Sensor and Simulation Notes

Note 244

November 1977

Surface Field Measurements with Image and Ground Planes

V. V. Liepa
D. L. Sengupta
J. E. Ferris
T. B. A. Senior

University of Michigan
Ann Arbor, MI 48109

Abstract

Results obtained from the measurement of currents and charges induced on some selected conducting bodies illuminated by plane electromagnetic waves are presented. The bodies considered are cylinders, bodies of revolution, and scale models of 747 aircraft. The measurements using the image plane technique were performed in the model frequency range of 0.45 GHz to 4.25 GHz. Data are presented for simulated conditions of free space, and in the presence of perfectly conducting and lossy ground planes. The cylinder length-to-diameter ratio, including its image, is 10; and the measurements cover the frequency range corresponding to $ka = 0.015\pi$ to $ka = 1.5\pi$. The body of revolution and the 747 results are shown at the full scale frequency ranges 1.13 MHz to 21.2 MHz and 0.98 MHz to 26.5 MHz, respectively. These full scale results have been deduced from the model frequency data.

Acknowledgment

It is a pleasure to acknowledge the assistance of Messrs. D. Sayre, R. Stoddard, J. Tedesco, and K. Young, all of the Radiation Laboratory, in performing the measurements, computer programming, data processing and other tasks involved in this study.

Sensor and Simulation Notes

Note 244

November 1977

Surface Field Measurements with Image and Ground Planes

V. V. Liepa
D. L. Sengupta
J. E. Ferris
T. B. A. Senior

University of Michigan
Ann Arbor, MI 48109

Abstract

Results obtained from the measurement of currents and charges induced on some selected conducting bodies illuminated by plane electromagnetic waves are presented. The bodies considered are cylinders, bodies of revolution, and scale models of 747 aircraft. The measurements using the image plane technique were performed in the model frequency range of 0.45 GHz to 4.25 GHz. Data are presented for simulated conditions of free space, and in the presence of perfectly conducting and lossy ground planes. The cylinder length-to-diameter ratio, including its image, is 10; and the measurements cover the frequency range corresponding to ka = 0.015 π to ka - 1.5 π. The body of revolution and the 747 results are shown at the full scale frequency ranges 1.13 MHz to 21.2 MHz and 0.98 MHz to 2660 MHz, respectively. These full scale results have been deduced from the model frequency data.

Acknowledgment

It is a pleasure to acknowledge the assistance of Messrs. D. Say, R. Stoddard, J. Tedesco, and K. Young, all of the Radiation Laboratory, in performing the measurements, computer programming, data processing and other tasks involved in this study.

TABLE OF CONTENTS

(continued on next page)

TABLE OF CONTENTS
(Continued)

1. INTRODUCTION

During the past 20 months the fields and charges have been measured as functions of frequency at selected stations on a variety of bodies, many of them in the presence of lossy and/or metallic ground planes. One group of measurements was distinct from the rest in being concerned exclusively with scale models of the F-111 aircraft in simulated free space; and since the results have already been presented in a technical report [1], it is sufficient to confine attention to the remaining portions of the study.

The overall objectives were to obtain data under experimentally controlled conditions that will aid in better understanding the material interaction of horizontally and vertically polarized hybrid and dipole simulators with test objects, and that will also serve as a data base for comparison with calculations using any of the computer codes available. The objects to be considered were circular cylinders, a body of revolution model of an aircraft, and a scale model of the 747 aircraft. All were to be probed in the presence of a perfectly conducting ground or image plane and, in some cases, a lossy ground plane as well, modelling the earth in the vicinity of the Achilles/Athamas simulators at Kirtland Air Force Base. It was therefore necessary to convert our free space measurement facility into an image plane set-up by constructing a large metallic plane in one of our anechoic chambers.

The 20-month duration of the contract saw a number of changes in our experimental facilities and in the techniques used for the acquisition and processing of surface field data. Some of these changes were voluntary and aimed at improving efficiency and the quality of the data obtained; however, one was involuntary and though it ultimately led to an improvement in capability, the change itself was disruptive, and costly in both time and effort. Because these evolutions have had an impact on the performance of the work, it would seem appropriate to give a brief historical account.

---

[1] Valdis V. Liepa, "Surface Field Measurements on Scale Model F-111 Aircraft," The University of Michigan Radiation Laboratory Report No. 014449-1-T; Interaction Application Memos, Memo 13, September 1977.

In the early stages of the contract two anechoic chambers were available. The first was a tapered room 50 ft. in length with a rectangular (test) section 12 ft. high, 18 ft. wide and long. This was specifically designed for surface field measurements and has VHP-48 absorber on the back wall and VHP-18 absorber on critical areas of the sidewalls, ceiling and floor. The other was a larger multipurpose room 15 ft. high, 30 ft. wide, and 100 ft. long of somewhat poorer electrical performance. It was our original intention to use the tapered room (actually, a predecessor of the one just described); but because of the necessity of having the image plane vertically in this, it was felt that the modification would be too disruptive of the other measurement programs for which this room was required. The decision was therefore made to use the multipurpose room at Willow Run Airport where the image plane could be installed horizontally.

Since the cement floor of this room was remarkably flat, the image plane was constructed by removing the absorber and then laying 4 ft. by 8 ft. sheets of 1/2 inch thick drywall (or sheetrock) sheets directly on the floor over an area 20 ft. by 48 ft. The joints were filled, taped, and subsequently sanded to obtain the required smoothness, and the whole was then covered with overlapping strips of 0.0015 inch thick aluminum foil to make the surface conducting. Edges were fastened with Scotch tape. In critical areas near the transmitting antenna and the test objects, 1/8 inch thick aluminum sheets were used instead of foil, and these were placed on top of 3/8 inch thick drywall to ensure a level surface for the plane. Probe and sensor leads were taken out through channels cut in the drywall sheets. While this construction was underway, the necessary probes and models were being fabricated; and by early November we had completed our probing of the field in the vicinity of the image plane, and had just started measurements on the cylindrical models.

The major disruption came at the beginning of December when the University of Michigan announced the sale of Willow Run Airport effective 1 January 1977. Although we were immediately given access to a nearby anechoic room which, though smaller, was actually better in electrical performance, there was no way to transfer the ground plane without effectively destroying it. We were therefore faced with a massive relocation operation and the construction of yet another image plane in the new facility.

The new chamber is 15 ft. high, 30 ft. wide and 50 ft. long and lined with absorbing material suitable for RF operation down to 0.4 GHz; and since time was now important, we were fortunate that its design made a simpler and better image plane possible. The floor is wood and has a recessed area (or crawl space) 8 ft. square and 4 ft. deep underneath. By performing the measurements in a region above this area, it was now possible to lay a purely metallic ground plane directly on the wooden floor, with the probe leads coming out into the recess. A plane was therefore constructed from 4 by 12 ft. sheets of 1/32 inch aluminum covering an area 24 by 44 ft. Joints were covered using conducting adhesive aluminum tape, and by late January we had a superior facility at our disposal and were in a position to carry on with the program where we had left off. However, two considerations suggested that it would be better to start the measurements from scratch. In the first place the ground plane (size and construction), the antenna location and the chamber itself were all different from before, and the changes would almost certainly show up when data for different and/or different-sized bodies were compared; and, secondly, we were now in the process of converting to an automatic data acquisition system to avoid the tedious and error-producing task of digitizing analog data manually. The developments in our data acquisition and processing systems in this period of time have been described by Liepa [2, 3]. It was therefore decided that we should repeat all the measurements that had previously been performed in the old chamber, and in effect the data presented here are the product of a nine-month investigation.

In Section 2 we describe the physical setup, including the ground planes, models, sensors and instrumentation used. The data are presented in Section 3 in the form of amplitude and phase plots as functions of the full scale frequency in the case of the aircraft models, and as functions of ka for the cylinders, where a is the cylinder radius. A brief discussion of the data is given in Section 4.

---

[2] Valdis V. Liepa, "Surface Field Measurements on Scale Model EC-135 Aircraft," The University of Michigan Radiation Laboratory Report No. 014182-1-F; Interaction Application Memos, Memo 15, August 1977.

[3] Valdis V. Liepa, "Surface Field Measurements on Scale Model EC-4 Aircraft," The University of Michigan Radiation Laboratory Report No. 014182-2-F, Interaction Application Memos, Memo 17, March 1977.

2. PHYSICAL DESCRIPTIONS

2.1 The Chamber and Its Image Plane

The measurements presented in this report were all made in an anechoic chamber 15 ft. in height, 30 ft. in width and 50 ft. long designed to operate down to at least 0.4 GHz. The chamber occupies an entire building apart from a small room at one end containing metal and wood shop equipment, and a room at the other (front) end for instrumentation, storage and personnel. An aperture in the wall separating the latter room from the chamber can be used for feeding cables into the room, placing antennas for pattern or scattering measurements, or merely observing work in progress in the chamber.

To convert the chamber from a free space measurement facility to a ground (or image) plane facility, a portion of the floor was stripped of absorber and then covered by 4 by 12 ft. aluminum sheets 1/32 inch in thickness. The joints were sealed using 1-1/2 inch wide adhesive conducting aluminum tape. The resulting 24 by 44 ft. image plane was placed symmetrically about the center line of the room and butted into the VHP-18 absorber on the backwall to provide a reasonable match for the currents flowing down the plane: see Figure 1 for a sketch emphasizing the image plane rather than the chamber. The transmitting antenna was located near the edge closest to the front wall, thereby creating a working area extending 30 ft. down the plane to the test location. Instrumentation was housed in the room behind the front wall.

2.2 The Ground Plane

In many applications a ground plane is a large metallic plate or screen placed horizontally, often on the ground, but in our case this is the image plane, and the ground plane is vertical as shown in Figure 2. Two types of ground plane were required: a metallic (perfectly conducting) plane, and a lossy one simulating the earth in the vicinity of Kirtland Air Force Base at suitably scaled frequencies.

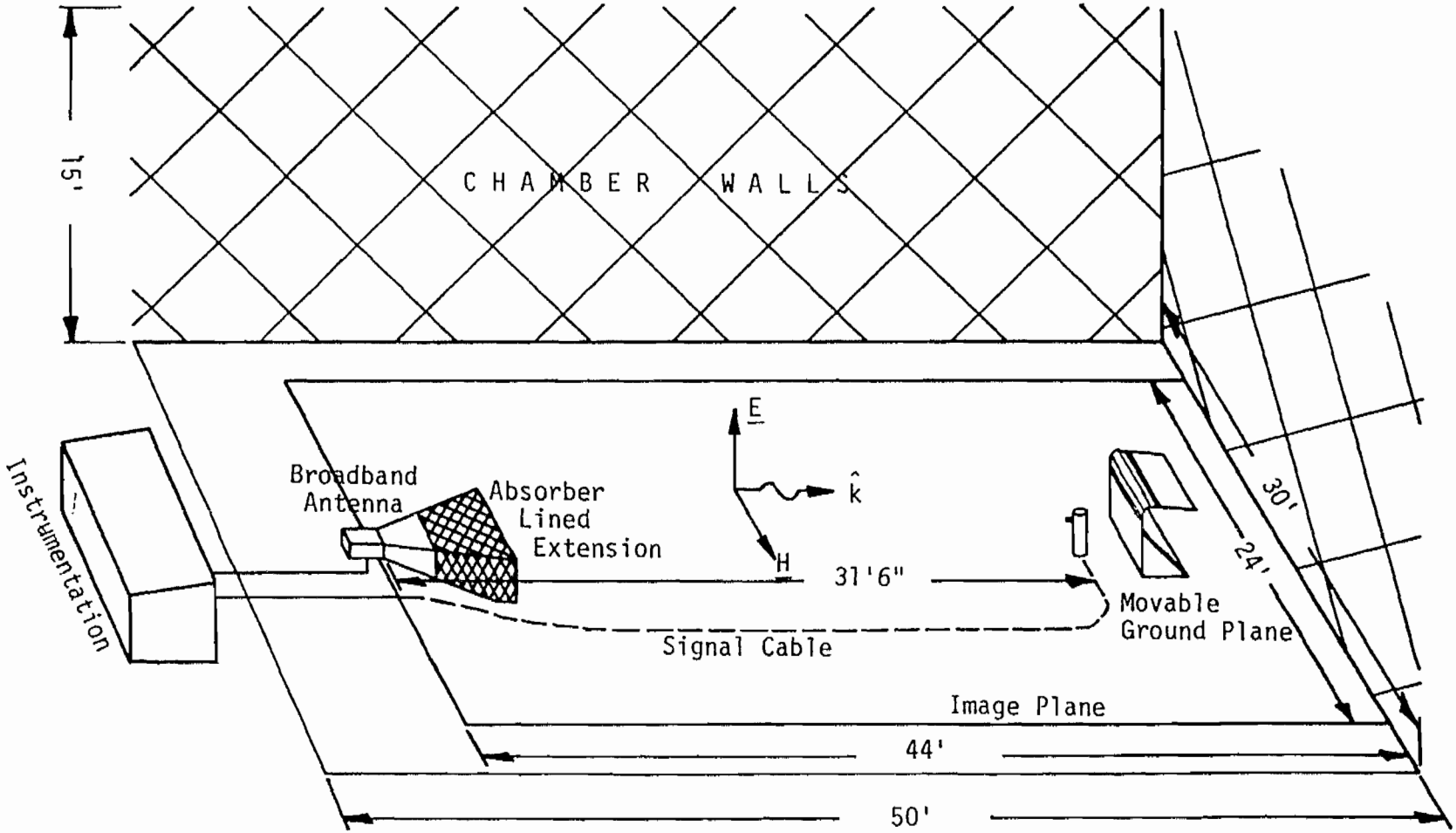

Figure 1. Image plane facility.

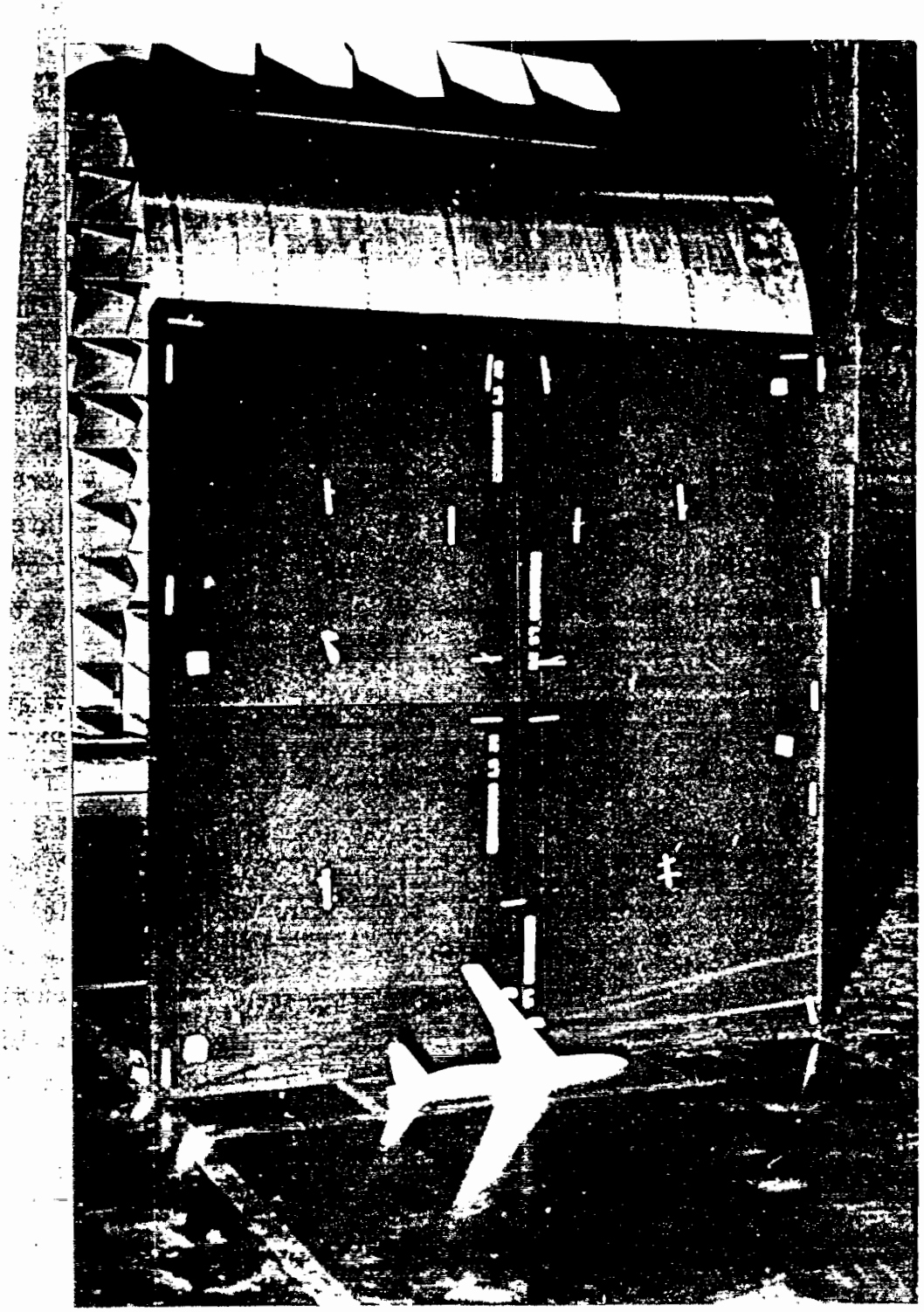

Figure 2. Lossy ground plane. The perfectly conducting ground plane is behind. The 747 model is 1/160.01 scale.

At first glance it might appear that the ground plane should be chosen as large as possible, but this is not necessarily true in practice. Any plane perpendicular to the direction of propagation will reflect most of the incident energy back to the transmitting antenna, where half is reradiated to create an effective incident field which is frequency dependent. In a previous study [2] the interaction between a 4 by 12 ft. metallic ground plane and the transmitting antenna produced oscillations of as much as 6 dB when the signal was recorded as a function of frequency. Various methods were explored for decreasing the interaction. One is obviously to rotate the plane to direct the reflected energy away from the antenna; but this was not deemed acceptable, and we were finally forced to reduce the plane to minimum size consistent with the maintenance of its image-forming property. In fact, all but a 4 by 4 ft. section of the ground plane had to be covered with absorber to reduce the oscillations to an acceptable level.

In view of this experience, we now chose immediately a 4 by 4 ft. ground plane mounted vertically on the image plane and corresponding to a 4 by 8 ft. ground plane under free space conditions, but special care was necessary to minimize the distortion of the surface field created by the edges. Since the incident field is vertically polarized the only significant component of the current is likewise vertical. The side edges of the ground plane then have only a negligible effect on the current, which is within 10 percent of its physical optics value at all points more than a small fraction of a wavelength from these edges [4]. However, a horizontal edge is another matter; and since this would reflect the current to produce a standing wave pattern, the ground plane was smoothly mated to a cylindrical surface at its upper edge, and the shadowed portion of the cylinder treated with absorber. The resulting ground plane structure weighs about 80 lbs. and can be moved as required. When in position, its bottom edge is fastened to the image plane using metallic tape to ensure continuity of the current from the image plane to the ground plane.

---

[4] J.J. Bowman, T.B.A. Senior and P.L.E. Uslenghi, "Electromagnetic and Acoustic Scattering by Simple Shapes," North-Holland Publishing Co., Amsterdam, 1969.

The lossy ground plane was required to provide simulation at suitably scaled frequencies of the ground at Kirtland Air Force Base, and the measured electrical properties of the ground expressed in terms of complex permittivity [5] are shown in Figure 3. The soil is practically nonmagnetic, so that its permeability is that of free space. In order to specify the complex permittivity desired for our ground plane material, it is necessary to take into account the scale factor p relating the laboratory frequencies to the full scale ones. Thus

$$\varepsilon'_{lab.} = \varepsilon'$$

$$\varepsilon''_{lab.} = \varepsilon''/p$$

where p ranges from 39.25 for the large cylinder to 460.25 for the small 747 model. More complete scaling factor information is given in Section 2.4.

Some of the considerations that went into the selection of a suitable material are given in Appendix A, and ultimately the LS-26 dielectric manufactured by Emerson and Cuming, Inc. was chosen. Its electromagnetic properties have been measured by the Avionics Laboratory of Wright-Patterson Air Force Base, and the data are presented as functions of frequency in Figures 4 and 5. Based on these values, the performance expected of our ground plane is discussed in Appendix A.

The metallic ground plane was used as the support structure for the lossy ground plane. The LS-26 material is 3/4 inch in thickness and comes in 2-foot square panels. A total of 12 panels were acquired and assembled into a three-layer sandwich 4 by 4 ft. in size. This was then attached to the metallic ground plane.

---

[5] R.D. Carrol, W.R. Eberle, D.R. Cunningham and M.J. Cunningham, "Electrical Properties of Earth at the AFSWC Dipole Facility and Horizontally Polarized Simulator Sites at Kirtland Air Force Base, New Mexico," U.S. Geological Survey, Special Project 27, February 1970.

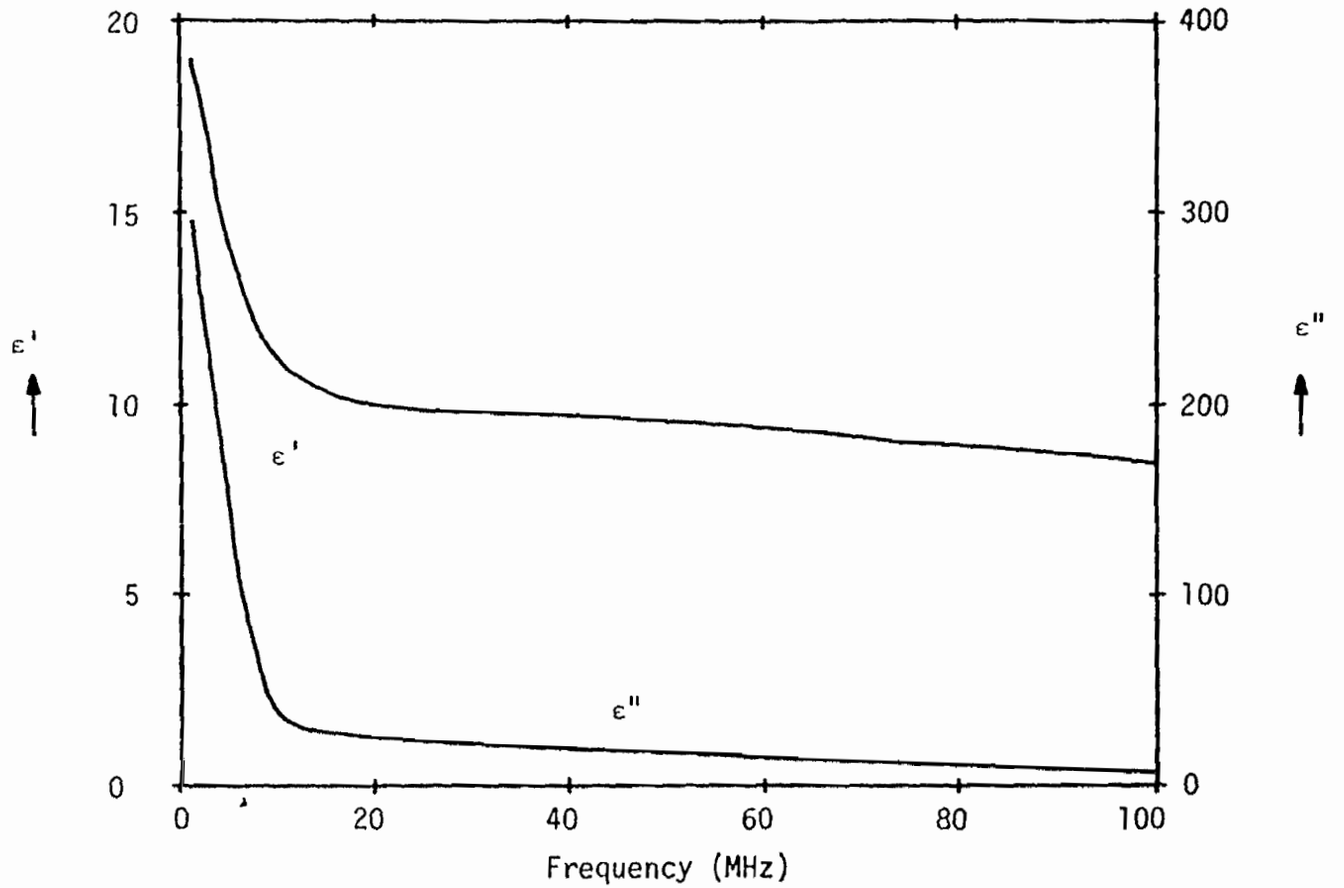

Figure 3. Average values of ε' and ε'' vs. frequency for the earth beneath the Dipole Facility [5]. $\mu = \mu_o$.

Figure 4. Measured ε' and μ' of LS-26 used.

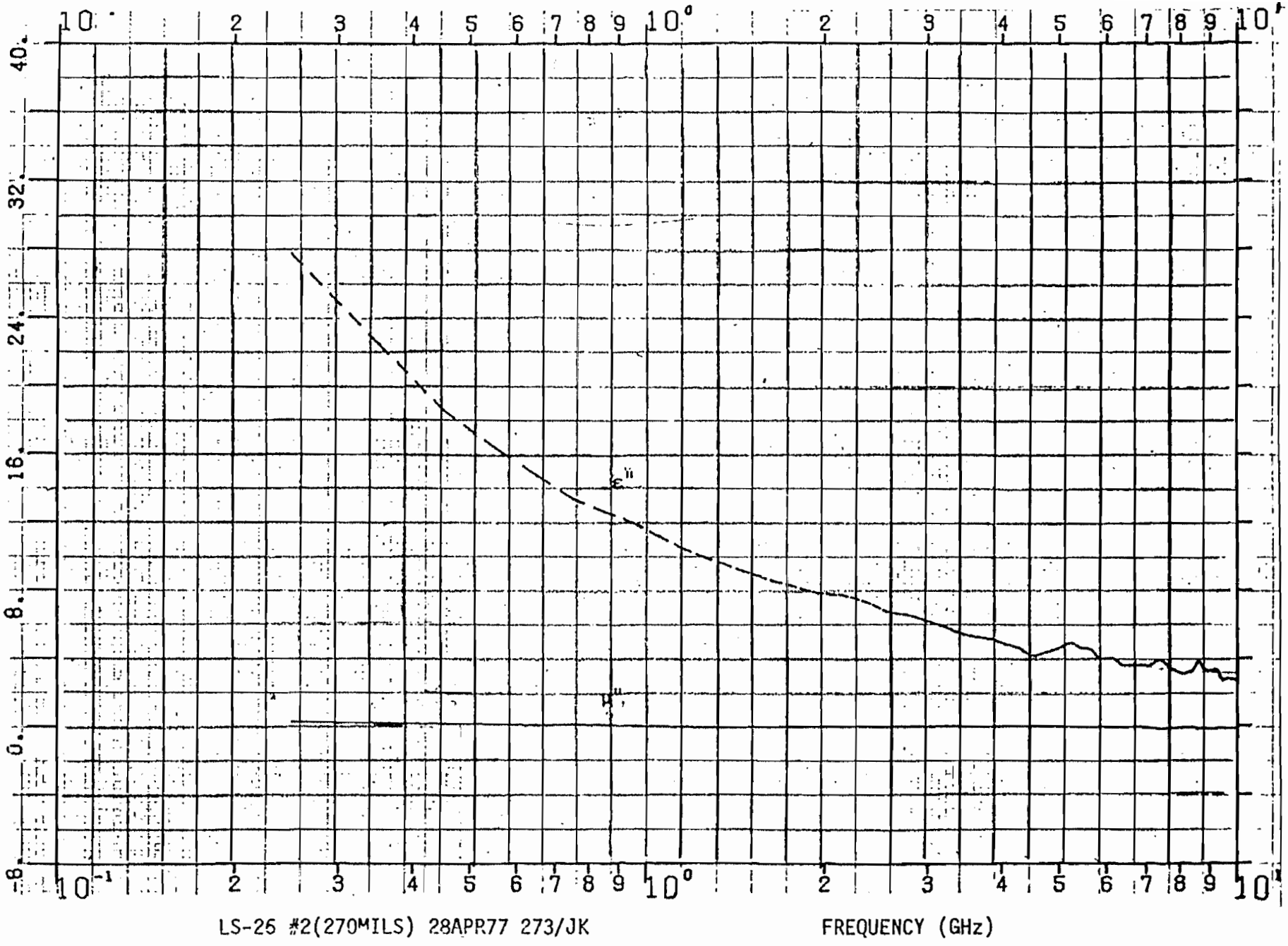

Figure 5. Measured ε'' and μ'' of LS-26 used.

2.3 Excitation Antenna

The wide bandwidth requirement somewhat limits the choice of antenna for illuminating the facility. Both the log periodic and rudimentary horn antennas meet this requirement; but in the case of the former, the backward wave characteristic produces an effective phase center whose location varies as a function of frequency in a manner which is difficult to compensate for. Attention was therefore given to the rudimentary horn which, for an image plane facility, is essentially a strip line with exponentially increasing separation between the strip and the plane. Various designs were tried including one where the strip extended all the way to the ceiling . Although most exhibited a tolerable VSWR, all had large side lobes, and the resulting signals bouncing off the chamber walls significantly degraded the uniformity of the field in the test area.

For these reasons it was decided to use the same broadband horn antenna previously employed in our free space measurements. This covers the required frequency range and has 8 to 12 dB gain with a maximum VSWR of 3:1 over the band. Because of its relatively low gain, its beamwidth in free space is at least 30°.

The horn was mounted with the center (phase center) of its aperture at a height h_t = 29.5 cm above the image plane and at a distance d = 960 cm from the center of the test region. The variation in the incident field amplitude as a function of the height y of the probe above the plane is then

$$\cos\left(\frac{2\pi h_t y}{\lambda d}\right)$$

The 3 dB point ranges from y = 271 cm at the lowest frequency to 28.7 cm at the highest, and the only model for which the variation is significant is the largest cylinder whose physical length ℓ is 50.83 cm. We remark that with this body the variation in illumination over its length is less than 3 dB if $f \leq 2.40$ GHz, but even at higher frequencies the fact that the cylinder is primarily excited at its base will somewhat reduce the effect of the illumination taper.

2.4 Test Models

Induced current and charge measurements were made on three types of metallic models over a 10:1 frequency range from 0.45 to 4.25 GHz. The models were right circular cylinders, bodies of revolution models of an aircraft, and scale models of the 747 aircraft, and these are described below.

Cylinders

All the cylinders were required to have $\ell/a = 10$ where ℓ is the physical length and a is the radius, and frequency coverage such that the characteristic parameter ka varied from 0.015π to 1.5π. Two sizes of cylinder were used to produce this coverage. The small ones were 0.55 cm in radius and 5.55 cm long, while the large one had a = 5.085 cm and ℓ = 50.83 cm. One large and five small cylinders were fabricated, and these are shown along with their vital dimensions in Figures 6 and 7. Because of the size of the small cylinders, it was not possible to employ our usual external sensors, and the cylinders which were fabricated had built-in sensors appropriate to the locations and types of measurement to be made.

The contract called for charge measurements on and near the top of the cylinder, and current measurements at the midpoint and near the base (see Figure 6). Near was specified as a distance of 5 sensor diameters, but this is ambiguous in our measurements since the models are scaled but not the sensors. On the large cylinder the sensors employed were the MGL-8 and ACD-1, and considering the sizes of these and our small ones, an average sensor diameter was defined, which was then used to find the desired measurement locations near to the ends of the cylinders. These turned out to be 9.04 percent of the cylinder length from the ends.

On the top of the small cylinder, a charge sensor was made by drilling a small hole through which a 0.020 inch diameter coax was passed and soldered to the cylinder. The outer shield was then removed and the center conductor and dielectric trimmed back to a 2 mm projection. The charge probes near the top and the center were produced in a similar fashion on the second and third small cylinders, the idea of mounting more than one sensor on the same model having been abandoned because of the fragile nature of the probes and the

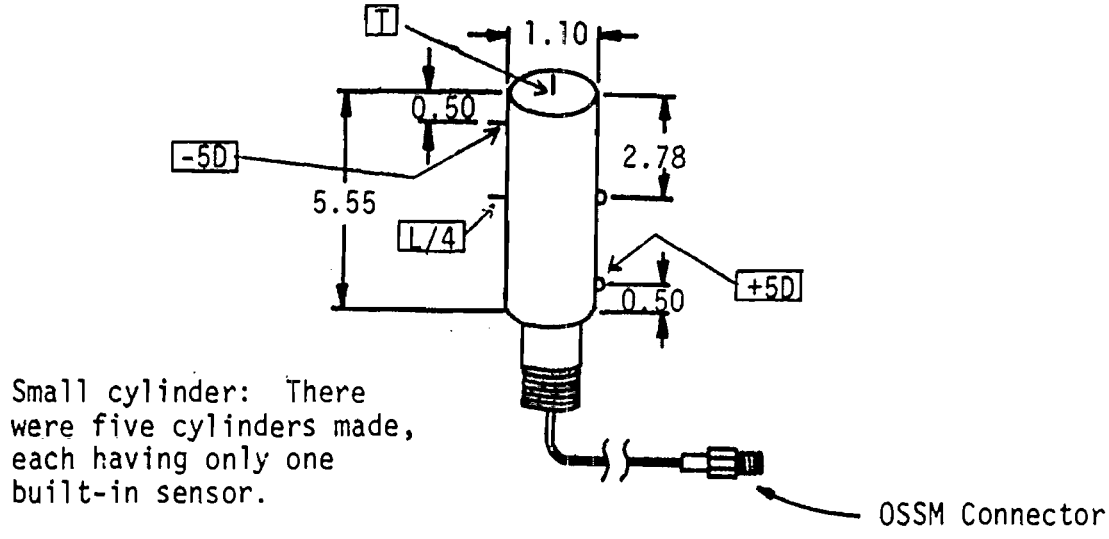

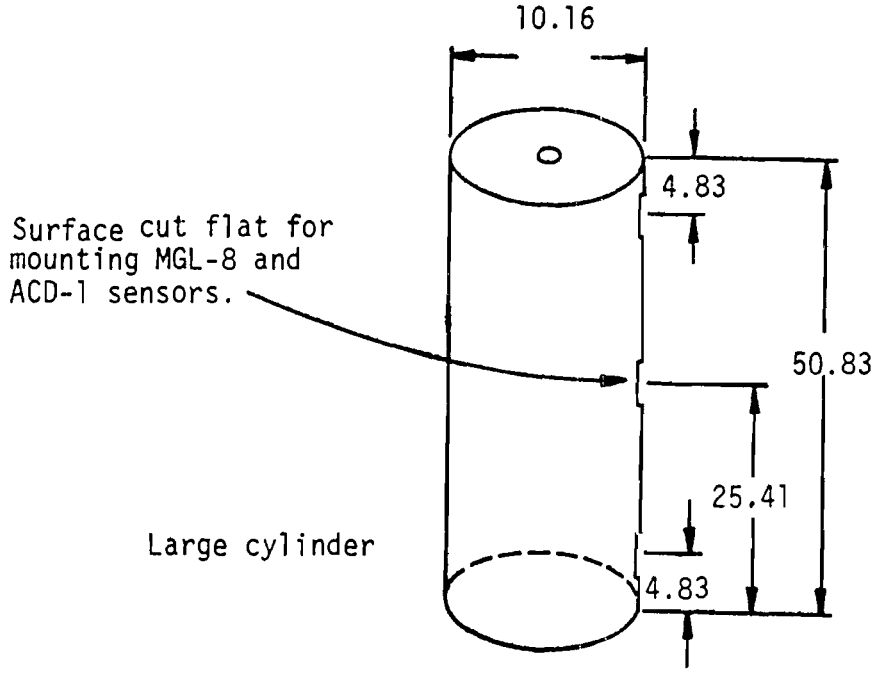

Figure 6. Cylinders used in measurements. (Dimensions in cm.)

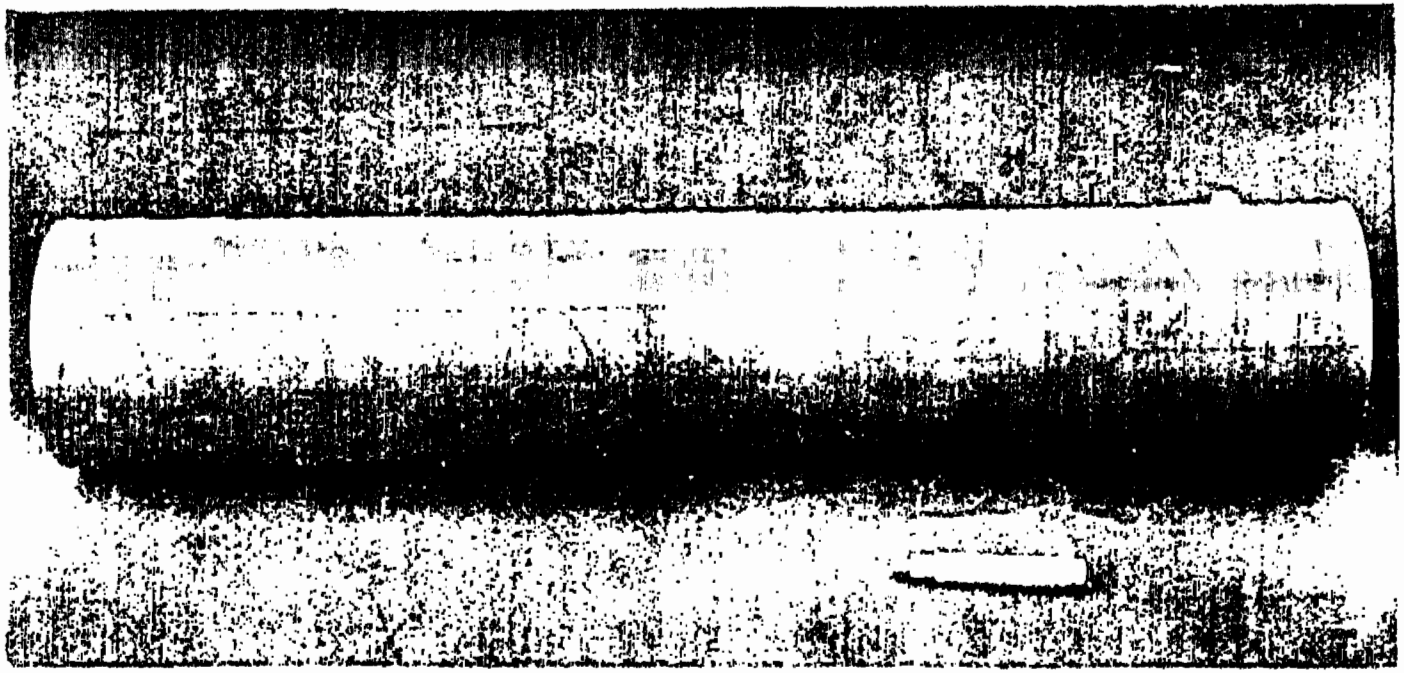

Figure 7. Cylinder models. Note the ACD-1A(A) sensor mounted on the large cylinder.

sensor leads. Magnetic loop (current) sensors were built at the center and near the base of the remaining two small cylinders. The sensors were of standard design and were made by drilling two holes about 2 mm apart in a cylinder, through which a coax was passed to form a half loop. A slot (or gap) was then cut in the outer shield at the surface of the cylinder.

Body of Revolution

For their computer analyses Taylor et al. [6] designed a conglomerate of ellipsoids and cylinders to simulate the EC-135 aircraft, and the shape and (full scale) dimensions of this structure are given in Figure 8. Our body of revolution is a scaled version of this. It was required that we cover the range $ka = 0.015\pi$ to 0.27π where a is the radius of the (central portion of the) fuselage; and to achieve this with the 10:1 range of frequencies available, it was necessary to construct two different sized models. These are shown in Figure 9. Their actual scale factors are 1/199.35 and 1/399.20 (nominally 1/200 and 1/400), and together they provide coverage from $ka = 0.015\pi$ to 0.28π.

The models were machined from solid brass and because of the tapered shapes of the various members, the construction was a complicated task involving almost 80 hours of machinists' time. The tapering was first done in staircase fashion, and the piece was then smoothed to the shape prescribed by the appropriate equation in [6]. Because of our image plane, only a half-model was needed; but for the fuselage and the vertical fin, the complete members were constructed and the right sides ground off on a milling machine. The wings and fins were then attached (soldered for the smaller model and with screws for the larger) to form the left side of the aircraft. Finally, each model was mounted on a metal plate approximately 20 by 30 cm in size, and the minute gap between the fuselage and plate was filled with silver paint to ensure good electrical contact.

---

[6] C.D. Taylor, K.T. Chen and T.T. Crow, "Electromagnetic Pulse Interaction with the EC-135 Aircraft," Interaction Application Memos, Memo 10, July 1975.

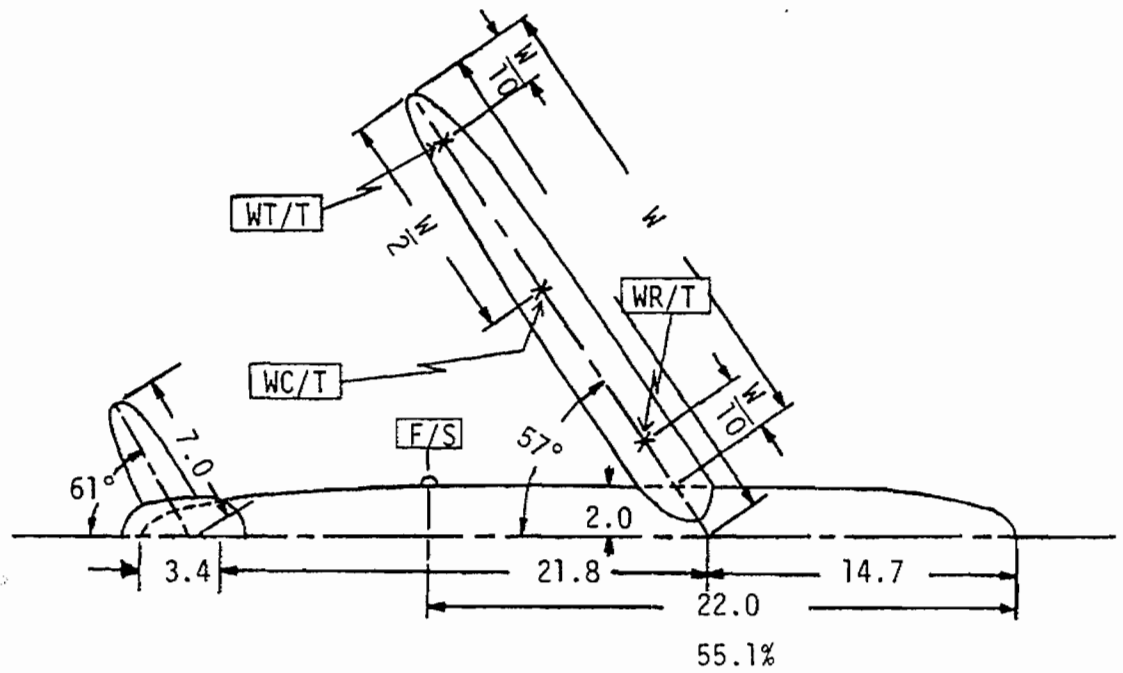

Station Legend

WT/T - Wing Tip, Top

WC/T - Wing Center, Top

WR/T - Wing Root, Top

F/S - Fuselage, Side

Figure 8. Body of revolution; full scale dimensions in meters.

Figure 9. Lady of revolution map.

747 Aircraft

Two plastic scale model kits for the 747 aircraft were purchased. Only the left sides were assembled and these were filled with plastic (auto body fiberglass) to help in mounting the models on aluminum plates. The models were smoothed and painted with conducting (silver) paint, and finally the contact edges with the plates were touched up to avoid any gaps. The fuselages were of lengths 14.54 and 44.08 cm, but since the excitation was antisymmetric, the wingspan provides the critical dimension. On this basis the scale factors for the two models were 1/460.75 and 1/160.01. Drawings and photographs of the models are shown in Figures 10 and 11.

2.5 Sensors and Their Implementation

Three types of sensors were used in this study: built-in ones for the small cylinders, the MGL-8 and ACD-1 for the large cylinder, and miniature surface probes for the bodies of revolution and the 747 aircraft.

The built-in ones were an integral part of the model and were described in the previous section. The large cylinder was big enough to accommodate the B-dot MGL-8A(R) and D-dot ACD-1A(A) sensors for current and charge measurements respectively. Each has a base plate and requires a hole to be drilled in the surface to take the signal lead into the interior of the model. Mounting was easy on the top of the cylinder, but on the side of the cylinder an area equal to that of the base plate was machined flat at each sensor location and then the hole drilled. To minimize the possibility of perturbing the surface fields, the milled areas which were not in use were taped over to bring the surface back to its original curvature.

The above sensors are too large for the body of revolution and 747 models, and our original idea of building in sensors was finally abandoned because of the difficulty in calibrating them. Special surface-mounted probes were therefore constructed and these are shown in Figure 12. Each is made from 0.020 inch

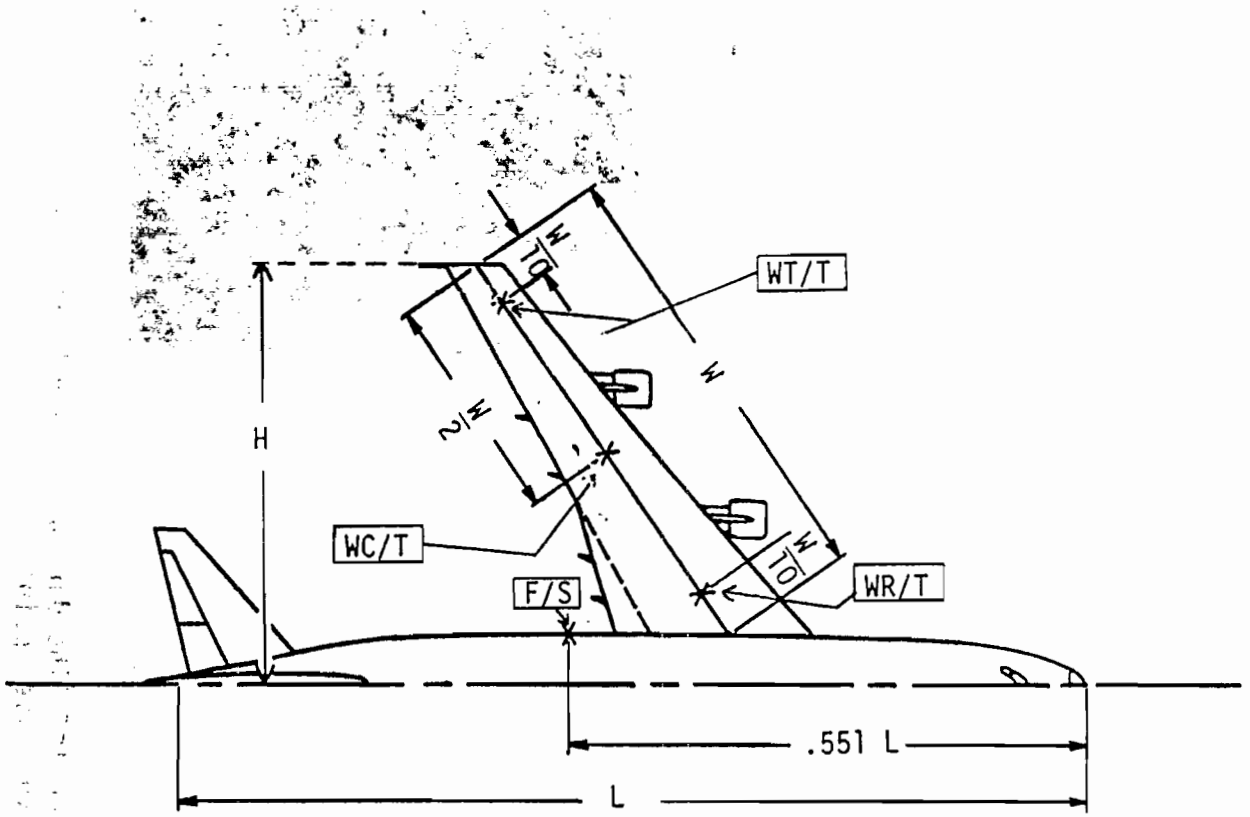

Station Legend

WT/T - Wing Tip, Top

WC/T - Wing Center, Top

WR/T - Wing Root, Top

F/S - Fuselage, Side

Figure 10. 747 aircraft. Full scale dimensions: fuselage length (L) = 68.63m, half wing-span (H) = 29.82m.

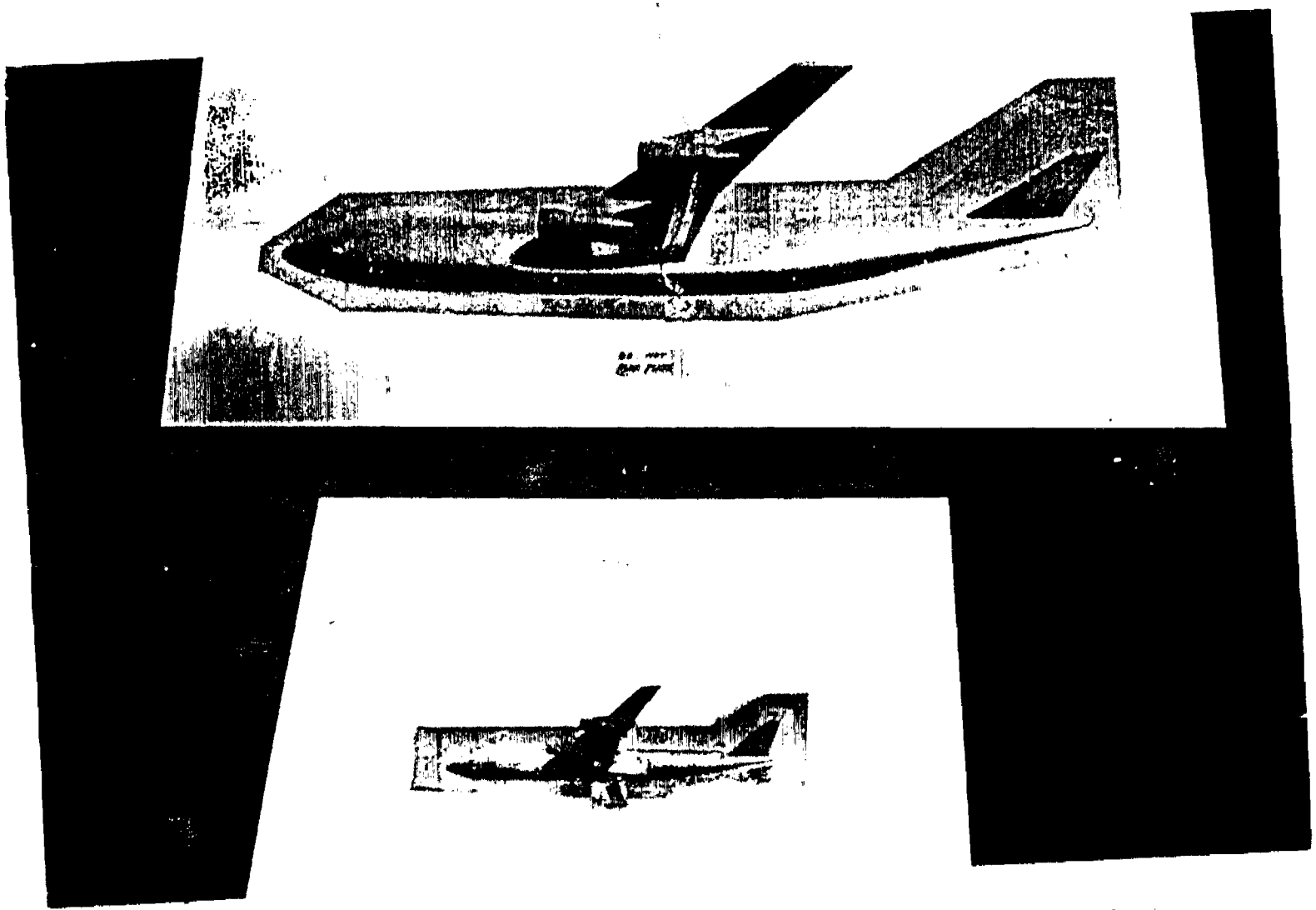

Figure 11. 747 scale models. The dark area around each fuselage is conductive silver paint.

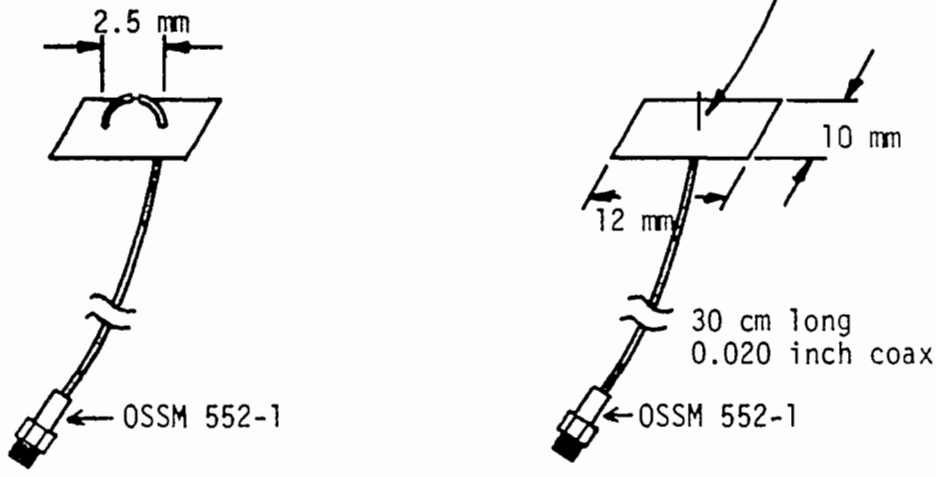

Current Sensor

Charge Sensor

Figure 12: Miniature external current and charge sensors.

diameter coaxial line about 30 cm long and a 10 by 12 mm 3-mil thick flexible brass plate. For the current probe two holes are drilled in the plate and a previously bent section of coaxial line is inserted through. The coax (including center conductor) is then soldered to the plate from the underside and, finally, a slot is cut in the outer shield at the center top of the loop. This last step is the most tricky part of the entire operation. There is a rather high probability of slicing through the center conductor as well, thereby destroying the sensor, and it usually took three attempts to make a single good probe. The charge probe was much easier to construct. The coax was simply passed through a hole in the plate where the outer conductor was soldered. From the short end the outer conductor was removed, being cut flush with the surface of the plate, leaving just the dielectric and the center conductor. With both probes, the output ends of the coaxial lines had connectors of the Omni-Spectra OSSM 551-1 (male) or -2 (female) type.

To use these probes on the body of revolution and 747 models, slots were cut at the desired locations on the wings and fuselages through which to pass the coaxial lead. The small sensor plate was then taped to the model with conducting tape and in addition the slots not in use were taped. The sensor lead emerged on the other side of the model (in the case of a wing, the underside), and from there was taped to the surface until it reached the image plane where it passed through a hole out of harm's way. It will be obvious that the process of mounting and taping a probe was tedious and time consuming, and required a good deal of care to ensure that the signal lead was not bent in a manner that would nullify the calibration.

2.6 Instrumentation

For the most part the instrumentation used was the same as in our previous [1, 2] free space model measurements, the only differences being in the cabling and (in some cases) the sensors. The main categories of equipment are shown in Figure 13, where the HP (Hewlett-Packard) numbers indicate the

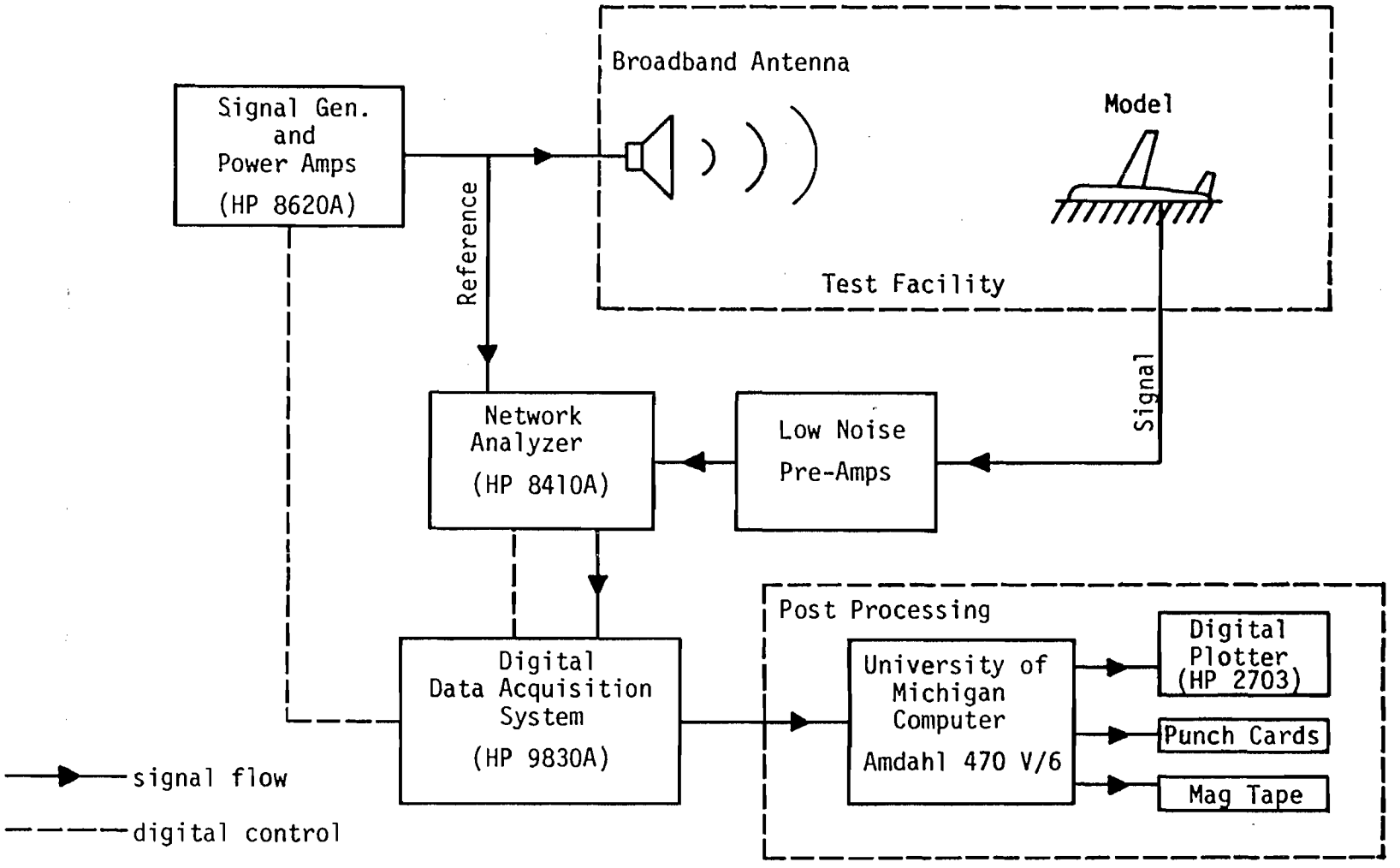

Figure 13. Block diagram of the experimental setup.

key items. However, each block may contain many individual pieces. Thus, the HP 9830A calculator in the digital data acquisition block is only one of almost a dozen pieces here, and represents only about a third of the total cost of the equipment in the block. The same is true for most of the other blocks.

The heart of the system is the data acquisition group which controls the transmitted frequencies and records and stores the measured surface field values. The process is as follows. Information is sent to the 8620A signal source to generate a particular cw signal, and the latter is then amplified to about 1 watt by a transistor or traveling wave tube amplifier and passed to a broadband ridged horn antenna where it is radiated. Just prior to the antenna, a small portion (-20 dB) of the signal is tapped and fed to the network analyzer as a reference. The radiated field excites currents and charges on the model. The sensor relates the current or charge to a voltage that is first amplified (20 to 40 dB depending on the frequency band) by a low noise preamplifier and then passed to the network analyzer which measures its amplitude and phase relative to those of the reference signal. The values are digitized by the data acquisition system and stored in its memory. The frequency is now incremented to a new value and the whole sequence repeated.

About 125 frequencies are used to cover a frequency band and the measurements take about 2 minutes. At the end of this, the data are transferred from the calculator core to a preassigned file on a cassette magnetic tape, and the equipment becomes available for the next set of measurements, e.g., a calibration run, measurements of a different field component or at a different station, or measurements in a different frequency band. A single transfer function such as those shown in Section 3 may require as many as nine sets of measurements: two models over each of three frequency bands, plus three calibration runs.

2.7 Measurement Procedure

The data recorded seldom resemble what one might initially expect. What is actually measured is the ratio of the received and reference signals at the terminals of the network analyzer, and this is quite different from the ratio of the field at the sensor to the field incident on the model. For example, the transmitted field is not frequency independent and may vary as much as ± 5 dB over the entire 10:1 band. It is virtually impossible to build an antenna which is frequency independent, yet reasonably efficient and directive, and there are also the effects caused by the chamber itself. On the receiving or sensing side, the frequency response of a small sensor is not ideal, and its output is further modified by the losses in the miniature semi-rigid coax used to make the sensor, the miniature connectors that may have a VSWR as high as 1.5:1, and the 50 or more feet of cable from the sensor to the recording equipment. The transistor preamplifiers with their input VSWRs of 2:1 will also introduce amplitude variations if their inputs are not properly padded, and a 4 dB attenuator is generally inserted to reduce the mismatch at the input. Finally, there is the network analyzer. When properly locked on to the frequency, the accuracy of this instrument is well within the accuracy desired of the final data; but sometimes due to the wide range over which the frequency is swept, plus the presence of harmonics generated by the power amplifier (or even noise per se), the instrument fails to lock and produces erroneous output. For the A-D conversion and the data processing, the accuracy is orders of magnitude better than in the other parts of the system, and is of no concern.

To obtain meaningful data from these measurements, it is obvious that the components must be calibrated. The critical ones are those on the paths followed by the reference and measurement signals from the directional coupler (ahead of the antenna) to the network analyzer. In the case of the latter signal, the path includes the antenna, chamber, sensor, cables, connectors and preamplifier, and with so many elements it is obviously impractical to

calibrate them individually. The system (including sensor) is therefore calibrated as a whole and it is this information which is used in processing the data.

The calibration consists of mounting the sensor in the image plane and recording the incident field over all three frequency bands. Mounting the surface sensors (see Figure 12) and the MGL-1 and ACD-1 was relatively straightforward, but the built-in sensors on the small cylinders required special attention. For each of the three cylinders with side probes, a cylindrical trough was cut in a 1/8-inch thick metal plate so it would rest snugly on the side of the cylinder. The trough was cut just through the plate to allow the probe to project through the locally plane surface, and the entire structure was then mounted in the image plane. For the cylinder with the top probe, a circular hole of the same diameter as the cylinder was cut in a metal plate, the cylinder pushed through until its top was flush with the plate, and the structure mounted in the image plane as before. Wherever appropriate, joints and cracks were sealed with metallic tape prior to measurement.

On completing the calibration of a probe, this same probe with all its cables and connectors attached is mounted on a model. The system is now inspected to make sure that the fragile probe has not been damaged, and that the cables and connectors have not been strained or distorted in a manner that would vitiate the calibration. If everything appears alright, the measurements are performed on the model at first one station and then another. On the other hand, if at any stage the probe and its associated cabling is damaged, repairs must be made, and the system then has to be recalibrated prior to the next measurement.

2.8 Data Reduction

When allowance is made for repeated measurements caused by equipment breakdowns and human errors, the study required almost 500 measurement

runs, and to keep track of these a log book is maintained listing models, stations, field components, frequency bands, calibrations, etc. On completion of a group of measurements, the 9830A calculator is used to normalize the measured fields to the incident field (calibration) values, and the reduced data are then stored back on the cassette. To avoid the possibility of accidentally erasing the raw data, this is stored in the odd files on the cassette, and the reduced data on the next adjacent (even) file. Using the 9830A calculator as a remote computer terminal, the reduced data are then transmitted to the central University of Michigan computer where it is further processed, leading ultimately to the form of plots presented in Section 3. Each such plot has a set of characters in the top right hand corner identifying the model, station, etc., as well as giving the file name where the data from which the plot was generated is stored. In addition to plots, the data can be printed out, written on magnetic tape or punched on cards.

3. DATA

The surface current and charge data are presented here in five groups, three devoted to the cylinder models and one each to the body of revolution and 747 aircraft. Each section provides such needed information as the phase reference plane and frequency scales used and, in addition, contains a summary table giving the figure numbers for the various measurement situations.

Six data sets (two models over each of three frequency bands) are required to generate a transfer function. The data are stored on magnetic tape and the file format is:

1. FILENAME (4A4)
2. Comments (18A4)
3. Comments (18A4)
4. TITLE used in plotting (18A4)
5. FMIN, FMAX, AMPMIN, AMPMAX, PHASEMIN, PHASEMAX, NN
   (4F8.3, 2F8.2, I5)
6. F(1) AMP(1) PHASE(1) F(2) AMP(2) PHASE(2) F(3) AMP(3)
   PHASE(3) (3(2F8.3, F8.2)

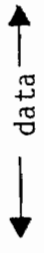

. . . . F(NN) AMP(NN) PHASE(NN)

where NN is the number of data points in the set. Table 1 is a listing of a typical file.

TABLE 1: ILLUSTRATION OF DATA SET

```
>      1     J2929
>      2     747S,F/T,JT1,BAND 1,J, FS,10/12/77,KY
>      3     460
>      4
>      5        0.982   2.405   1.303   8.017 -179.50  181.40  138
>      6        0.982   1.303  -92.10   0.992   1.380  -94.60   1.003   1.324  -96.10
>      7        1.013   1.358  -96.60   1.024   1.368  -95.50   1.034   1.439  -97.10
>      8        1.044   1.435  -97.90   1.055   1.355  -99.40   1.065   1.455  -97.50
>      9        1.076   1.439  -97.30   1.086   1.452 -100.90   1.096   1.486  -99.50
>     10        1.107   1.393 -101.40   1.117   1.479  -91.50   1.127   1.459  -91.90
>     11        1.138   1.545  -95.90   1.148   1.641  -96.80   1.159   1.667 -100.80
>     12        1.169   1.656  -99.40   1.179   1.600 -100.30   1.190   1.667  -96.50
>     13        1.200   1.706  -96.00   1.211   1.799  -98.60   1.221   1.820 -100.30
>     14        1.231   1.811 -101.30   1.242   1.799  -96.50   1.252   1.782  -96.50
>     15        1.263   1.932  -95.40   1.273   2.051  -97.80   1.283   2.188 -103.40
>     16        1.294   2.104 -105.20   1.304   1.968  -98.00   1.314   1.928  -99.20
>     17        1.325   2.118  -97.90   1.335   2.291 -100.60   1.346   2.393 -103.00
>     18        1.356   2.355 -104.60   1.366   2.239 -105.60   1.377   2.143 -103.40
>     19        1.387   2.213 -102.30   1.398   2.393 -100.10   1.408   2.588 -100.30
>     20        1.418   2.735 -102.40   1.429   2.716 -106.40   1.439   2.594 -108.50
>     21        1.449   2.606 -106.30   1.460   2.673 -105.00   1.470   2.805 -104.50
>     22        1.481   2.965 -106.40   1.491   3.020 -105.20   1.501   3.097 -105.20
>     23        1.512   3.027 -111.10   1.522   3.062 -111.90   1.533   3.199 -108.90
>     24        1.543   3.311 -109.40   1.553   3.334 -110.60   1.564   3.327 -113.60
>     25        1.574   3.412 -114.50   1.584   3.451 -113.00   1.595   3.499 -112.30
>     26        1.605   3.548 -111.40   1.616   3.681 -113.50   1.626   3.837 -115.60
>     27        1.636   3.917 -116.60   1.647   4.036 -118.90   1.657   3.981 -117.90
>     28        1.668   4.027 -119.50   1.678   4.055 -120.10   1.688   4.236 -116.80
>     29        1.699   4.365 -120.70   1.709   4.395 -119.70   1.720   4.426 -124.60
>     30        1.730   4.446 -122.90   1.740   4.592 -122.80   1.751   4.786 -123.80
>     31        1.761   5.000 -126.00   1.771   5.000 -127.20   1.782   5.023 -129.30
>     32        1.792   4.943 -129.20   1.803   4.909 -131.10   1.813   5.093 -130.50
>     33        1.823   5.346 -129.00   1.834   5.623 -129.30   1.844   5.808 -131.80
>     34        1.855   5.888 -134.80   1.865   5.808 -137.20   1.875   5.781 -139.60
>     35        1.886   5.875 -138.00   1.896   5.916 -136.20   1.906   6.180 -138.30
>     36        1.917   6.516 -139.80   1.927   6.699 -144.00   1.938   6.808 -146.70
>     37        1.948   6.668 -146.90   1.958   6.637 -147.30   1.969   6.683 -148.60
>     38        1.979   6.761 -151.40   1.990   7.047 -152.40   2.000   7.194 -153.20
>     39        2.010   7.379 -155.70   2.021   7.447 -157.30   2.031   7.295 -160.40
>     40        2.041   7.345 -162.30   2.052   7.396 -162.60   2.062   7.362 -162.60
>     41        2.073   7.482 -164.70   2.083   7.745 -166.30   2.093   7.816 -168.30
>     42        2.104   7.907 -173.40   2.114   8.017 -176.20   2.125   7.816 -177.30
>     43        2.135   7.621 -178.40   2.145   7.464 -179.50   2.156   7.586  181.40
>     44        2.166   7.586  178.10   2.176   7.709  176.90   2.187   7.727  174.30
>     45        2.197   7.638  172.20   2.208   7.551  171.10   2.218   7.534  170.50
>     46        2.228   7.413  168.90   2.239   7.430  167.40   2.249   7.413  166.00
>     47        2.260   7.499  163.60   2.270   7.621  161.10   2.280   7.295  159.20
>     48        2.291   6.982  157.40   2.301   6.887  155.60   2.312   6.808  157.00
>     49        2.322   6.871  156.90   2.332   7.063  156.40   2.343   6.966  155.80
>     50        2.353   6.902  152.10   2.363   6.730  149.50   2.374   6.761  147.60
>     51        2.384   6.546  147.80   2.395   6.353  147.10   2.405   6.223  145.80
END OF FILE
```

3.1 Cylinders

Of the three types of models considered, the largest amount of data was obtained for the cylinder, and for presentation purposes it is convenient to subdivide these data into categories corresponding to the measurements in simulated free space (F/S), and in the presence of perfectly conducting (GP) and lossy (LGP) ground planes. The measurements were made at four locations along the cylinder, and these are listed in Table 2.

TABLE 2: CYLINDER STATIONS

Station	Measurement	Location (see Figure 6)
+5D	J	near bottom of cylinder
L/4	J,Q	center of cylinder
-5D	Q	near top of cylinder
T	Q	top of cylinder

For the free space case, the measurements were made at 0°, 45°, 90°, 135°, and 180° azimuthal positions, while for the perfectly conducting and the lossy ground plane cases only the 180° measurement was made. The azimuthal angle is measured clockwise when viewed from the top of the cylinder, with $\phi = 0$ at the front (toward the transmitting antenna) and $\phi = 180$ at the back (in the shadow region). The phase reference plane is at the front of the cylinder, and the data are presented as functions of ka, where k is the wavenumber and a is the cylinder radius. To show more explicitly the resonant behavior of the cylinder, such as the resonant frequency and the height and the width of the peak, the resonant region data are also presented on an

expanded scale. For these plots, cleaning and slight filtering were applied on the data to remove some of the noise introduced by the equipment.

3.1.1 Cylinder in Free Space

The data presented for cylinders in free space are summarized in Table 3. To simplify the presentation, the four curves of data relating to the same measurement are presented under the same figure number, but subdivided by letters a and b designating the full plot amplitude and phase, and the expanded plot amplitude and phase, respectively.

TABLE 3: CYLINDER - FREE SPACE

STA	J/Q	Ø = 0°	45°	90°	135°	180°
+5D	J	Figure 14	Figure 15	Figure 16	Figure 17	Figure 18
L/4	J	19	20	21	22	23
L/4	Q	24	25	26	27	28
-5D	Q	29				
T	Q	30				

Each figure has two parts:

a) amplitude and phase, full plot

b) amplitude and phase, expanded plot

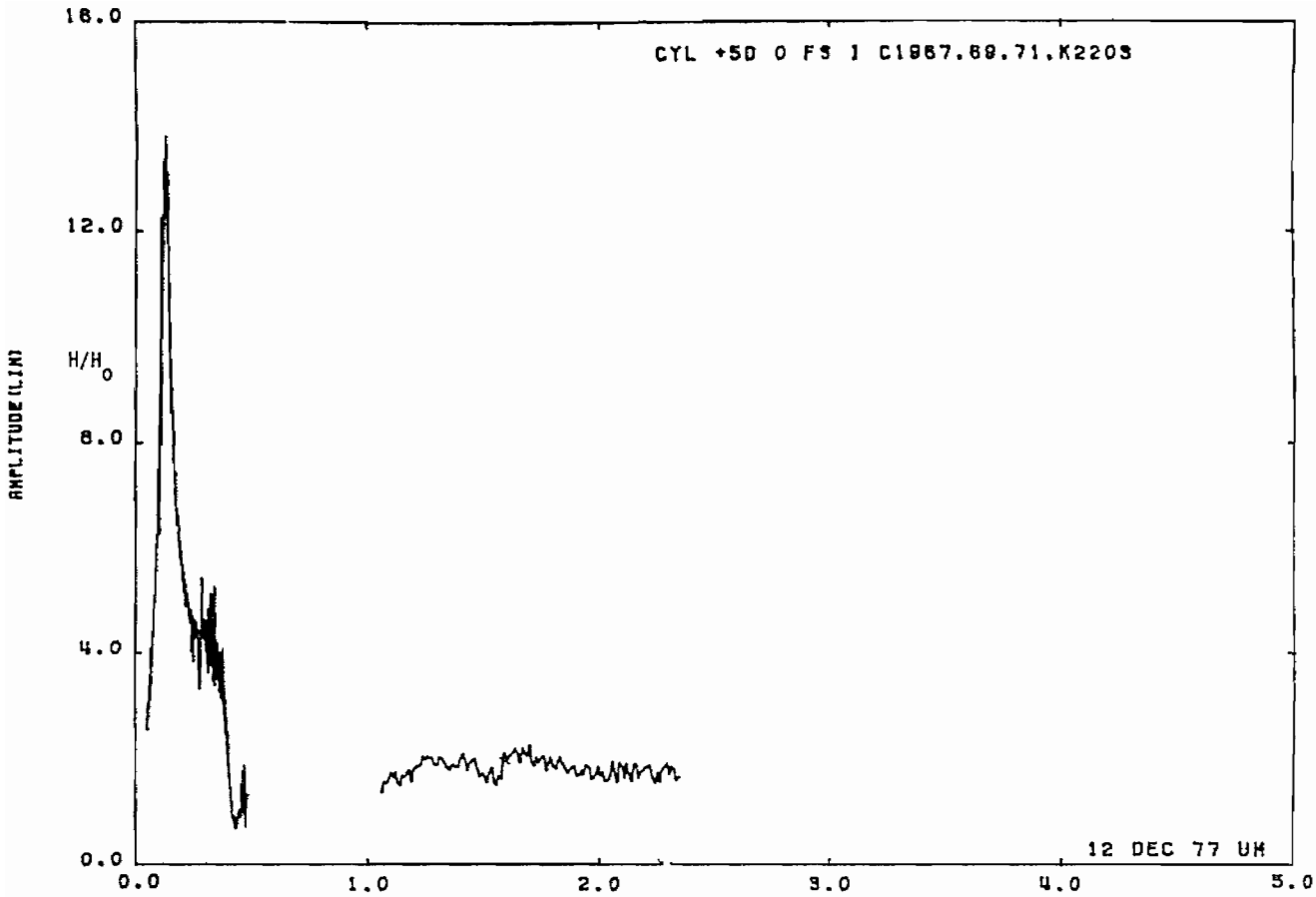

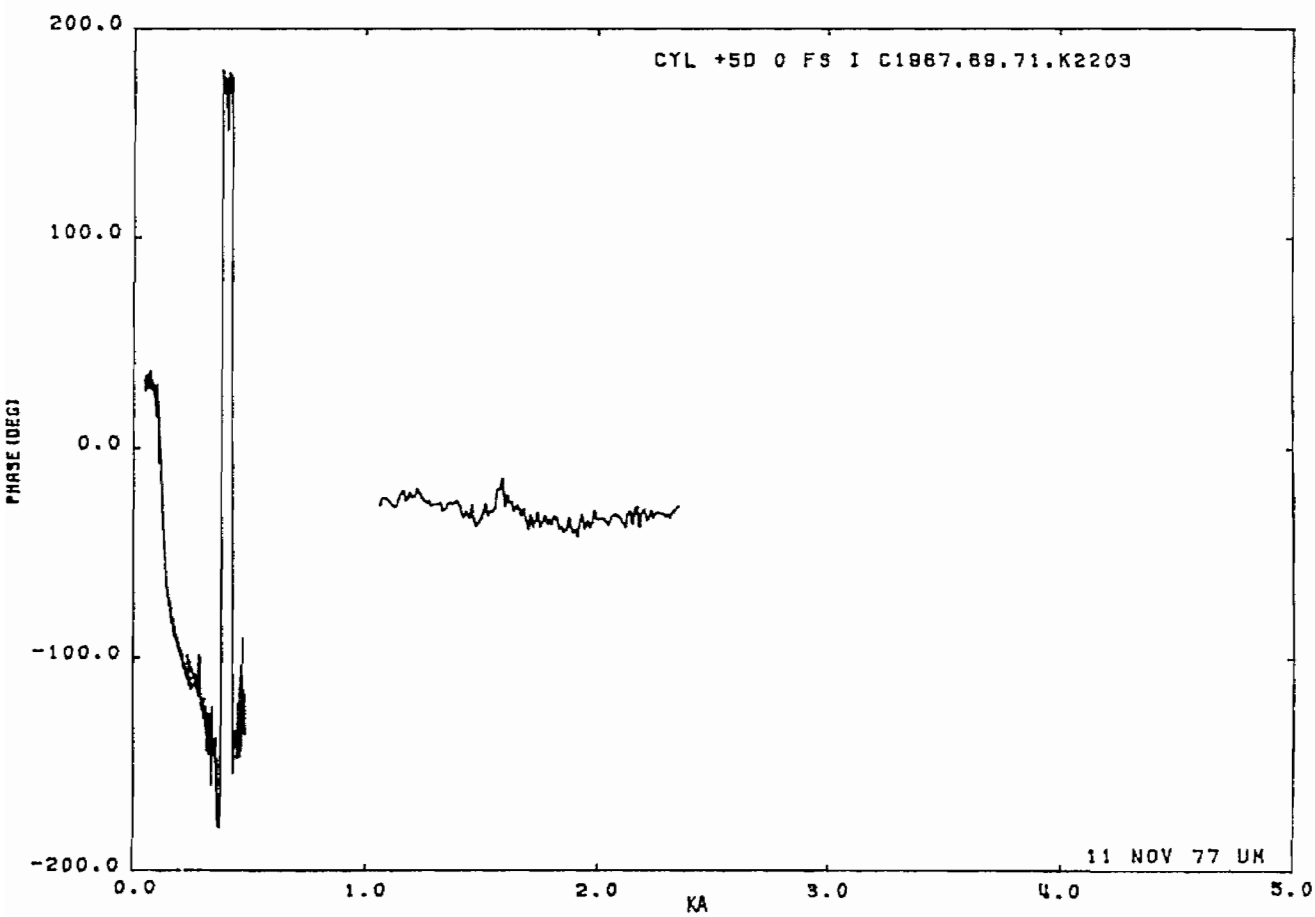

Figure 14a. Current on cylinder at STA:+5D; Ø = 0°, free space.

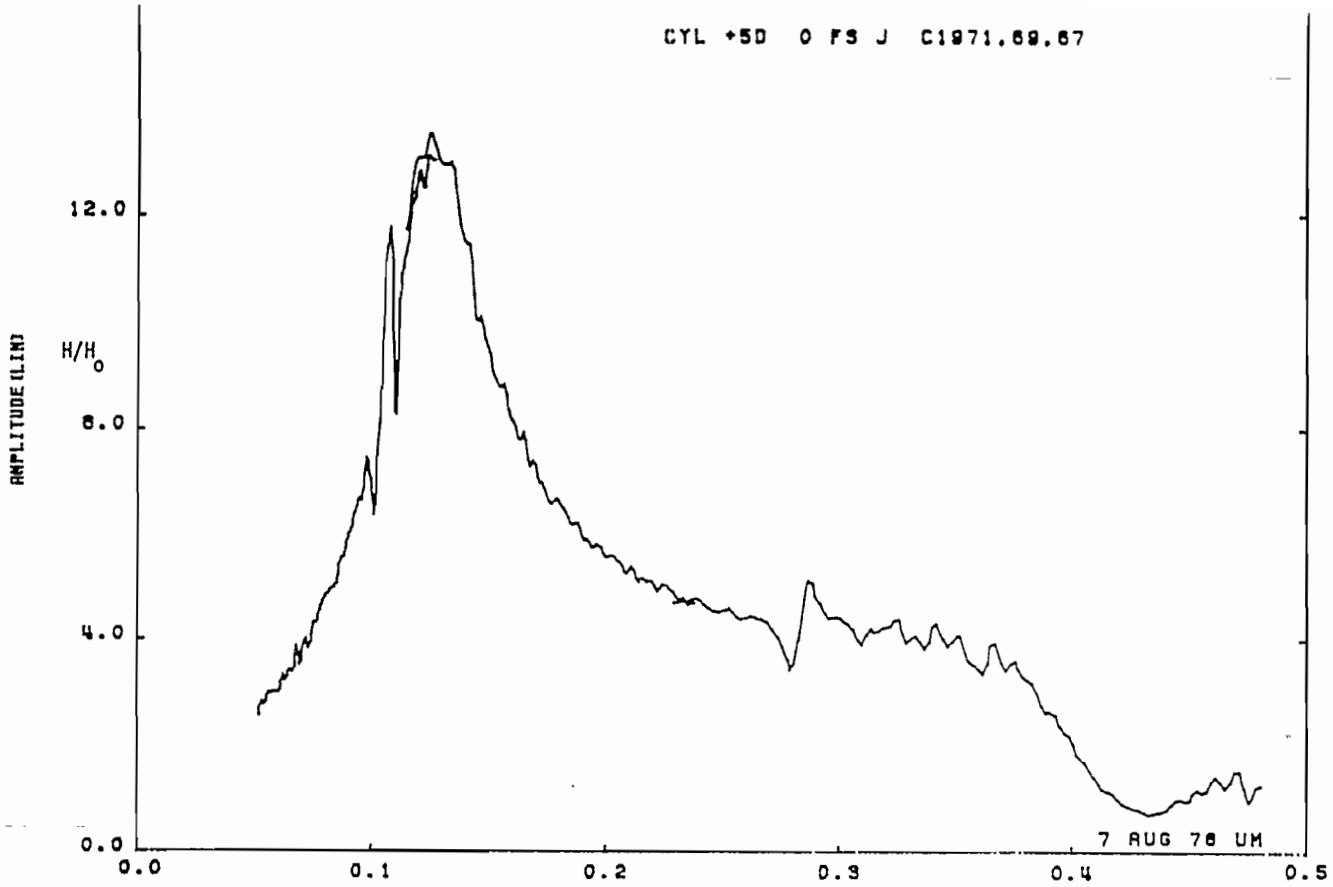

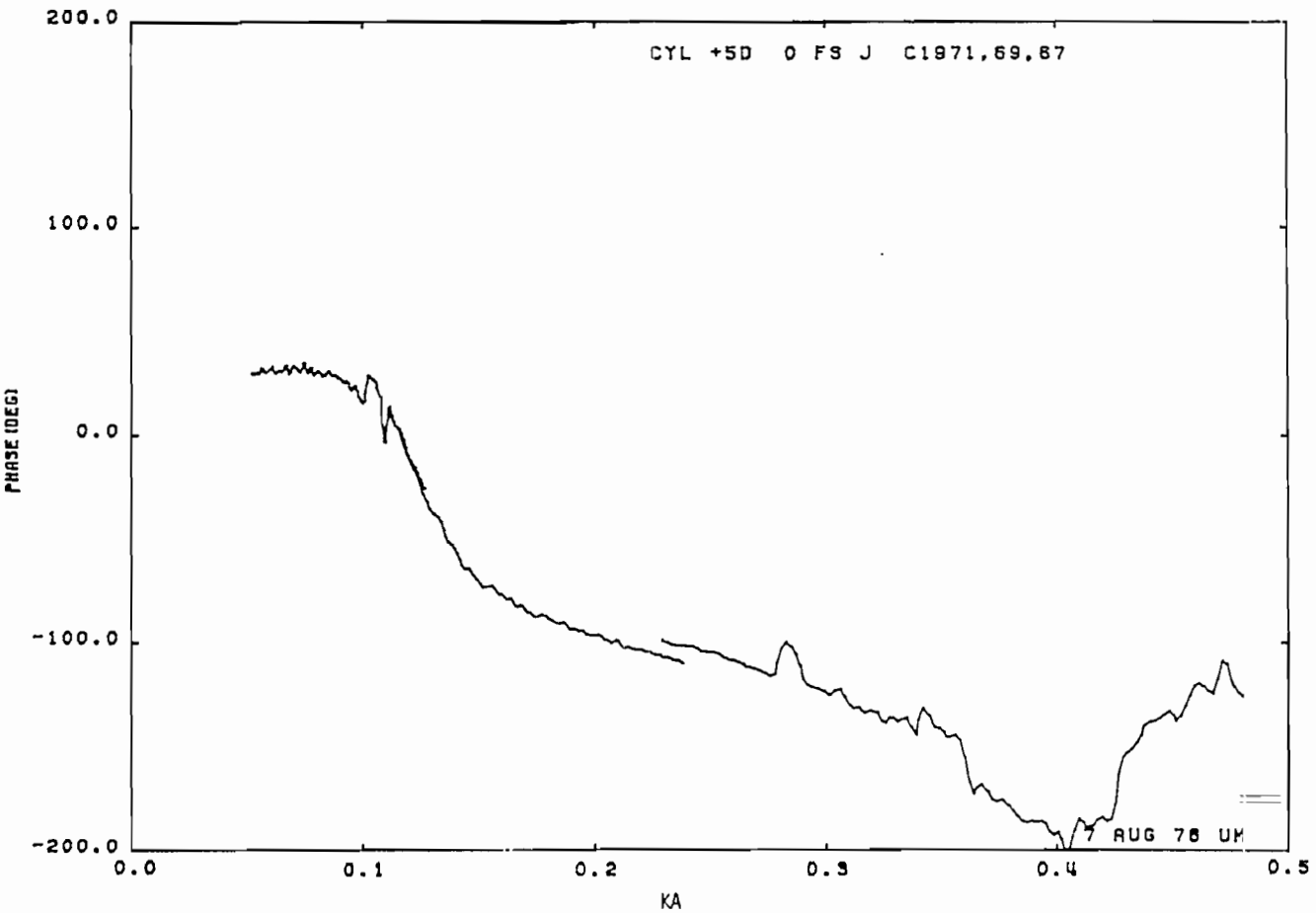

Figure 14b. Current on cylinder at STA:+5D; ϕ = 0°, free space (expanded scale).

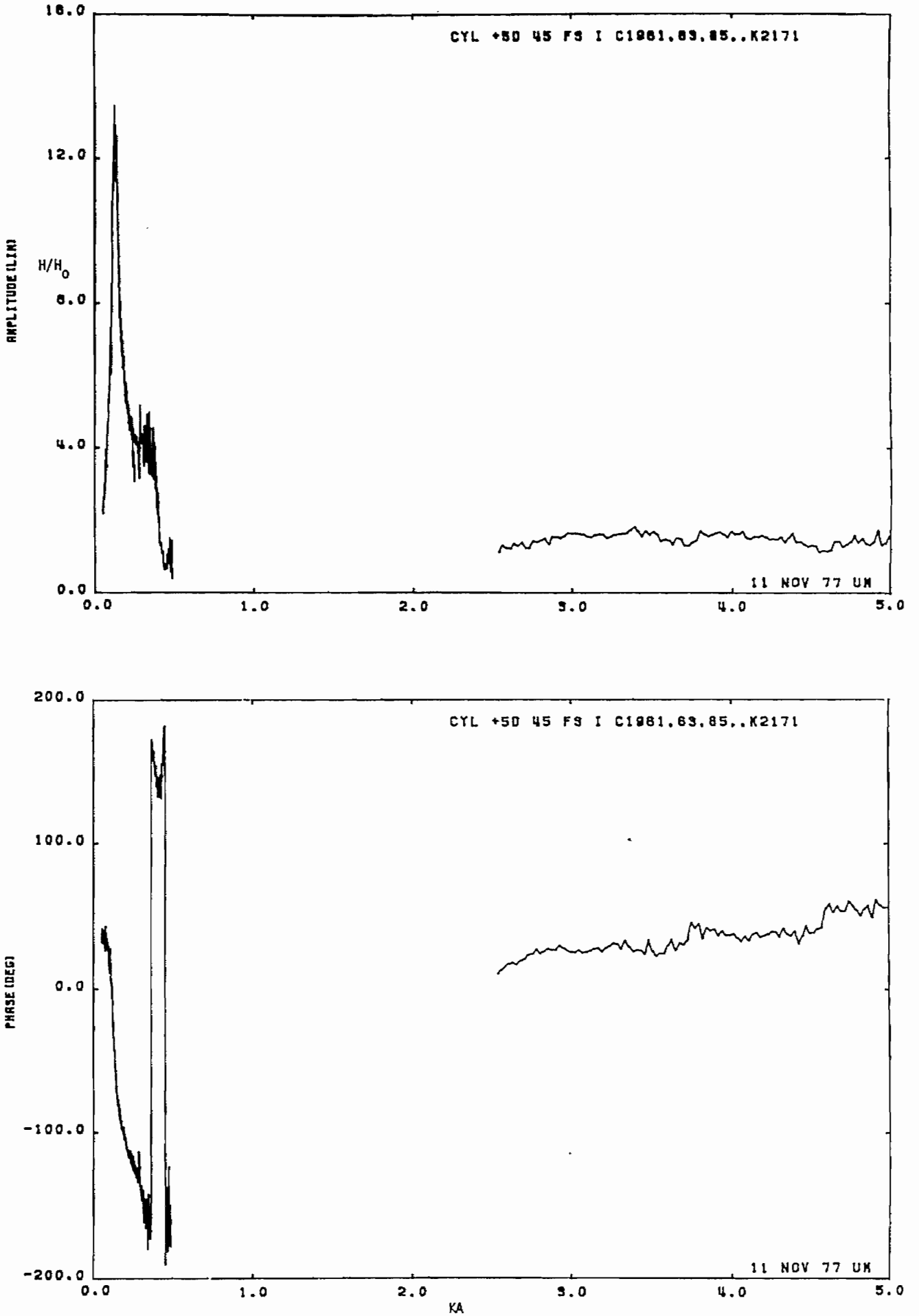

Figure 15a. Current on cylinder at STA:+5D; ϕ = 45°, free space.

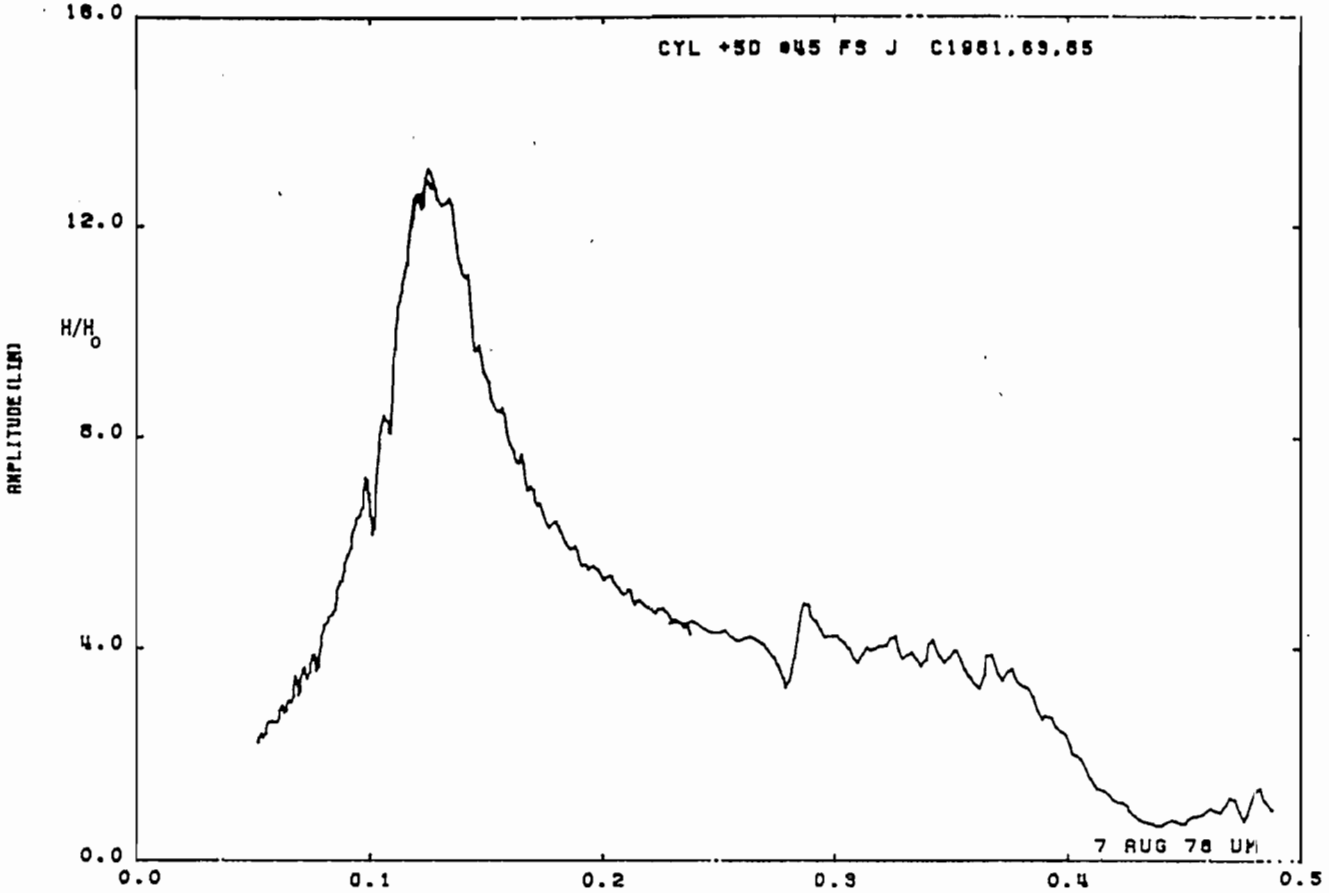

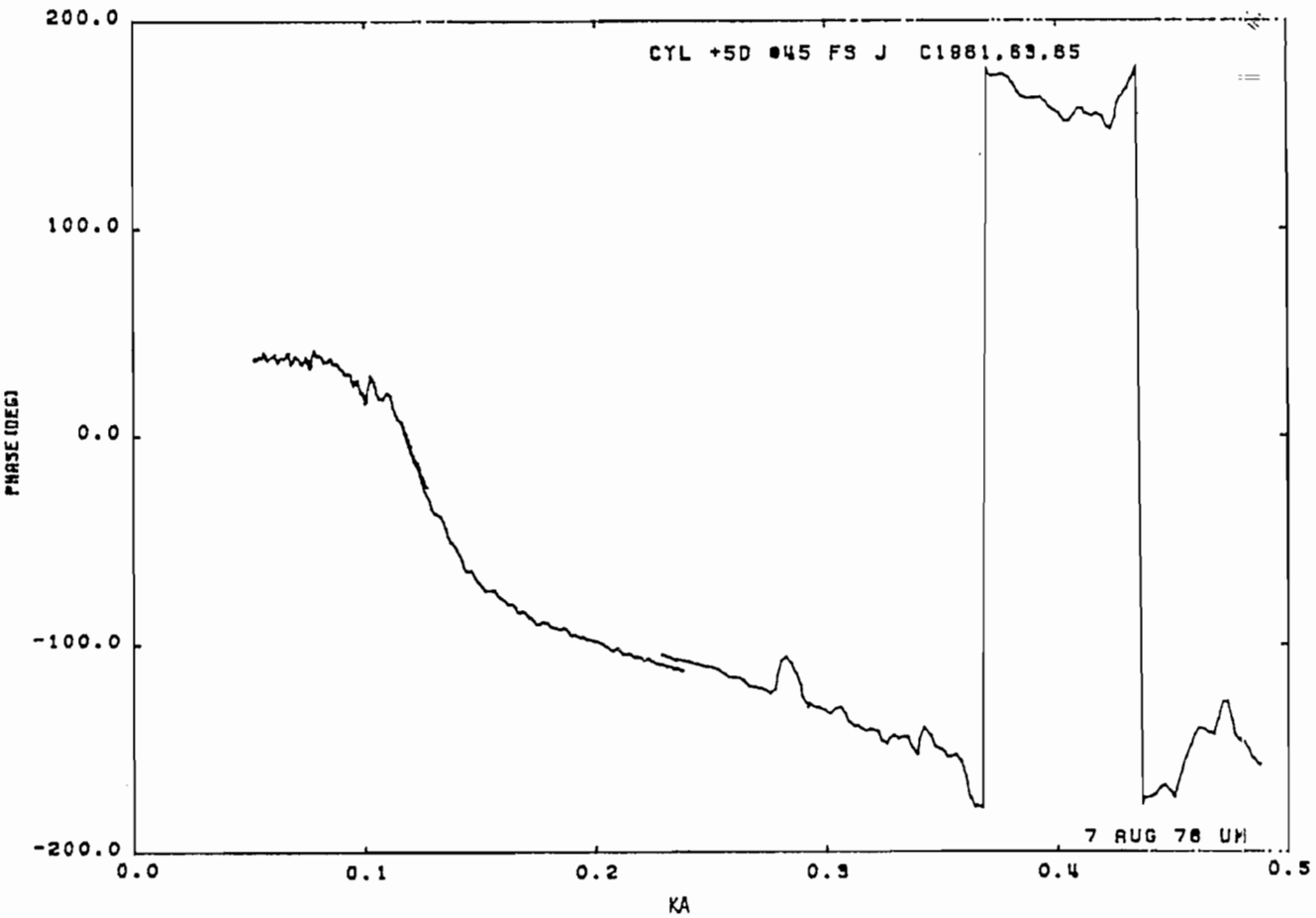

Figure 15b. Current on cylinder at STA:+5D; ø = 45°, free space (expanded scale).

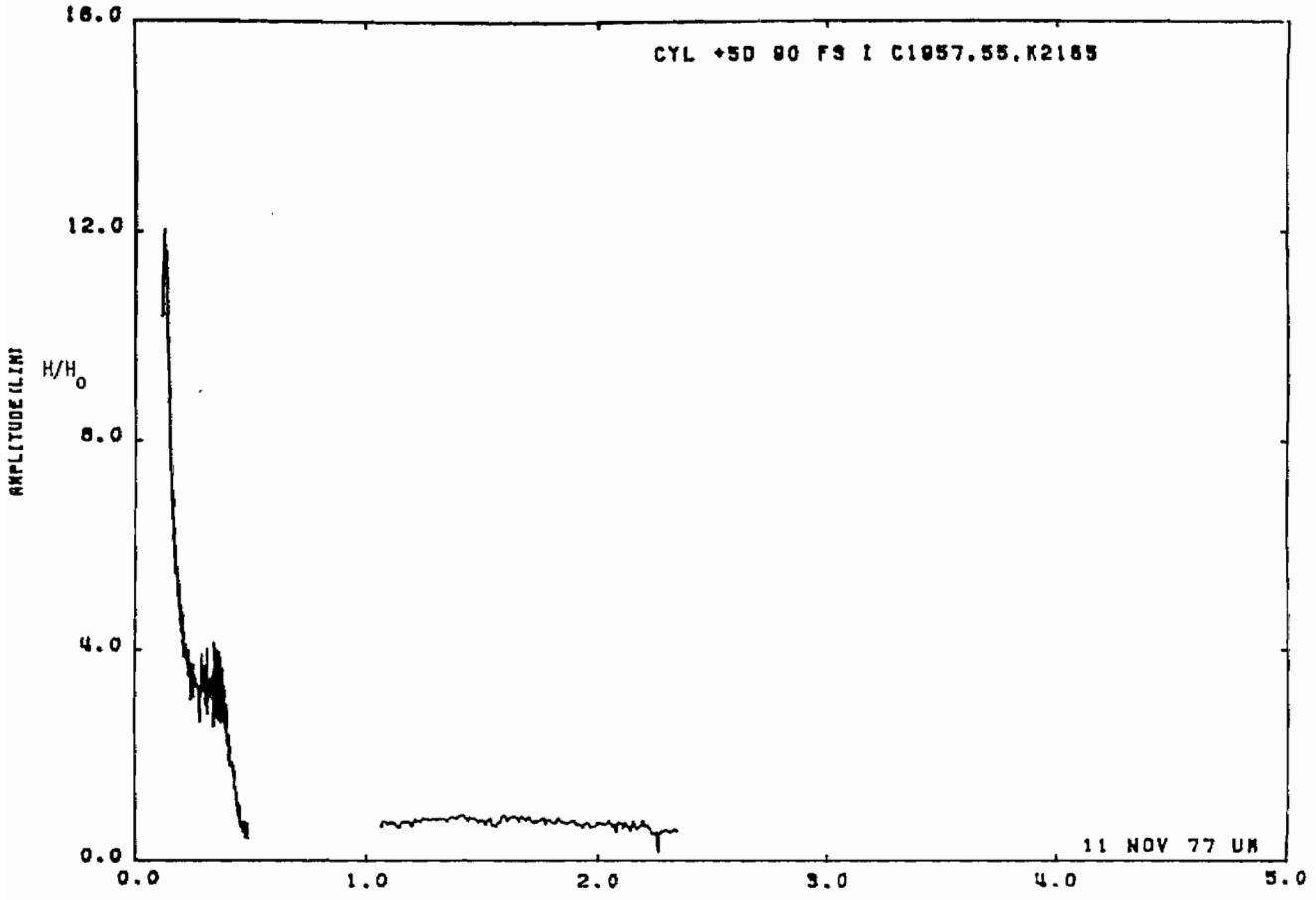

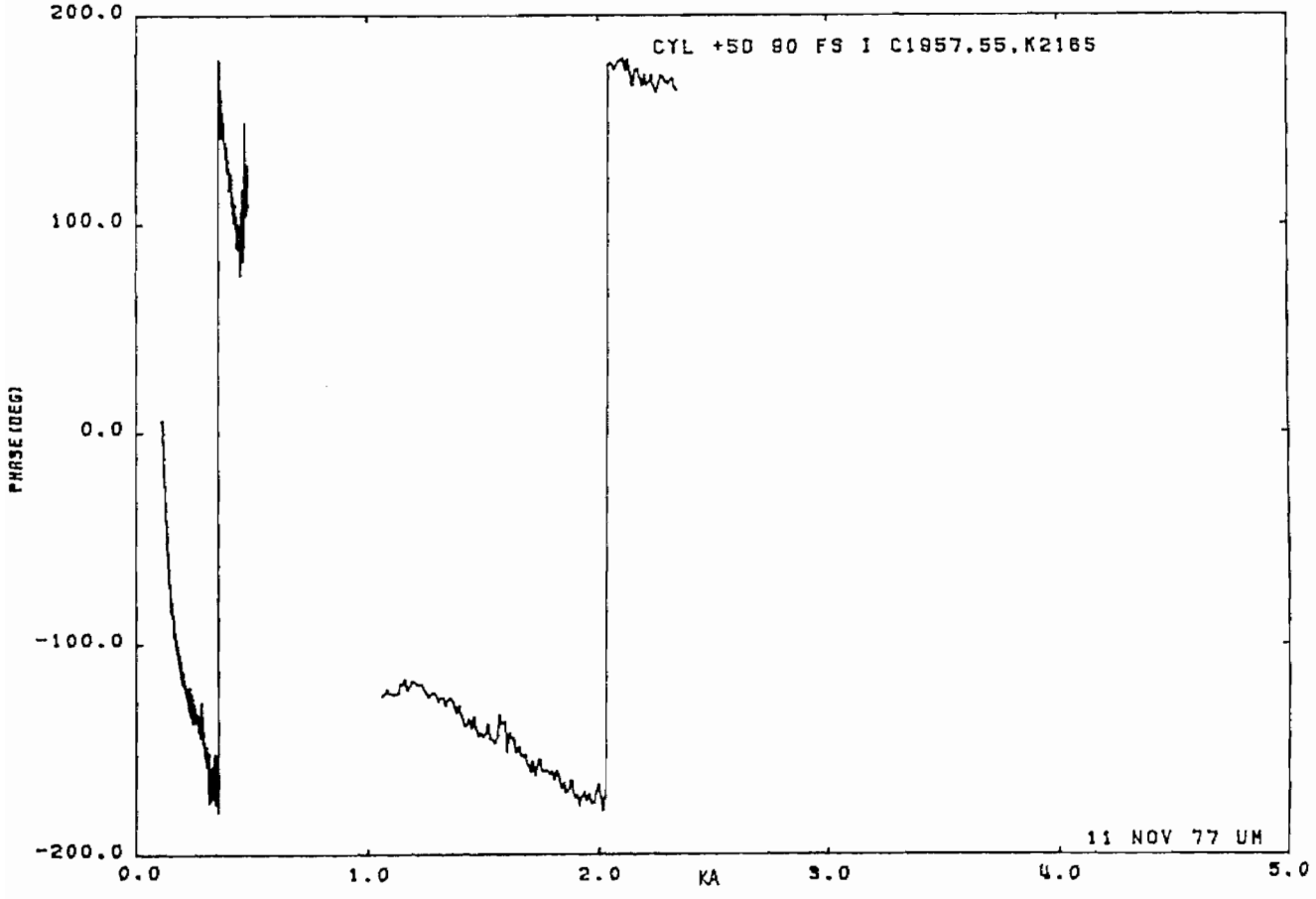

Figure 16a. Current on cylinder at STA:+5D; Ø = 90°, free space.

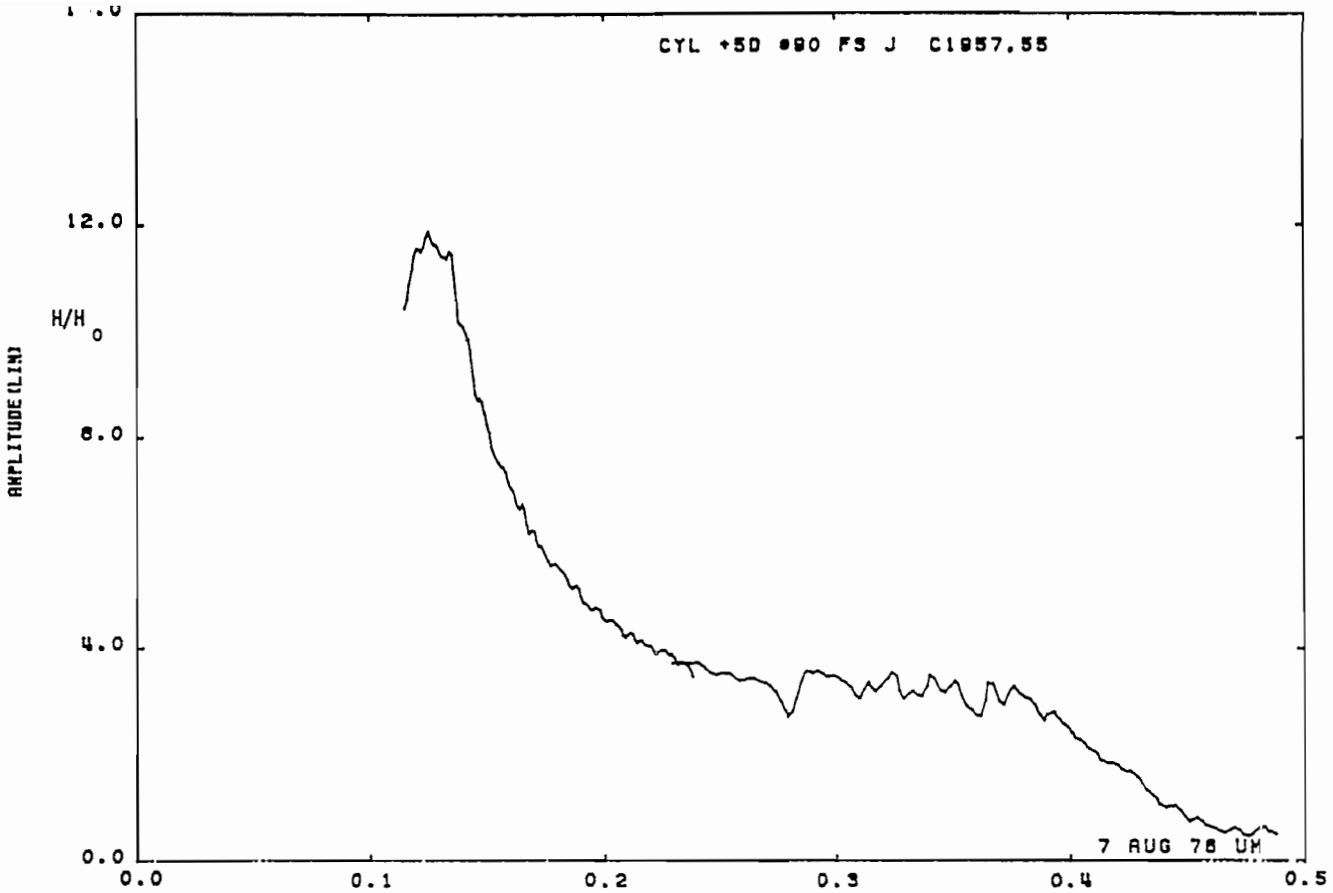

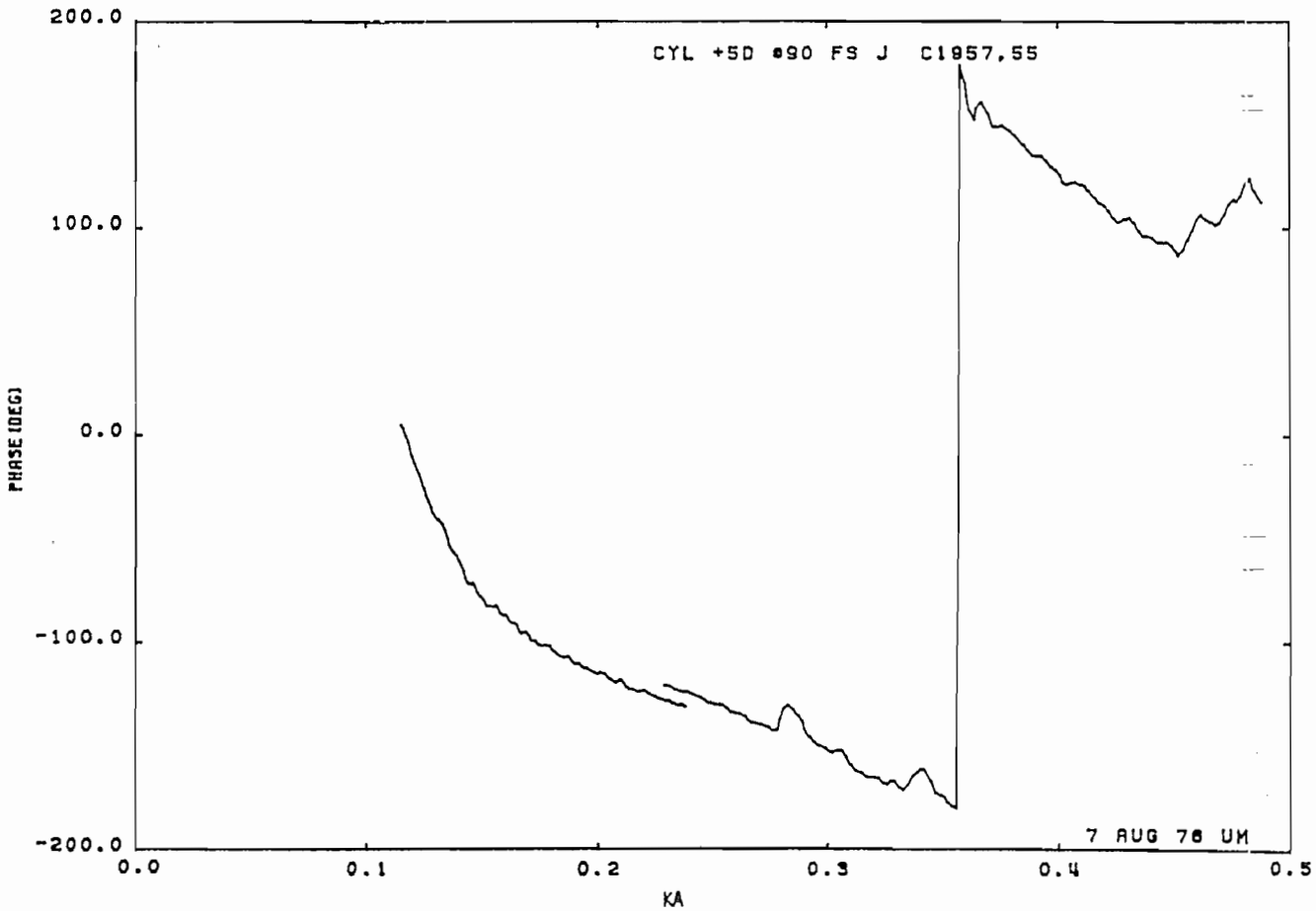

Figure 16b. Current on cylinder at STA:+5D; β = 90°, free space (expanded scale).

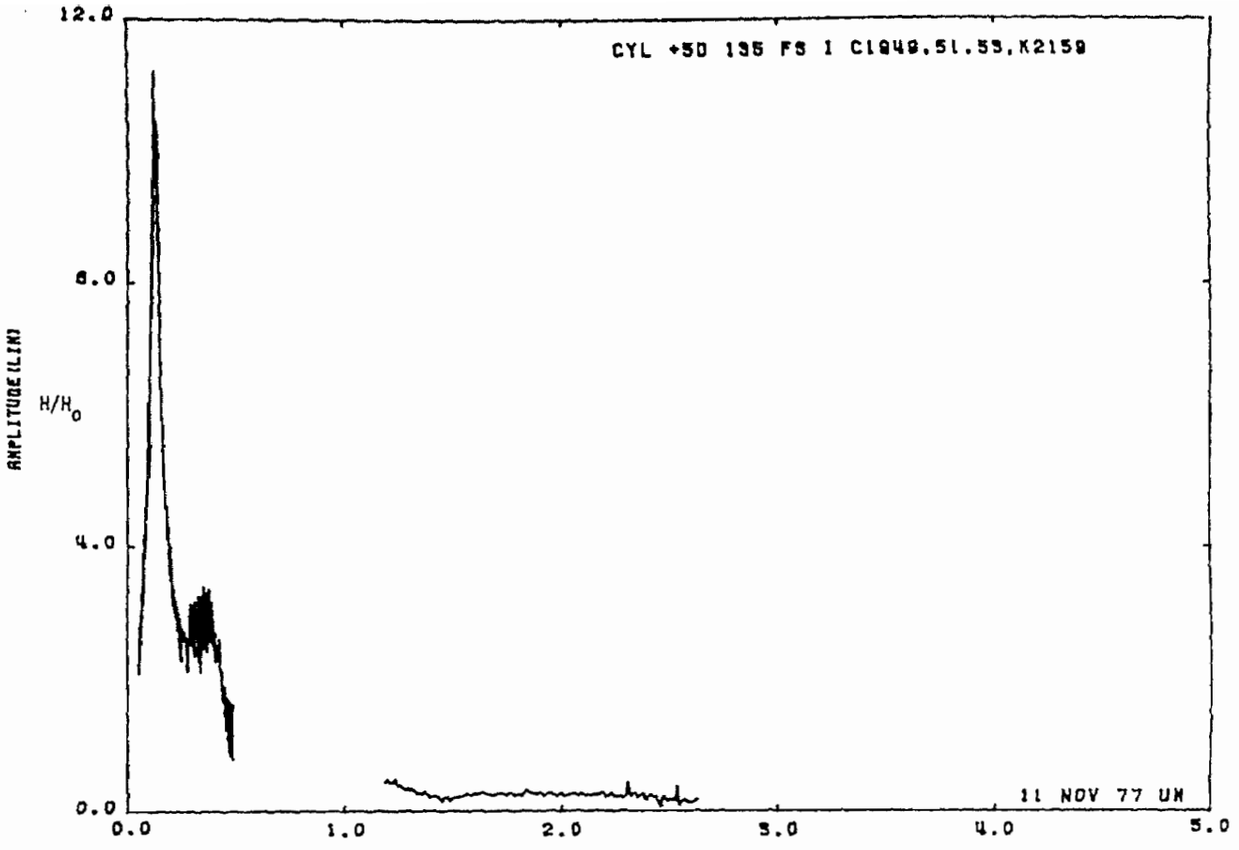

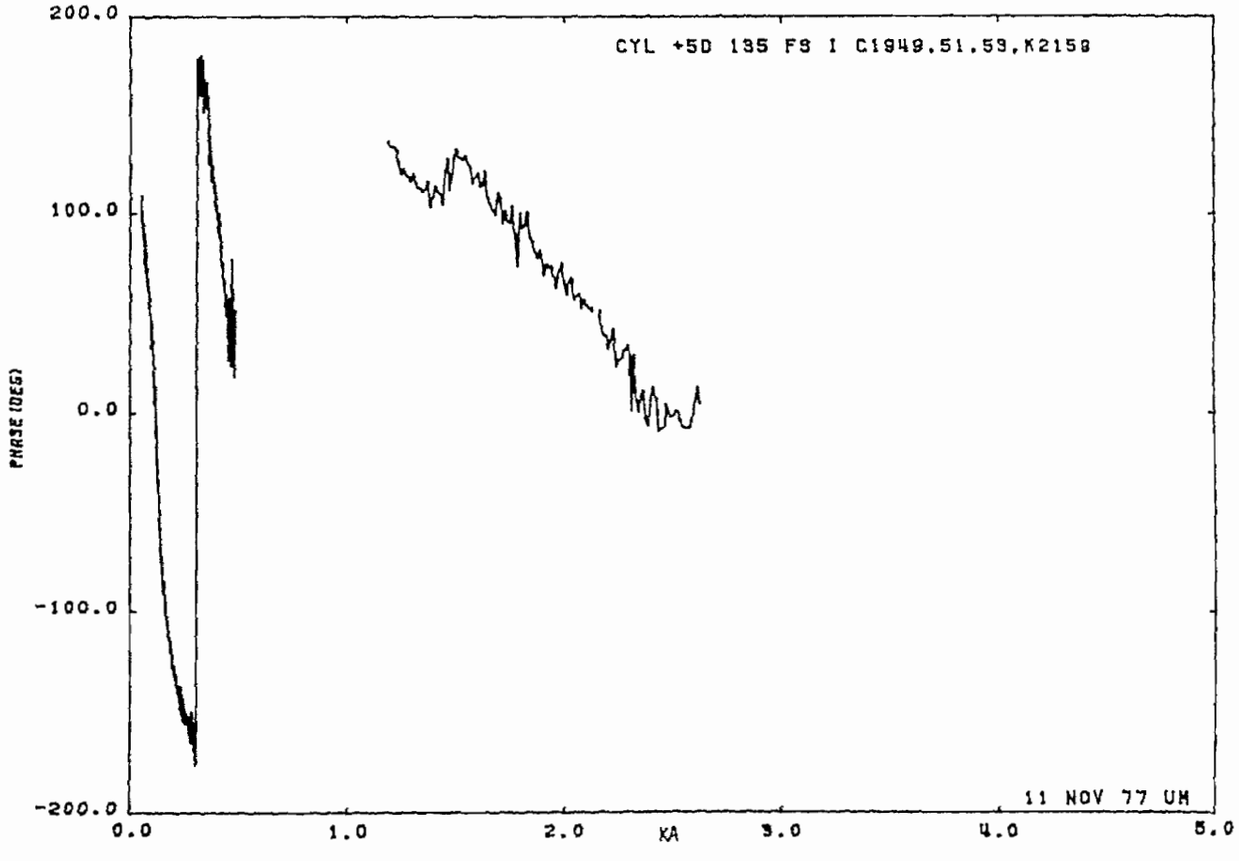

Figure 17a. Current on cylinder at STA:+5D; ϕ = 135°, free space.

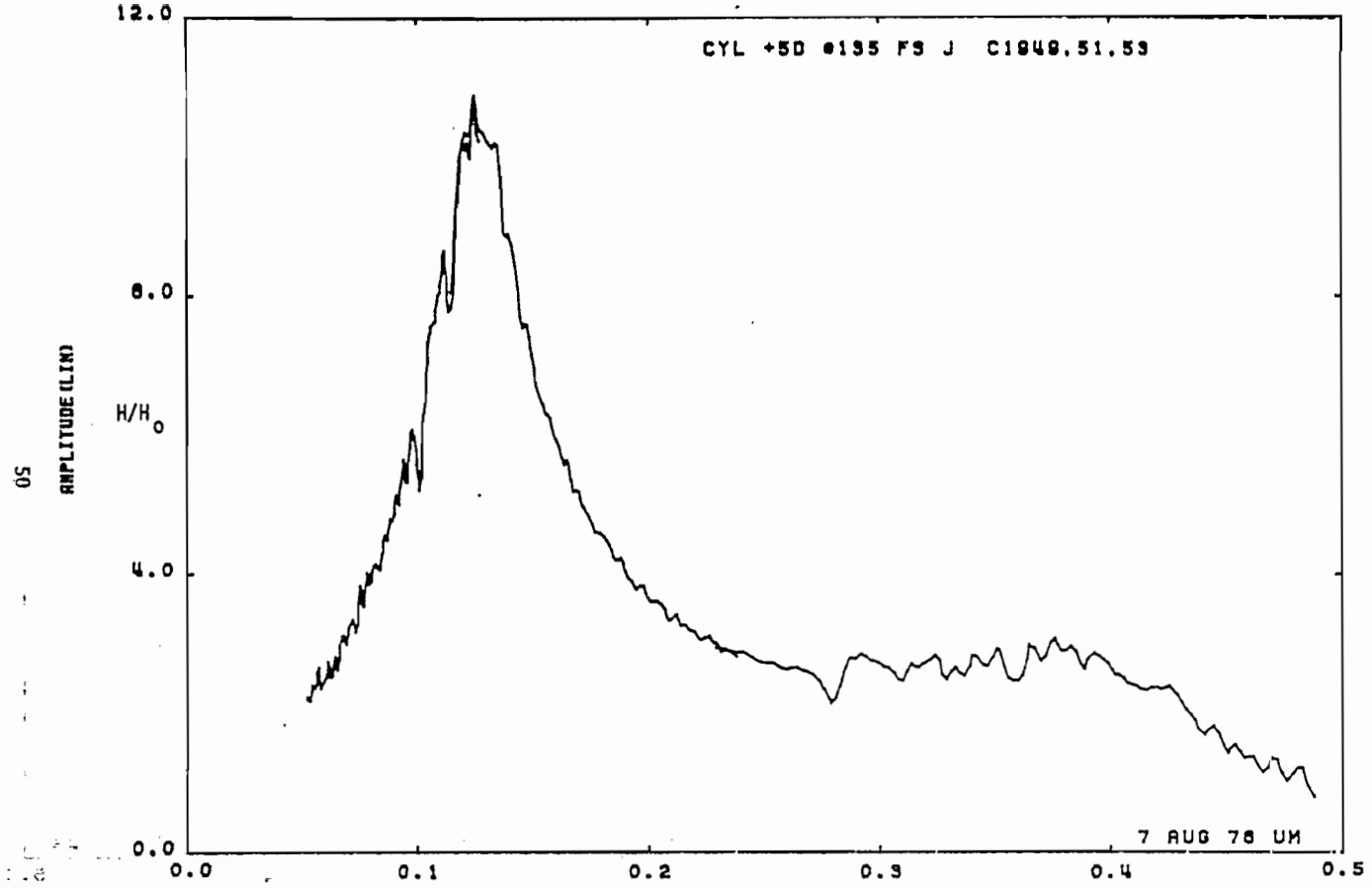

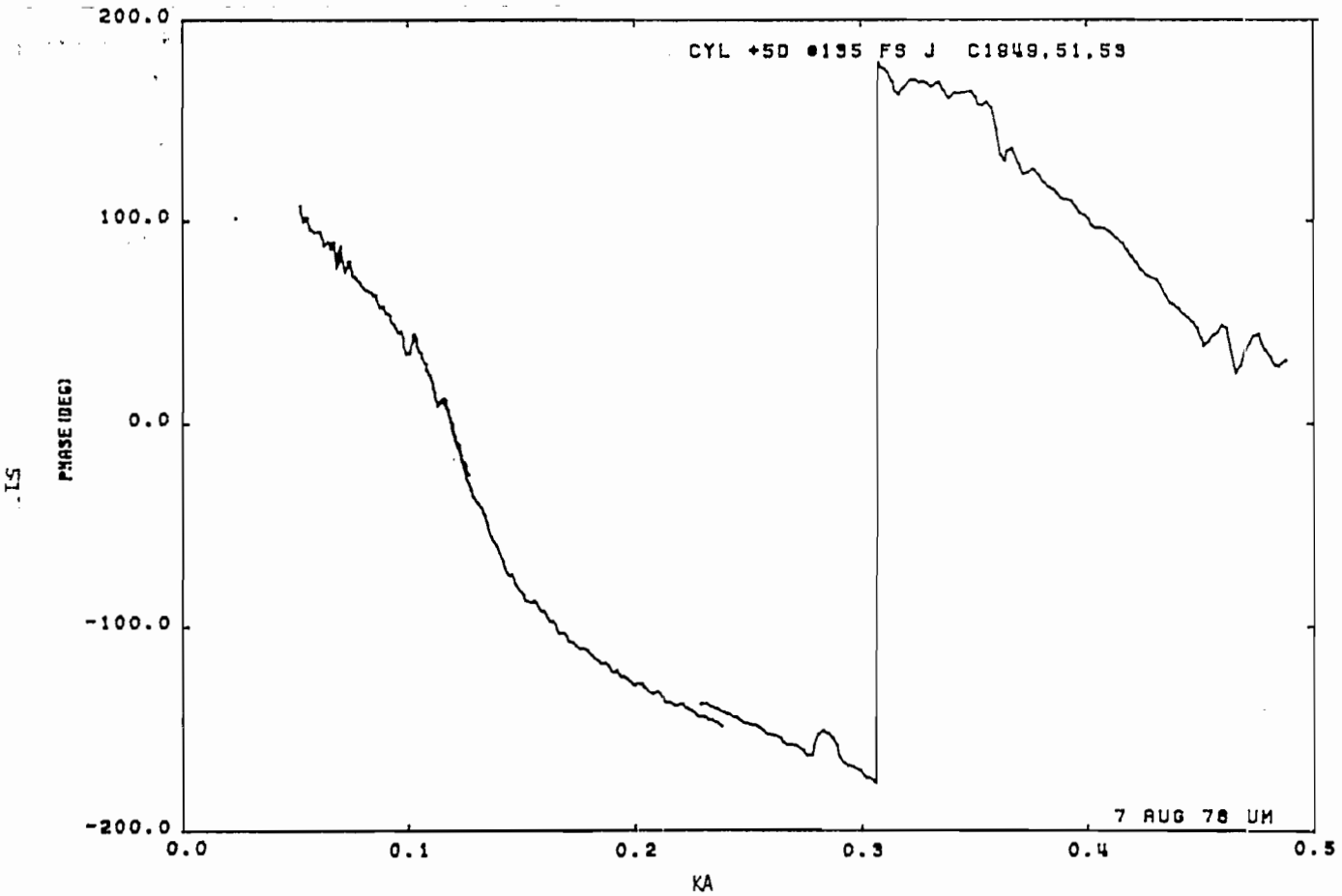

Figure 17b. Current on cylinder at STA:+5D; ϕ = 135°, free space (expanded scale).

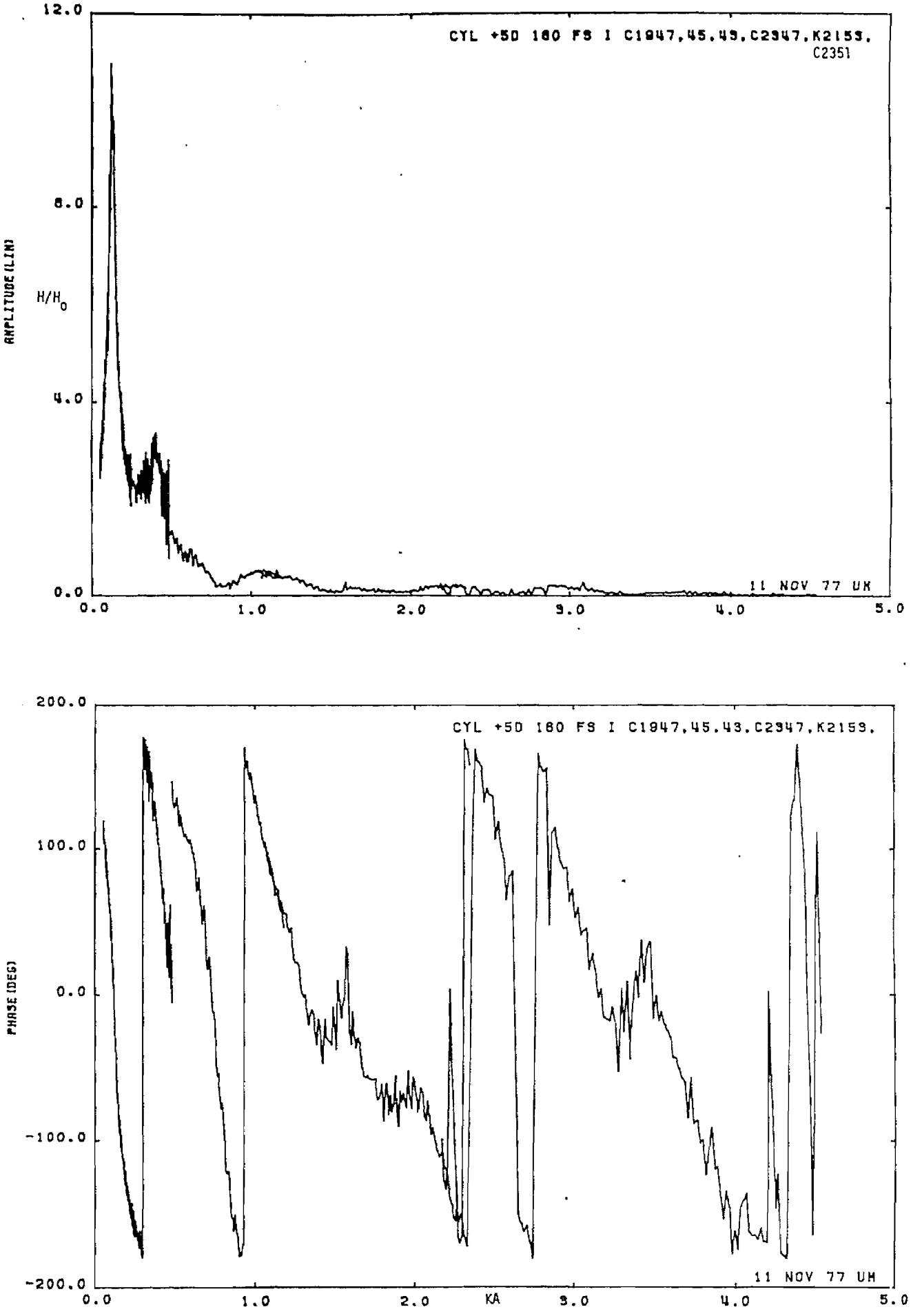

Figure 18a. Current on cylinder at STA:+5D; ϕ = 180°, free space.

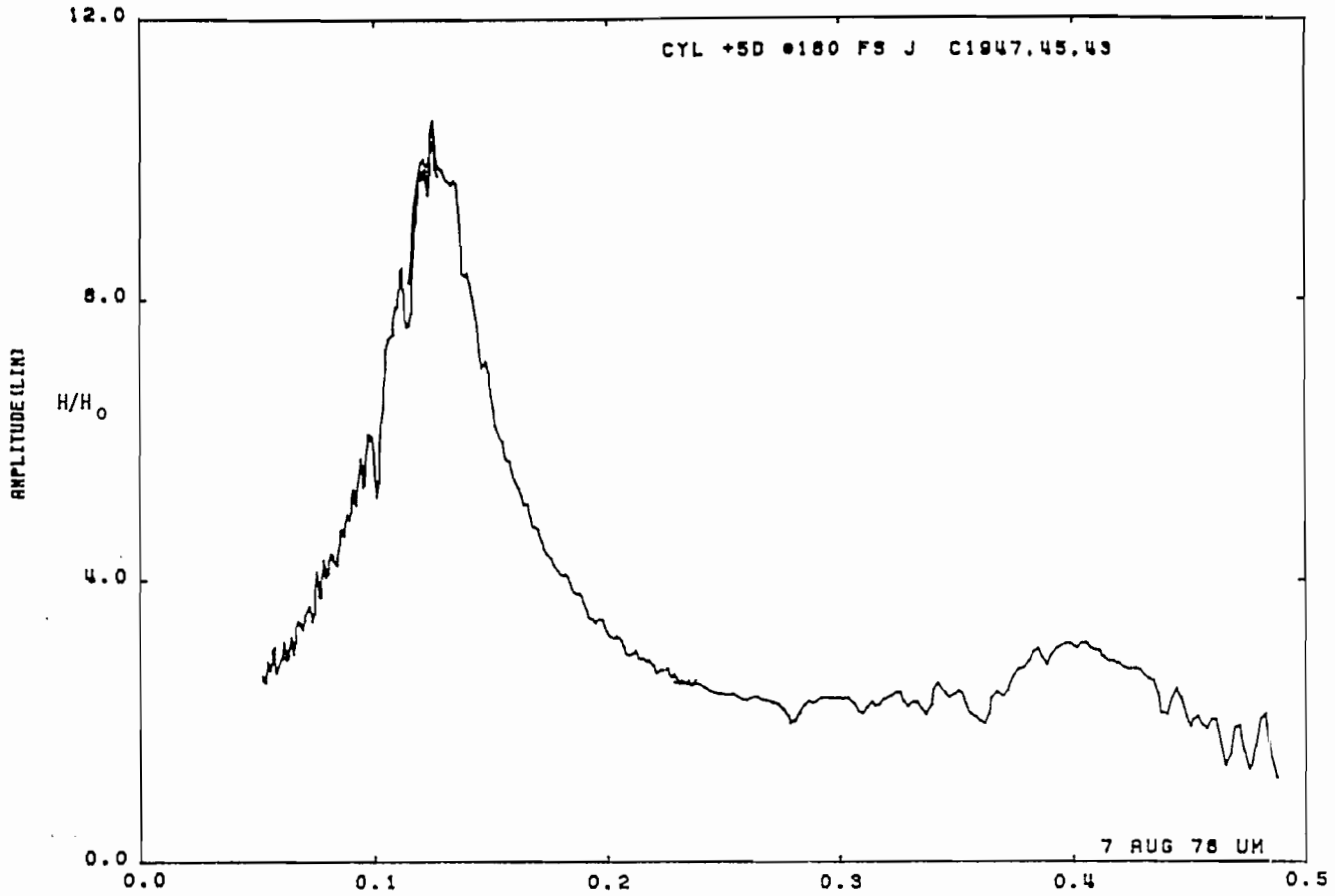

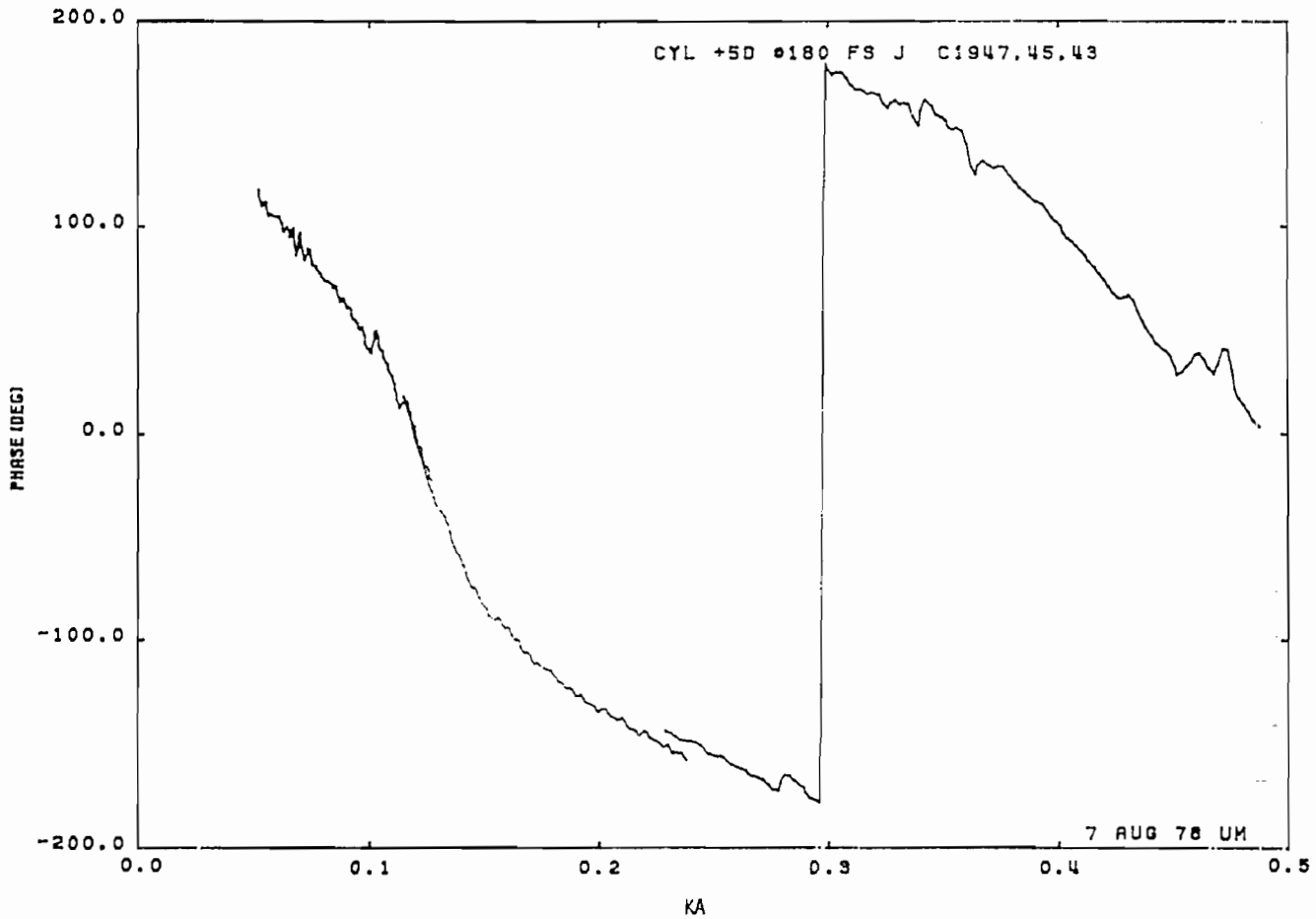

Figure 18b. Current on cylinder at STA:+5D; ϕ = 180°, free space (expanded scale).

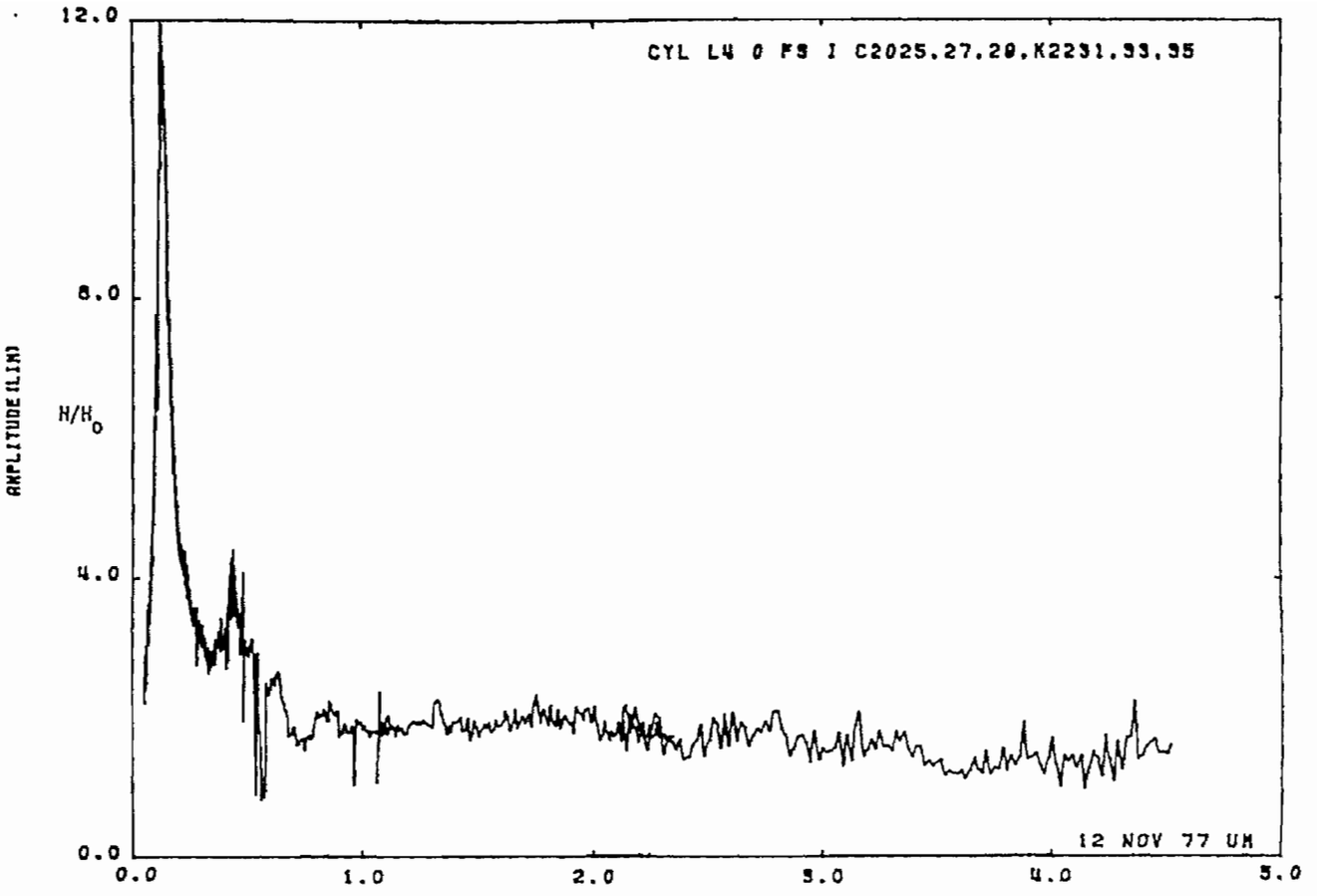

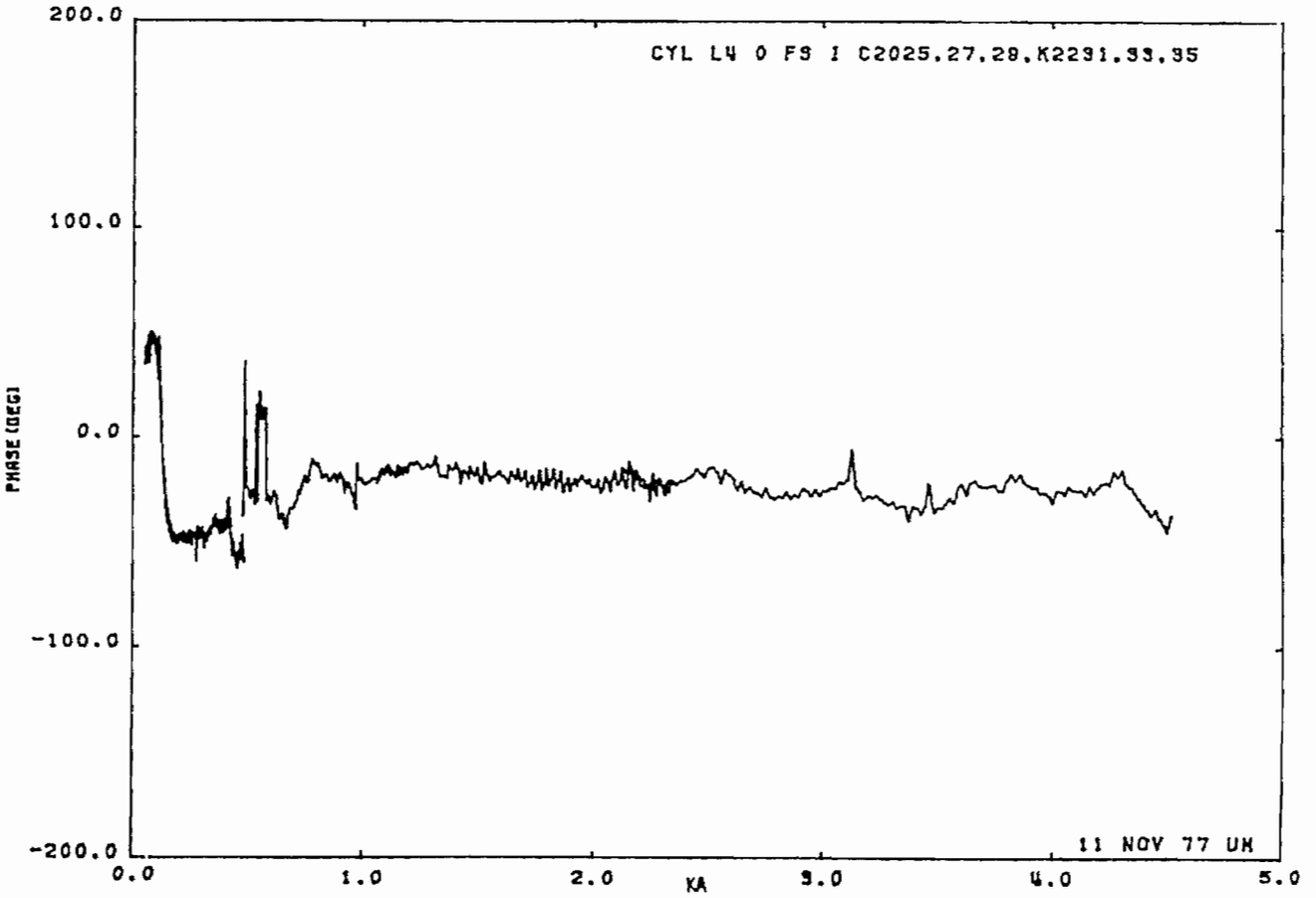

Figure 19a. Current on cylinder at STA:L/4; Ø = 0°, free space.

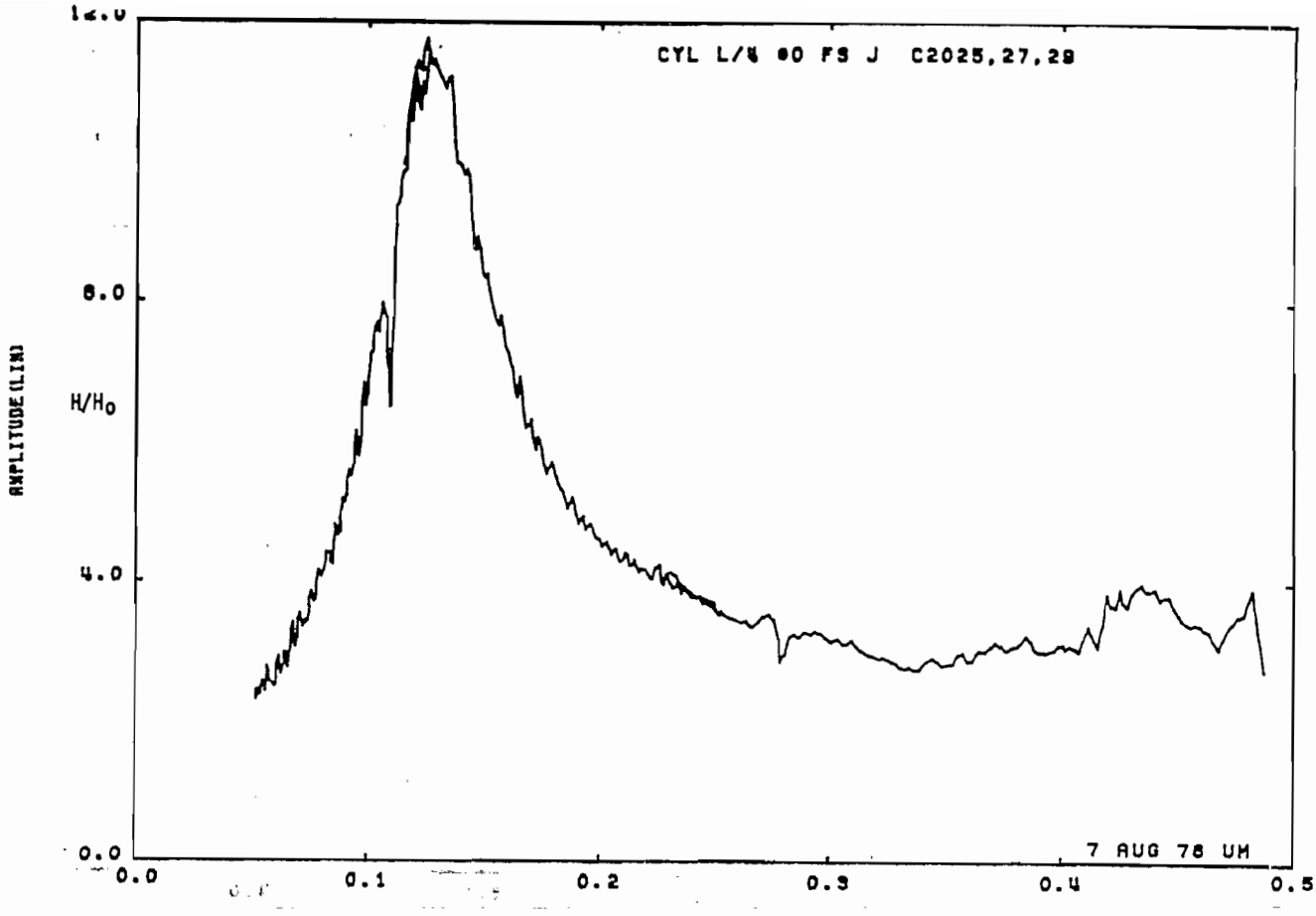

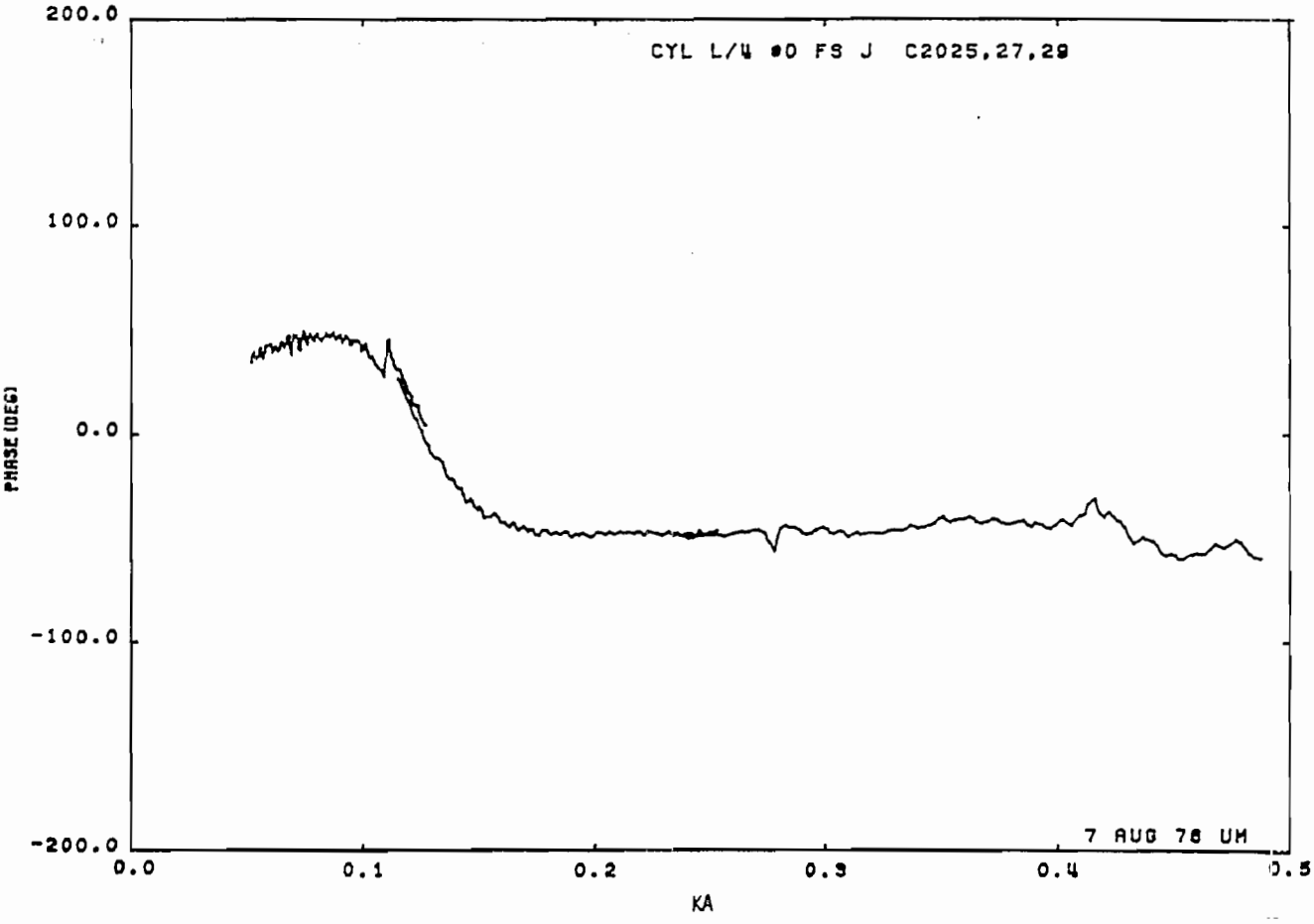

Figure 19b. Current on cylinder at STA:L/4; ø = 0°, free space (expanded scale).

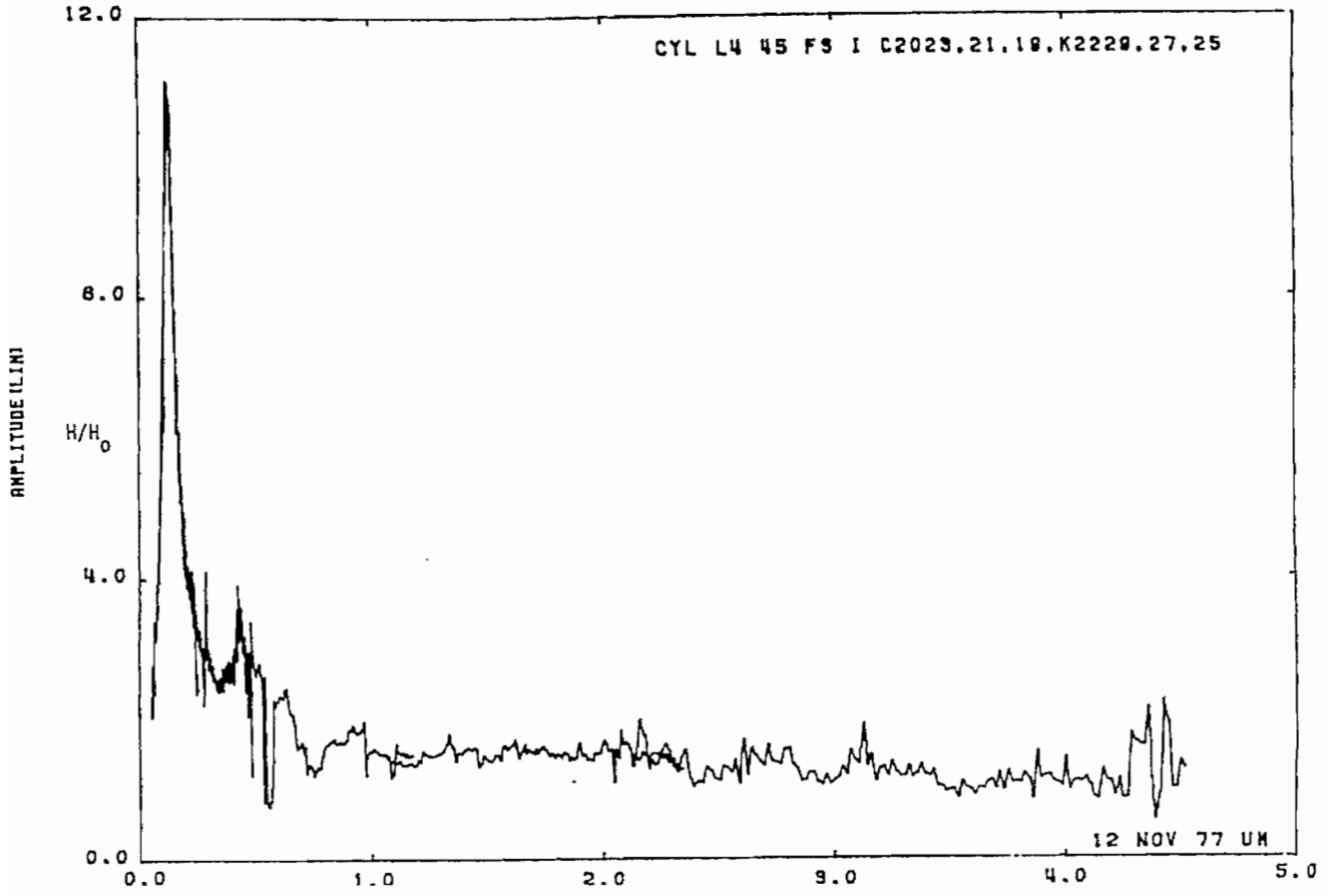

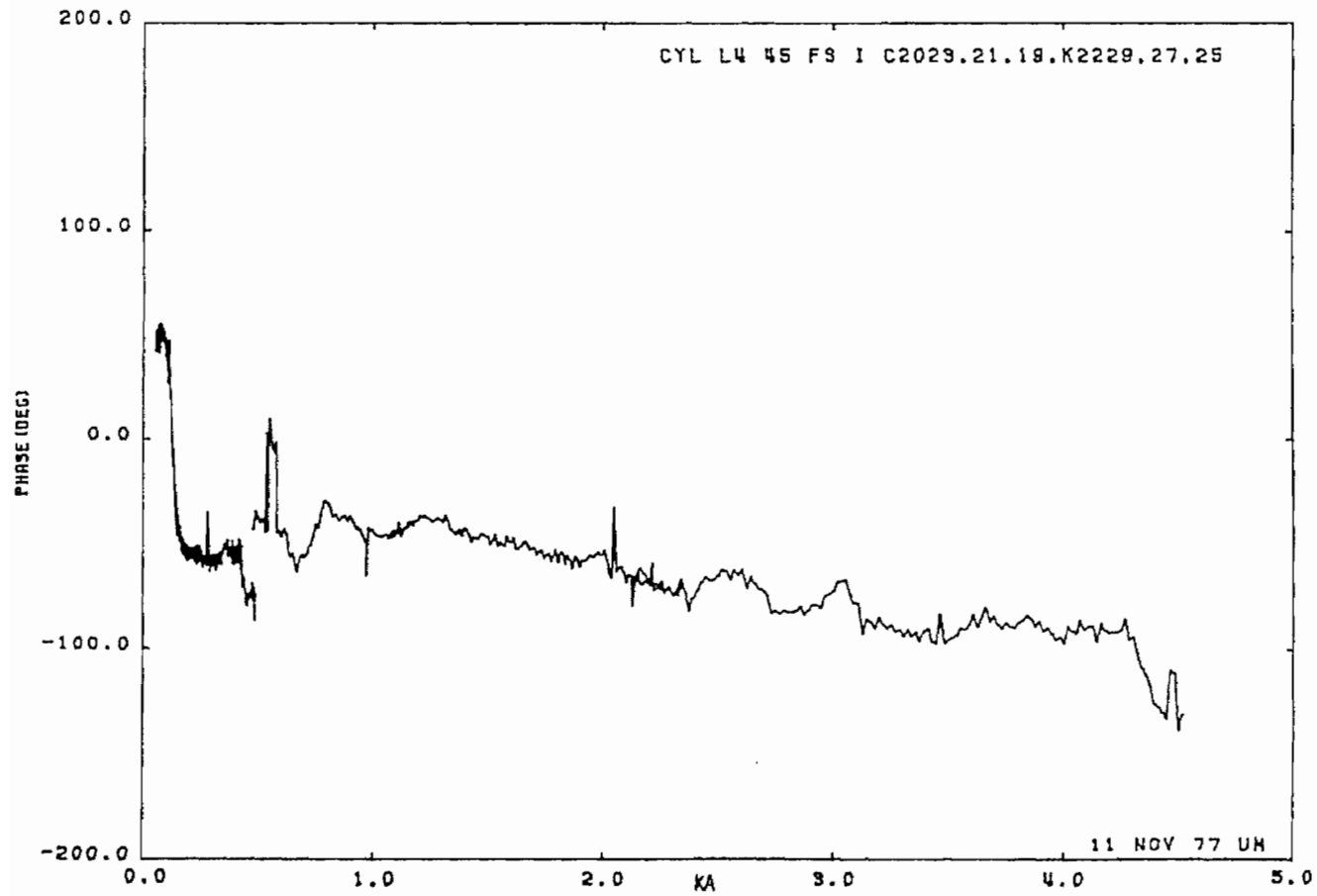

Figure 20a. Current on cylinder at STA:L/4; Ø = 45°, free space.

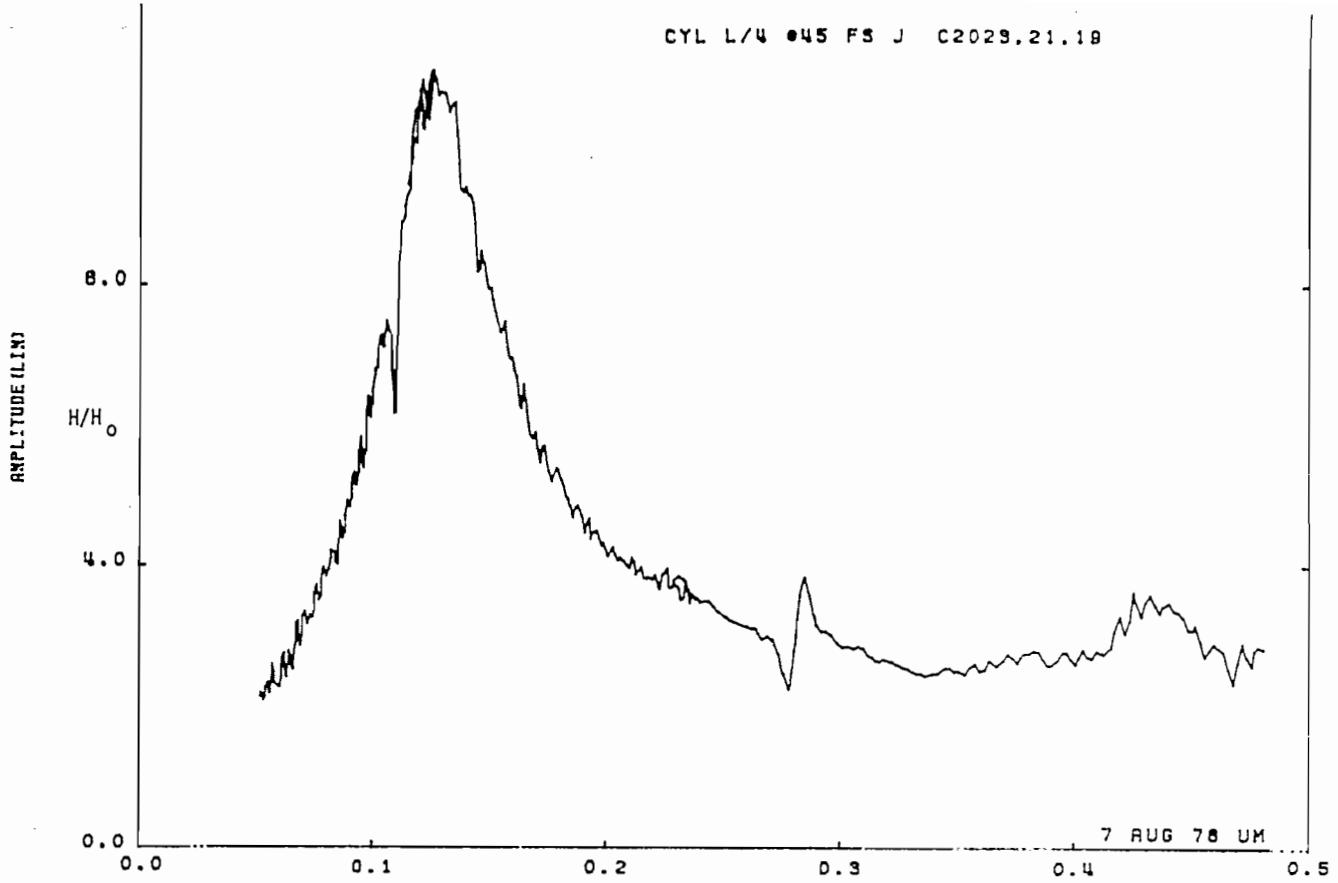

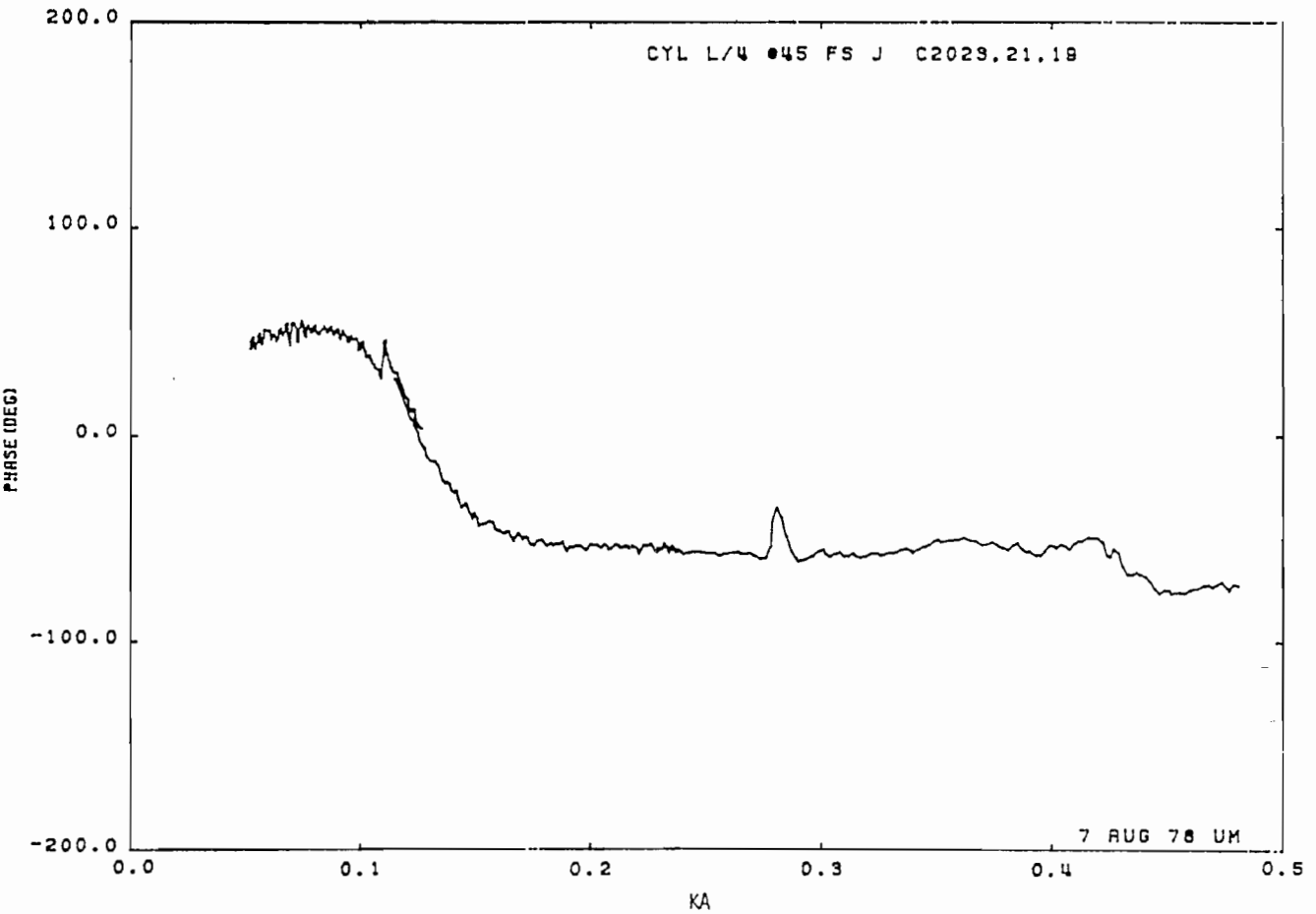

Figure 20b. Current on cylinder at STA:L/4; ø = 45°, free space (expanded scale).

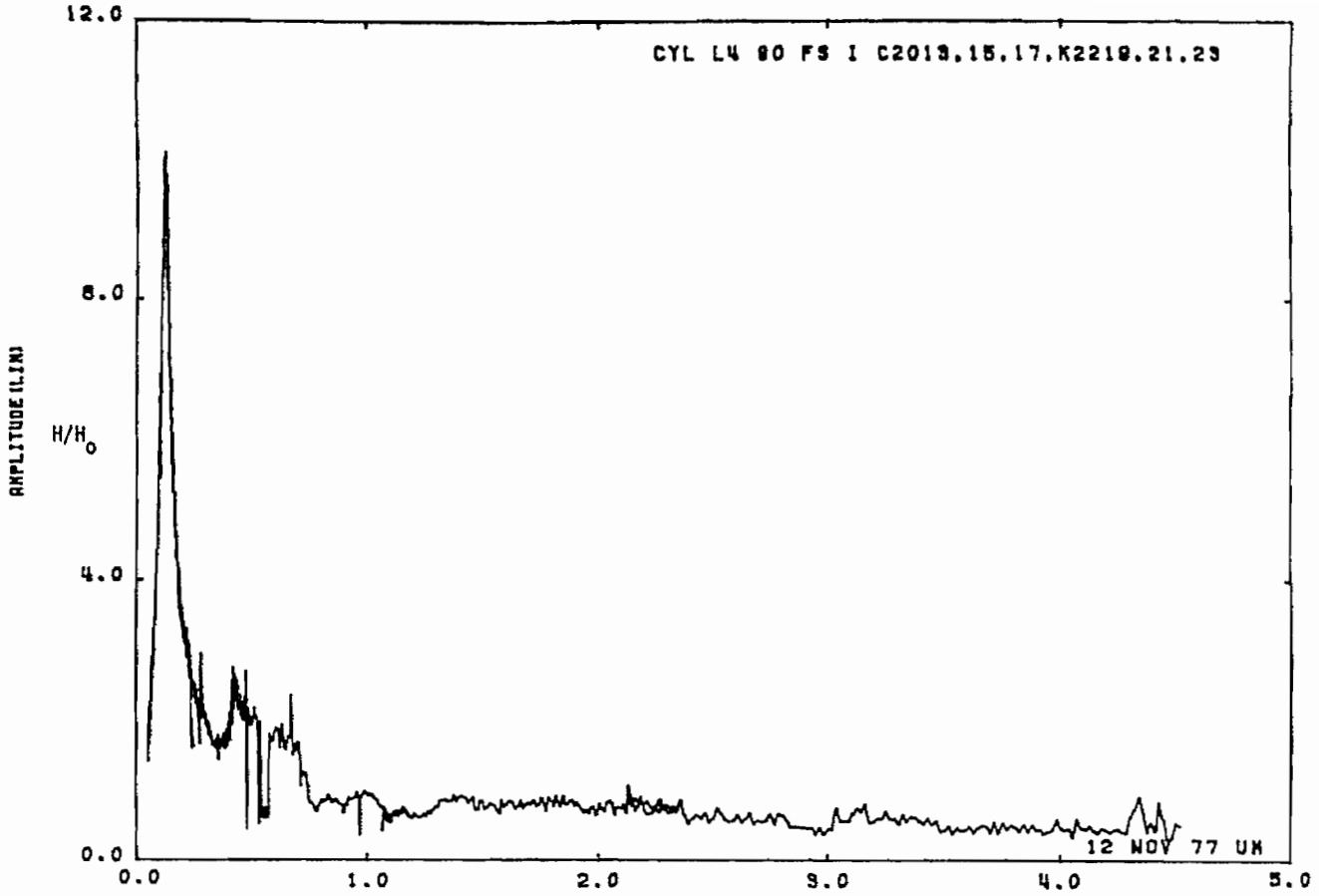

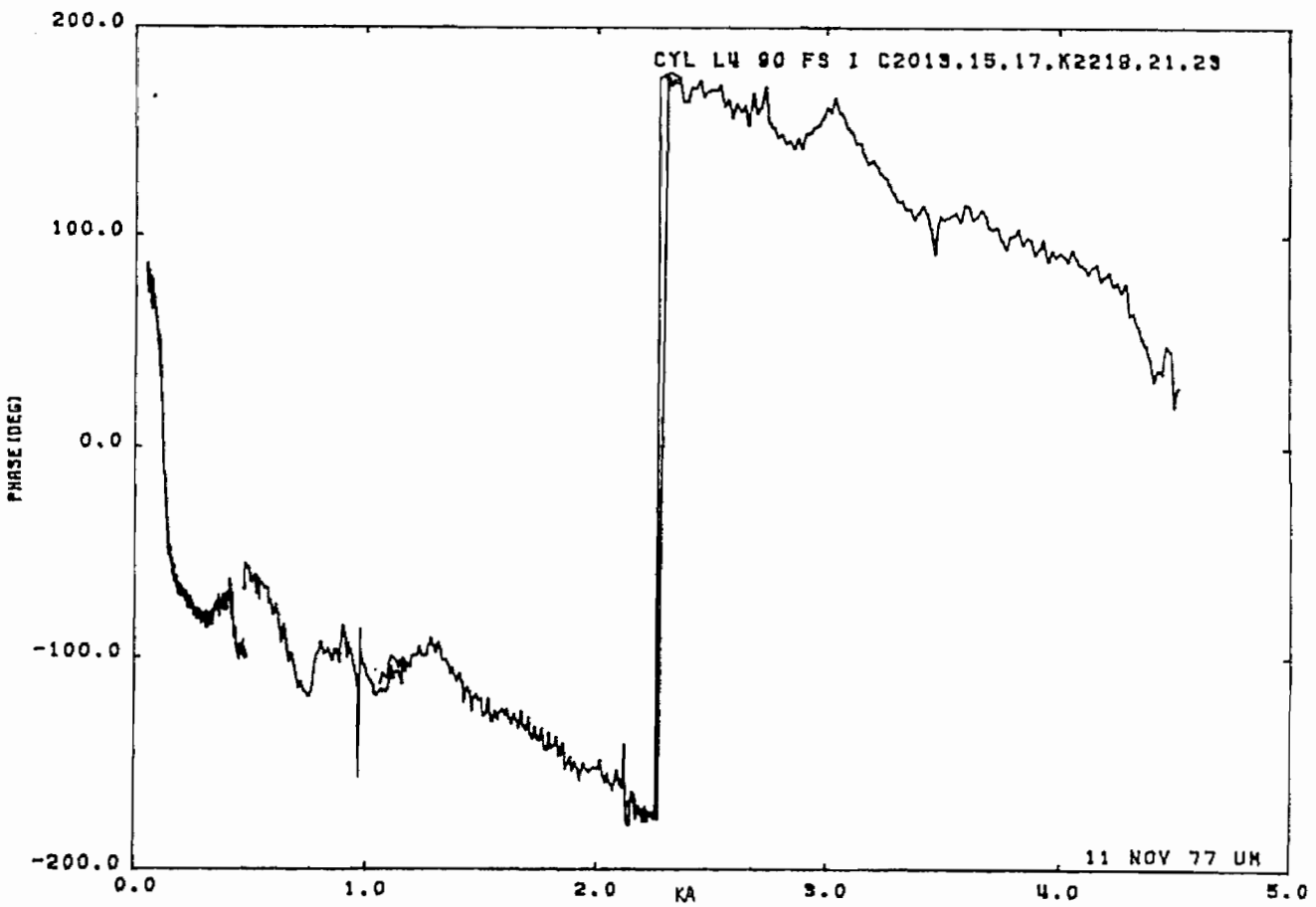

Figure 21a. Current on cylinder at STA:L/4; Ø = 90°, free space.

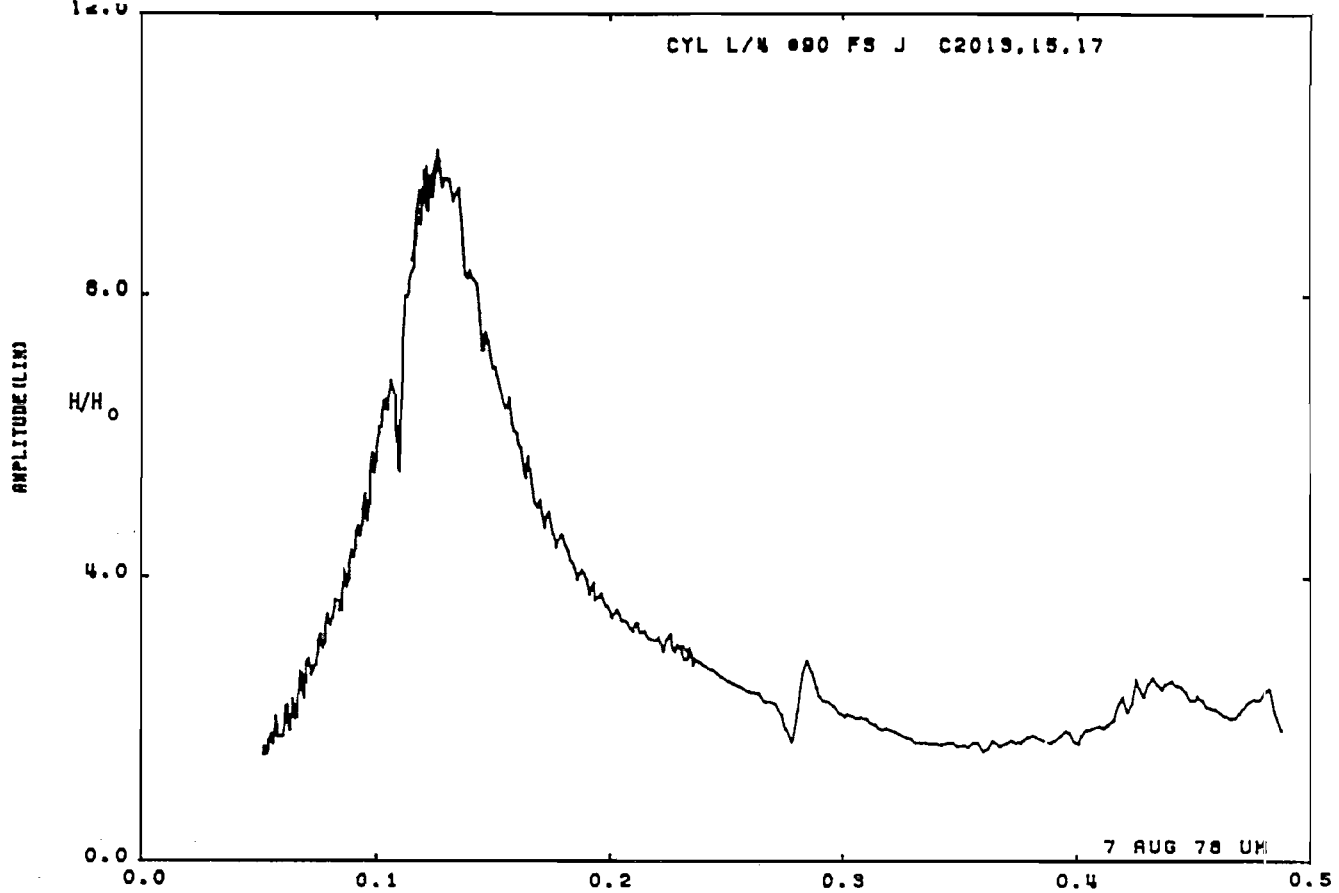

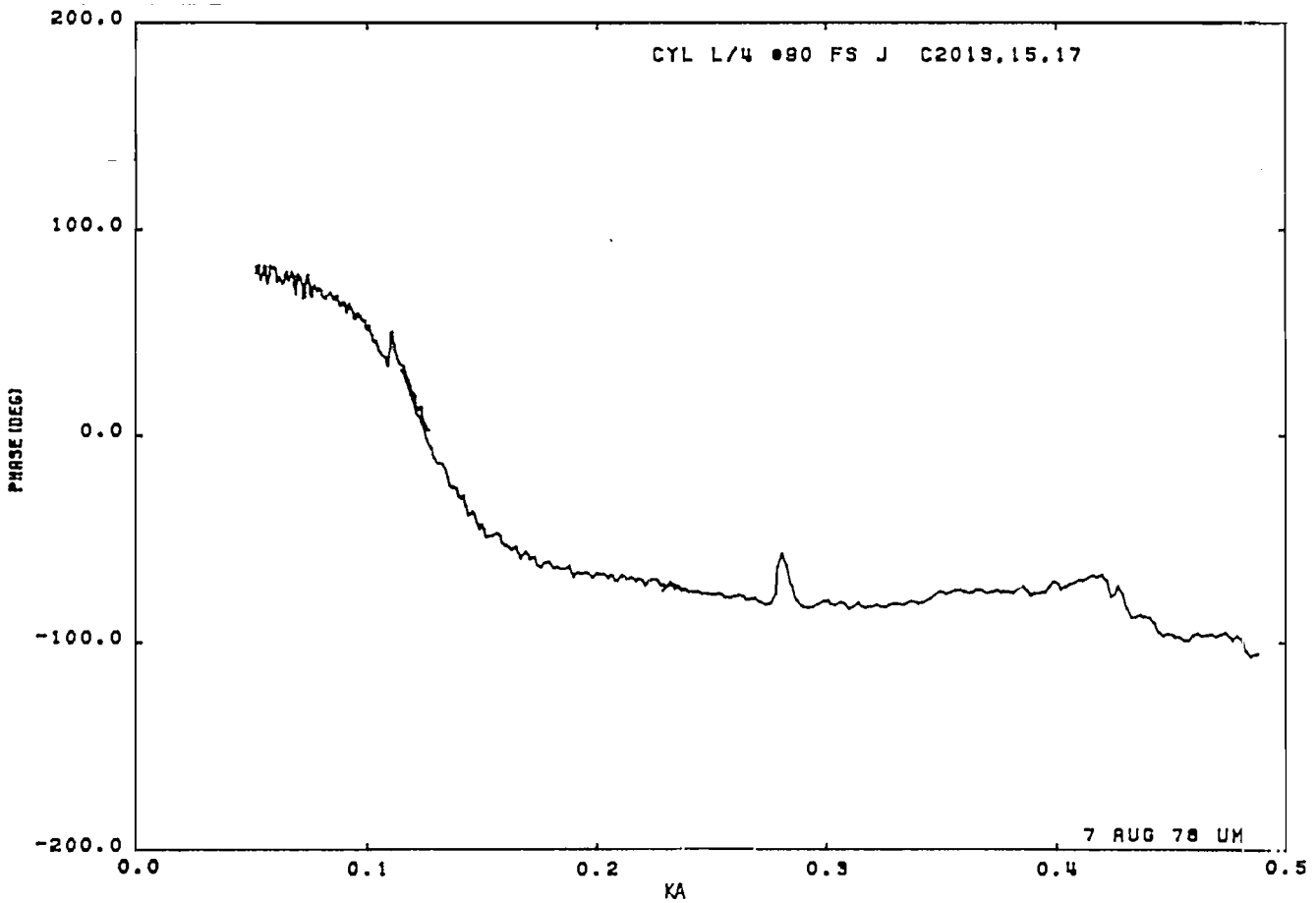

Figure 21b. Current on cylinder at STA:L/4; ϕ = 90°, free space (expanded scale).

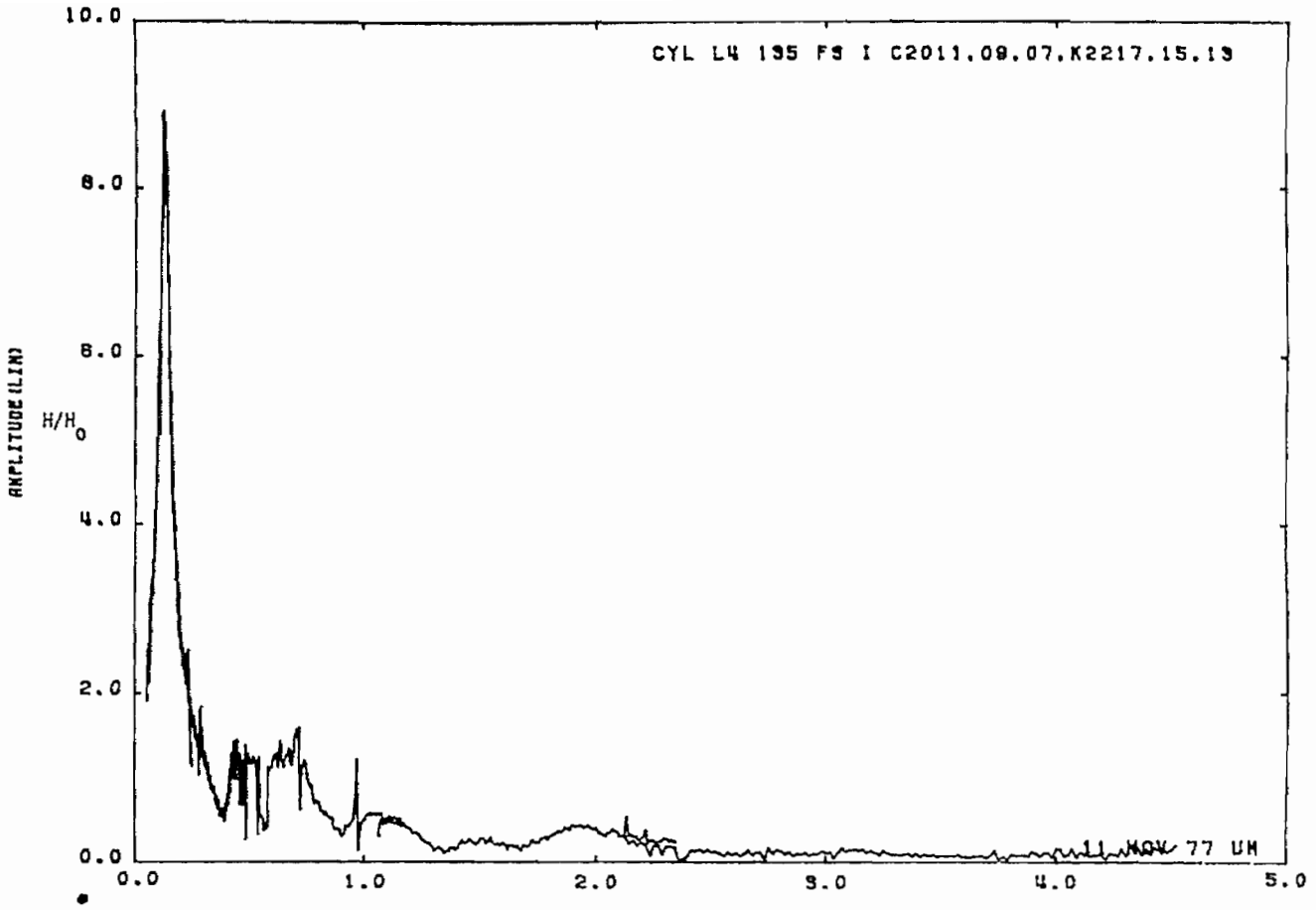

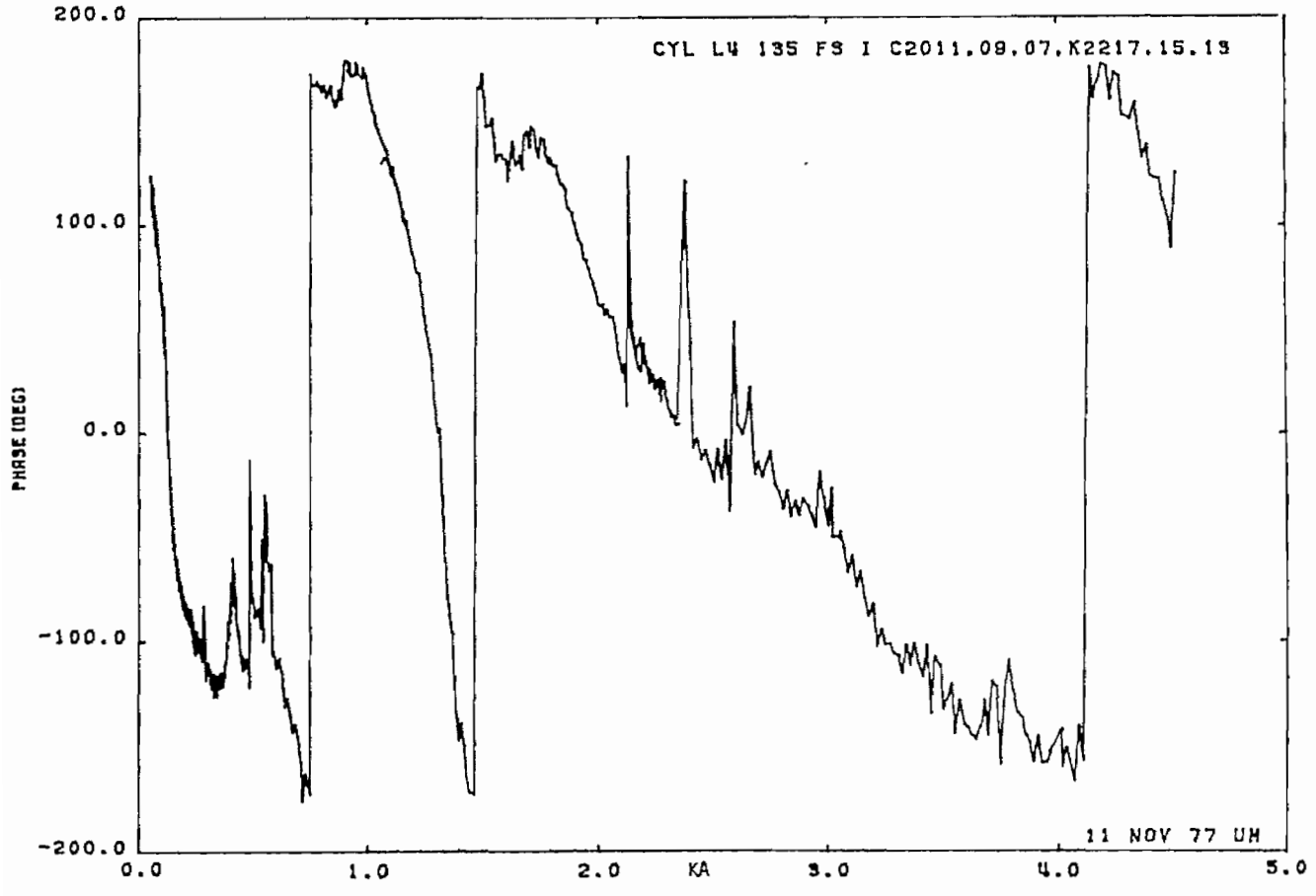

Figure 22a. Current on cylinder at STA:L/4; ϕ = 135°, free space.

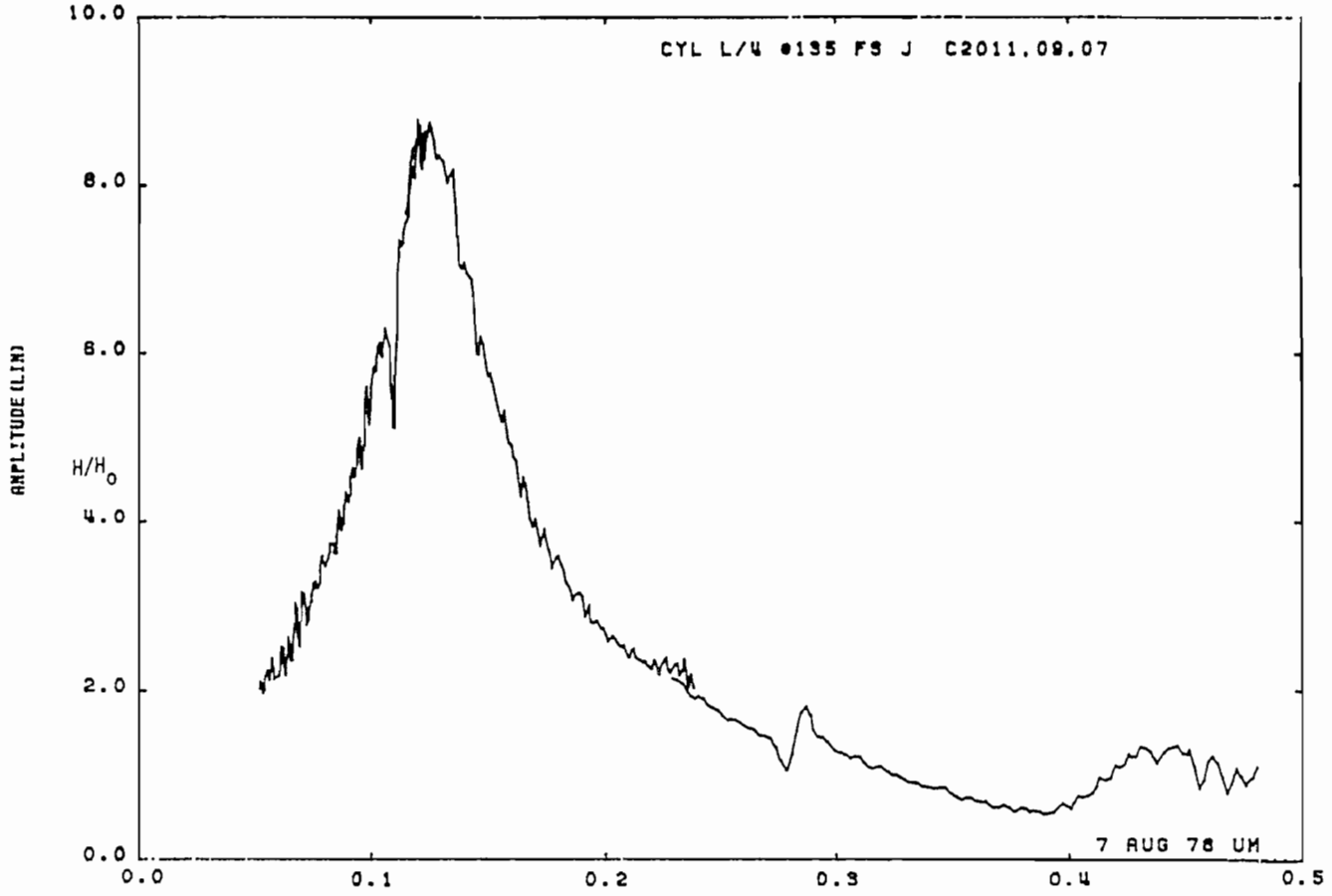

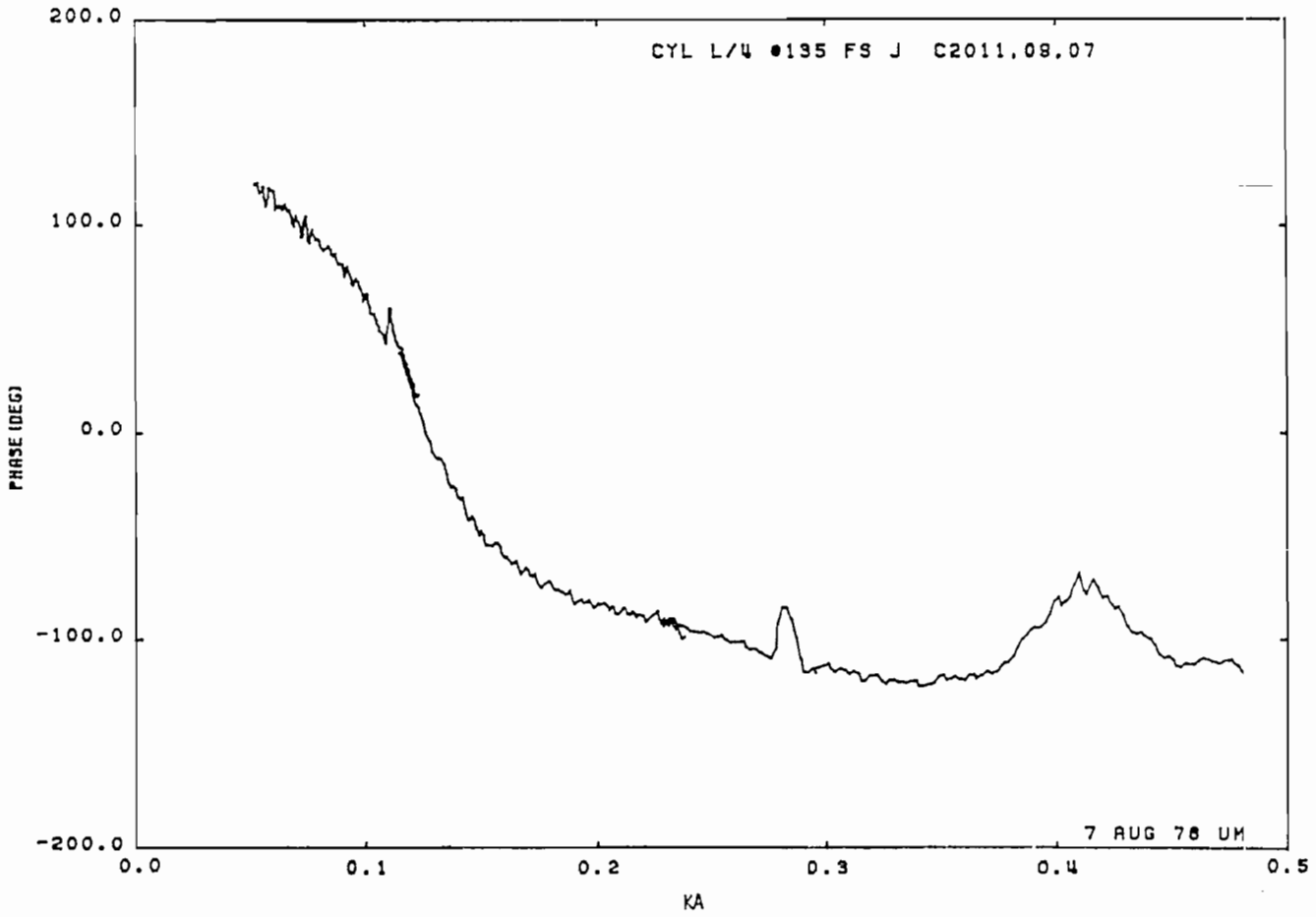

Figure 22b. Current on cylinder at STA:L/4; β = 135°, free space (expanded scale).

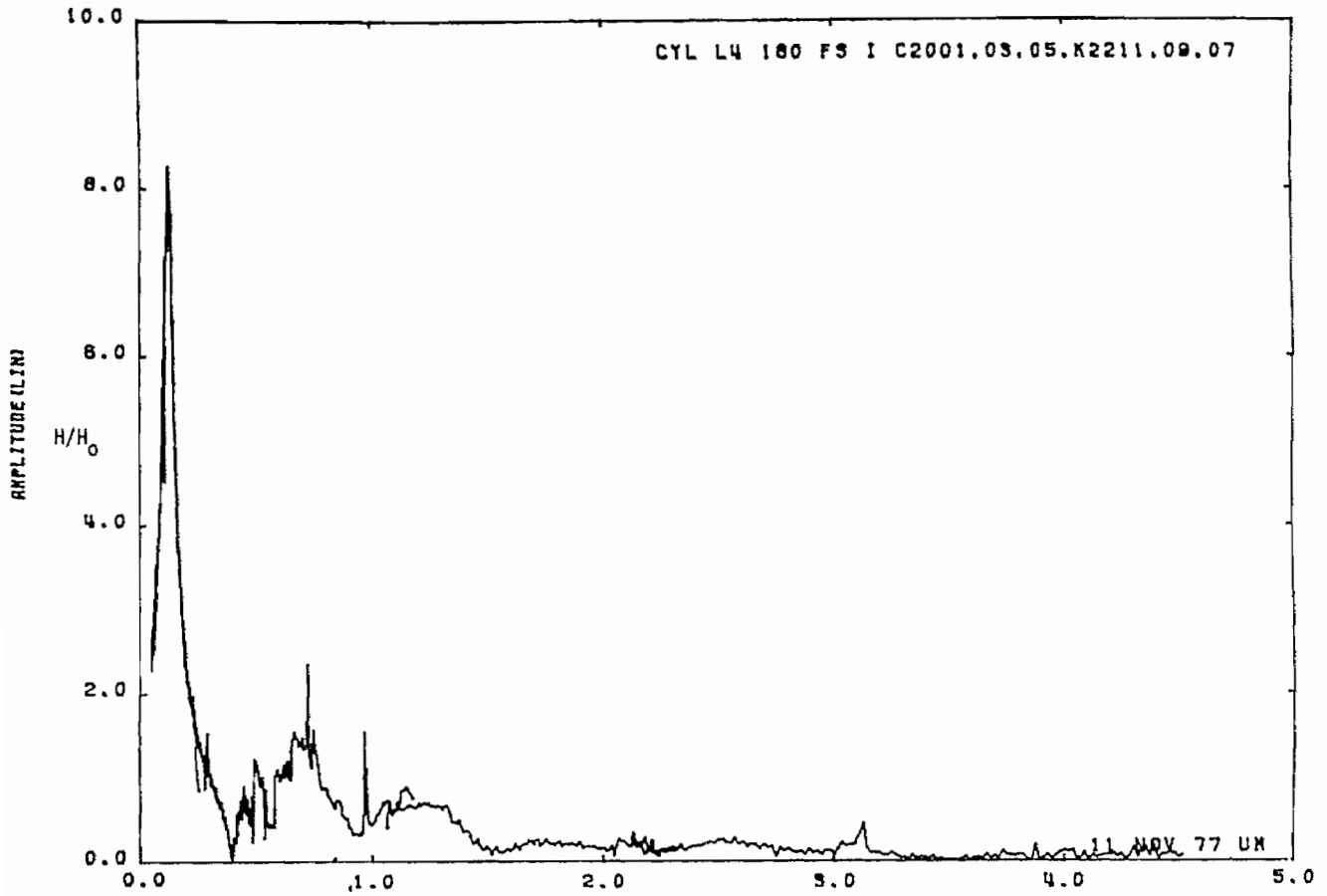

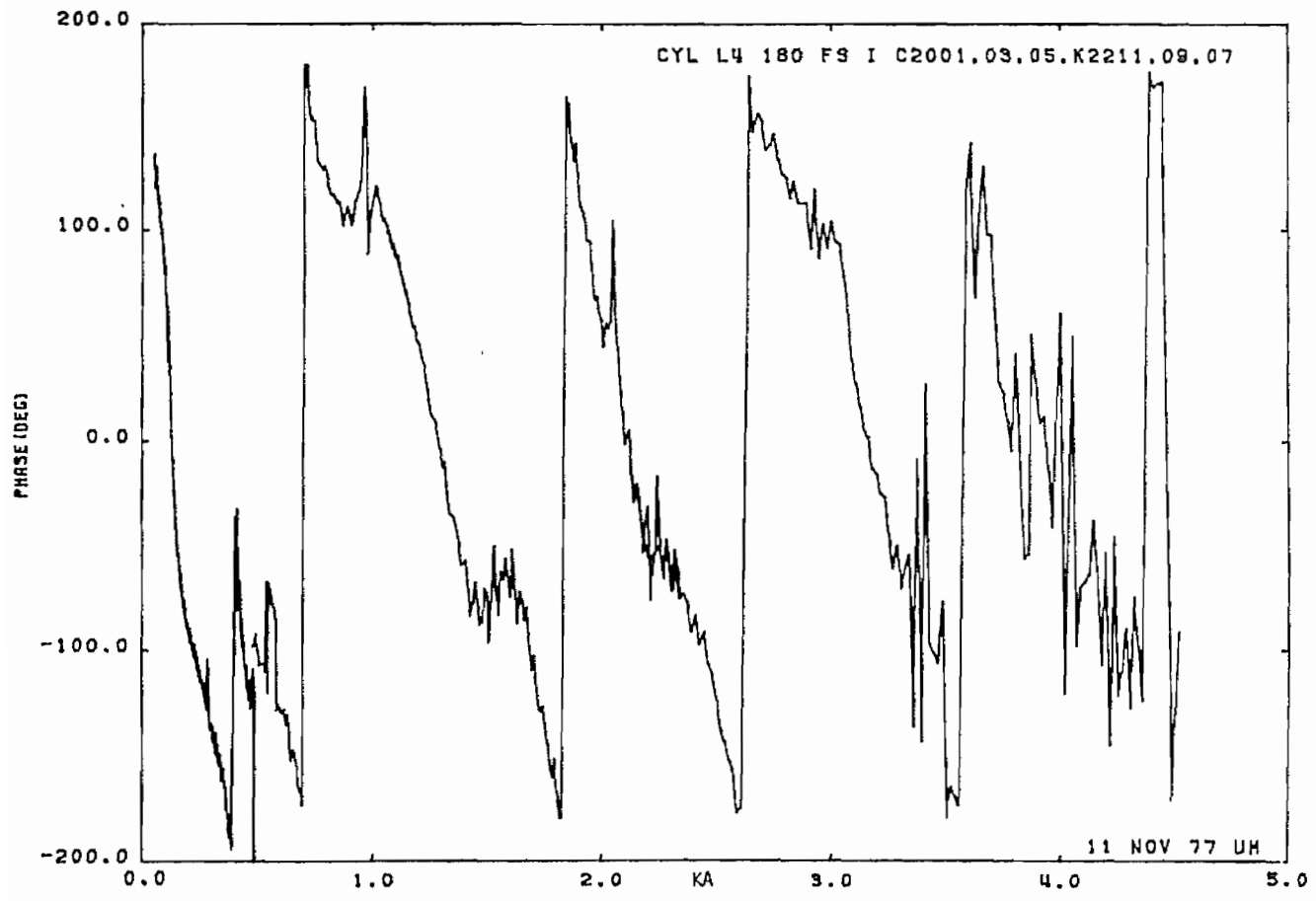

Figure 23a. Current on cylinder at STA:L/4; Ø = 180°, free space.

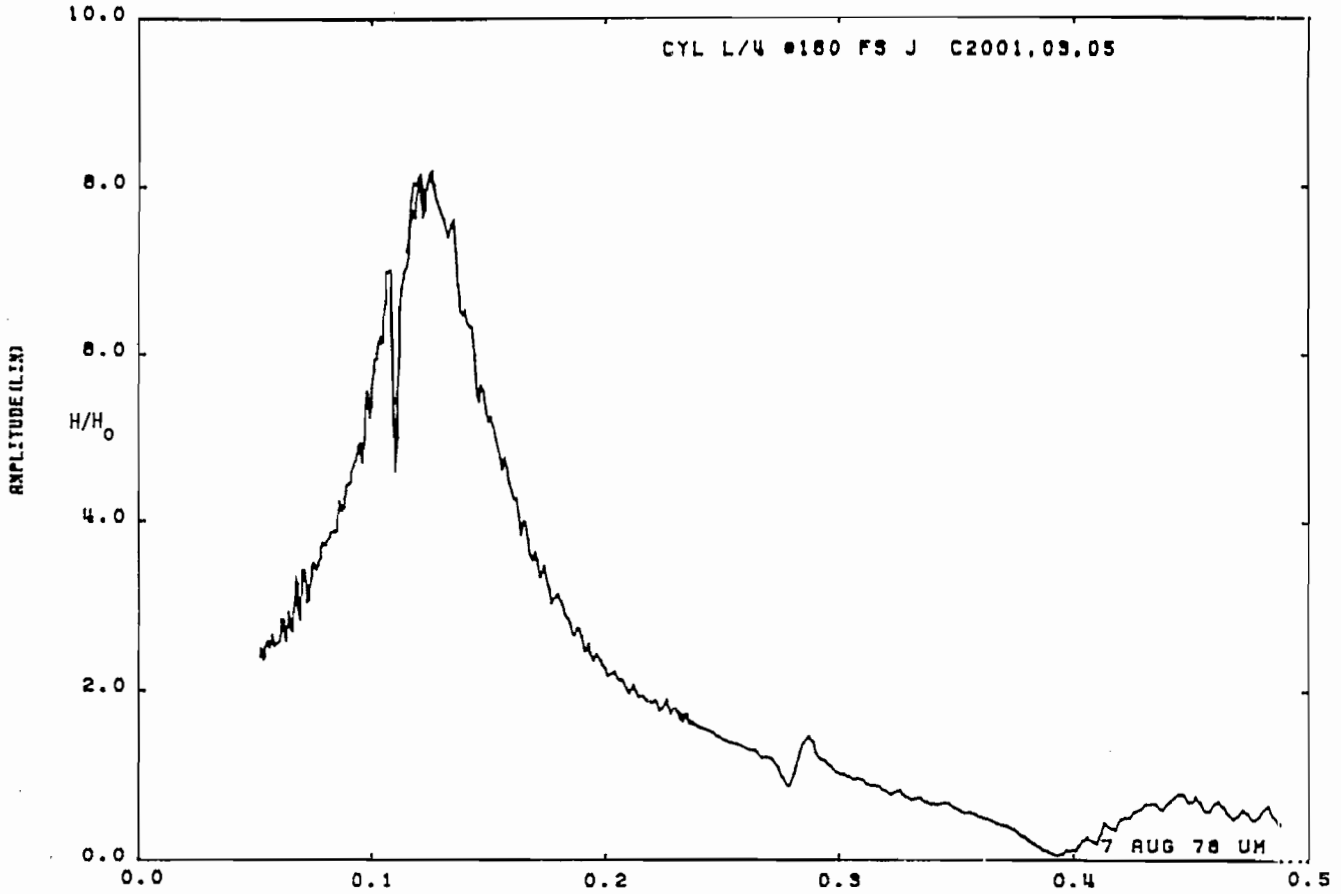

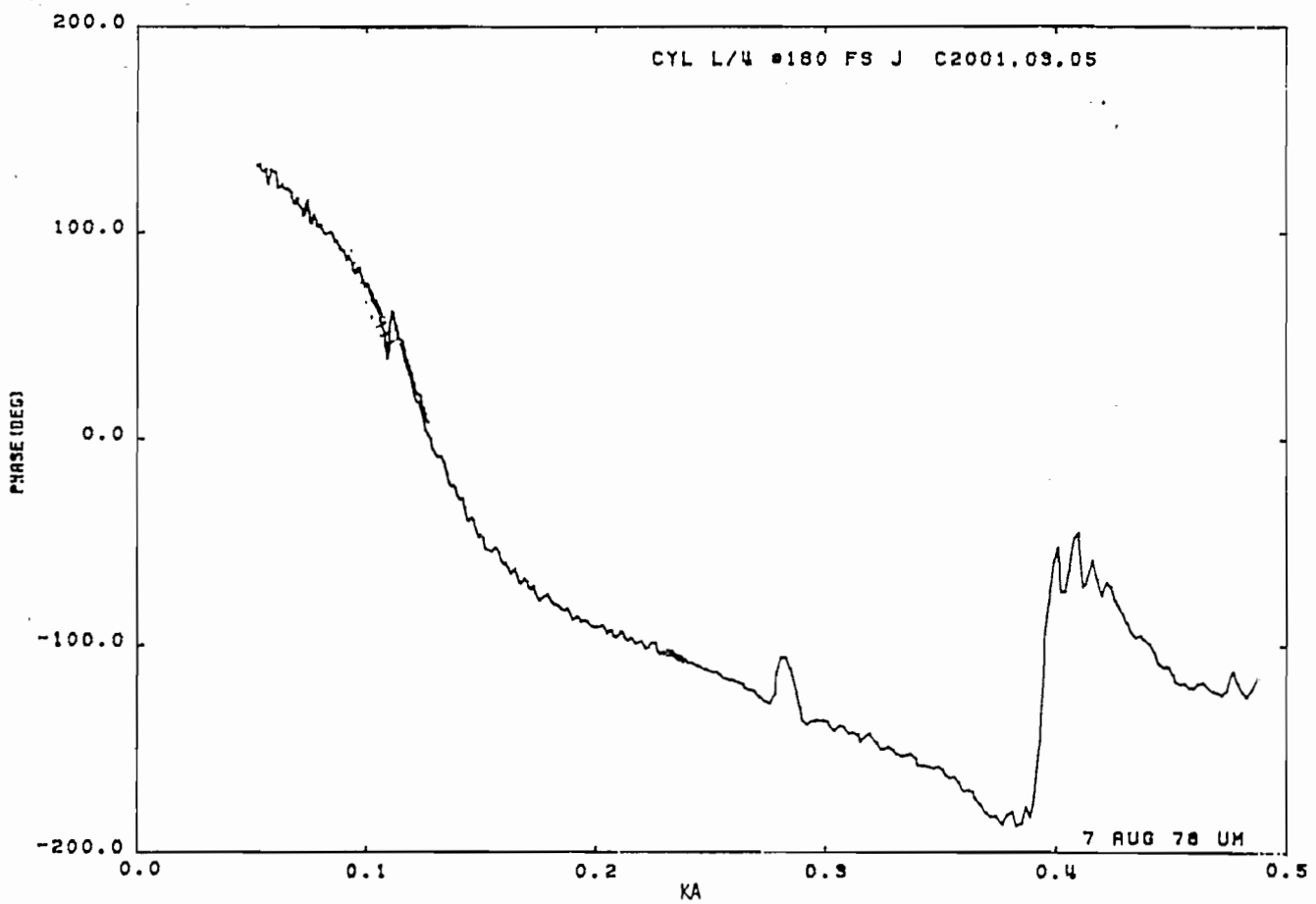

Figure 23b. Current on cylinder at STA:L/4; β = 180°, free space (expanded scale).

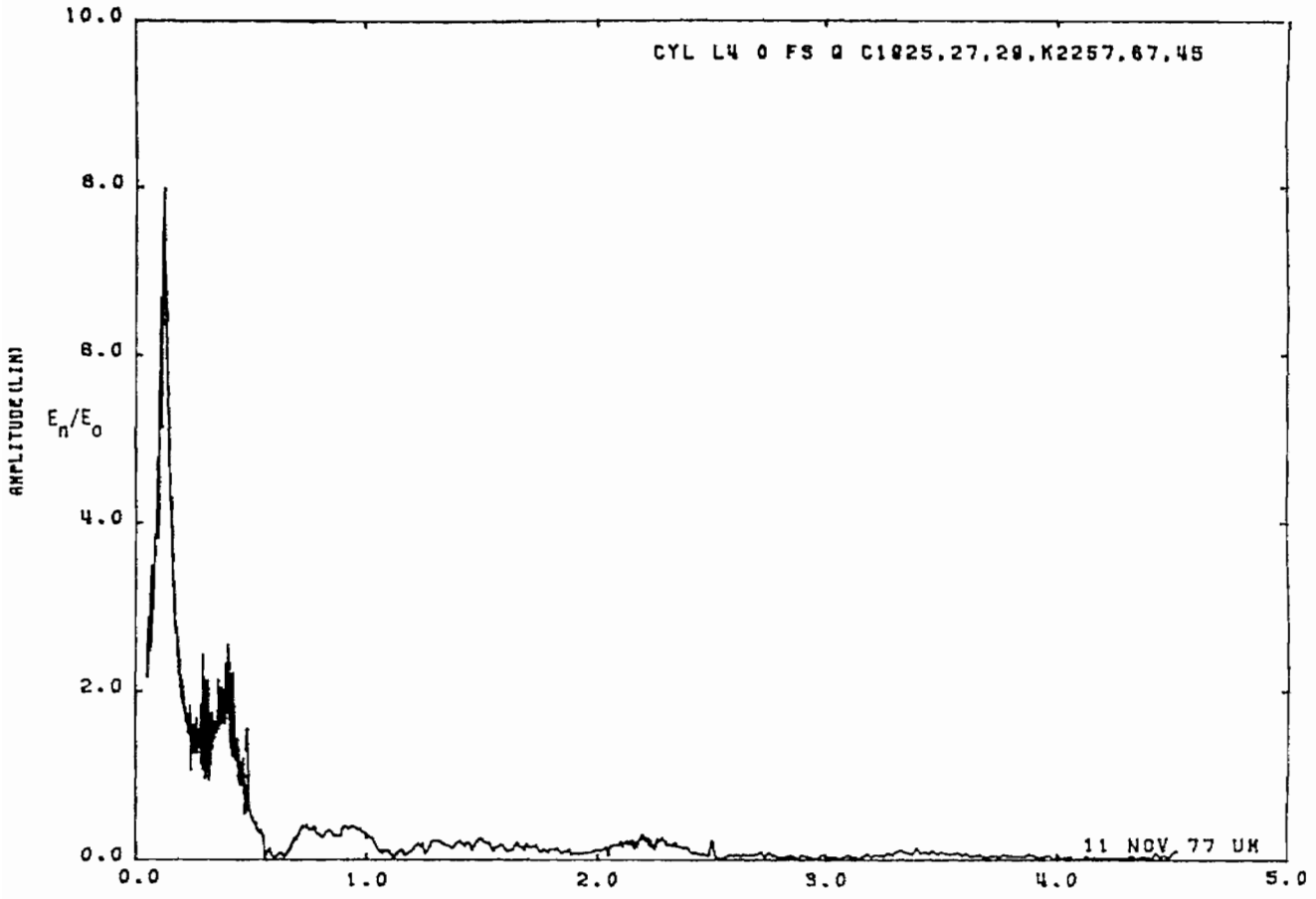

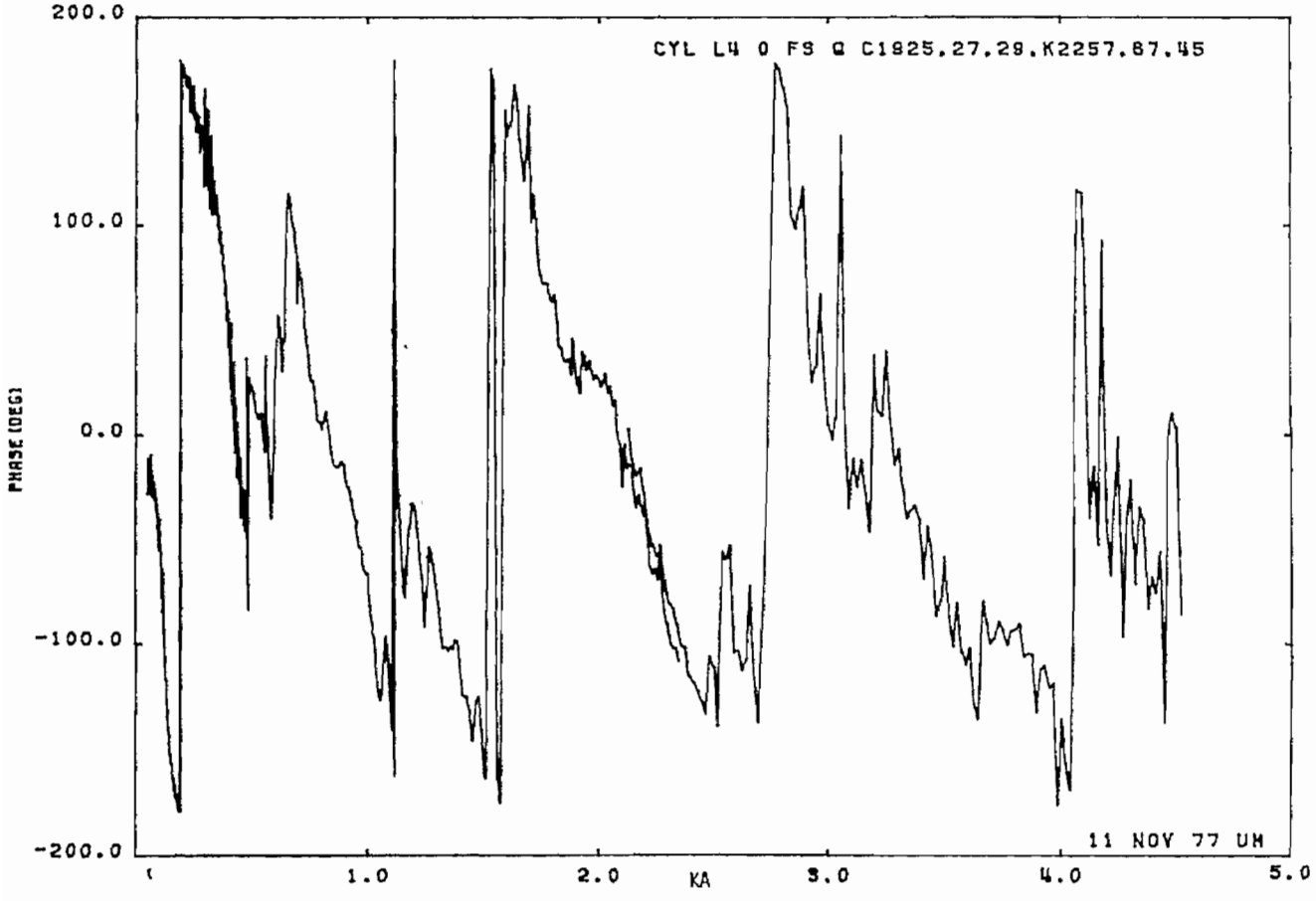

Figure 24a. Charge cylinder at STA:L/4; ϕ = 0°, free space.

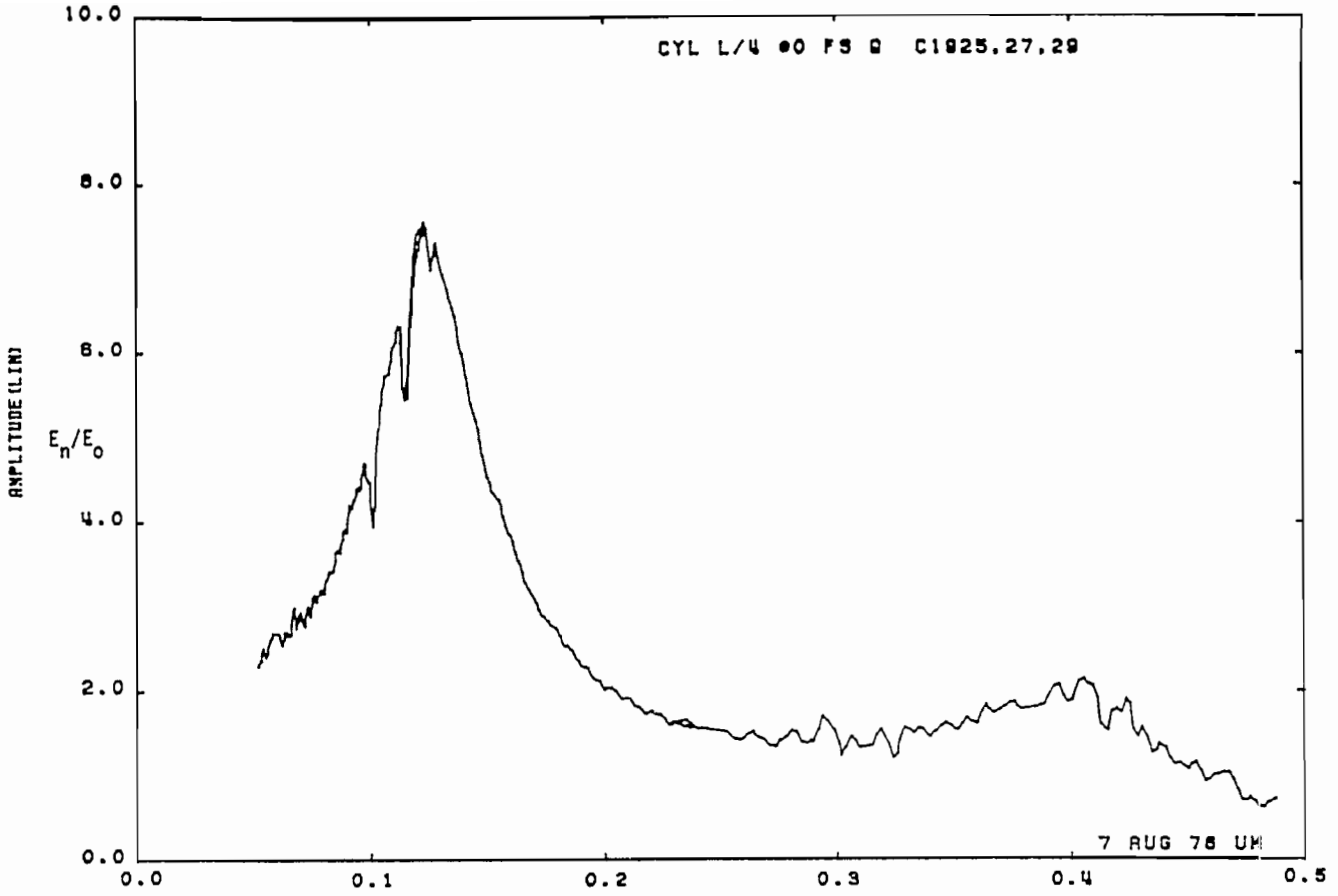

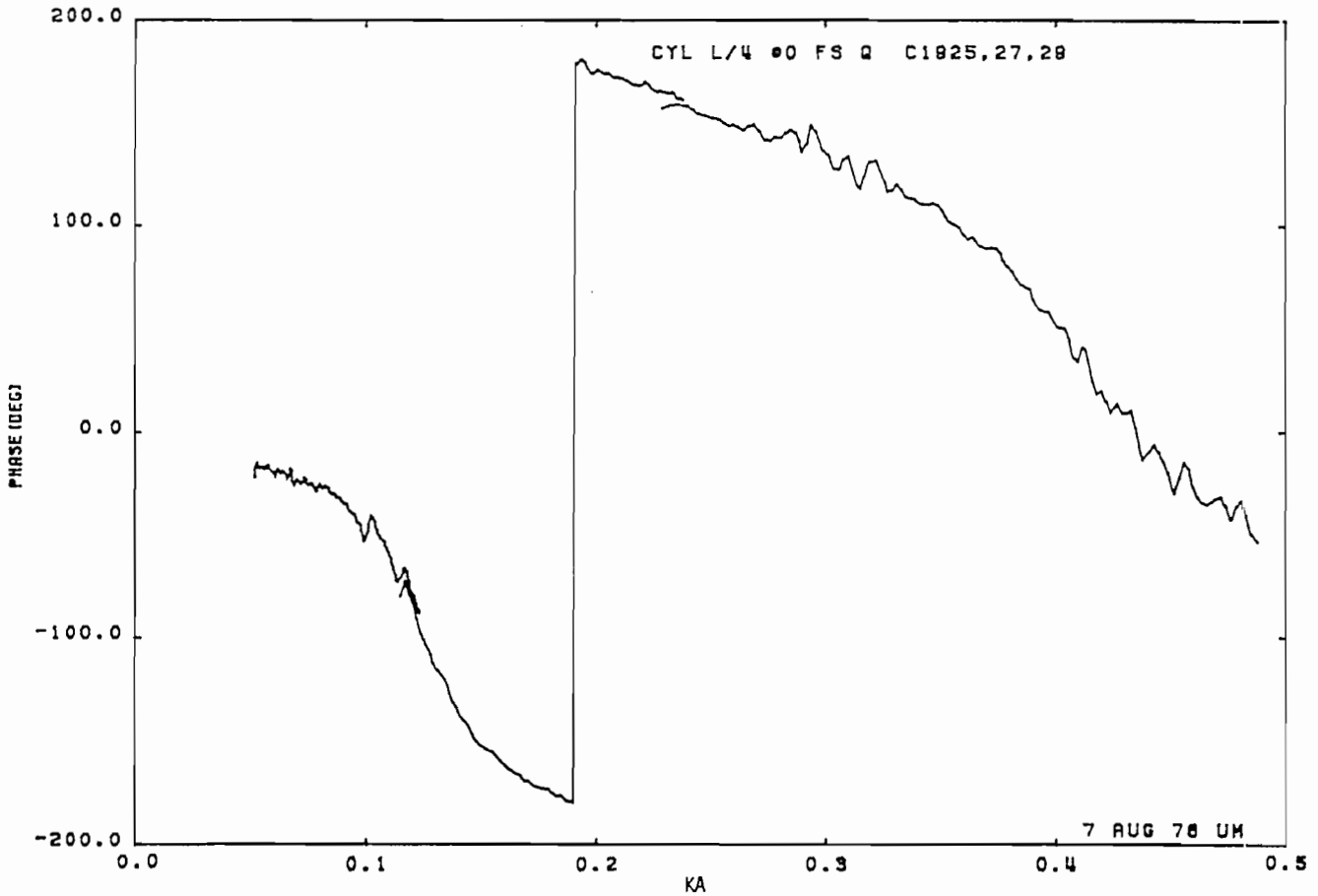

Figure 24b. Charge on cylinder at STA:L/4; β = 0°, free space (expanded scale).

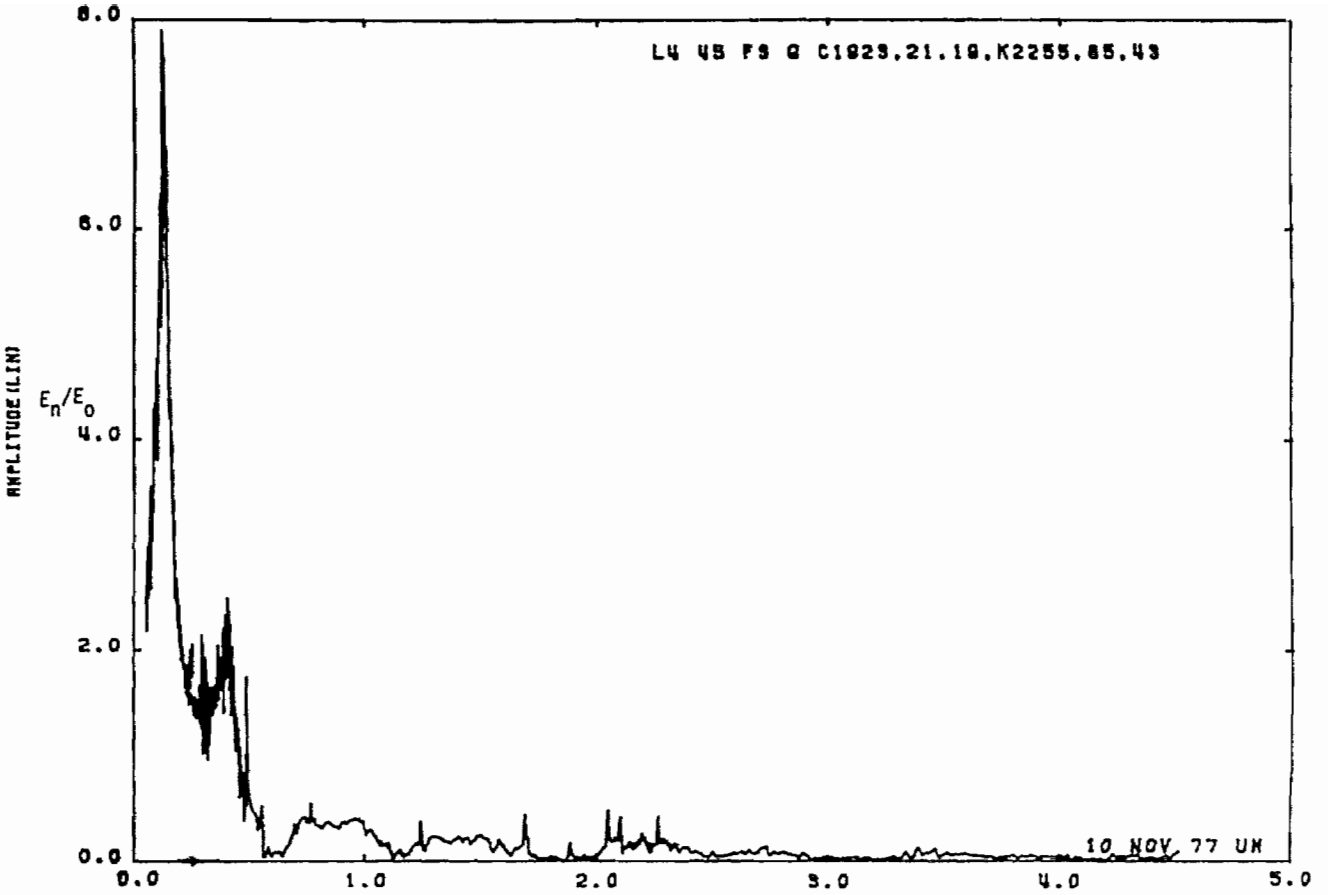

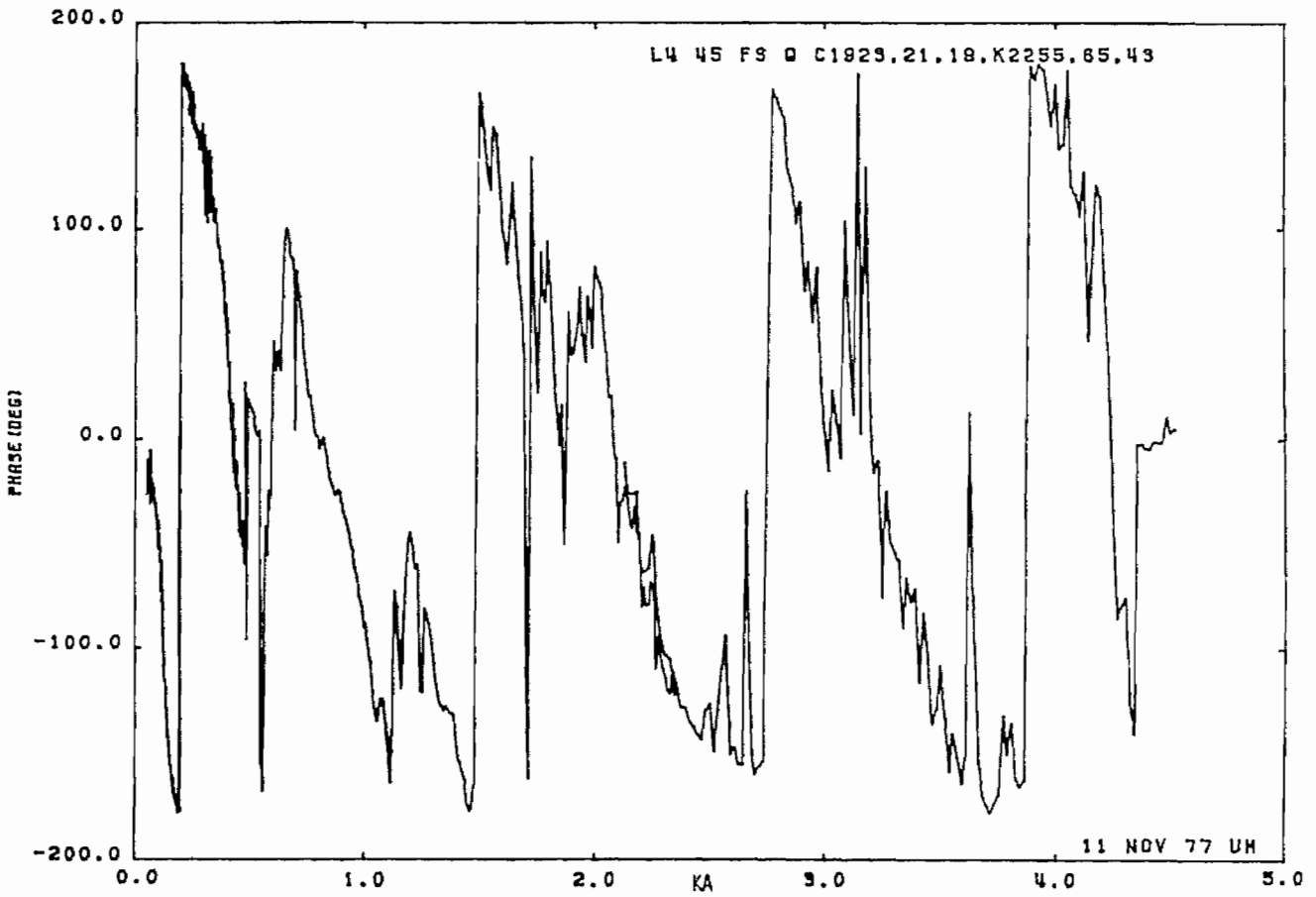

Fig Figure 25a. Charge cylinder at STA:L/4; Ø = 45°, free space.

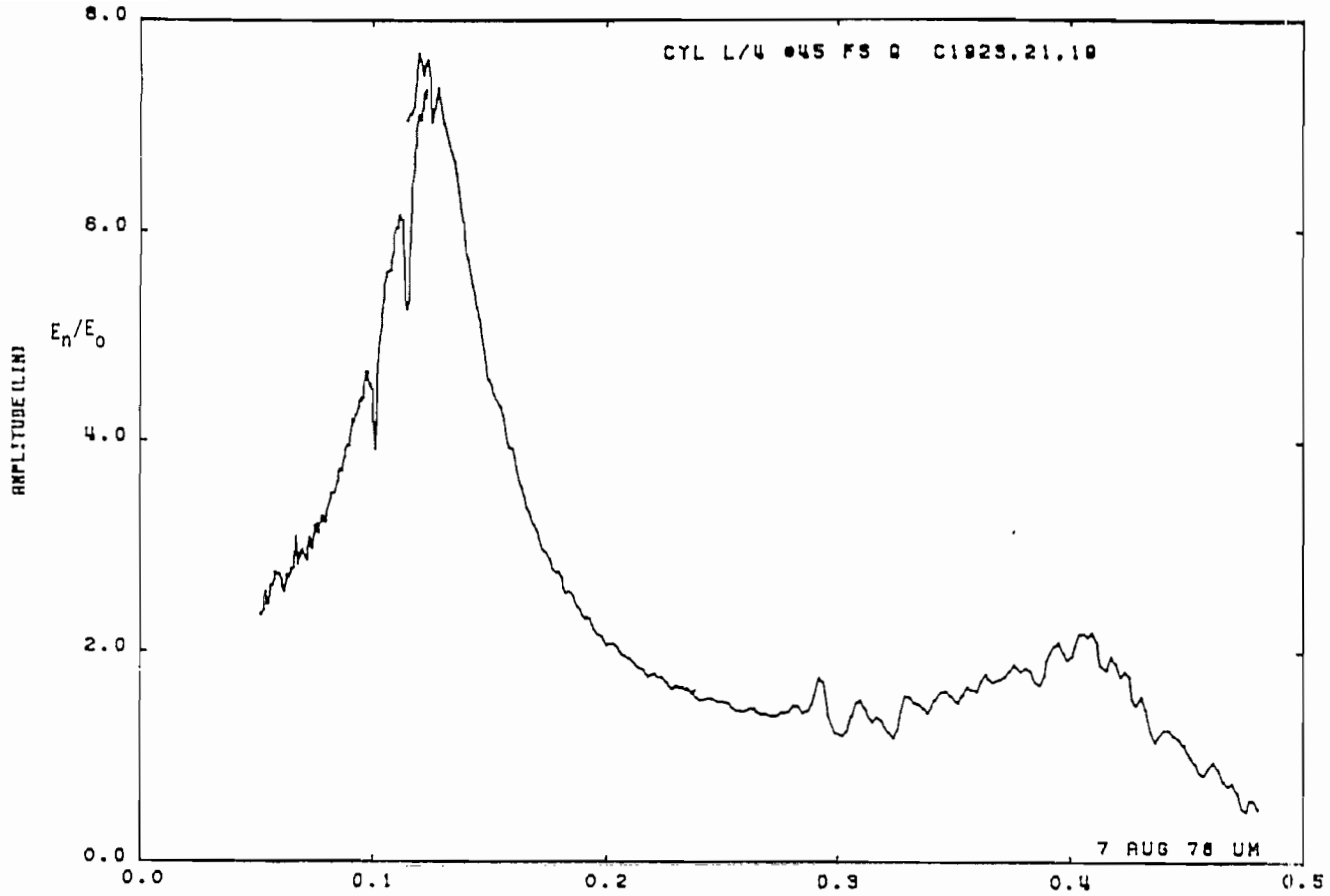

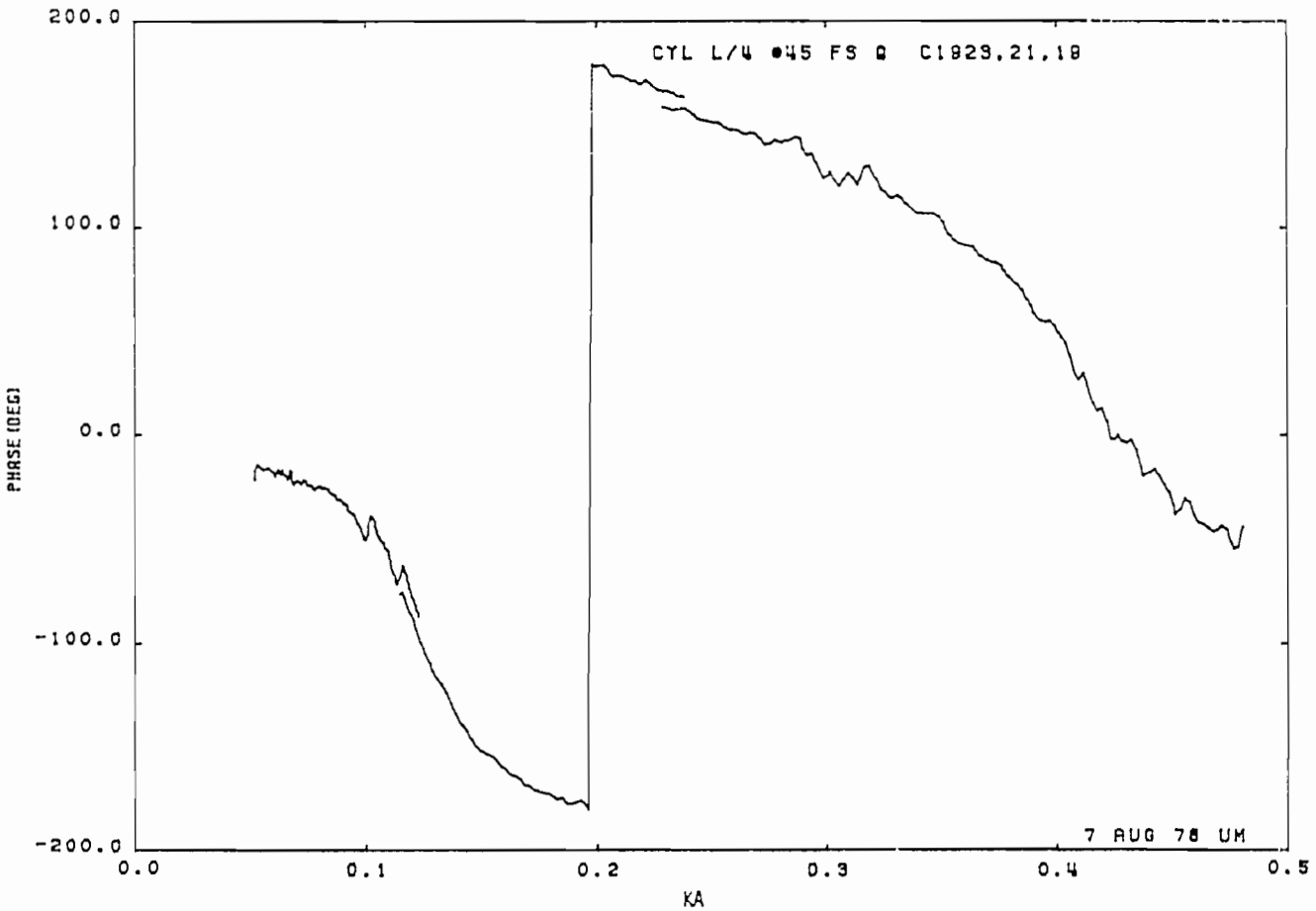

Figure 25b. Charge on cylinder at STA:L/4; ø = 45°, free space (expanded scale).

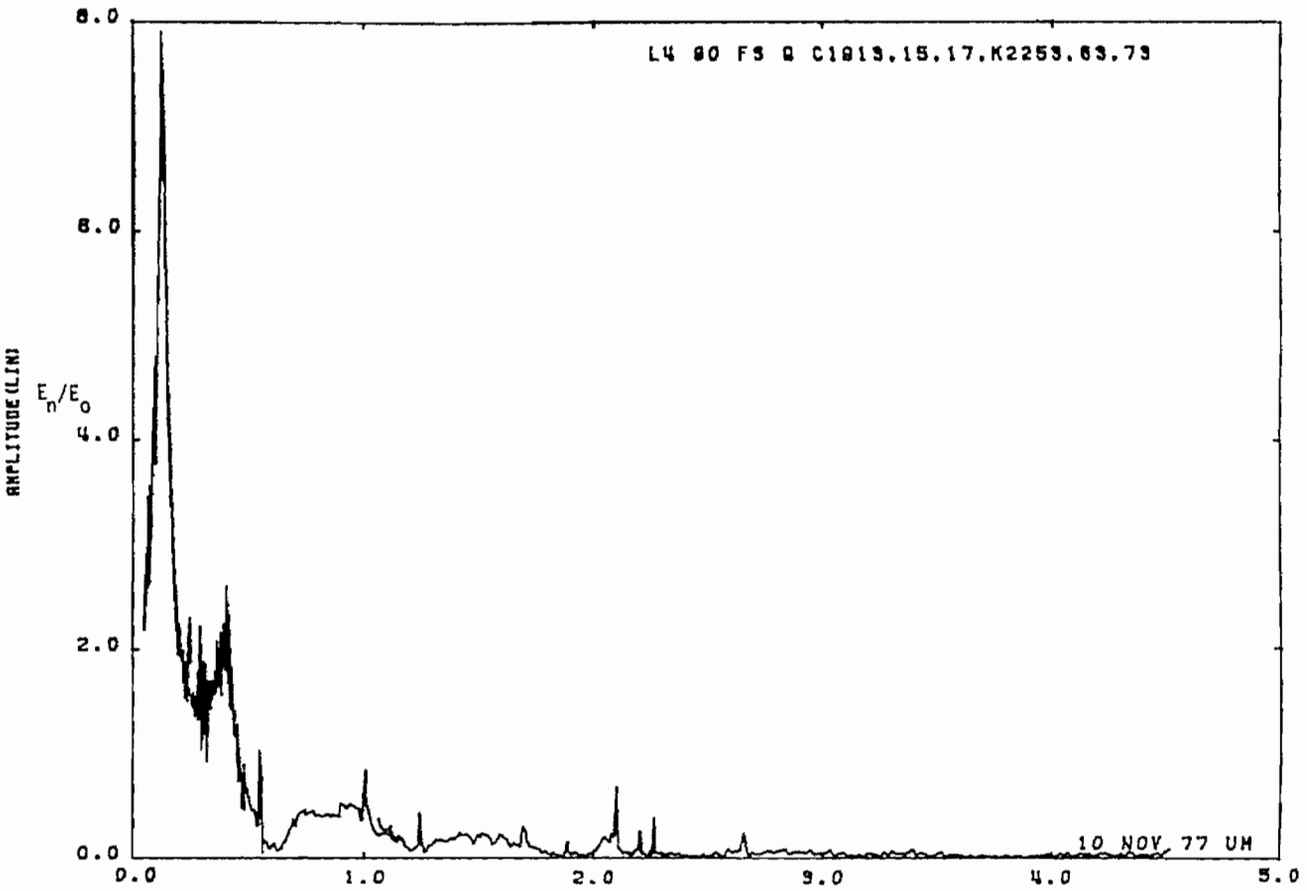

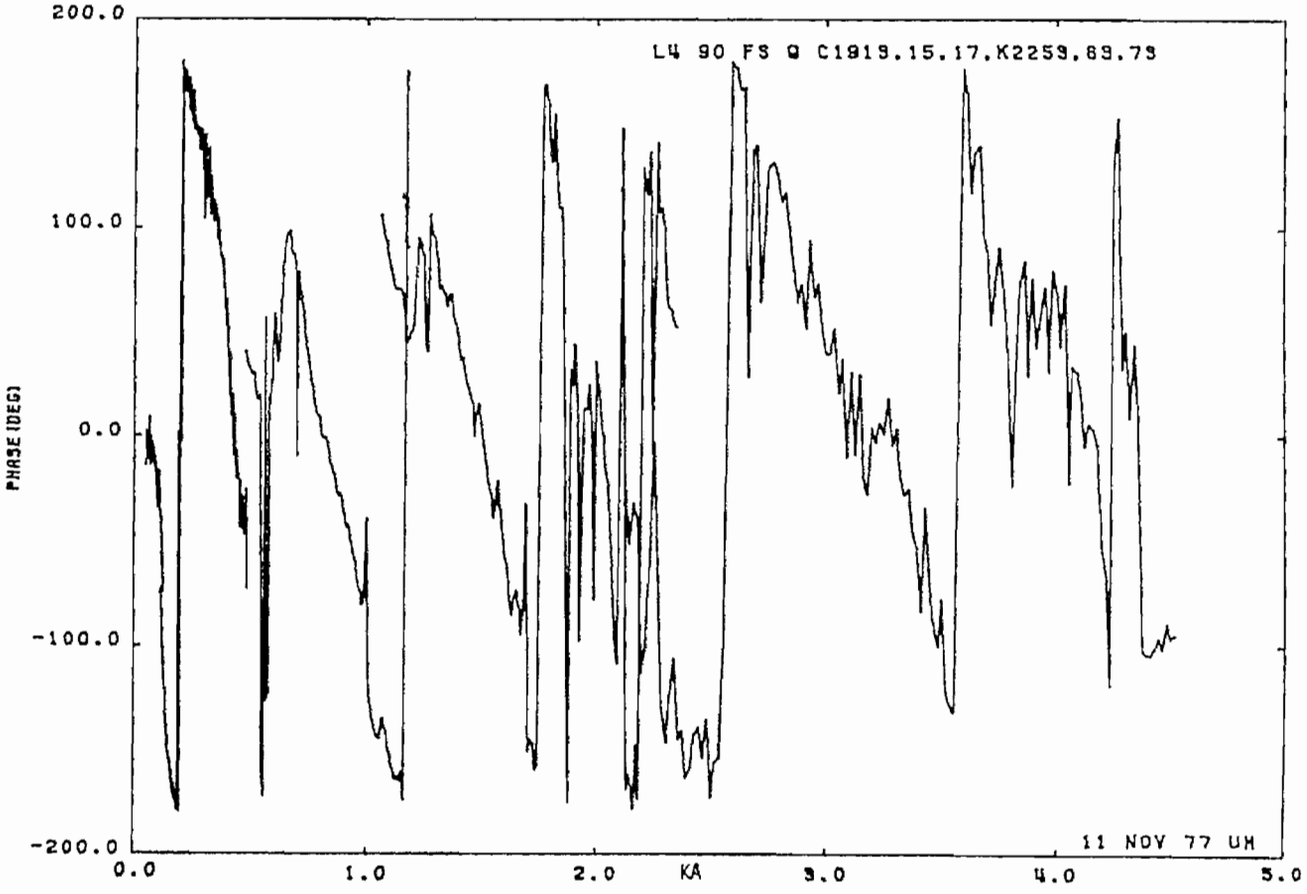

Figure 26a. Charge on cylinder at STA:L/4; ϕ = 90°, free space.

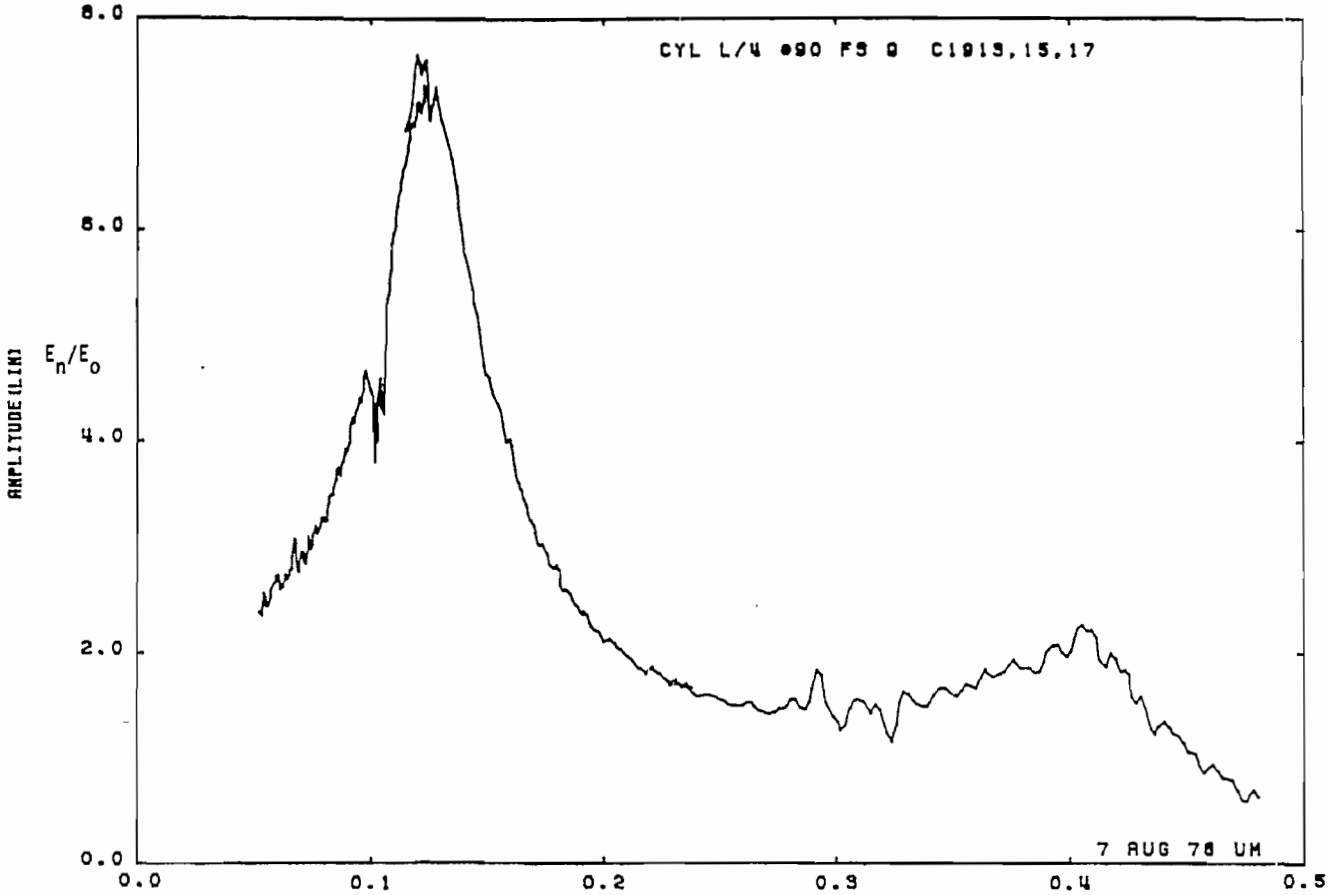

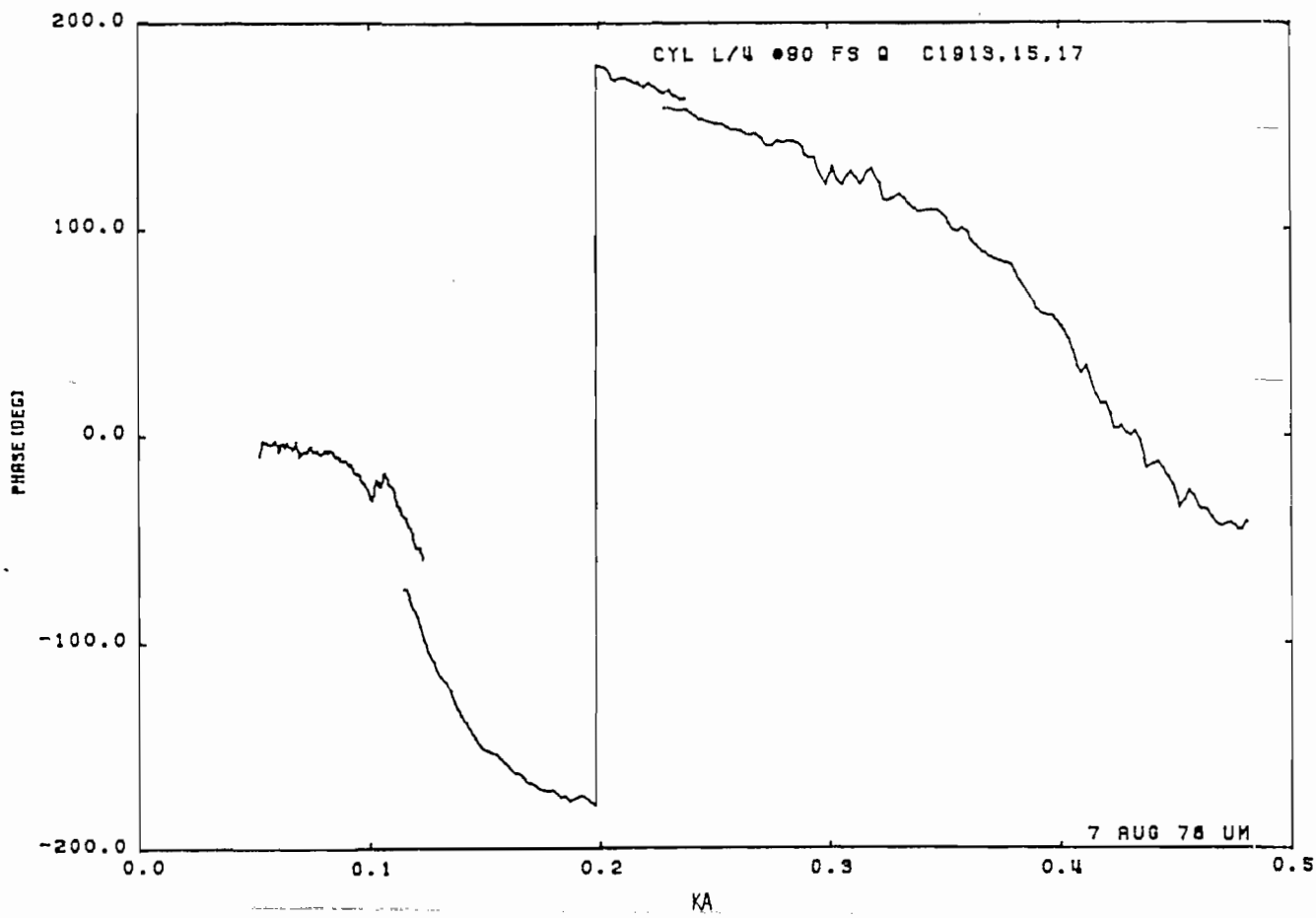

Figure 26b. Charge cylinder at STA:L/4; ϕ = 90°, free space (expanded scale).

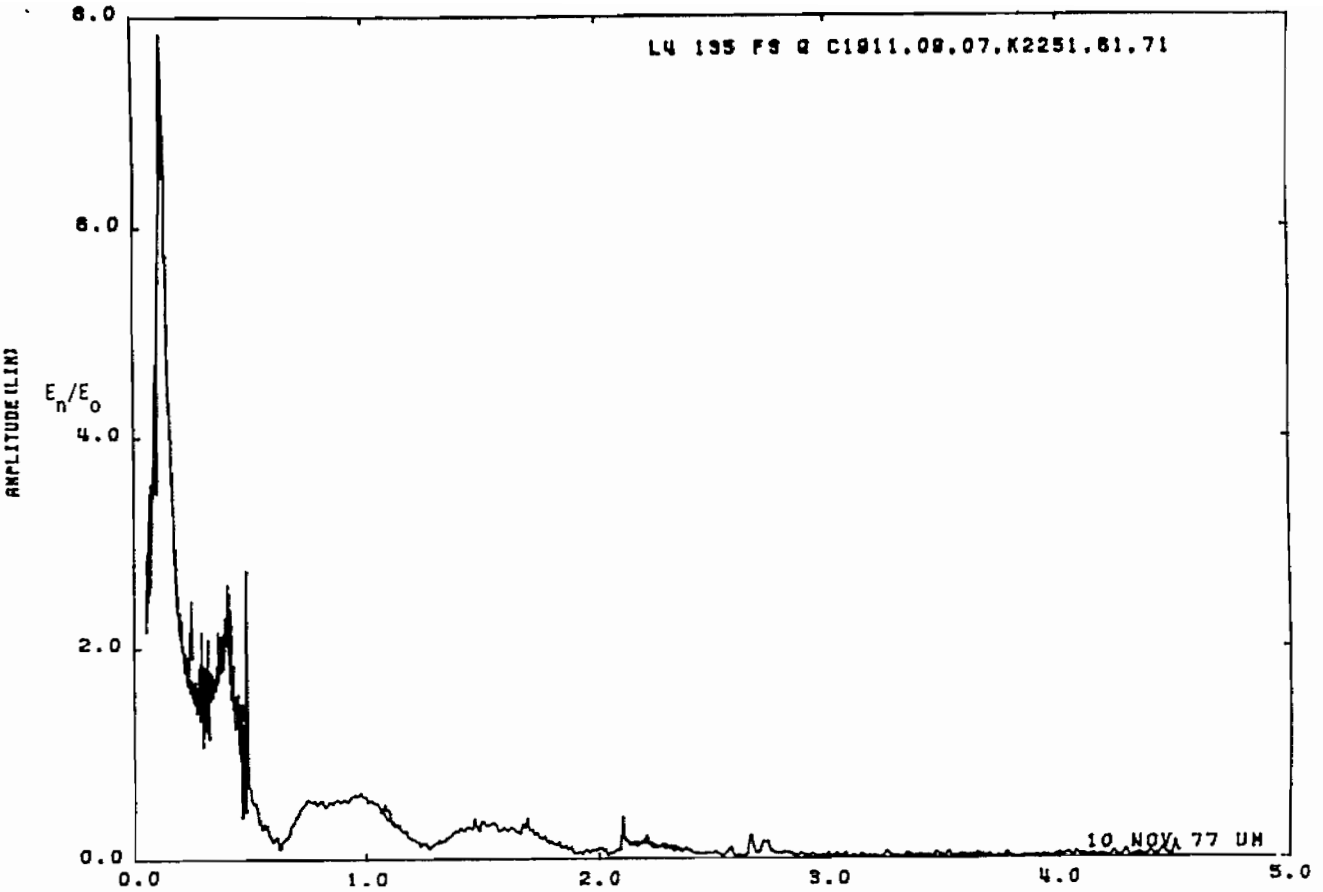

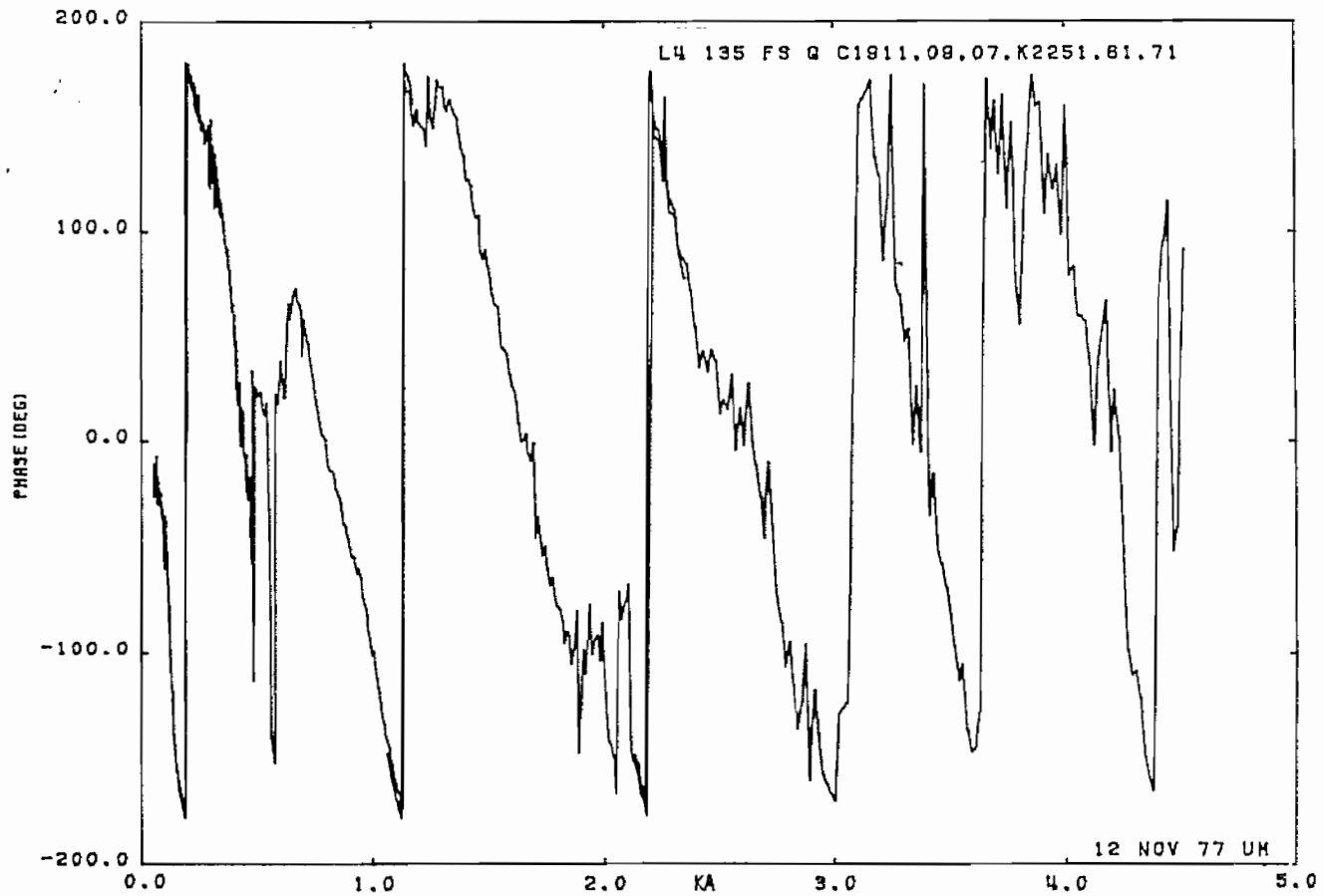

Figure 27a. Charge on cylinder at STA:L/4; ϕ = 135°, free space.

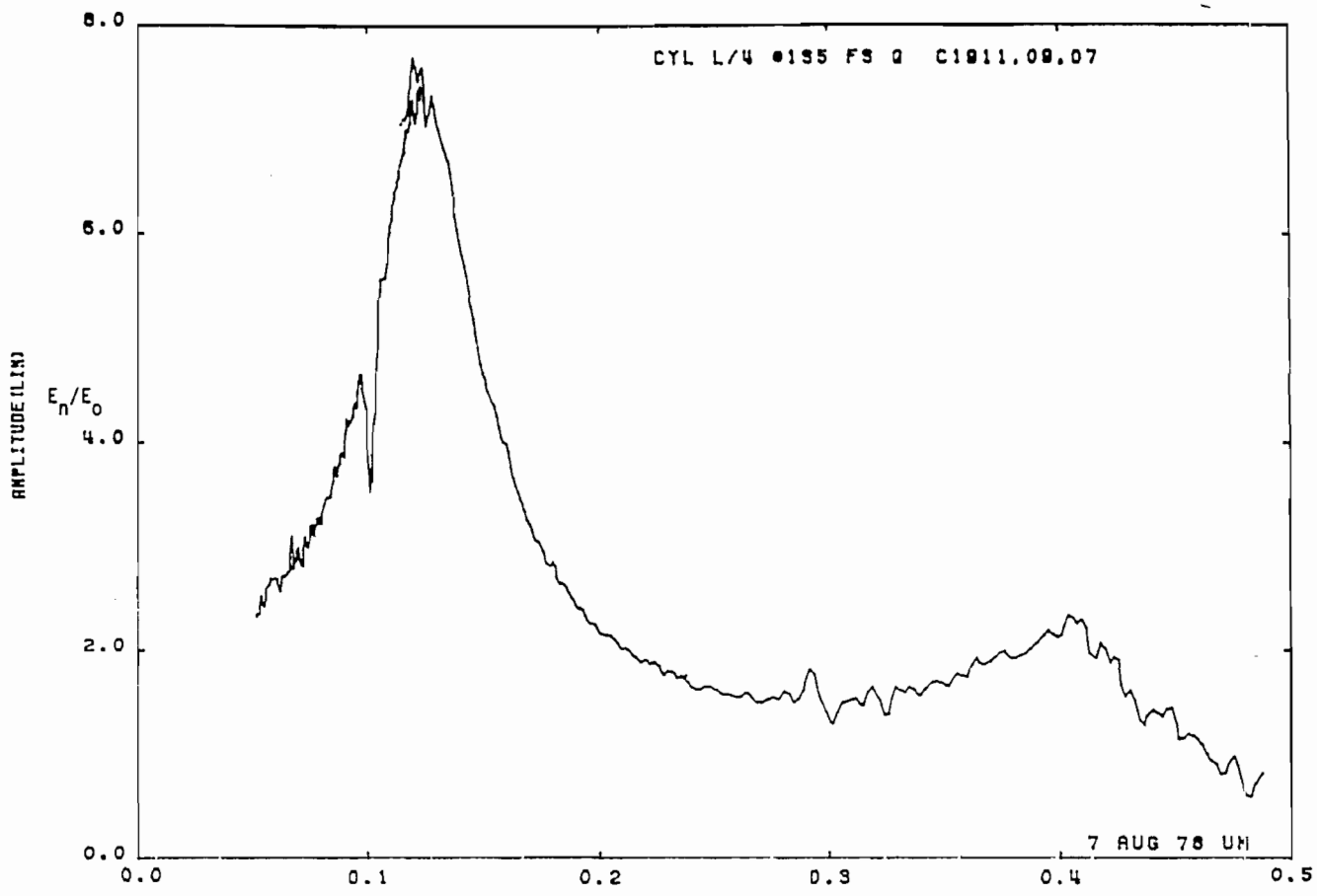

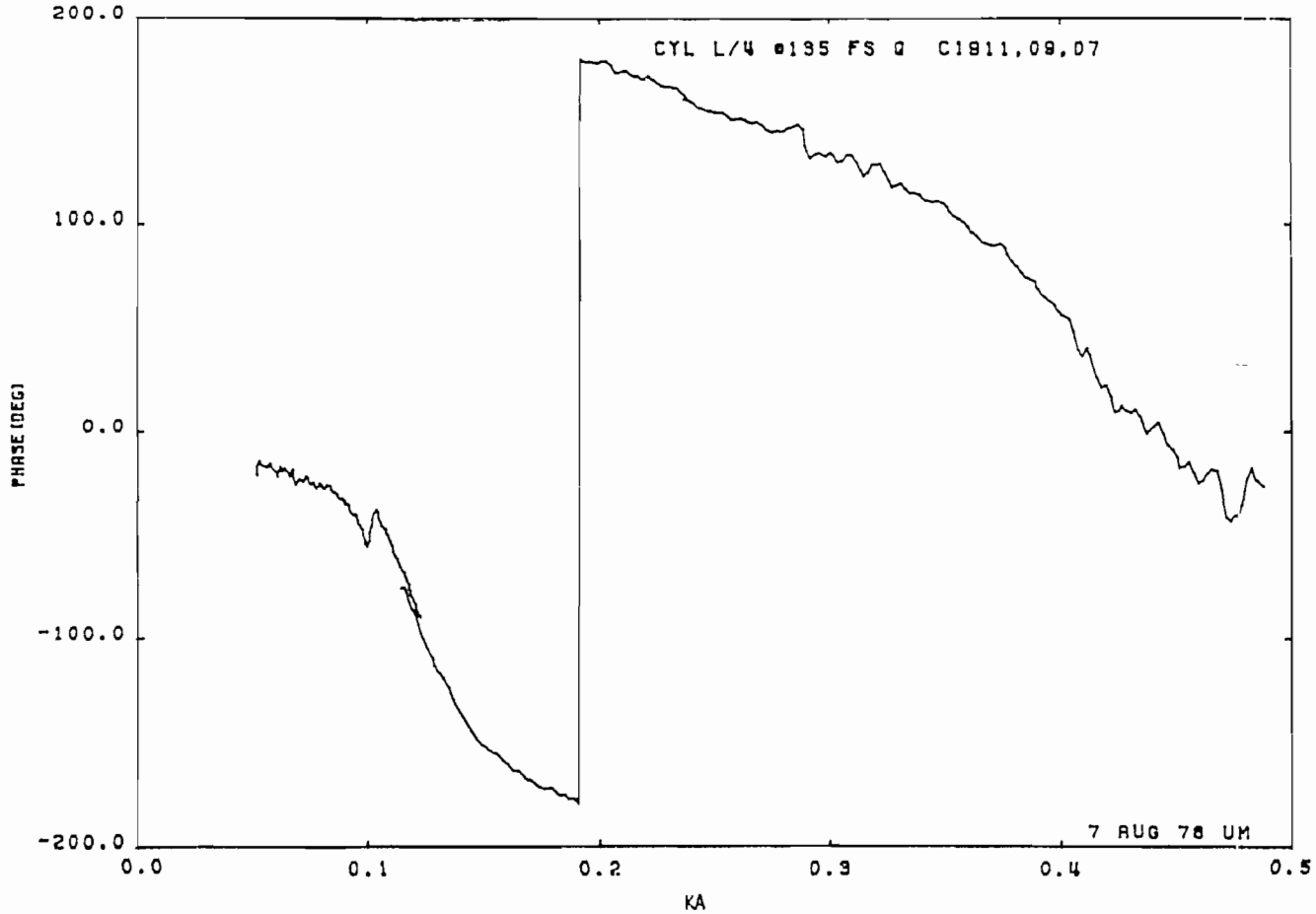

Figure 27b. Charge on cylinder at STA:L/4; ϕ = 135°, free space (expanded scale).

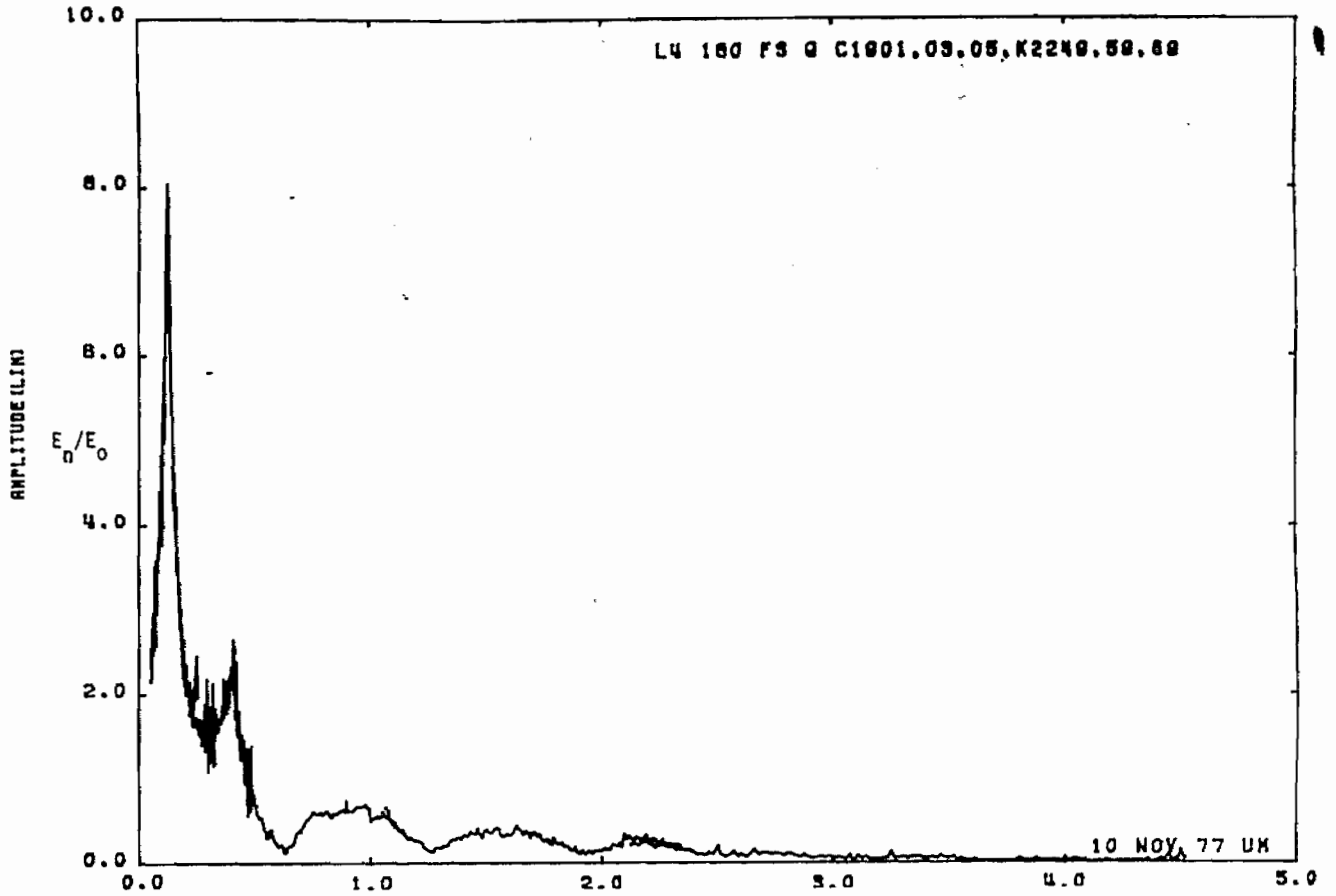

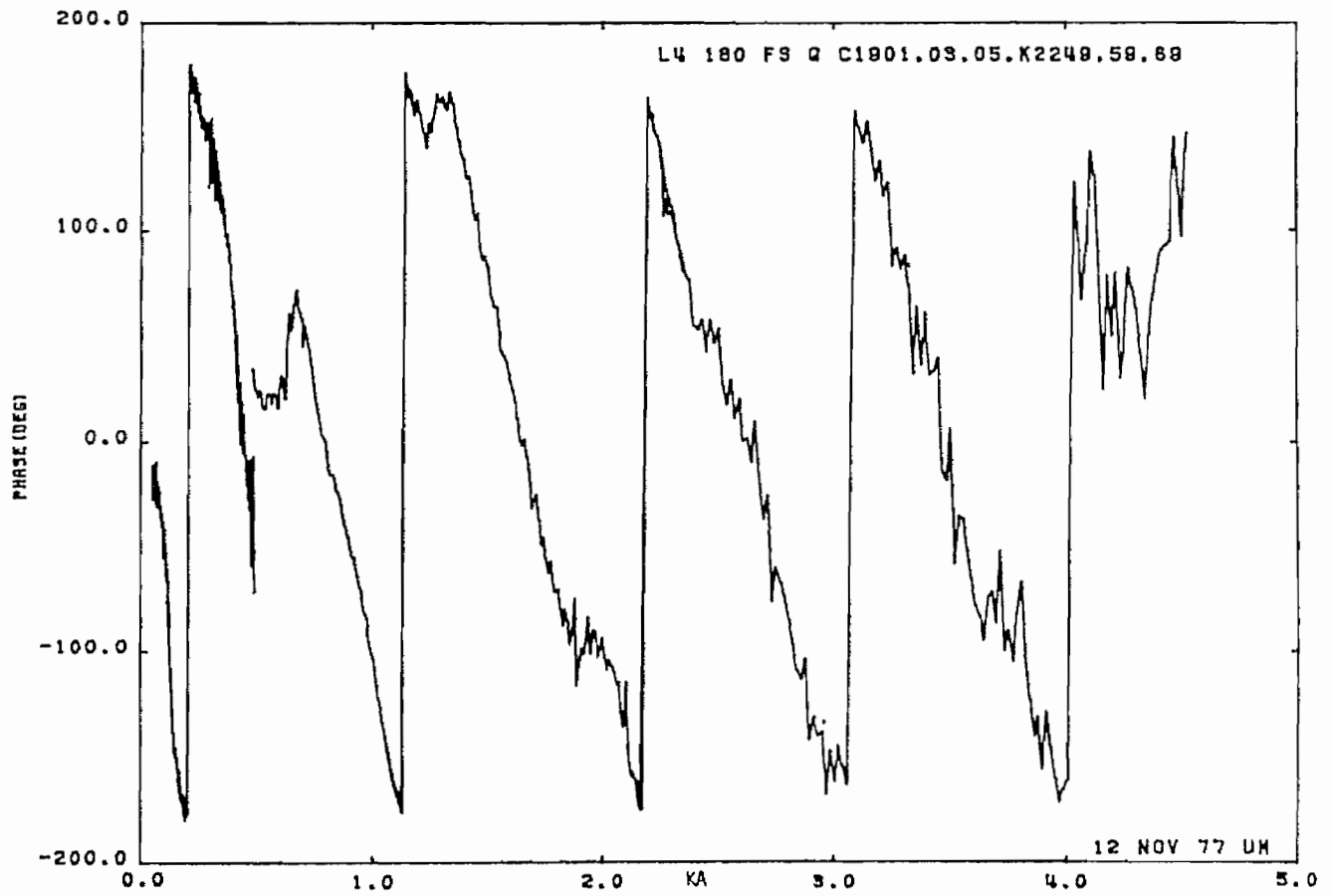

Figure 28a. Charge on cylinder at STA:L/4; ϕ = 180°, free space.

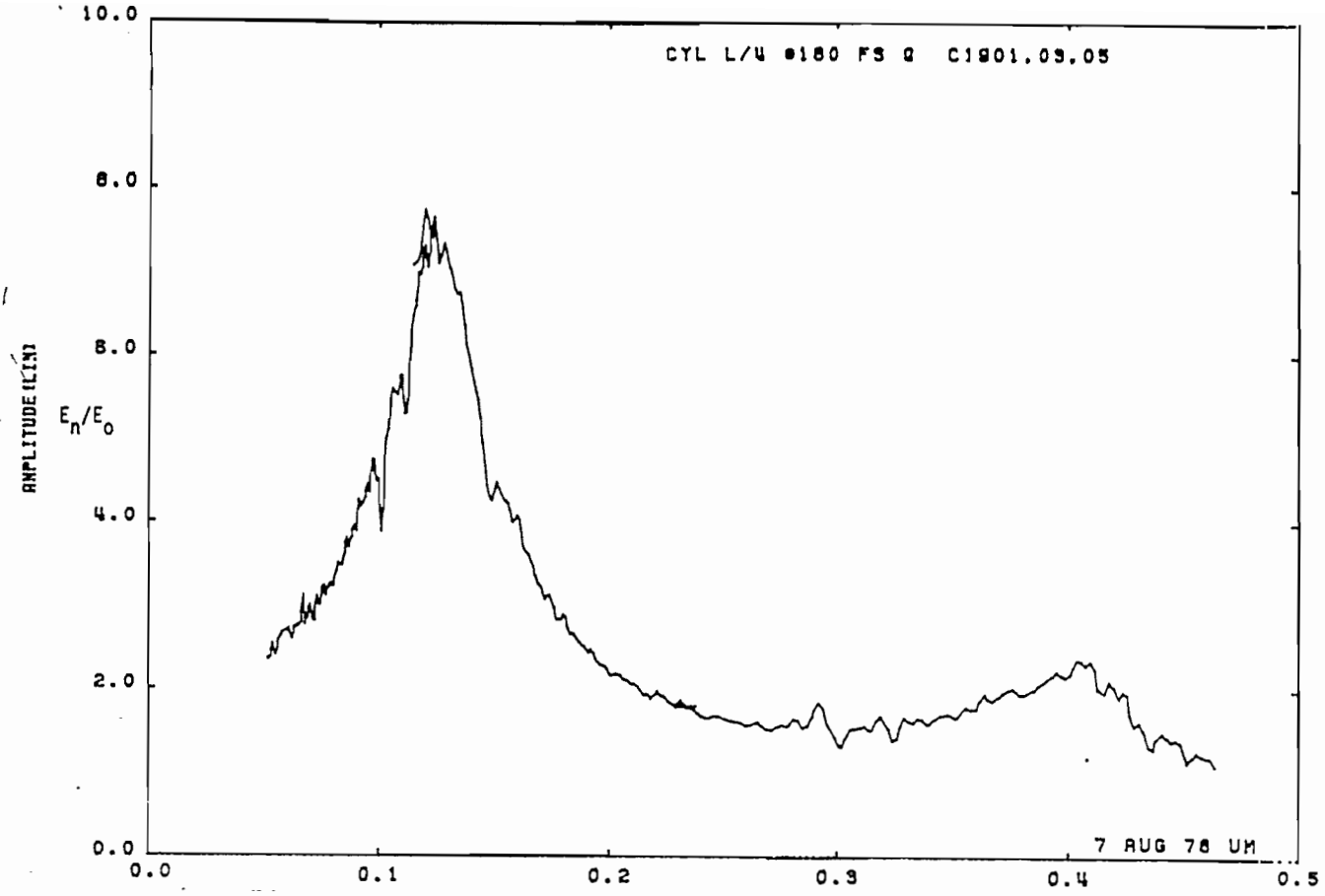

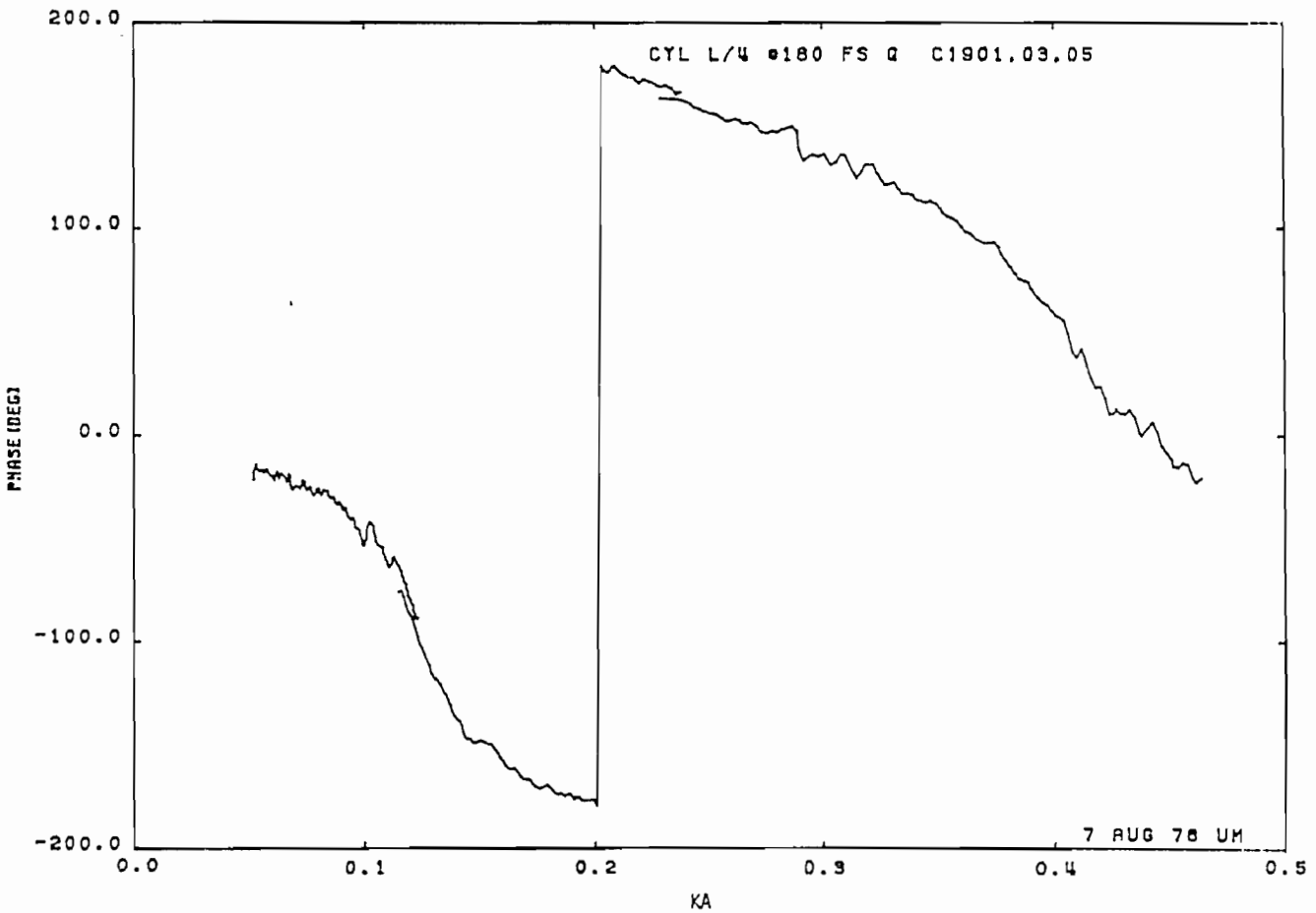

Figure 28b. Charge on cylinder at STA:L/4; ø = 180°, free space (expanded scale).

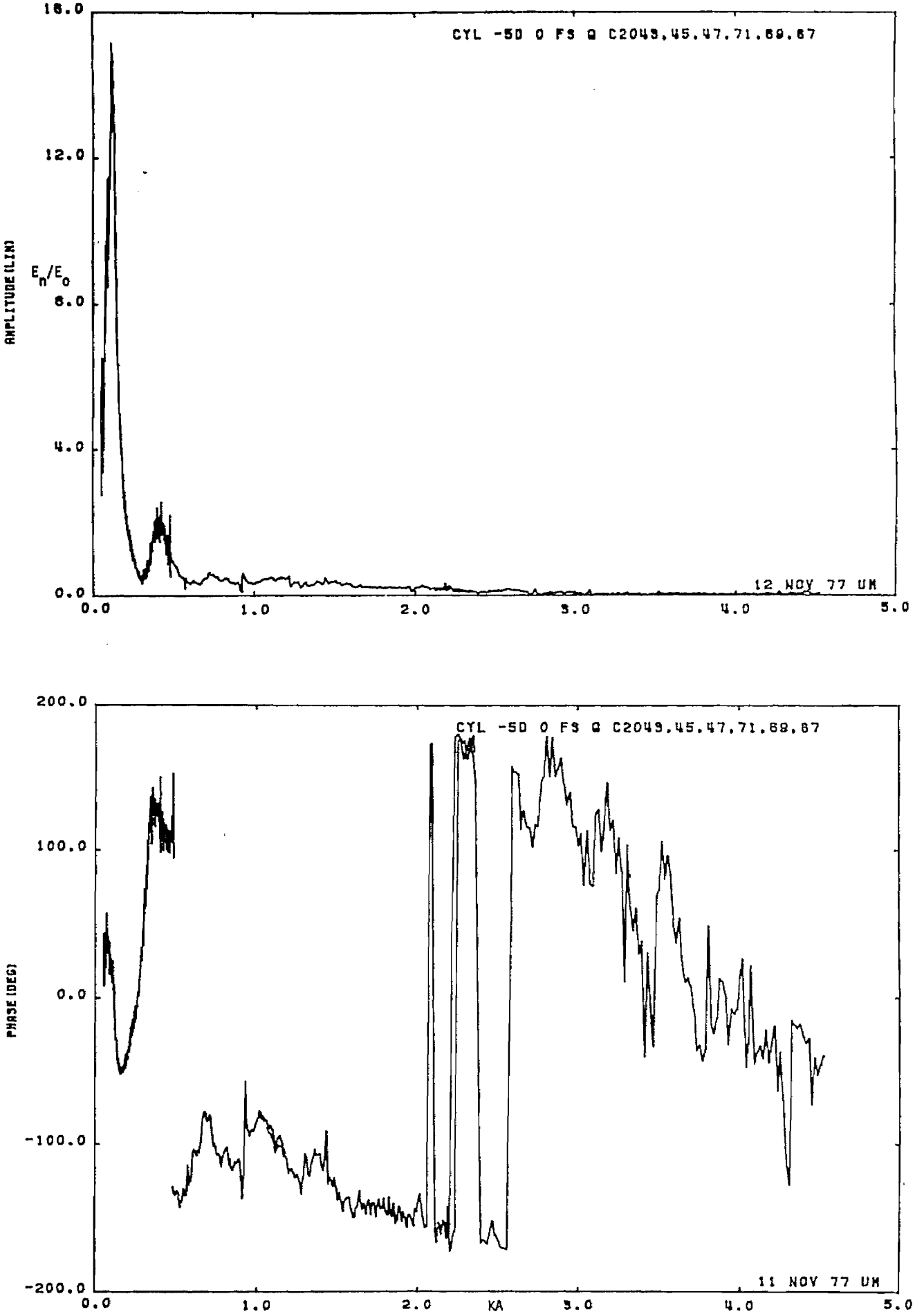

Figure 29a. Charge on cylinder at STA:-5D; ϕ = 0°, free space.

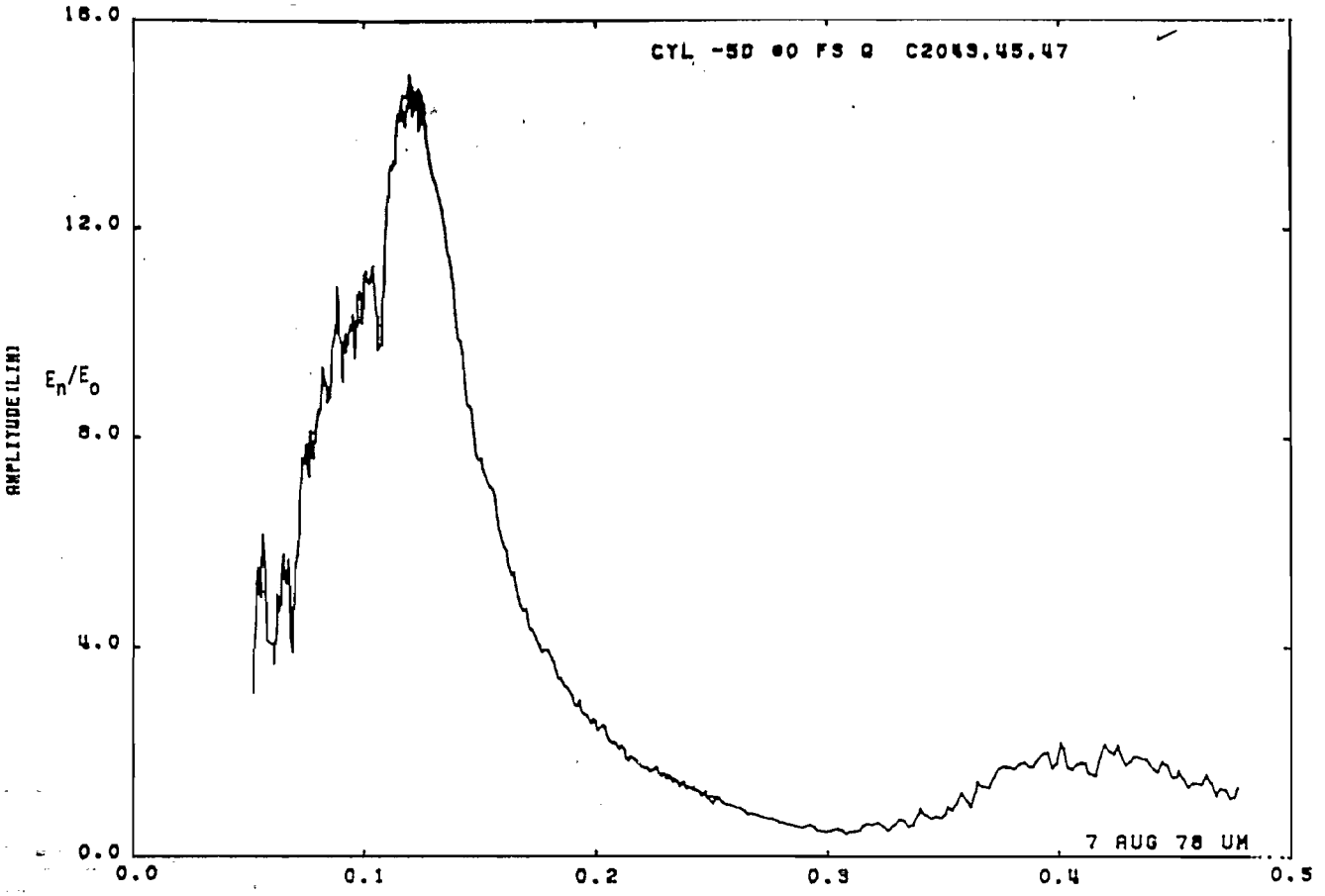

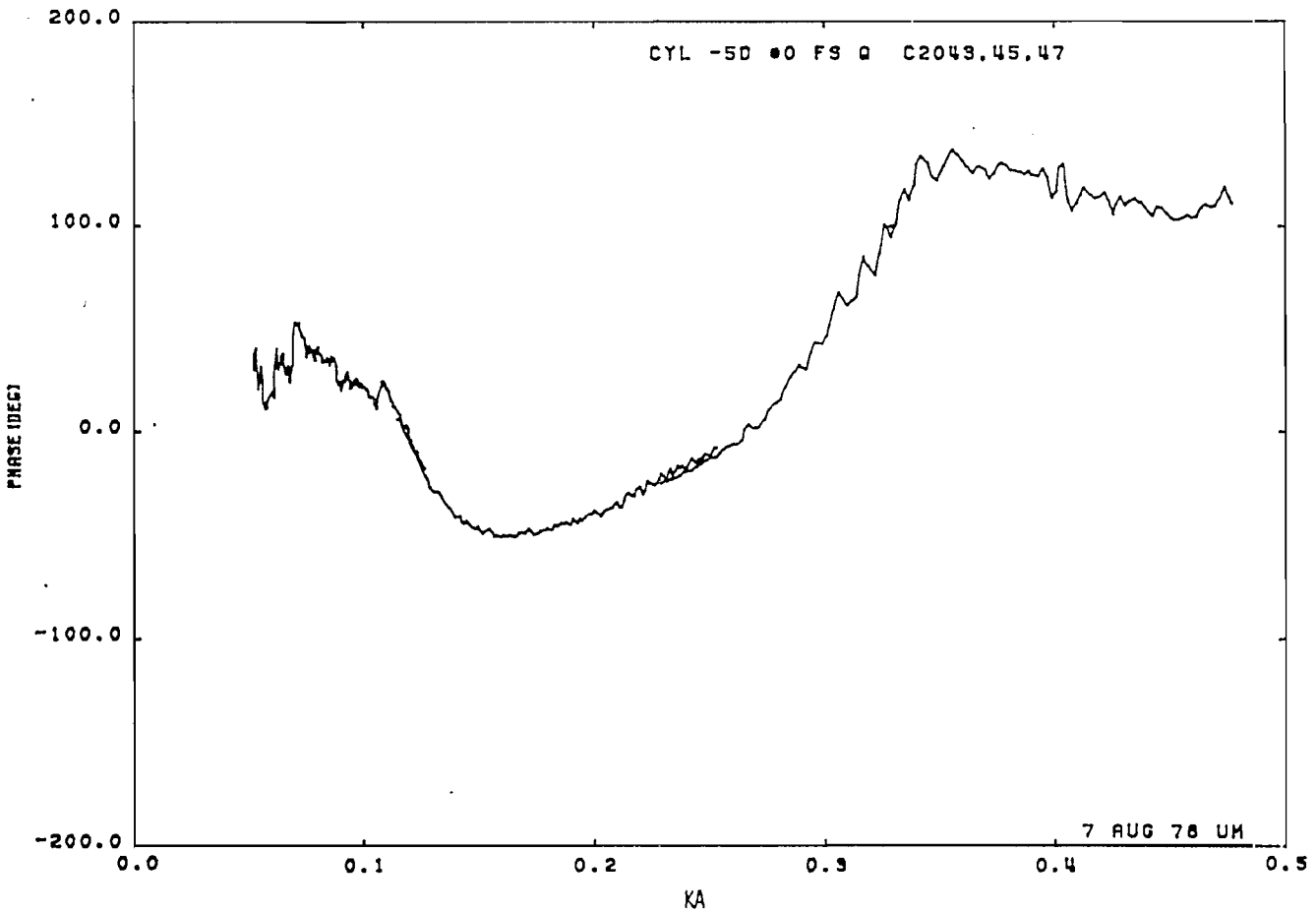

Fig. Figure 29b. Charge on cylinder at STA:-5D; ∅ = 0°, free space (expanded scale).

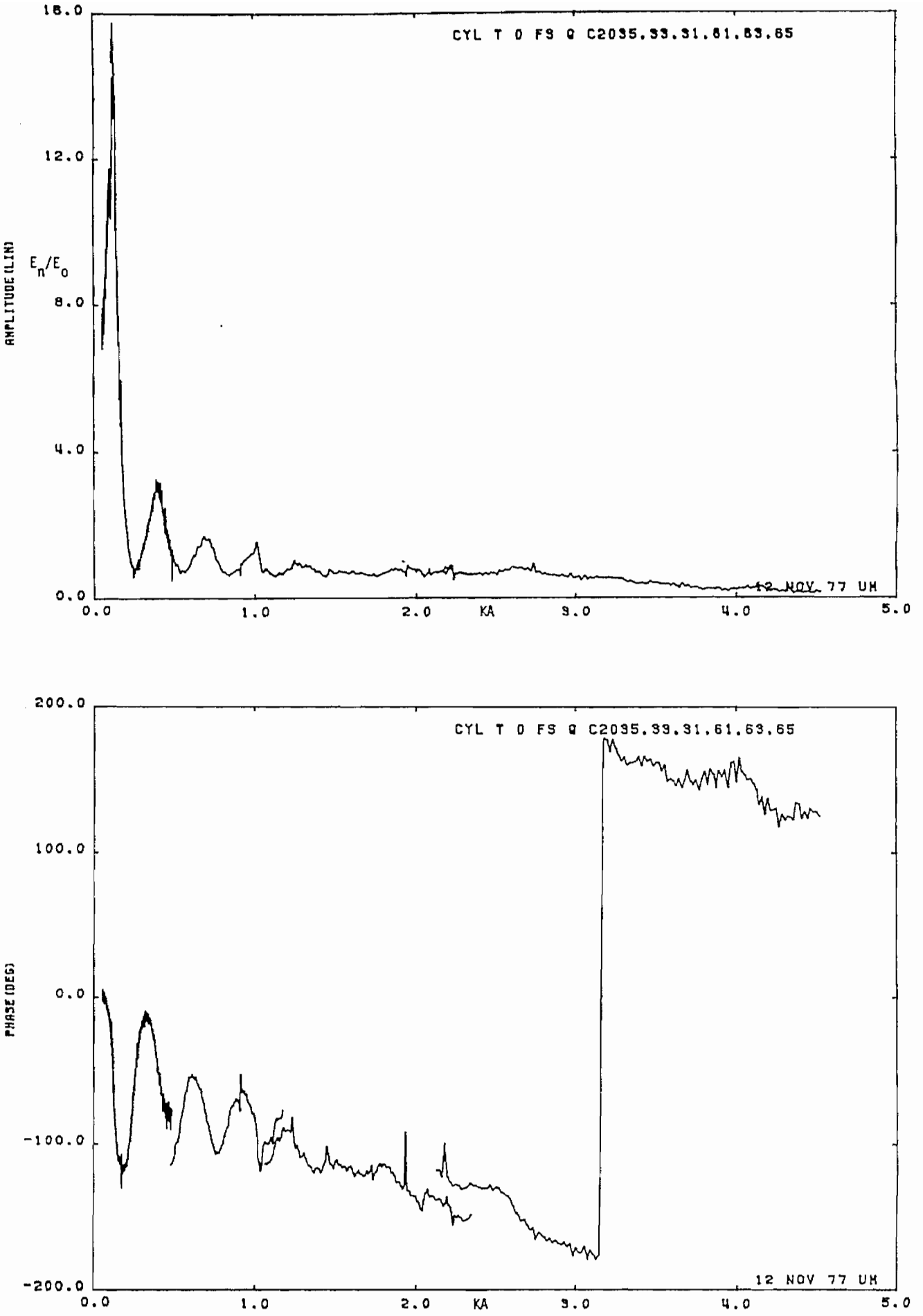

Figure 30a. Charge on cylinder at STA:T; free space.

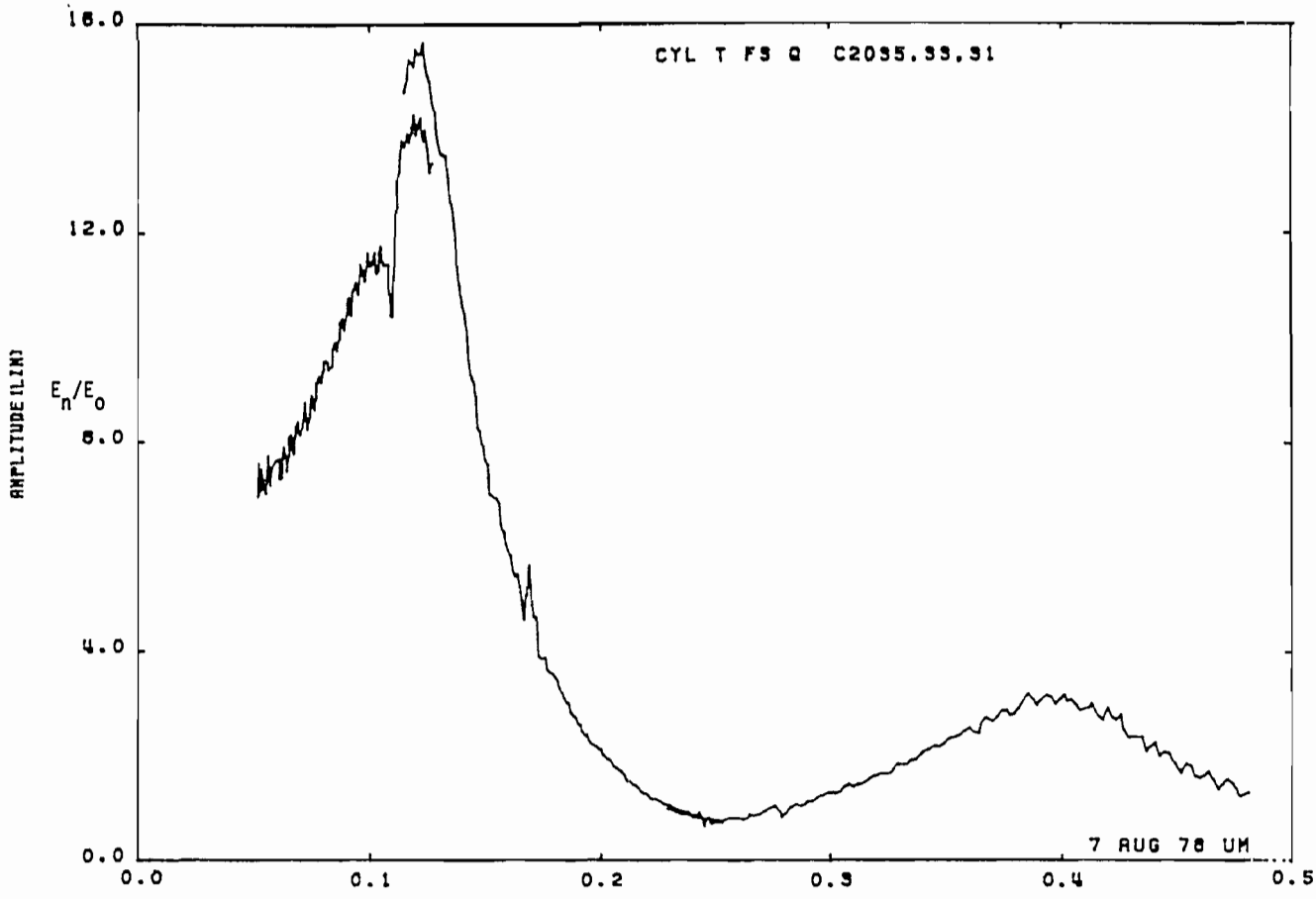

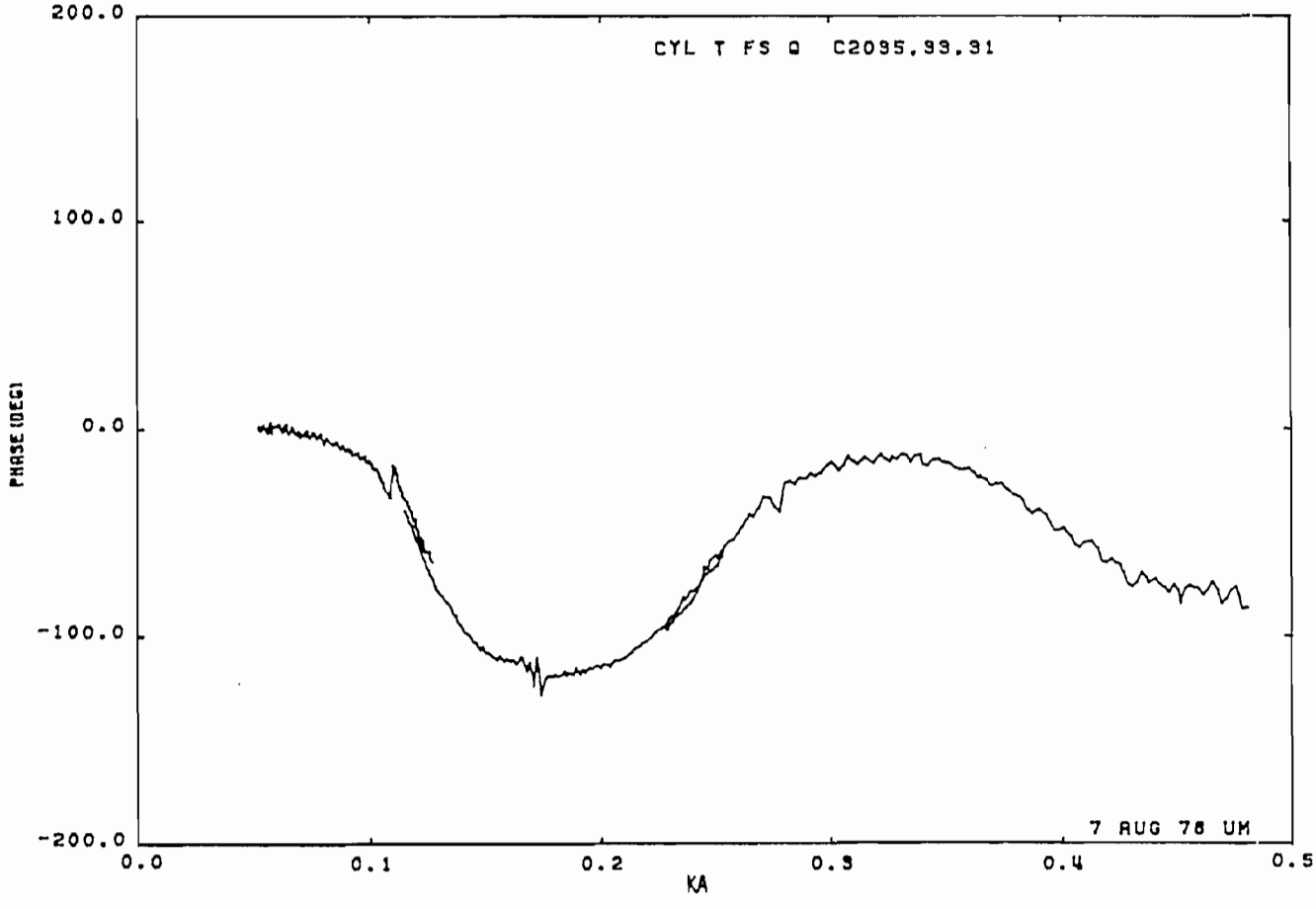

Figure 30b. Charge on cylinder at STA:T; free space (expanded scale).

3.1.2 Cylinder Near Perfectly Conducting Ground Plane

The current was measured at the back (ϕ = 180°) of the cylinder near the base (STA: +5D) and the charge at the top (STA: T) for various cylinder to ground plane spacings. The spacing h is measured from the center of the cylinder to the ground plane and is expressed in terms of the radius a. Data are presented for the full range of ka measured and in expanded form for the resonance region. Table 4 summarizes the data presented.

TABLE 4. CYLINDER NEAR PERFECTLY CONDUCTING GROUND PLANE

h	J. STA: +5D	Q, STA: T
1.5a	Figure 31	Figure 37
2a	32	38
5a	33	39
10a	34	40
20a	35	41
40a	36	42

Each figure has two parts:

a) amplitude and phase, full plot

b) amplitude and phase, expanded plot

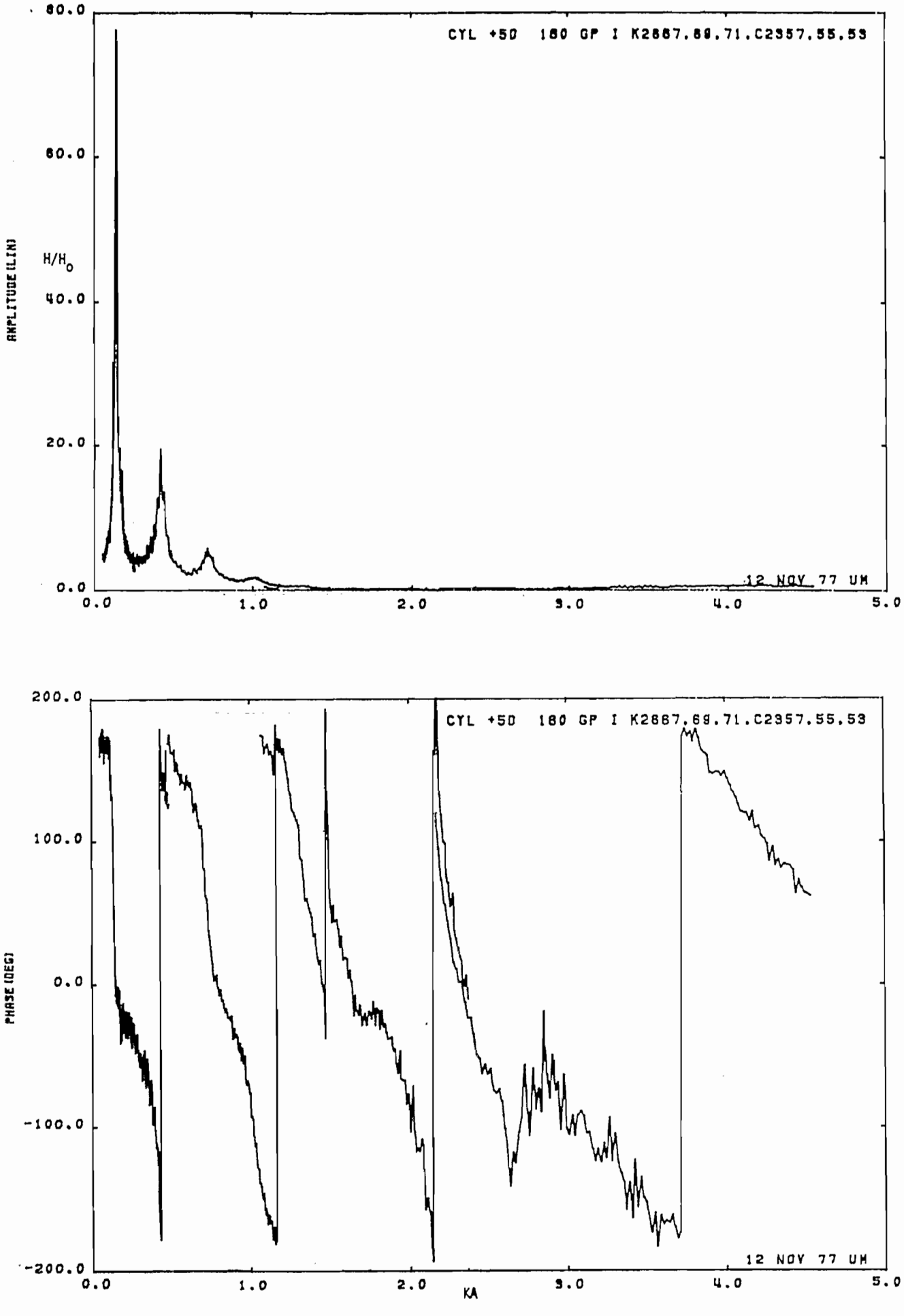

Figure 31a. Currention cylinder at STA:+5D; ϕ = 180°, h = 1.5a, near perfectly conducting ground plane.

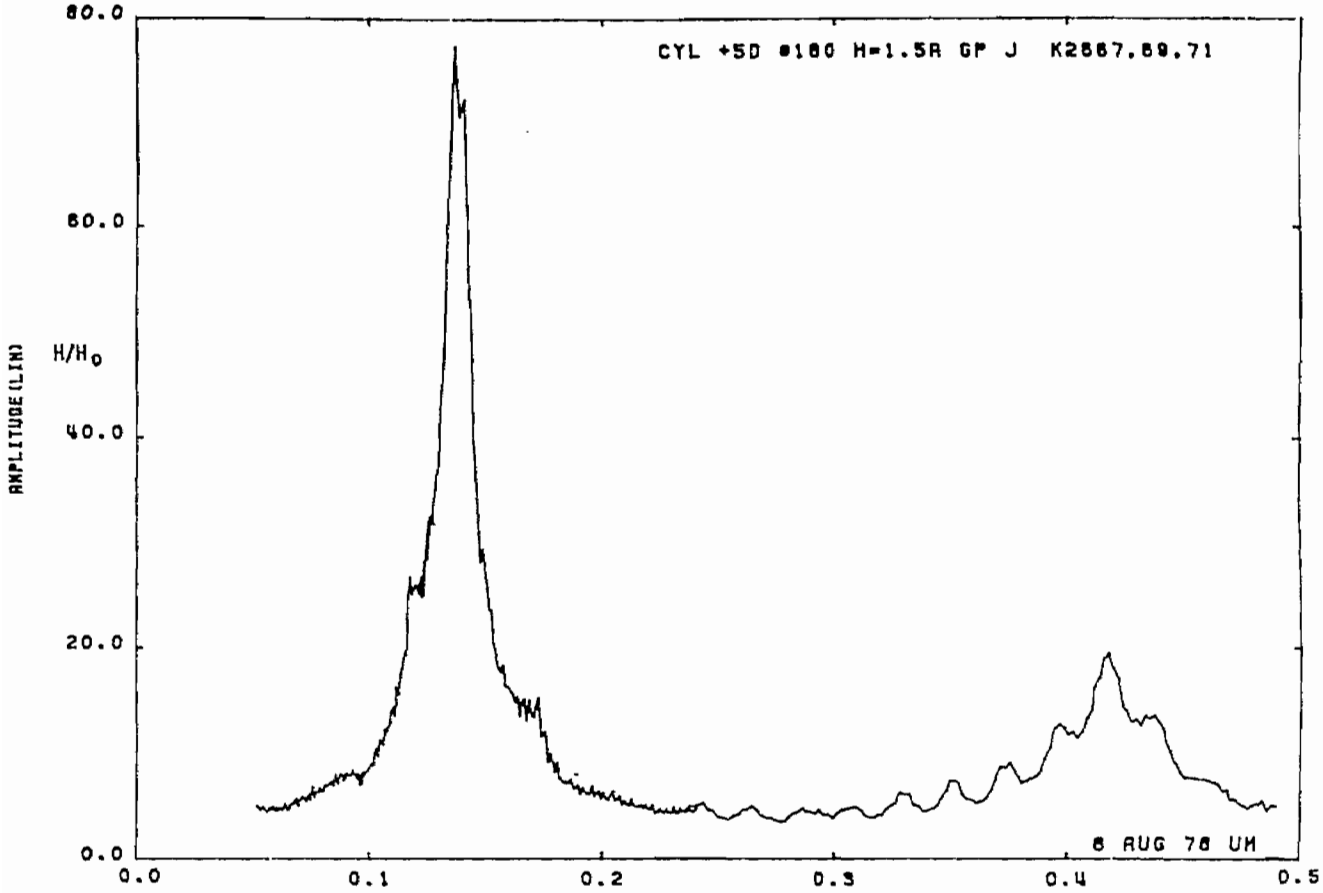

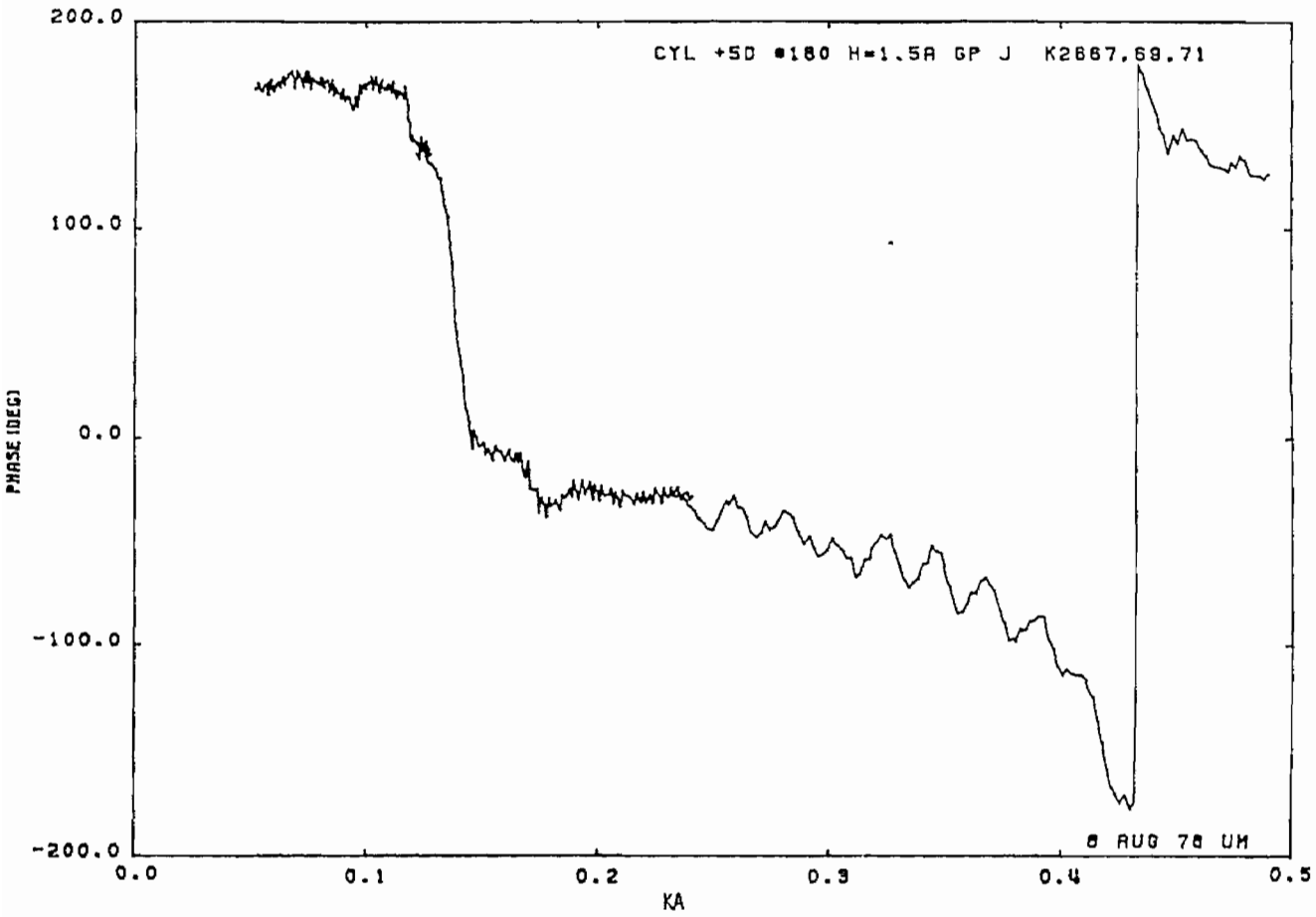

Figure 31b. Current on cylinder at STA:+5D; ϕ = 180°, h = 1.5a, near perfectly conducting ground plane (expanded scale).

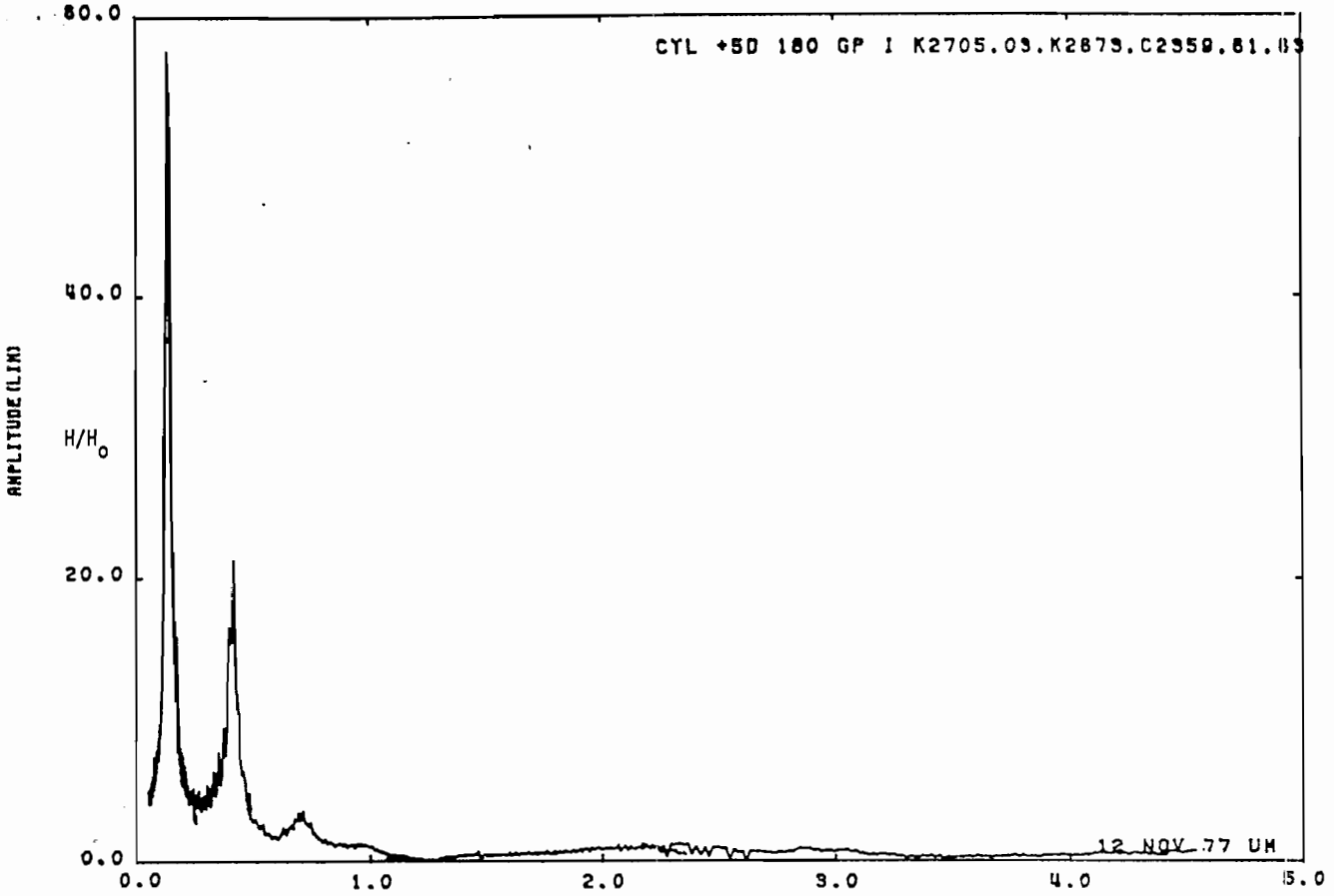

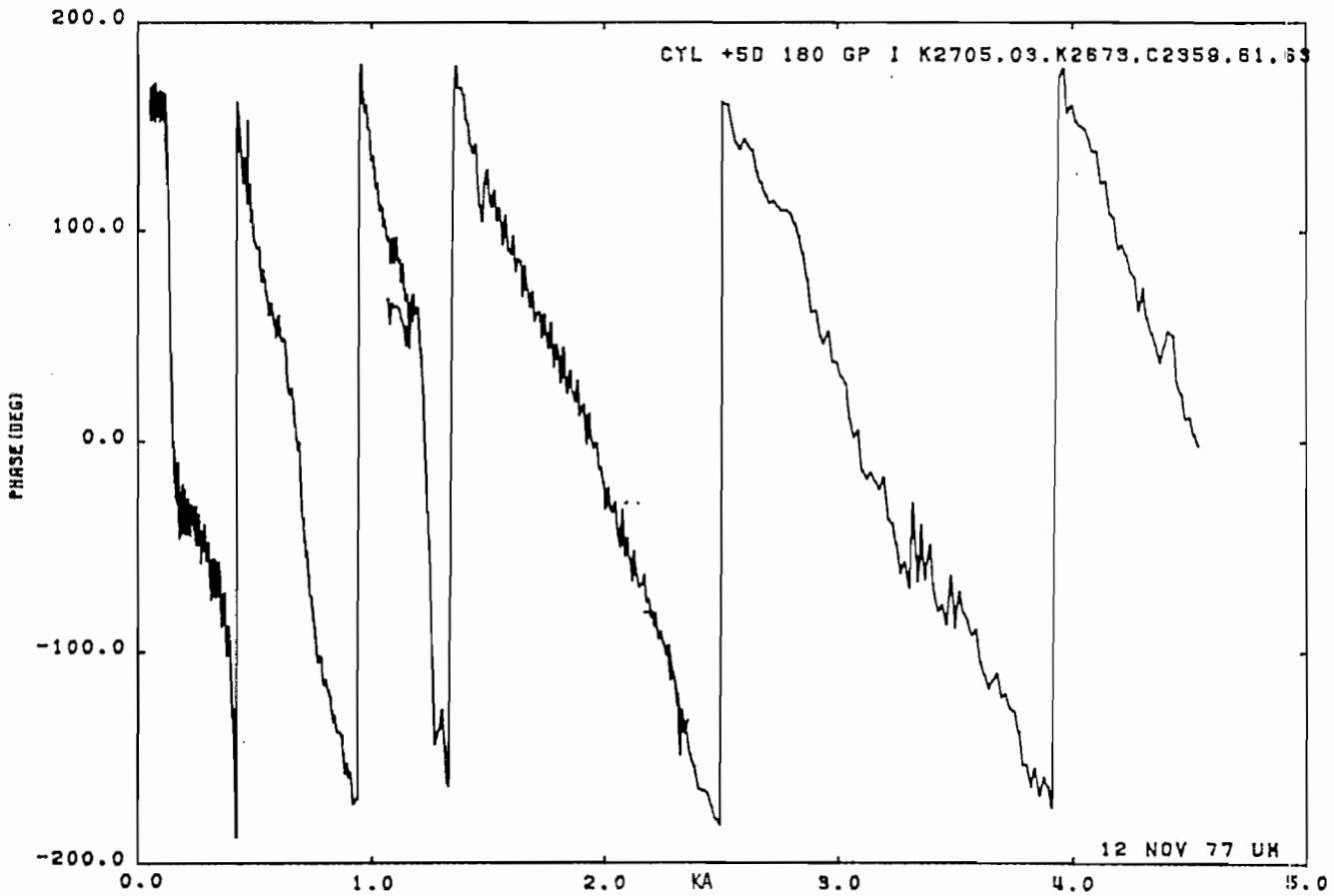

Figure 32a. Current on cylinder at STA:+5D; Ø = 180°, h = 2a, near perfectly conducting ground plane.

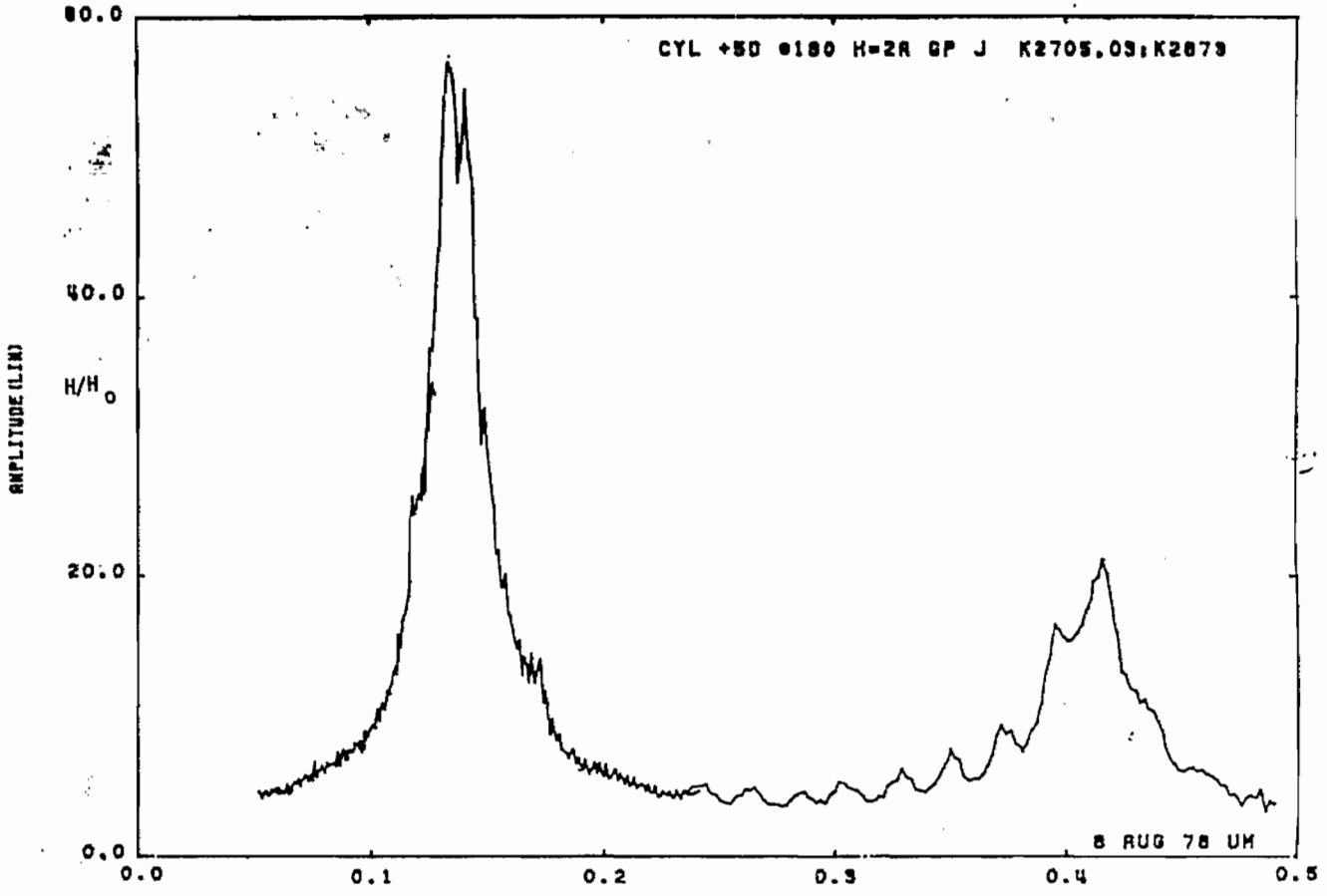

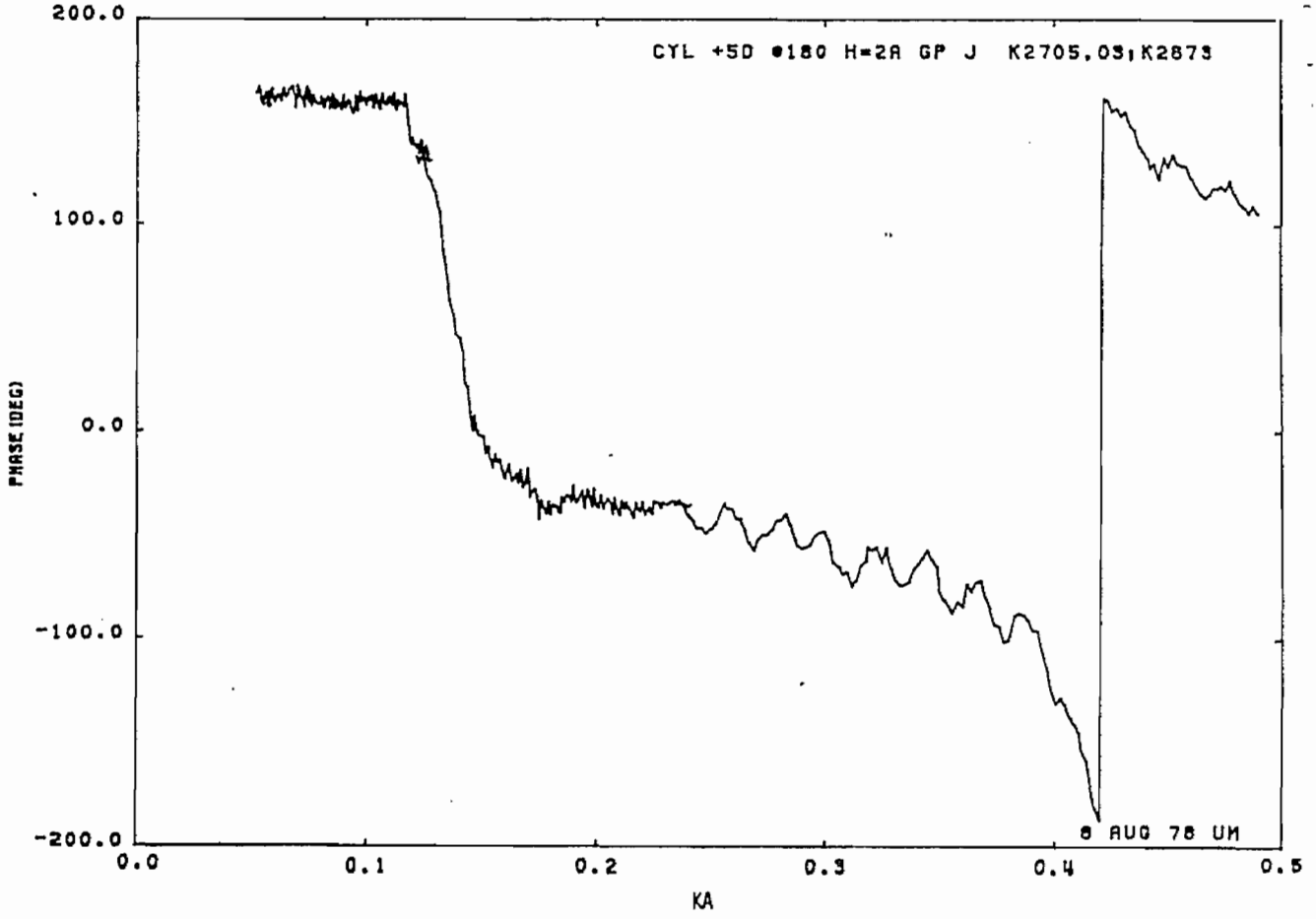

Figure 32b. Current on cylinder at STA:+5D; $\beta = 180°$, h = 2a, near perfectly conducting ground plane (expanded scale).

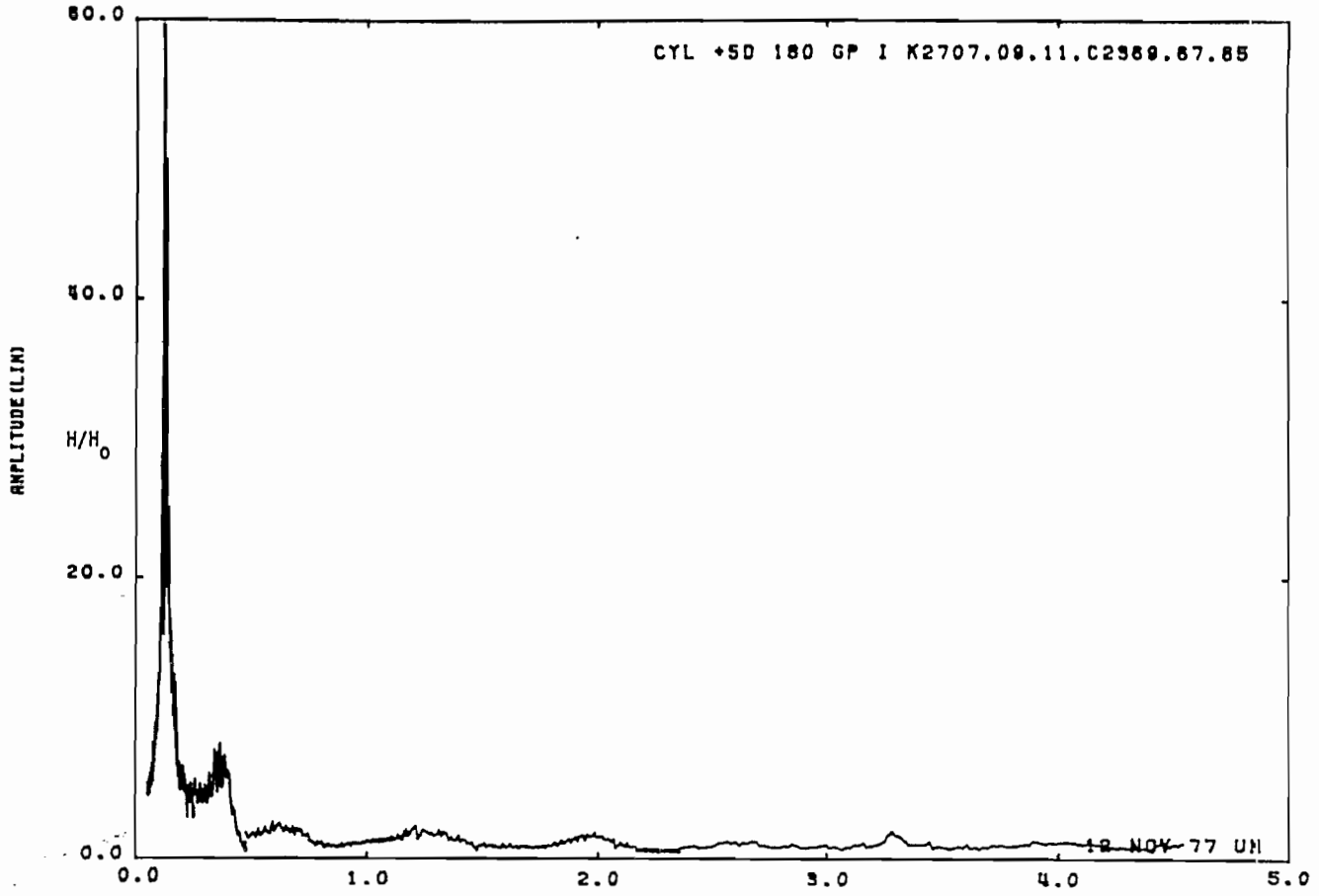

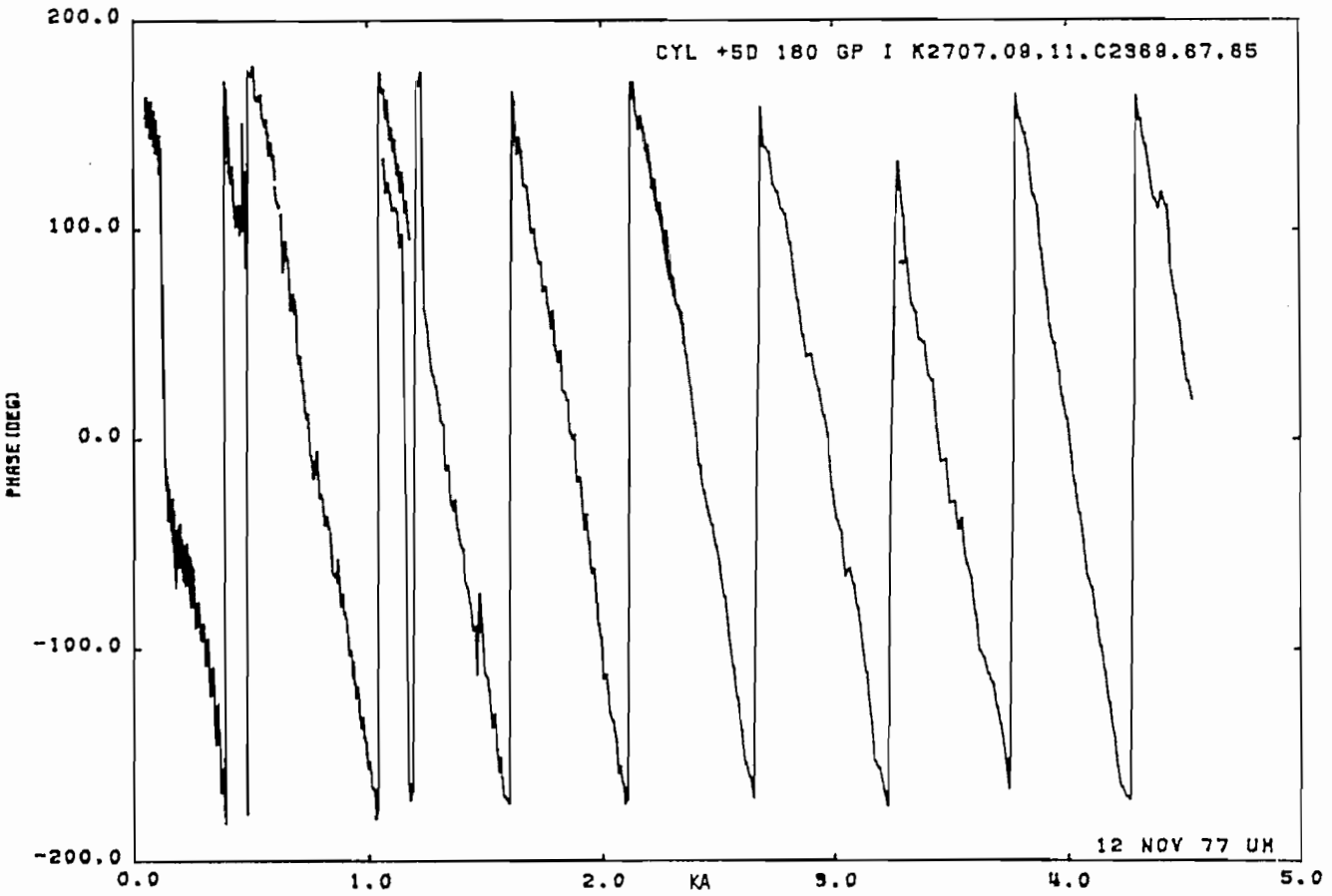

Figure 33a. Current on cylinder at STA:+5D; ϕ = 180°, h = 5a, near perfectly conducting ground plane.

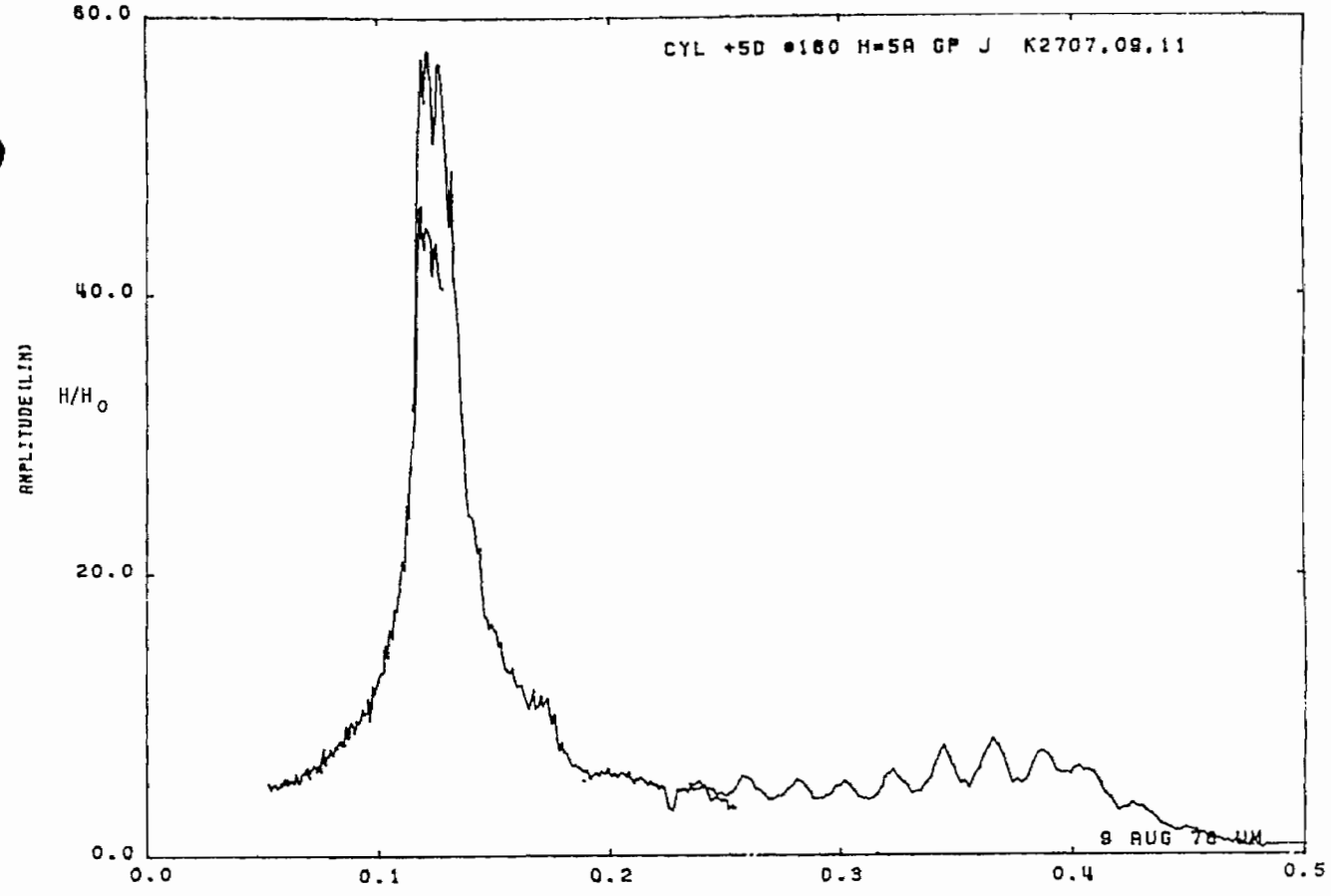

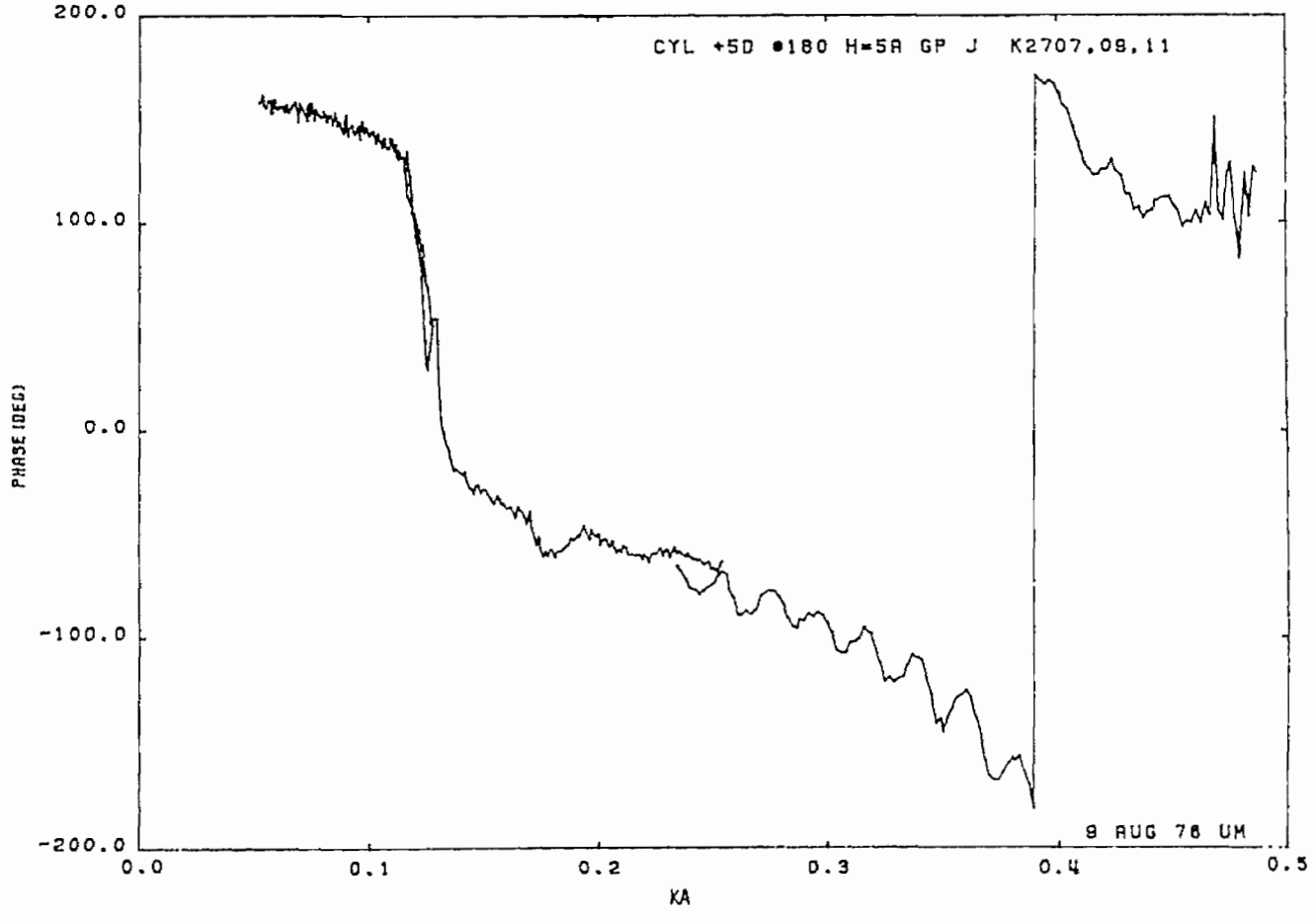

Figure 33b. Current on cylinder at STA:+5D; ø = 180°, h = 5a, near perfectly conducting ground plane (expanded scale).

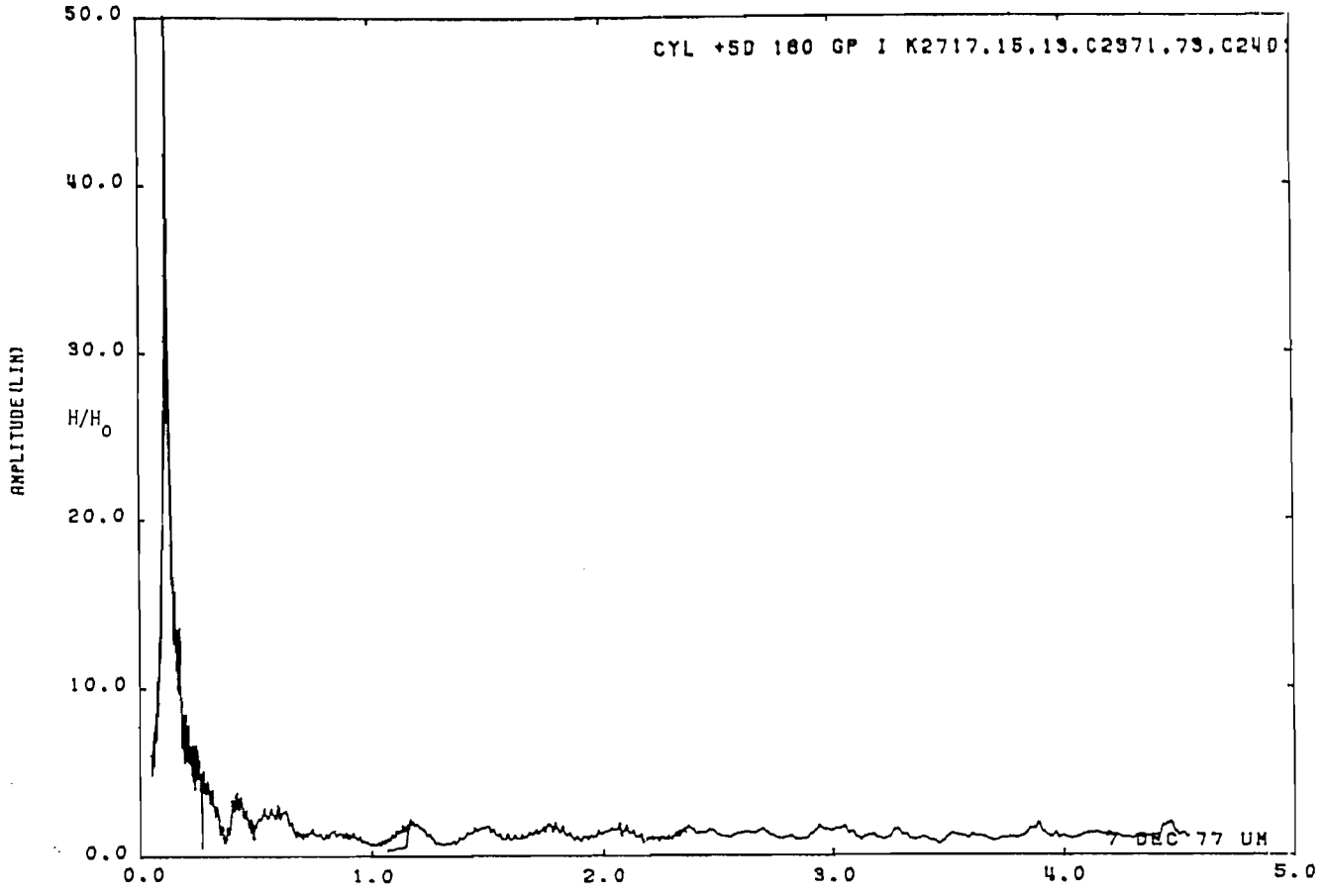

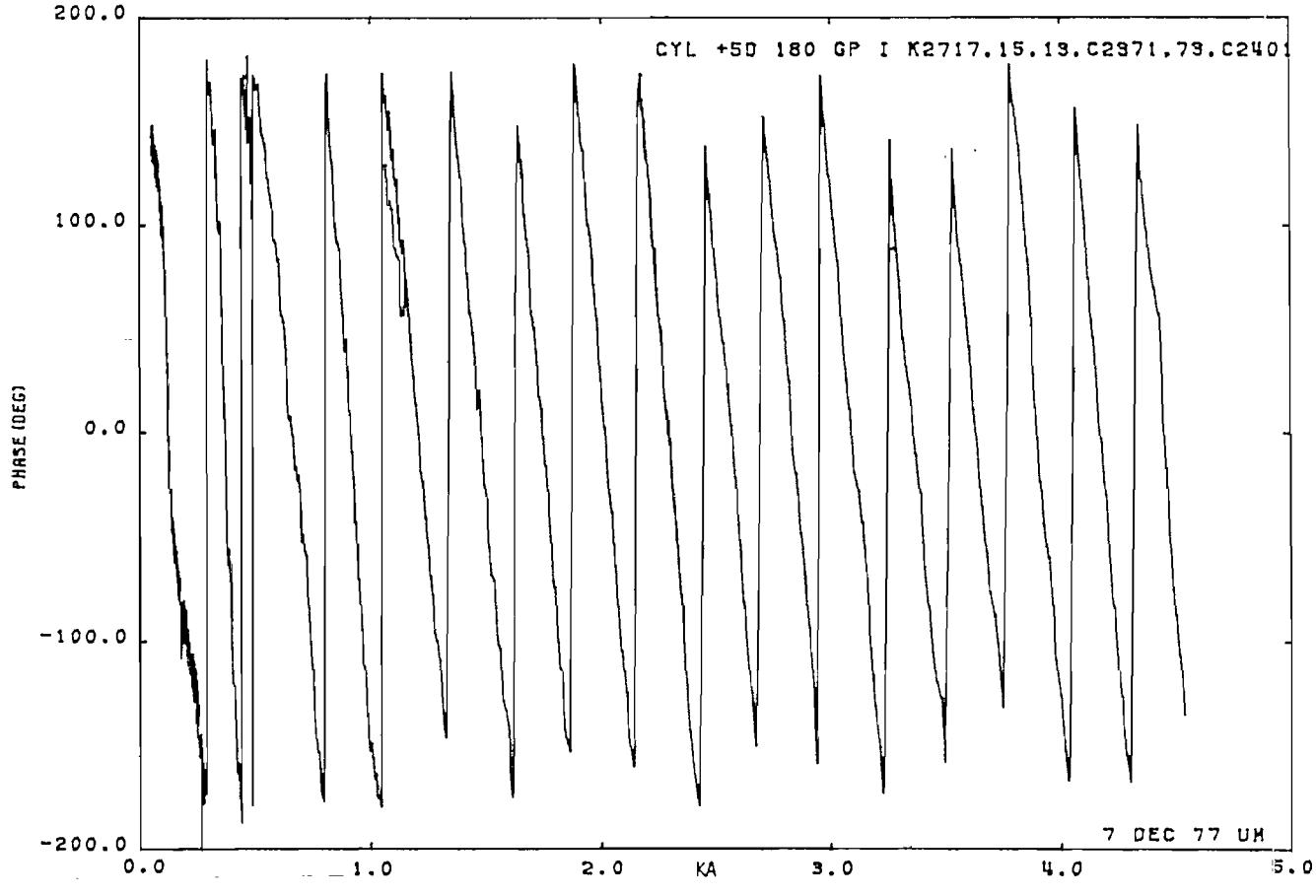

Figure 34a. Current on cylinder at STA:+5D; Ø = 180°, h = 10a, near perfectly conducting ground plane.

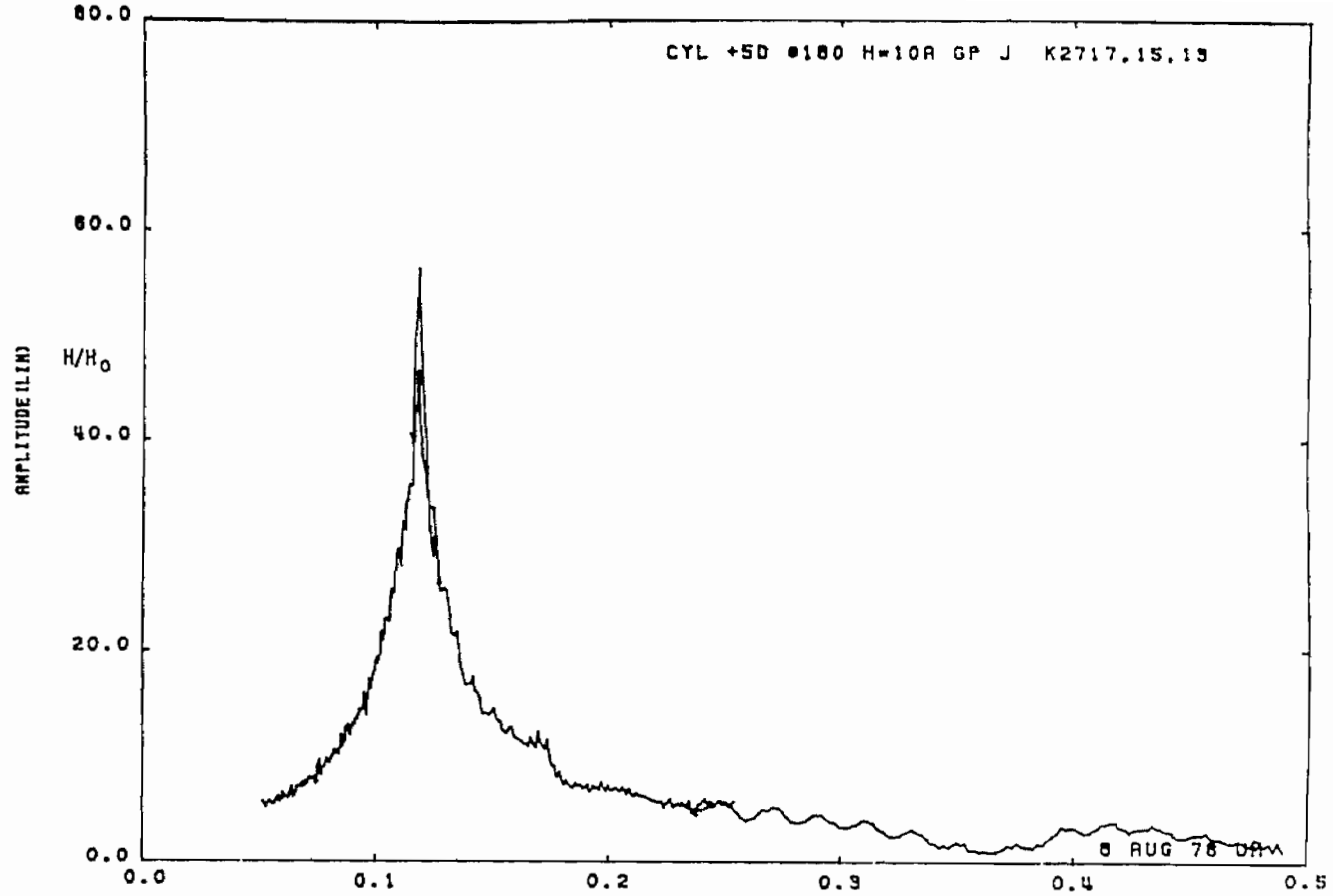

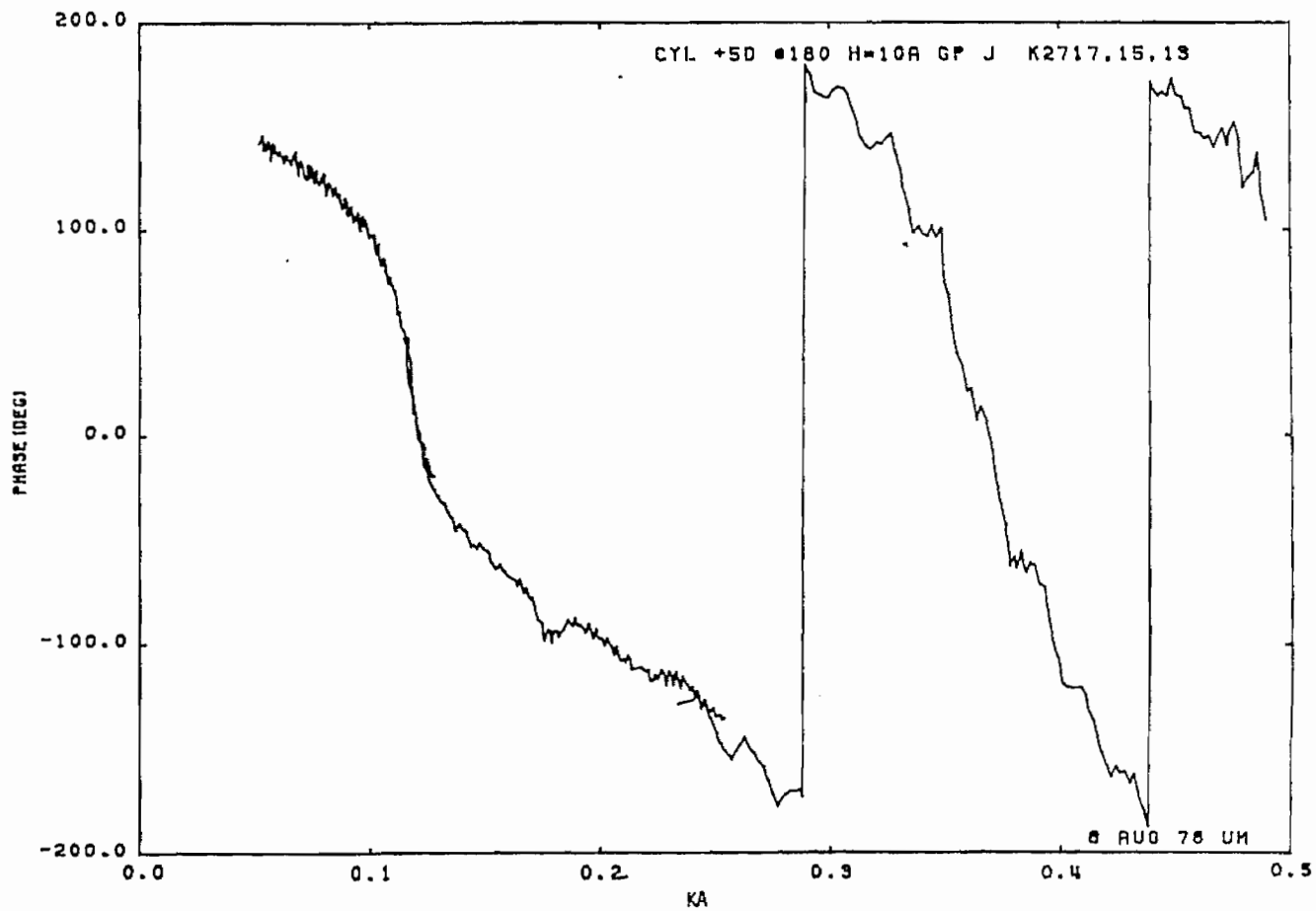

Figure 34b. Current on cylinder at STA:+5D; ø = 180°, h = 10a, near perfectly conducting ground plane (expanded scale).

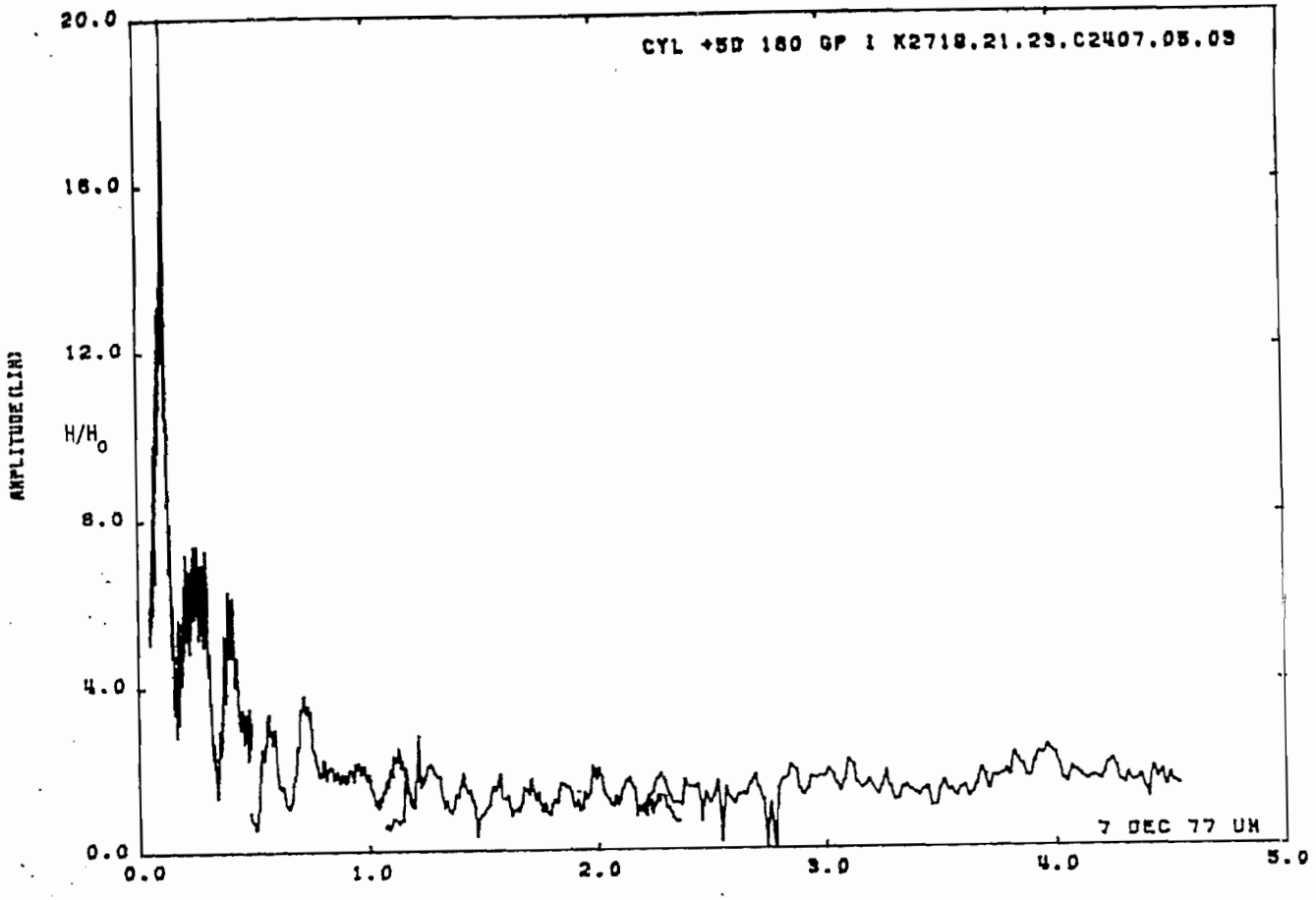

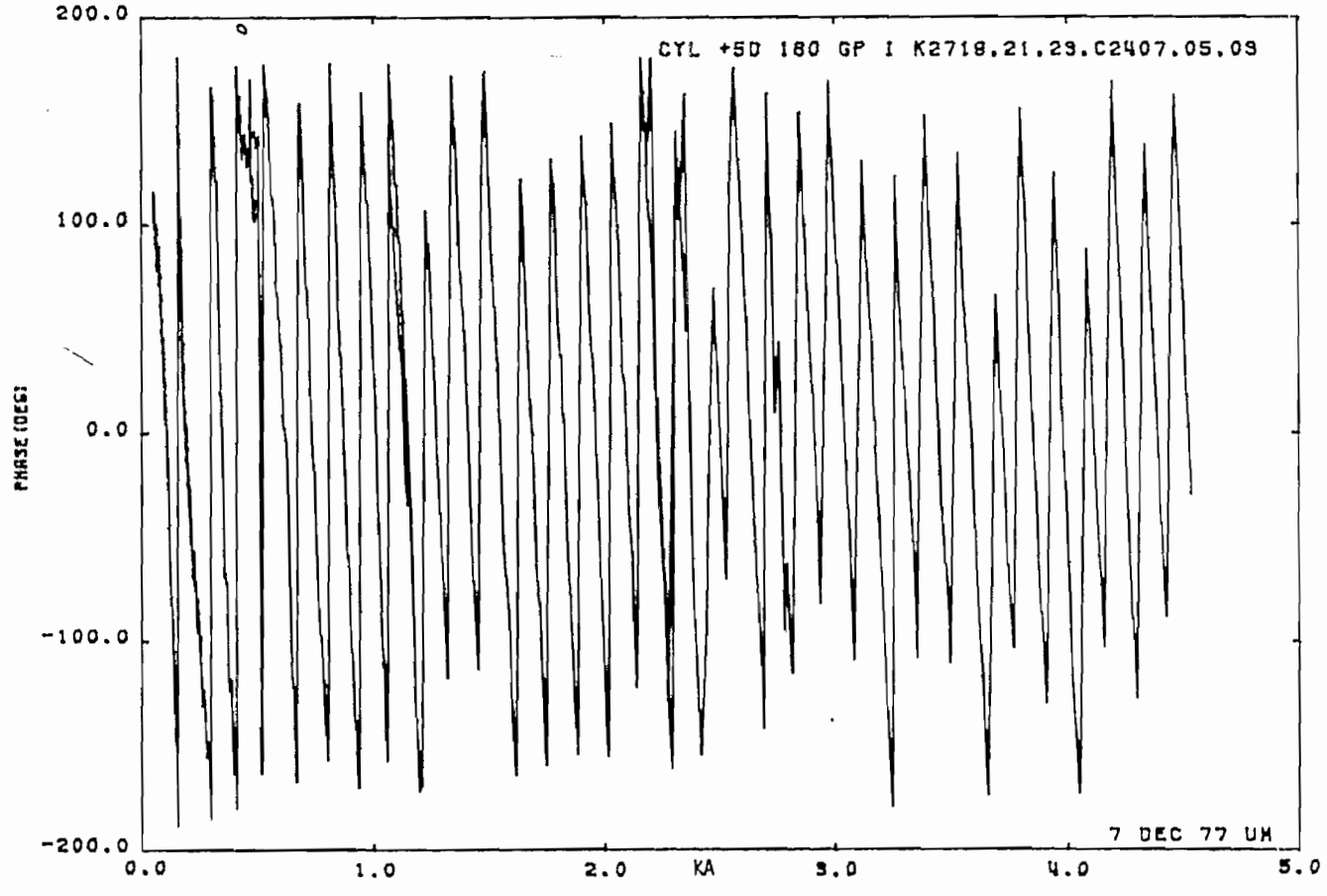

Figure 35a. Current on cylinder at STA:+5D; Ø = 180°, h = 20a, near perfectly conducting ground plane.

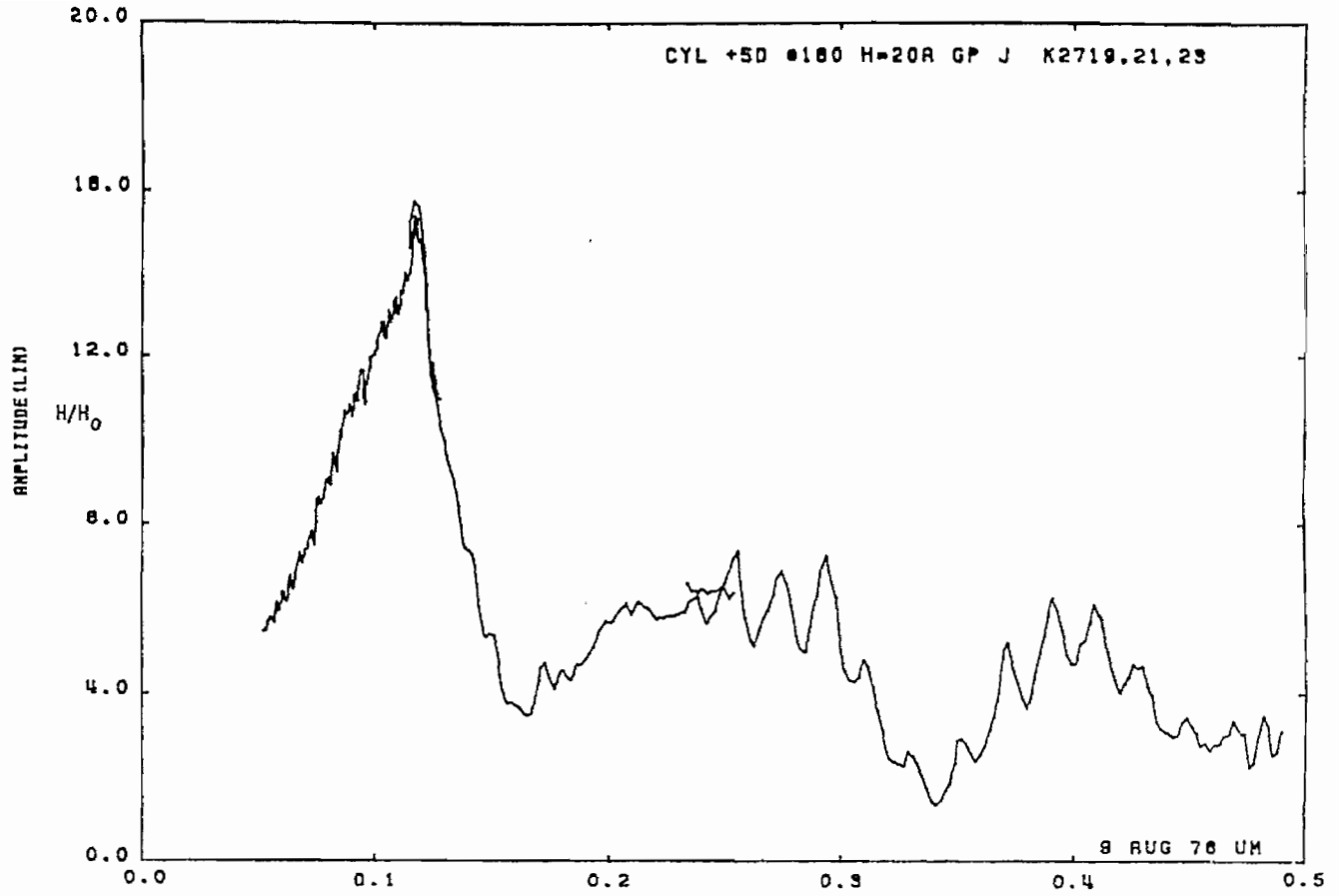

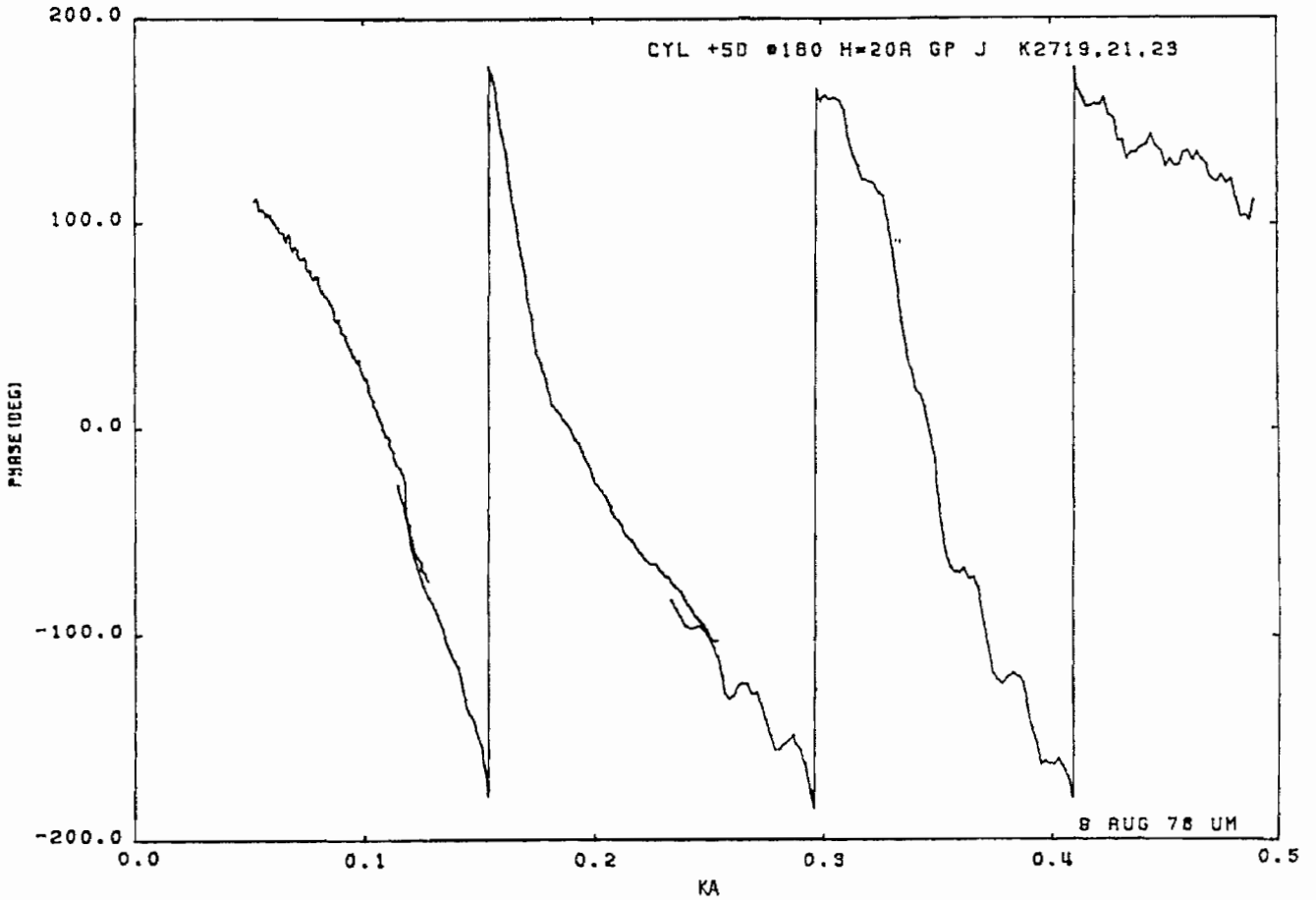

Figure 35b. Current cylinder at STA:+5D; ø = 180°, h = 20a, near perfectly conducting ground plane (expanded scale).

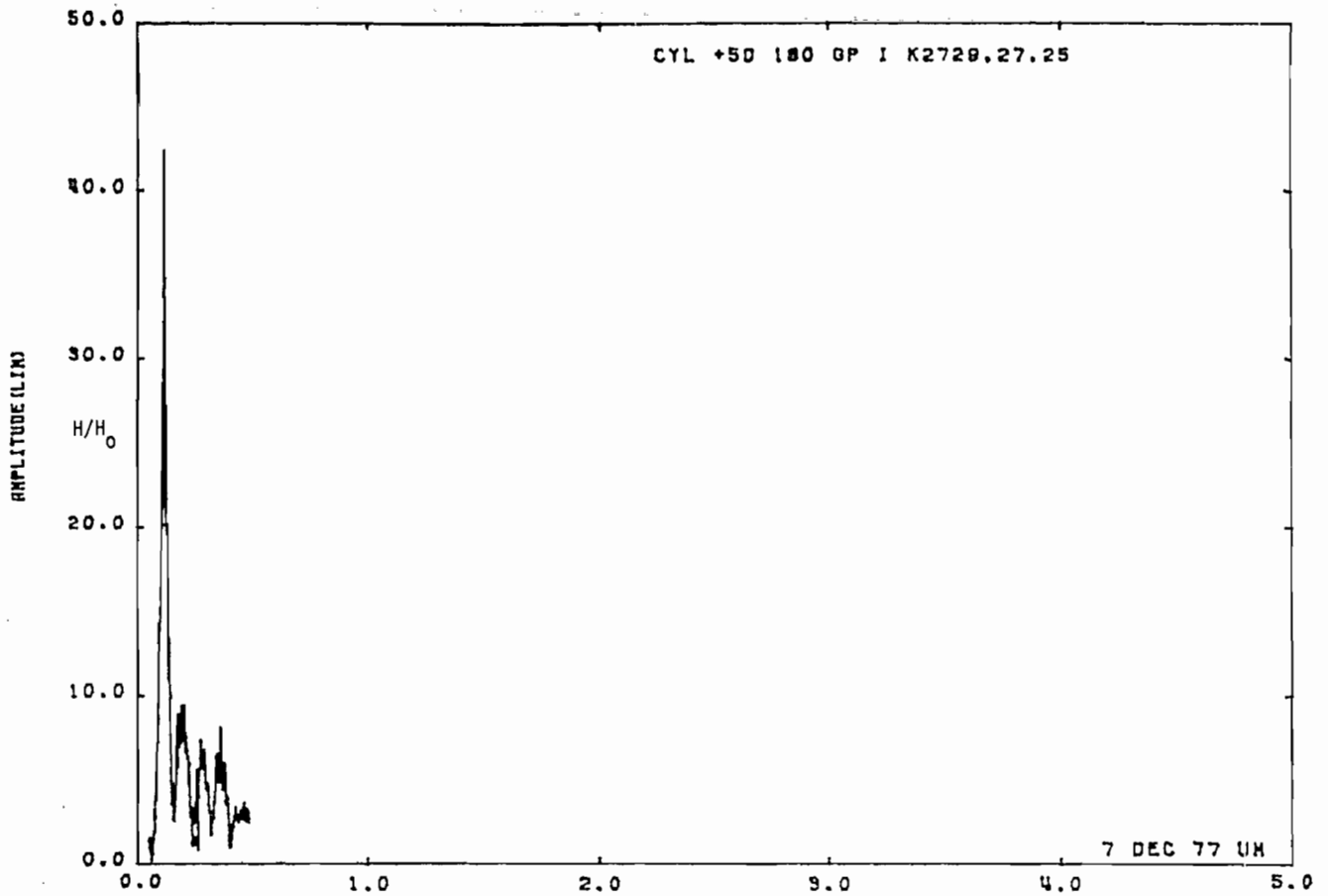

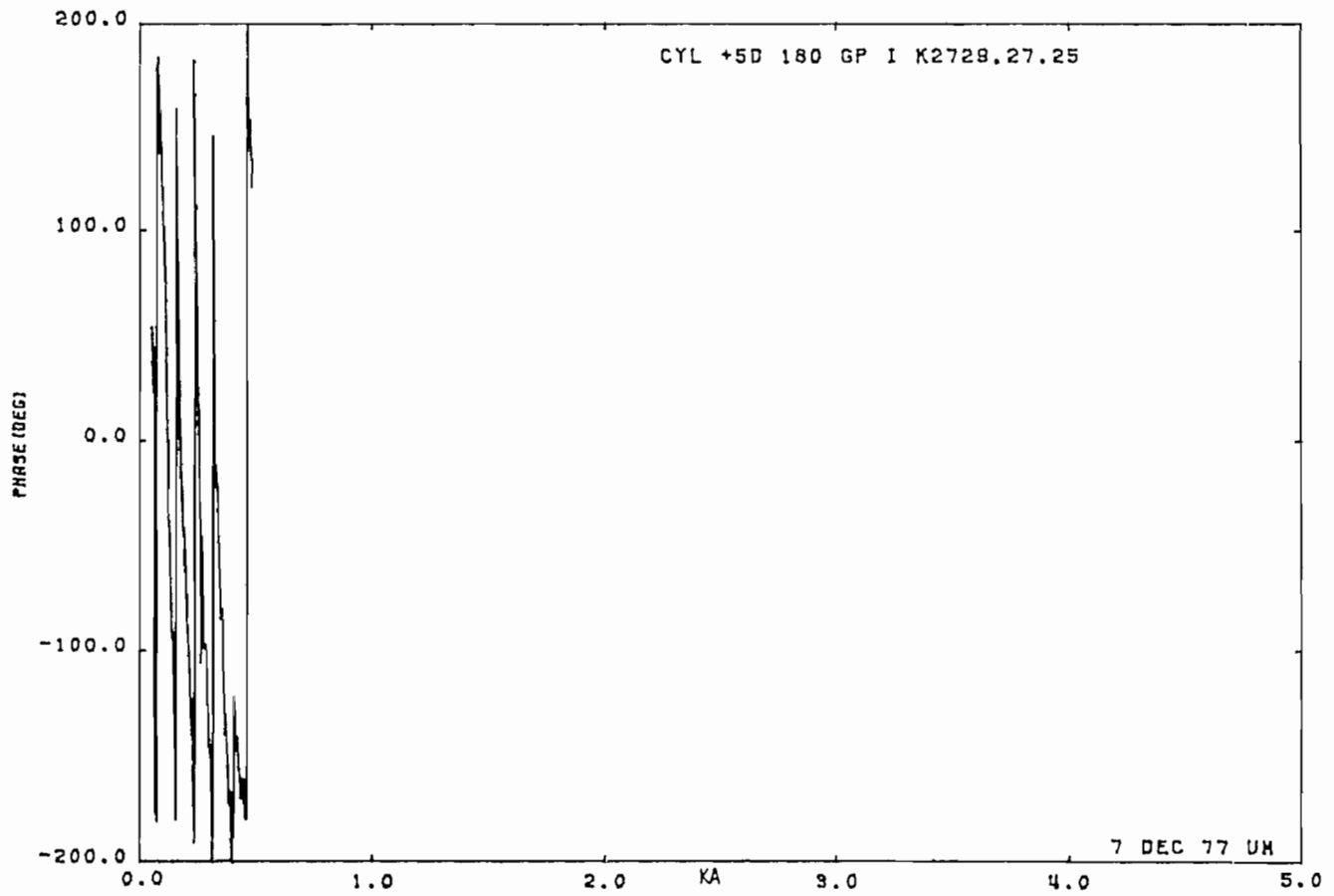

Figure 36a. Current on cylinder at STA:+5D; ϕ = 180°, h = 40a, near perfectly conducting ground plane.

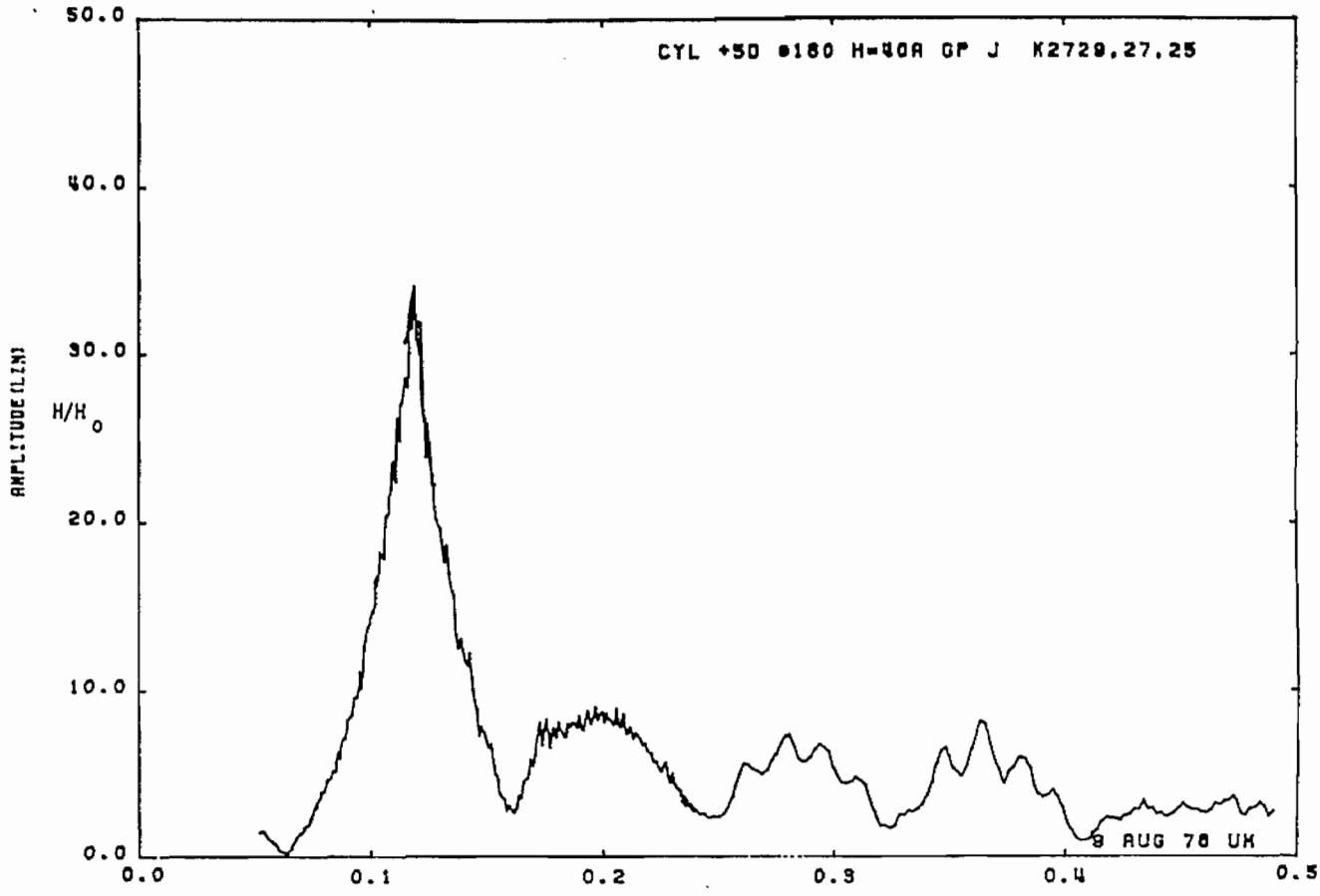

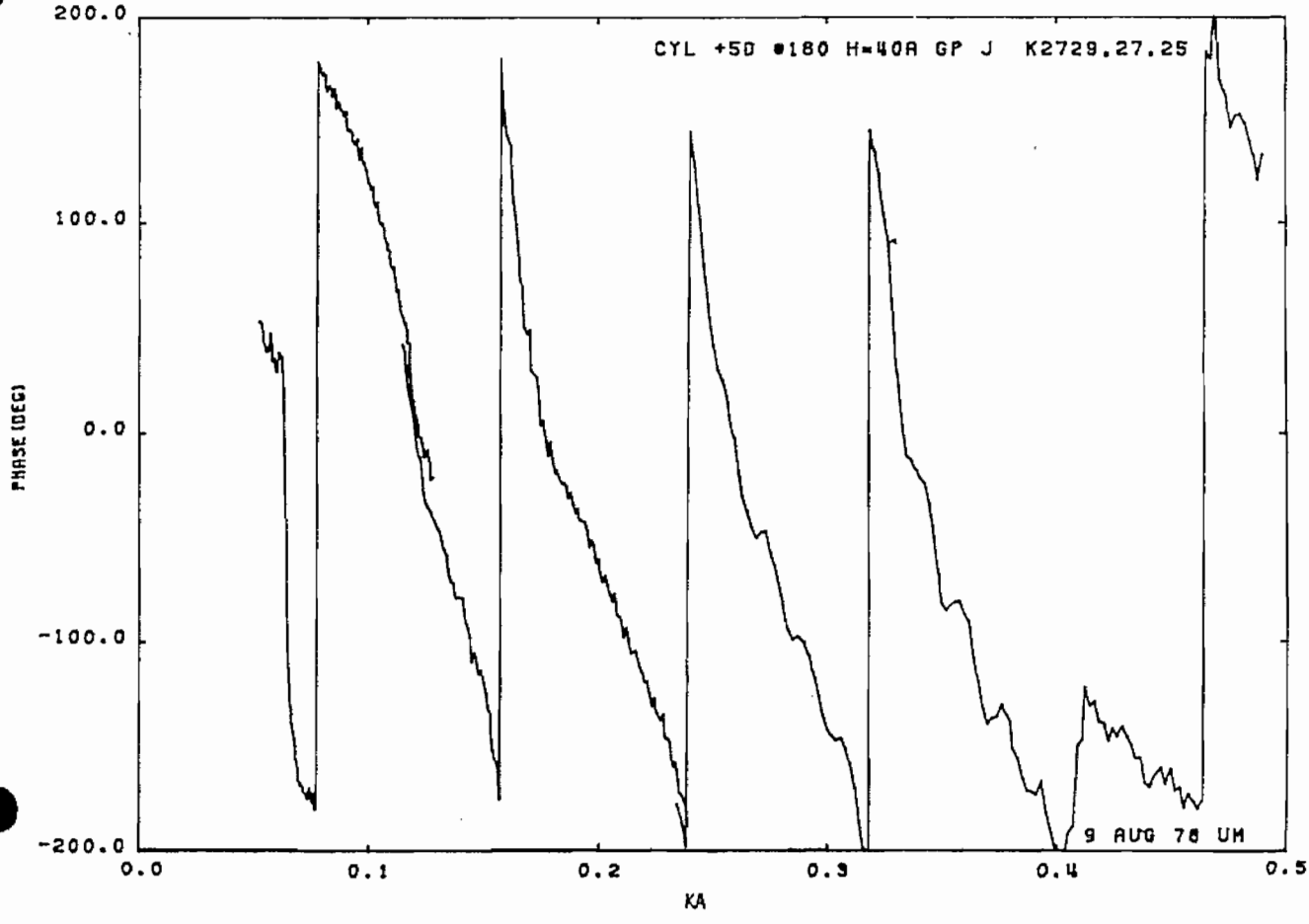

Figure 36b. Current on cylinder at STA:+5D; β = 180°, h = 40a, near perfectly conducting ground plane (expanded scale).

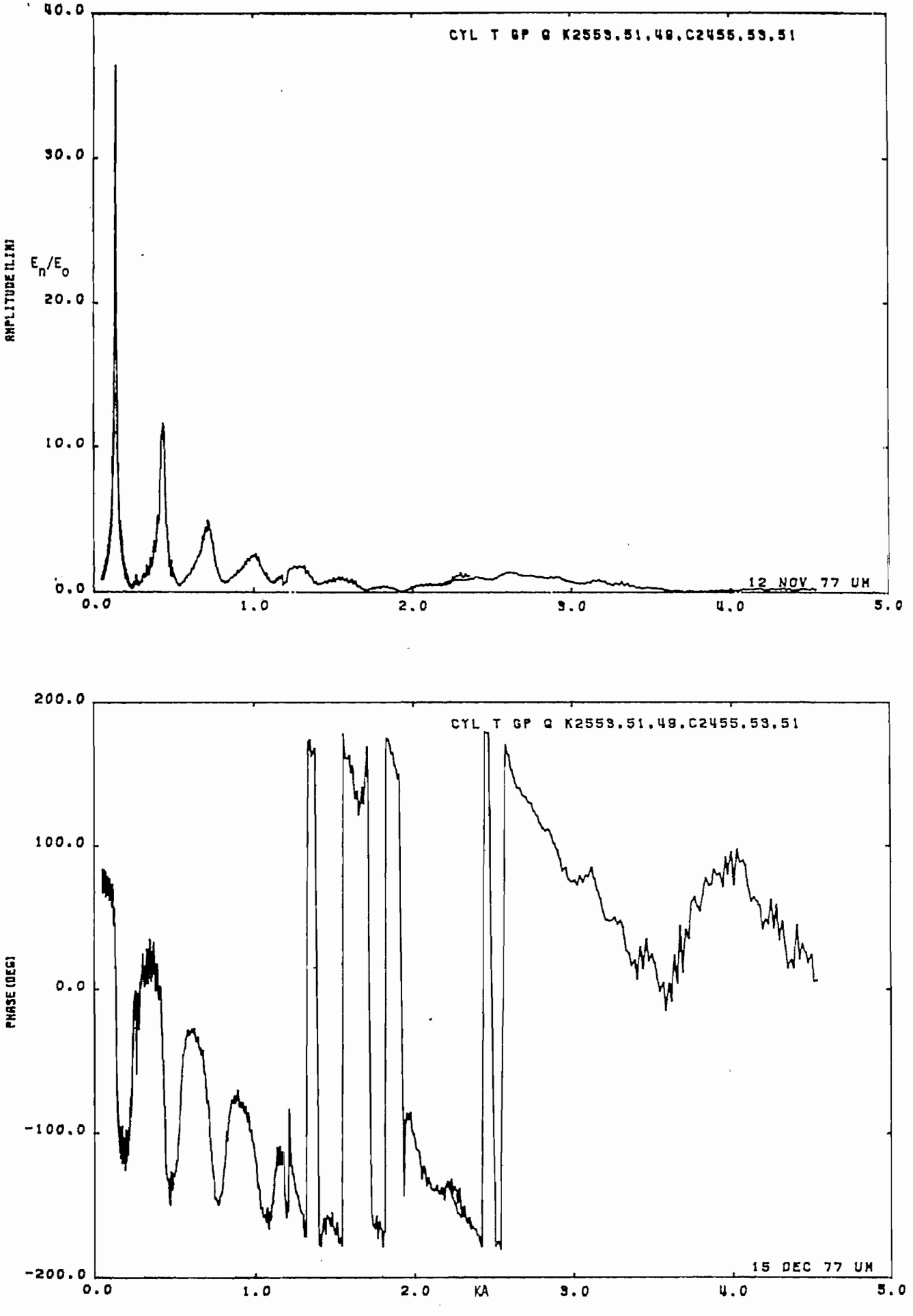

Figure 37a. Charge on cylinder at STA:T; h = 1.5a, near perfectly conducting ground plane.

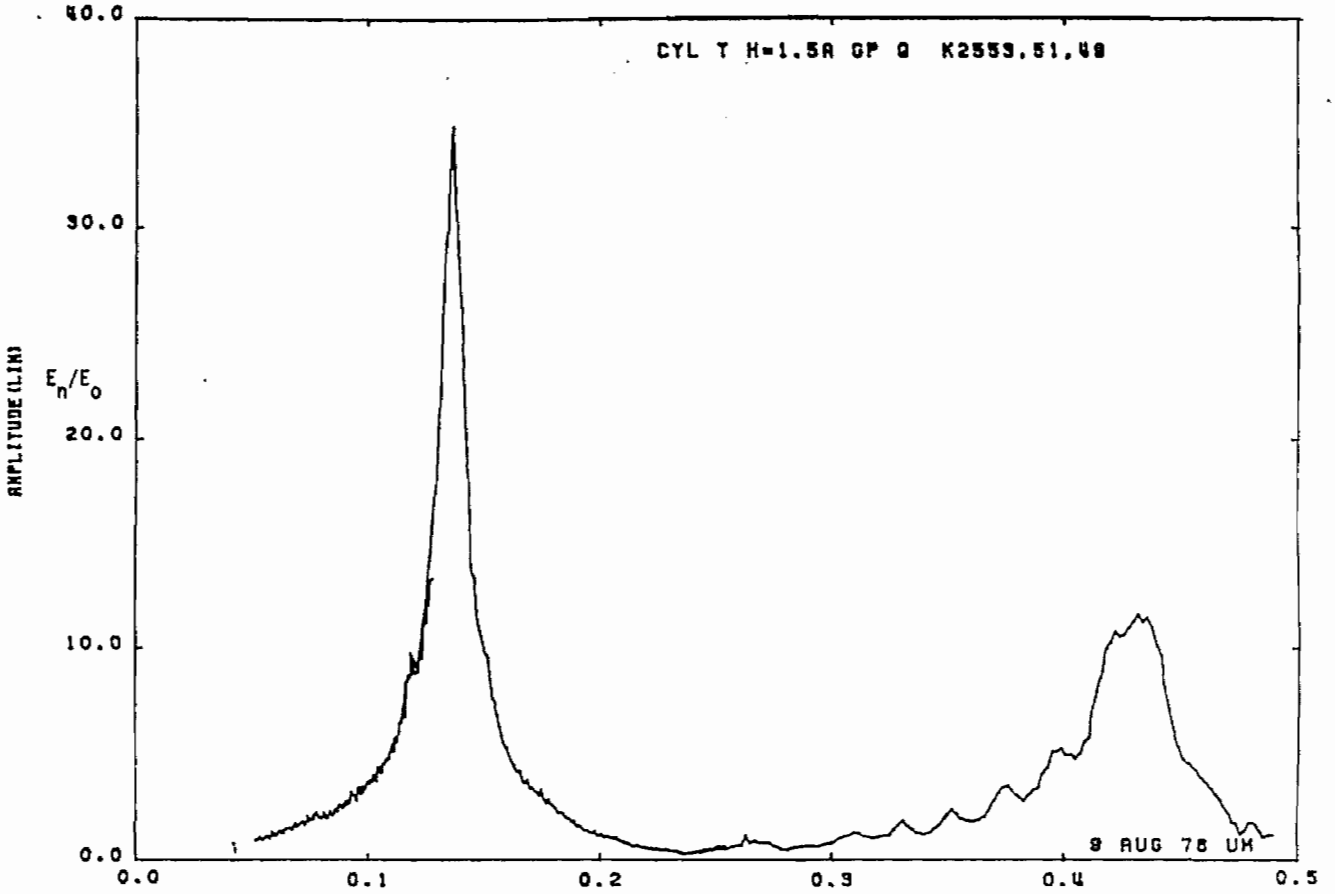

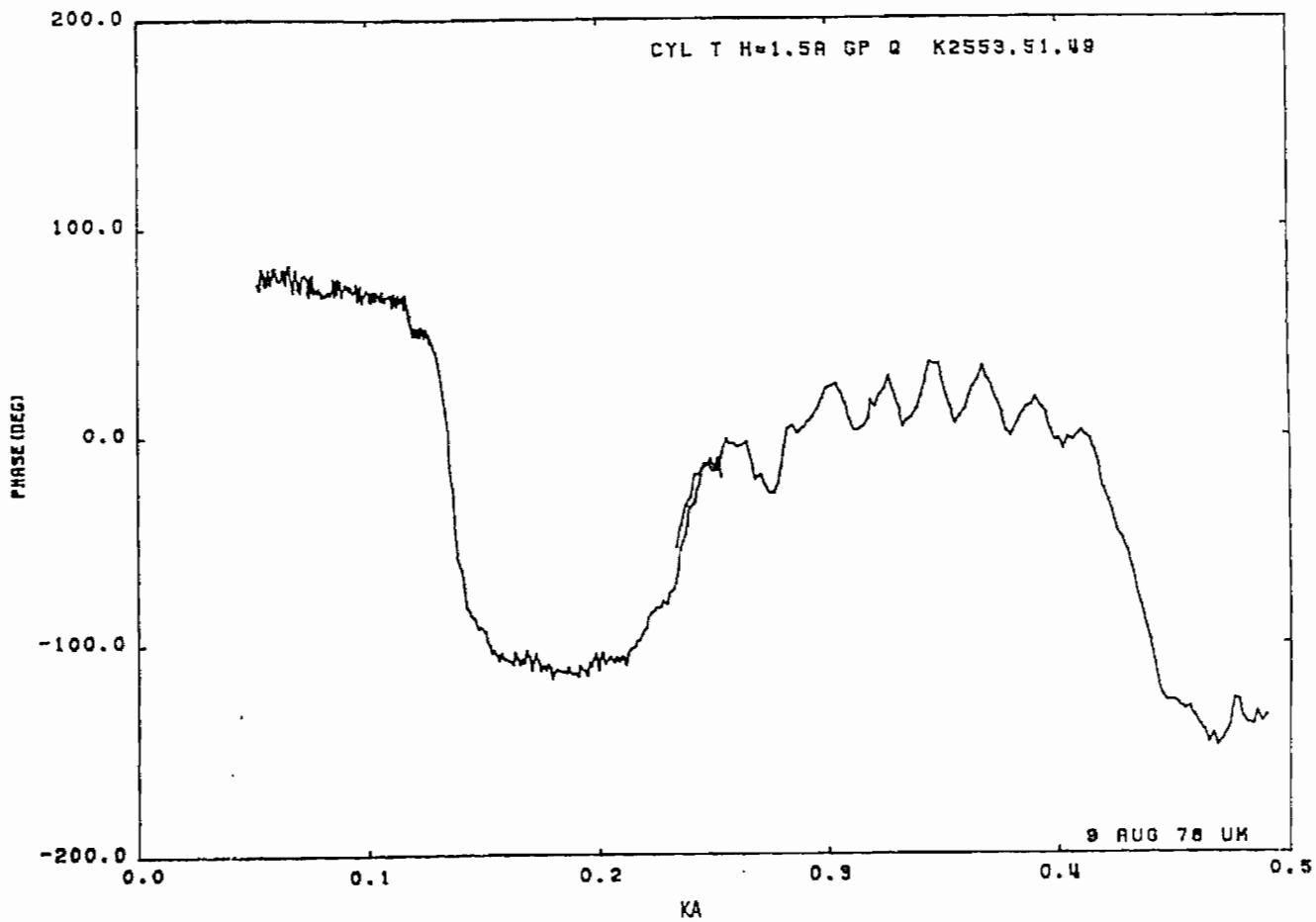

Figure 37b. Charge on cylinder at STA:T; h = 1.5a, near perfectly conducting ground plane (expanded scale).

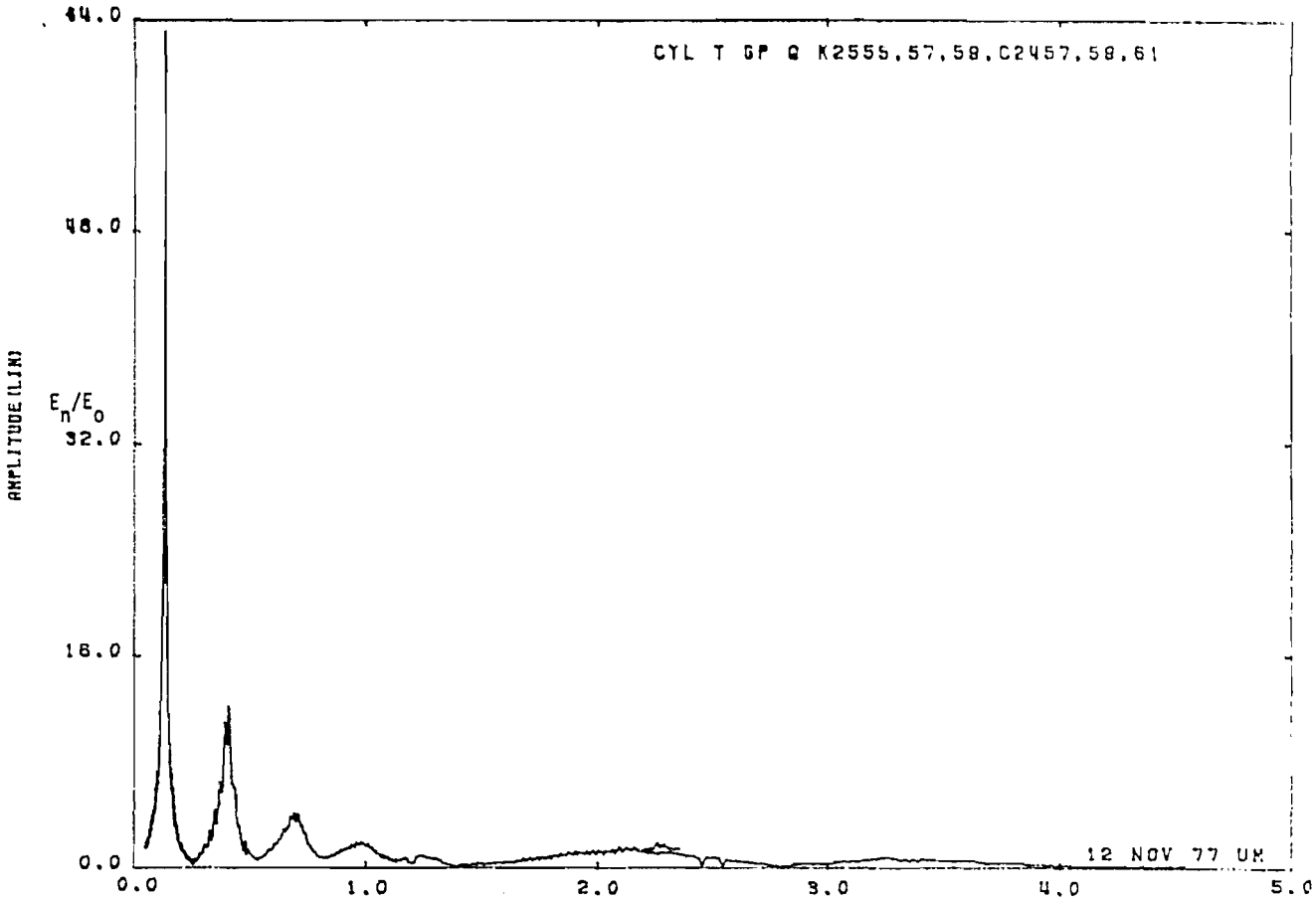

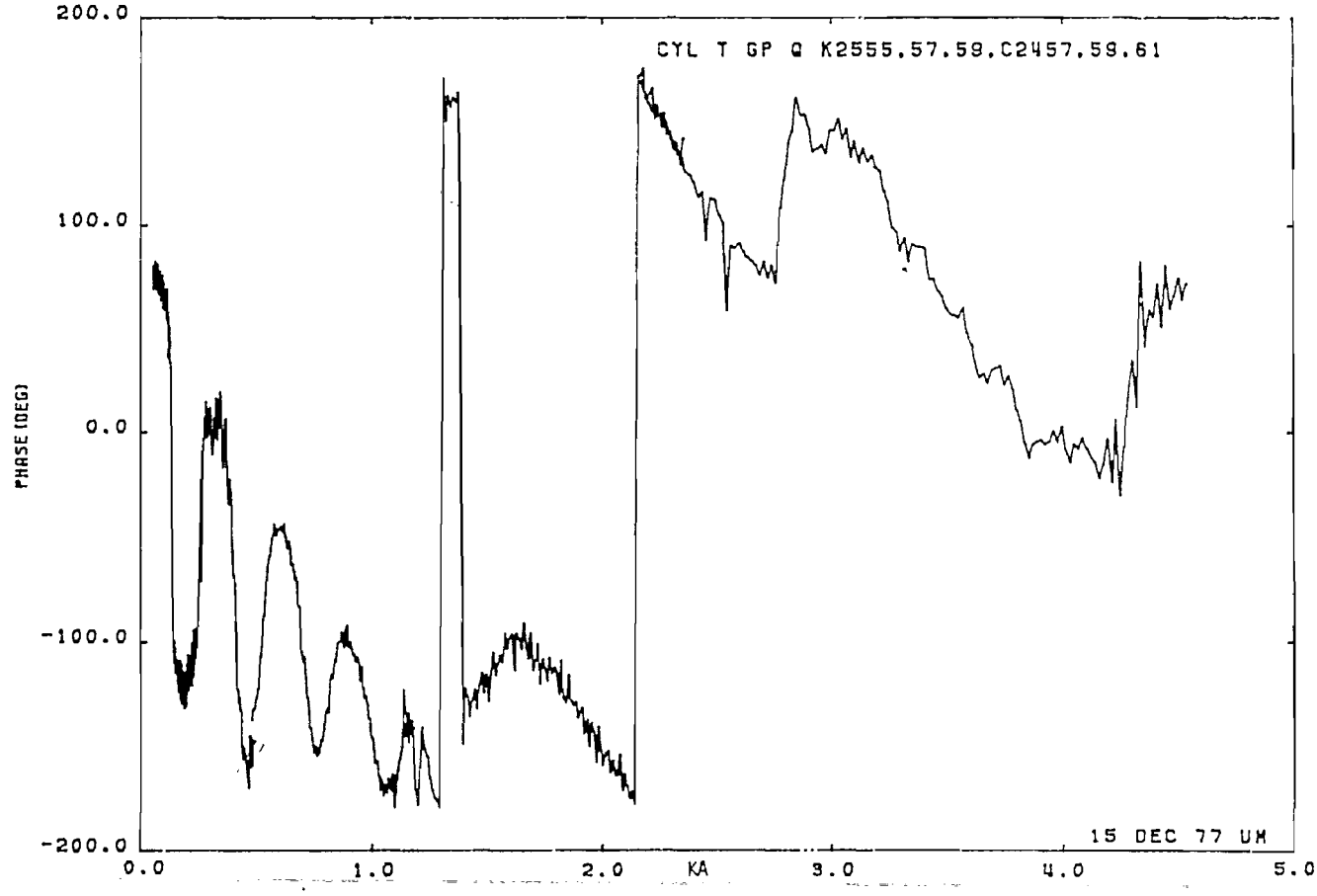

Figure 38a. Charge on cylinder at STA:T; h = 2a, near perfectly conducting ground plane.

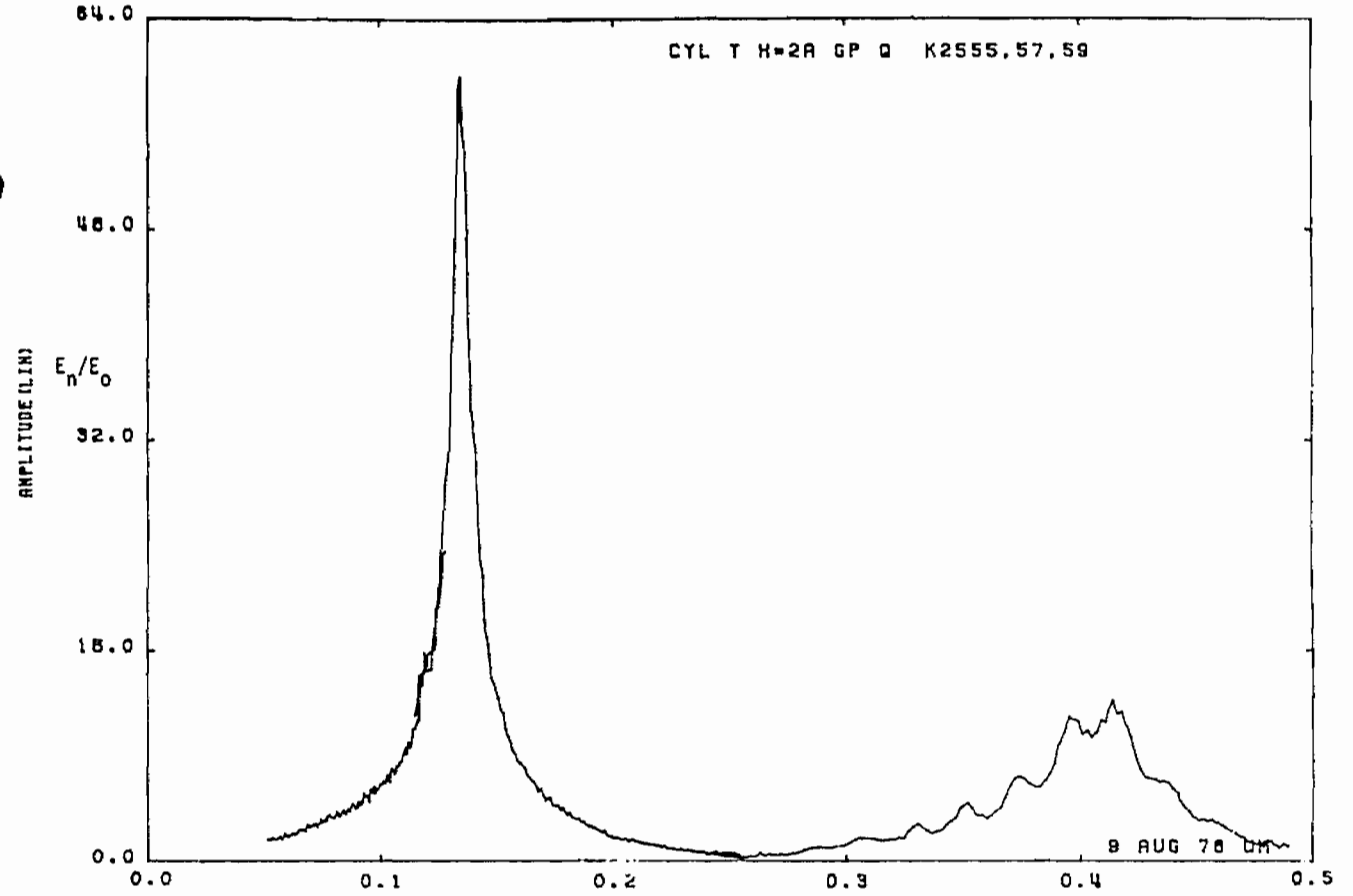

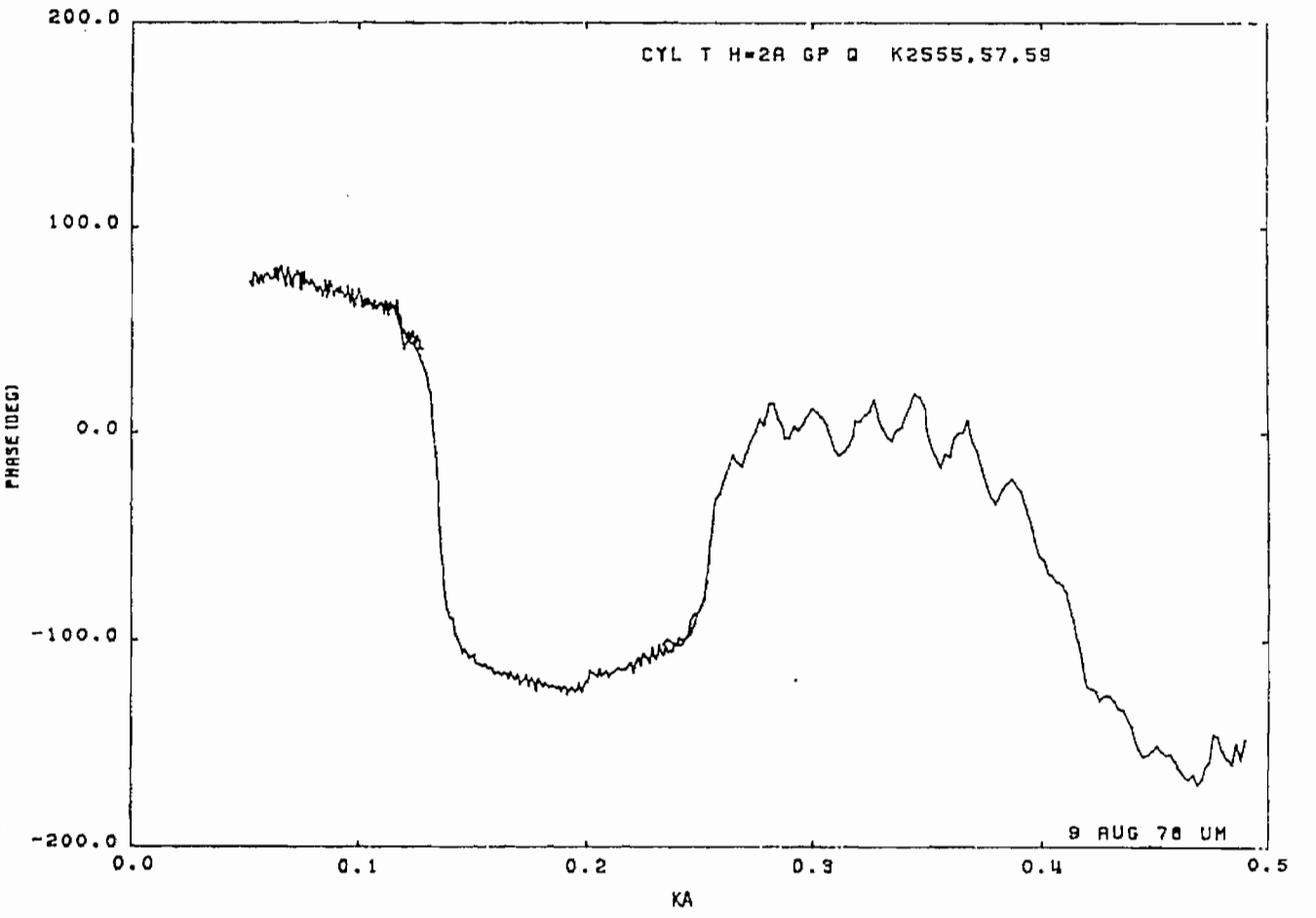

Figure 38b. Charge on cylinder at STA:T; h = 2a, near perfectly conducting ground plane (expanded scale).

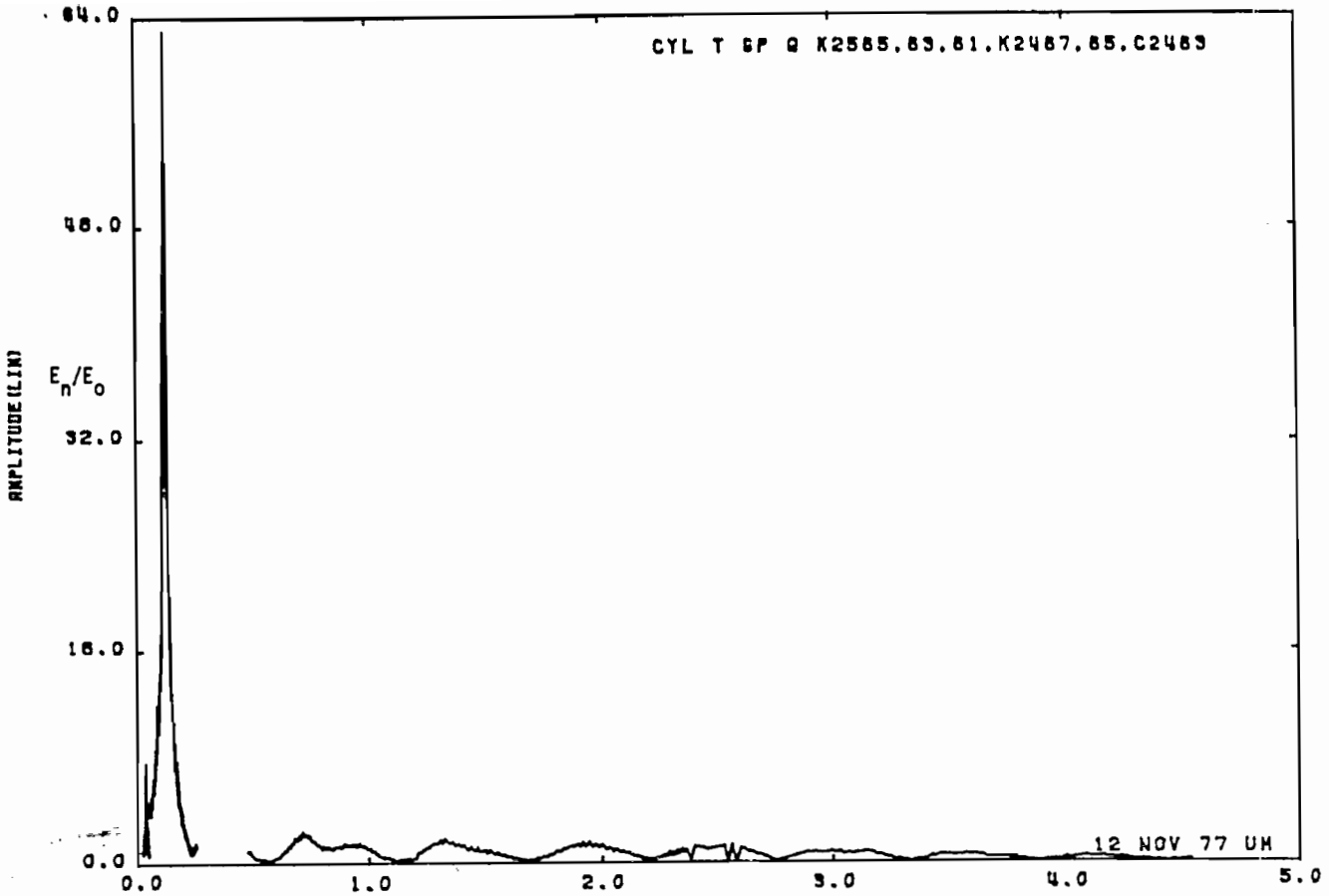

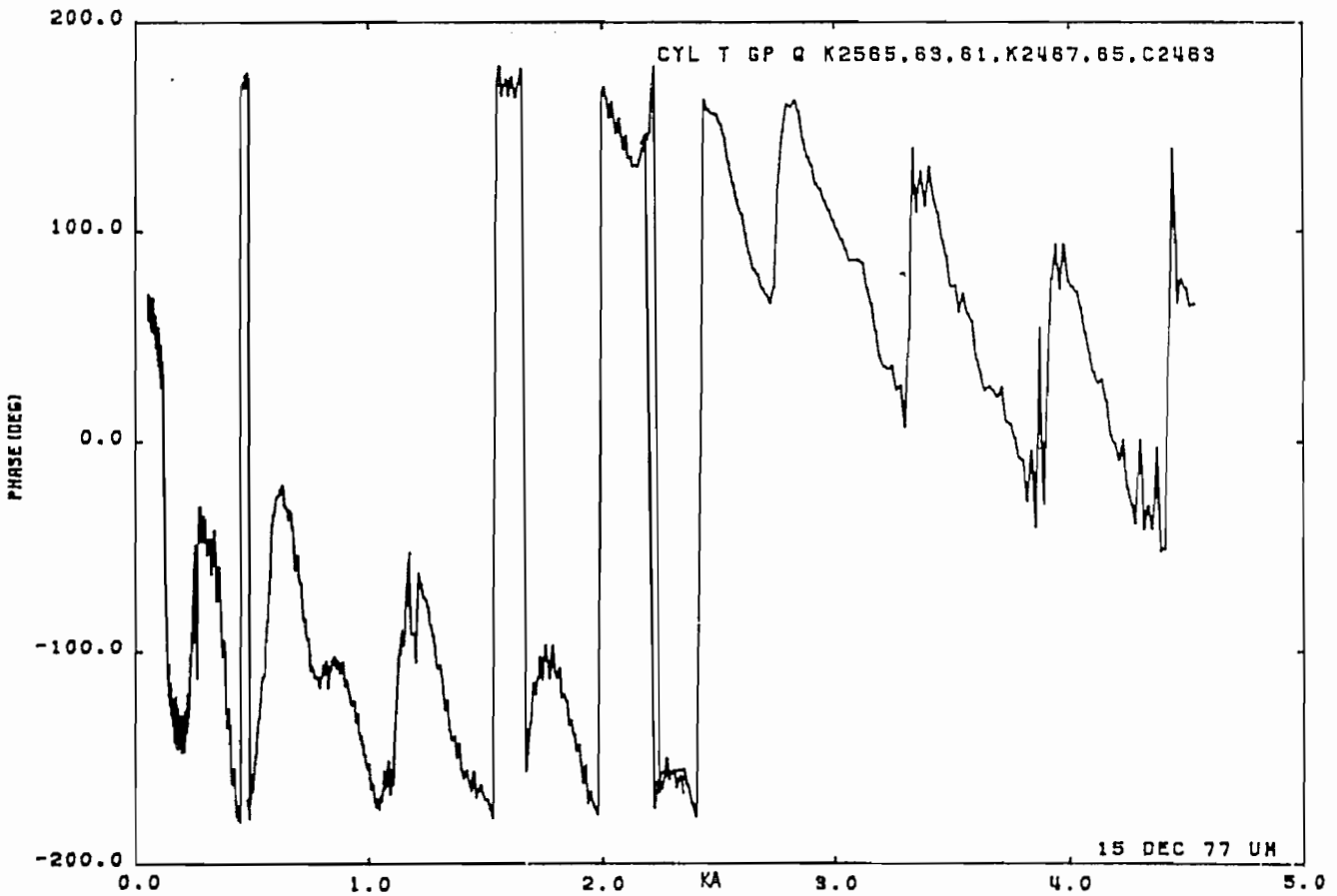

Figure 39a. Charge on cylinder at STA:T; h = 5a, near perfectly conducting ground plane.

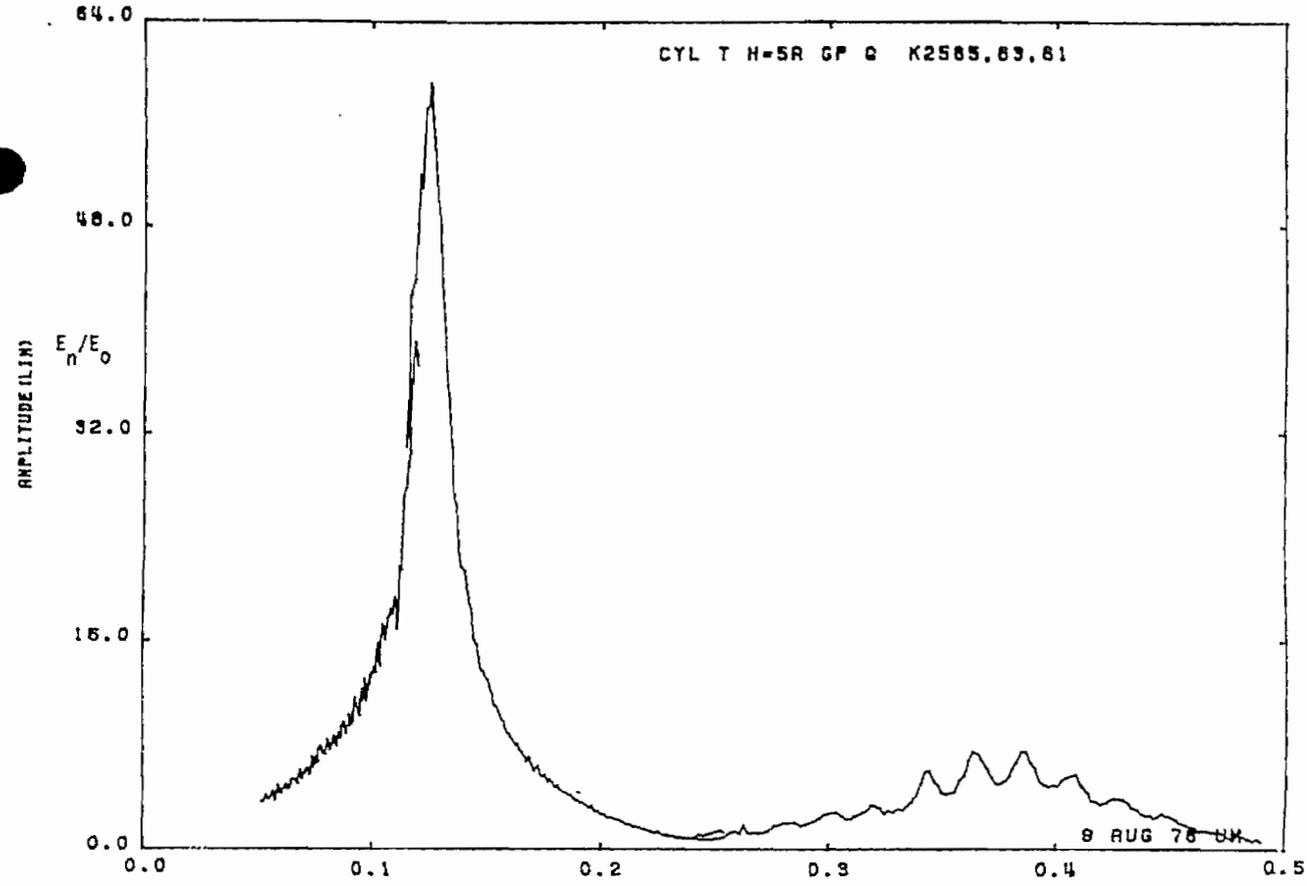

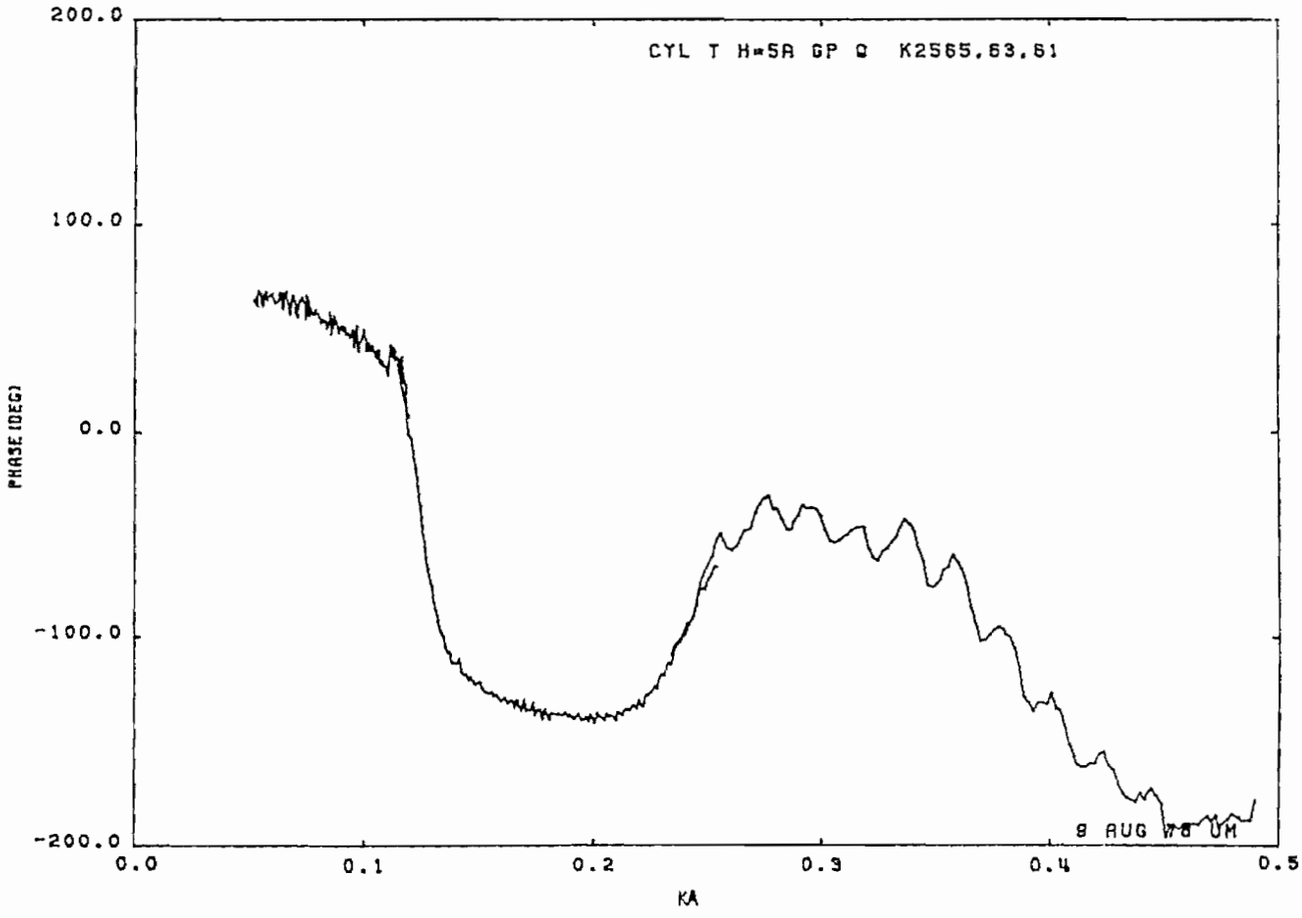

Figure 39b. Charge on cylinder at STA:T; h = 5a, near perfectly conducting ground plane (expanded scale).

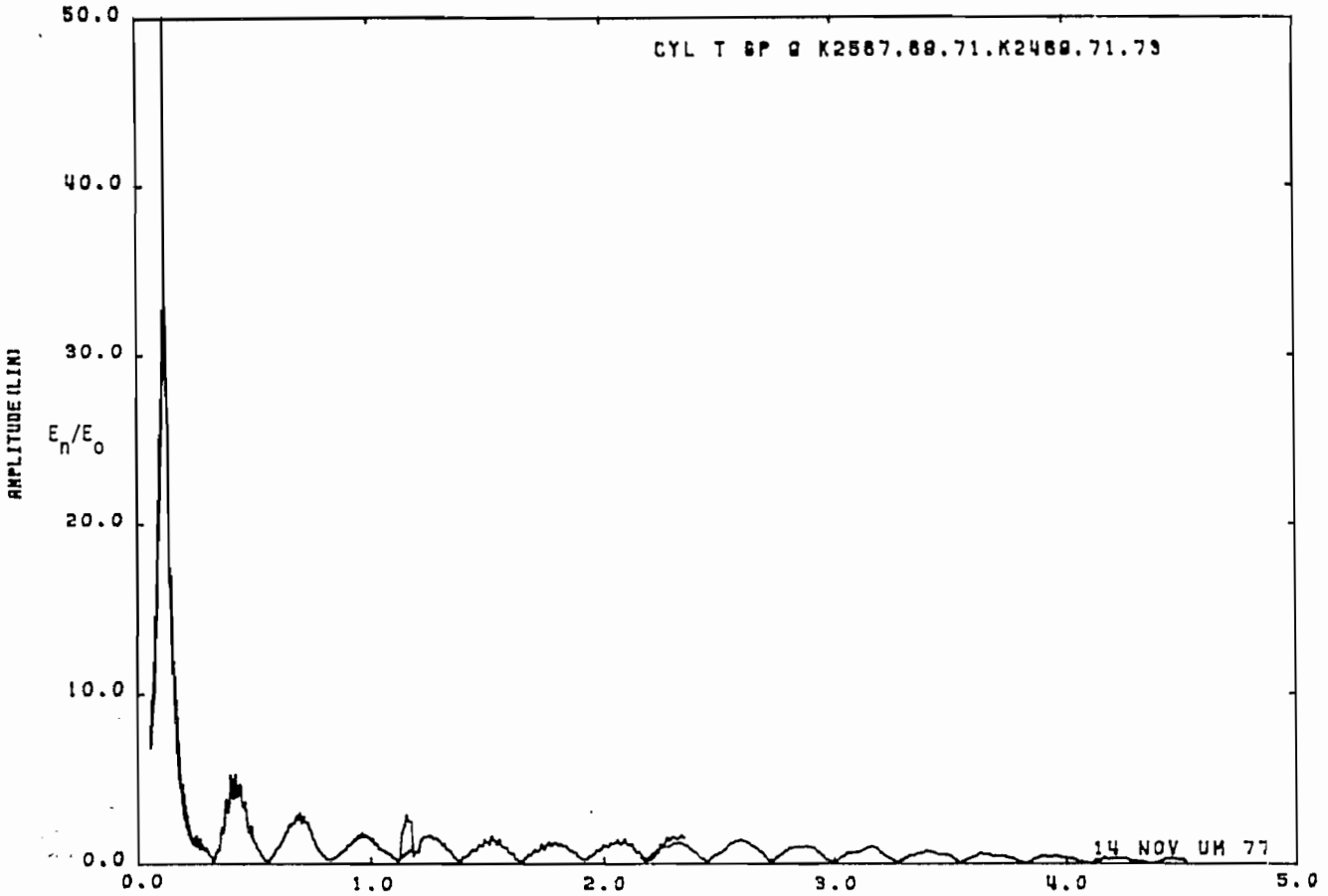

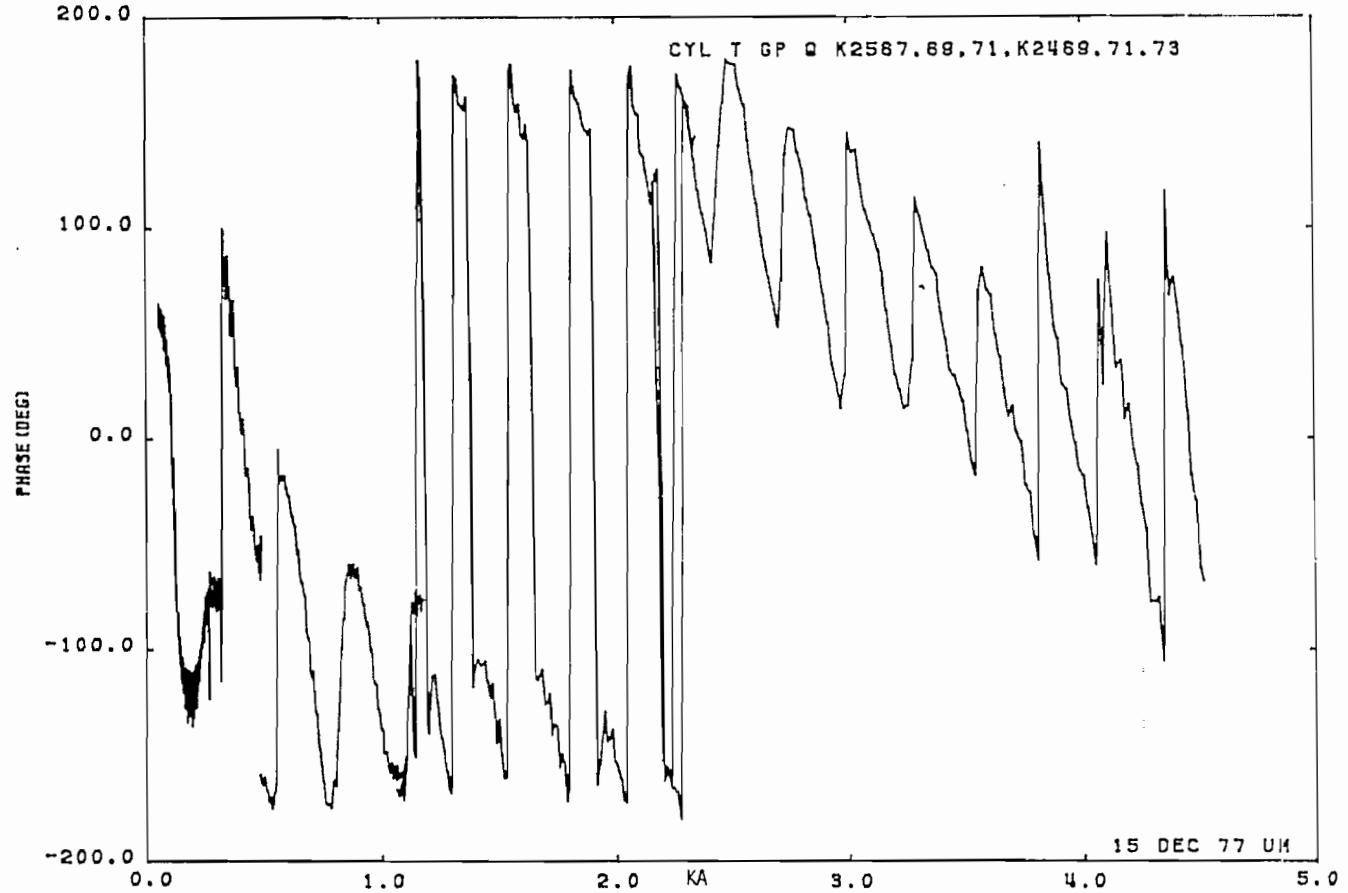

Figure 40a. Charge on cylinder at STA:T; h = 10a, near perfectly conducting ground plane.

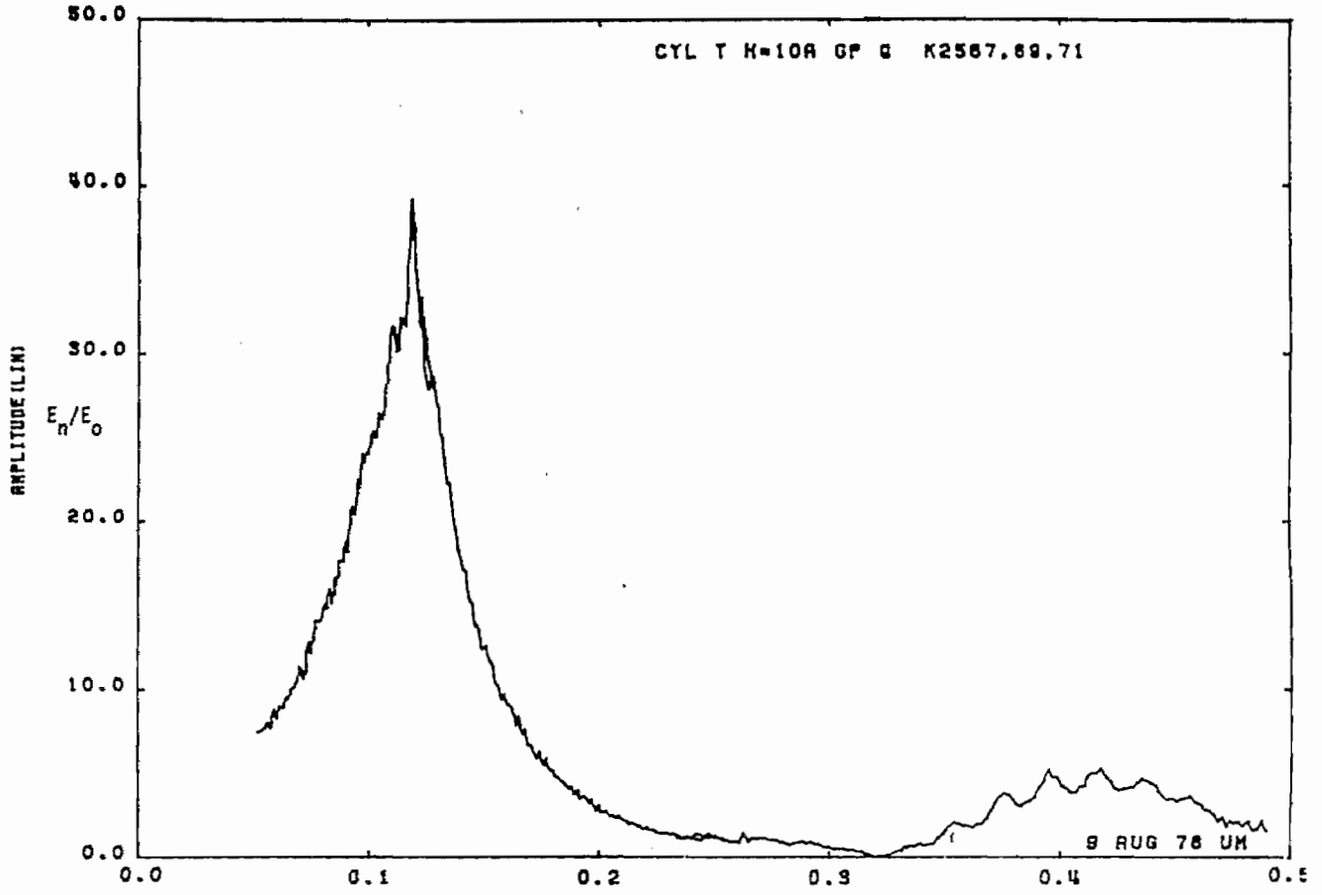

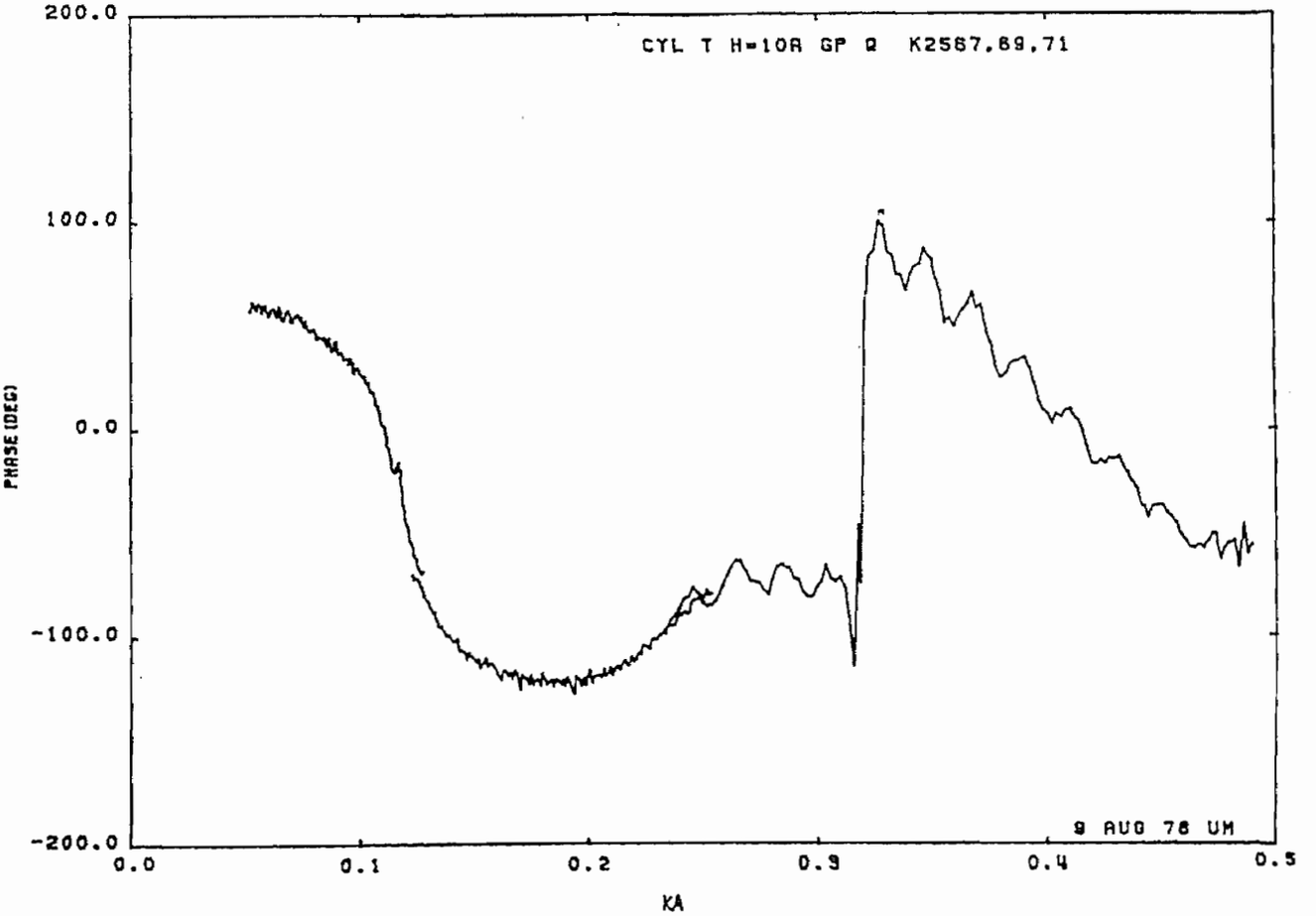

Figure 40b. Charge on cylinder at STA:T; h = 10a, near perfectly conducting ground plane (expanded scale).

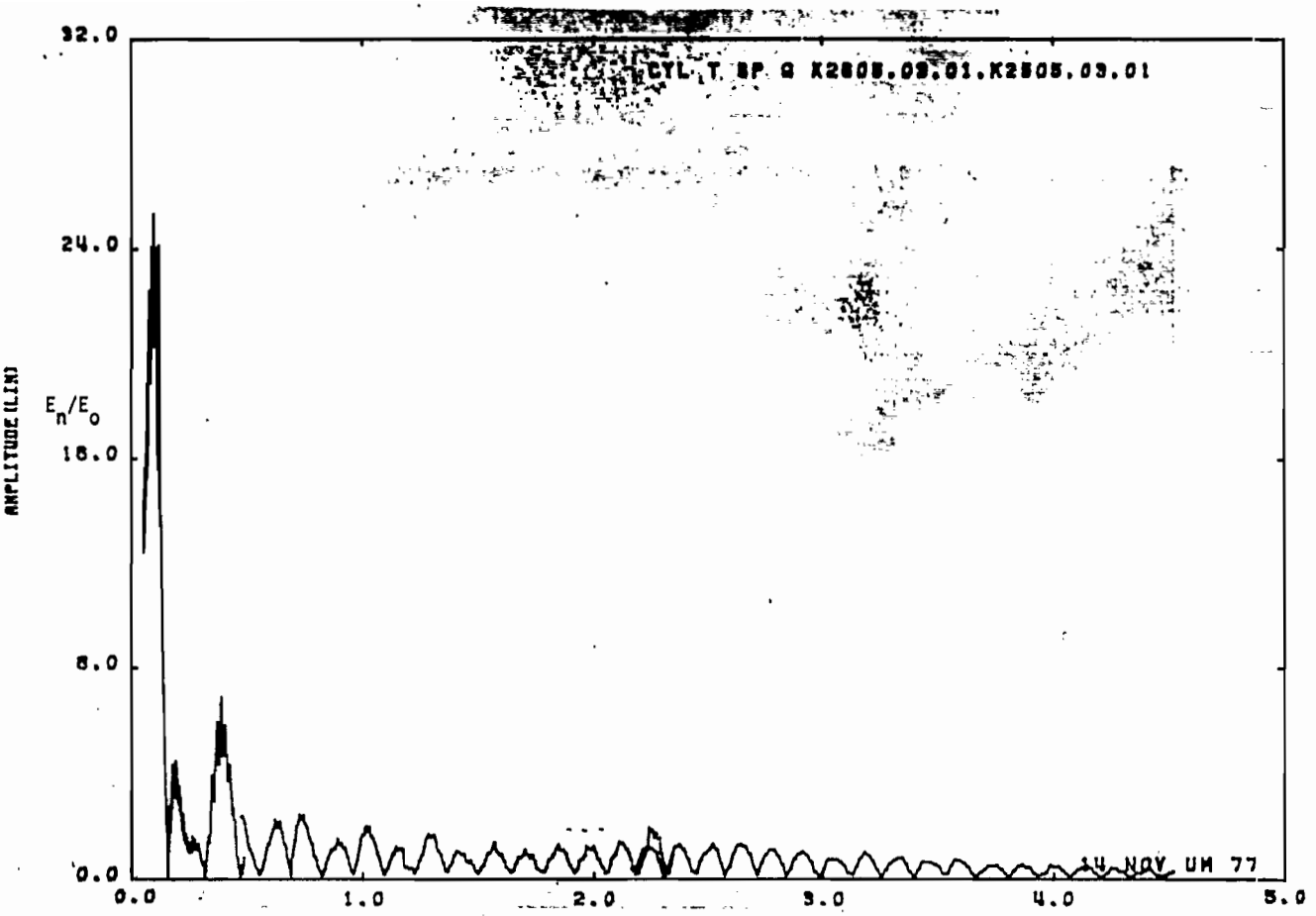

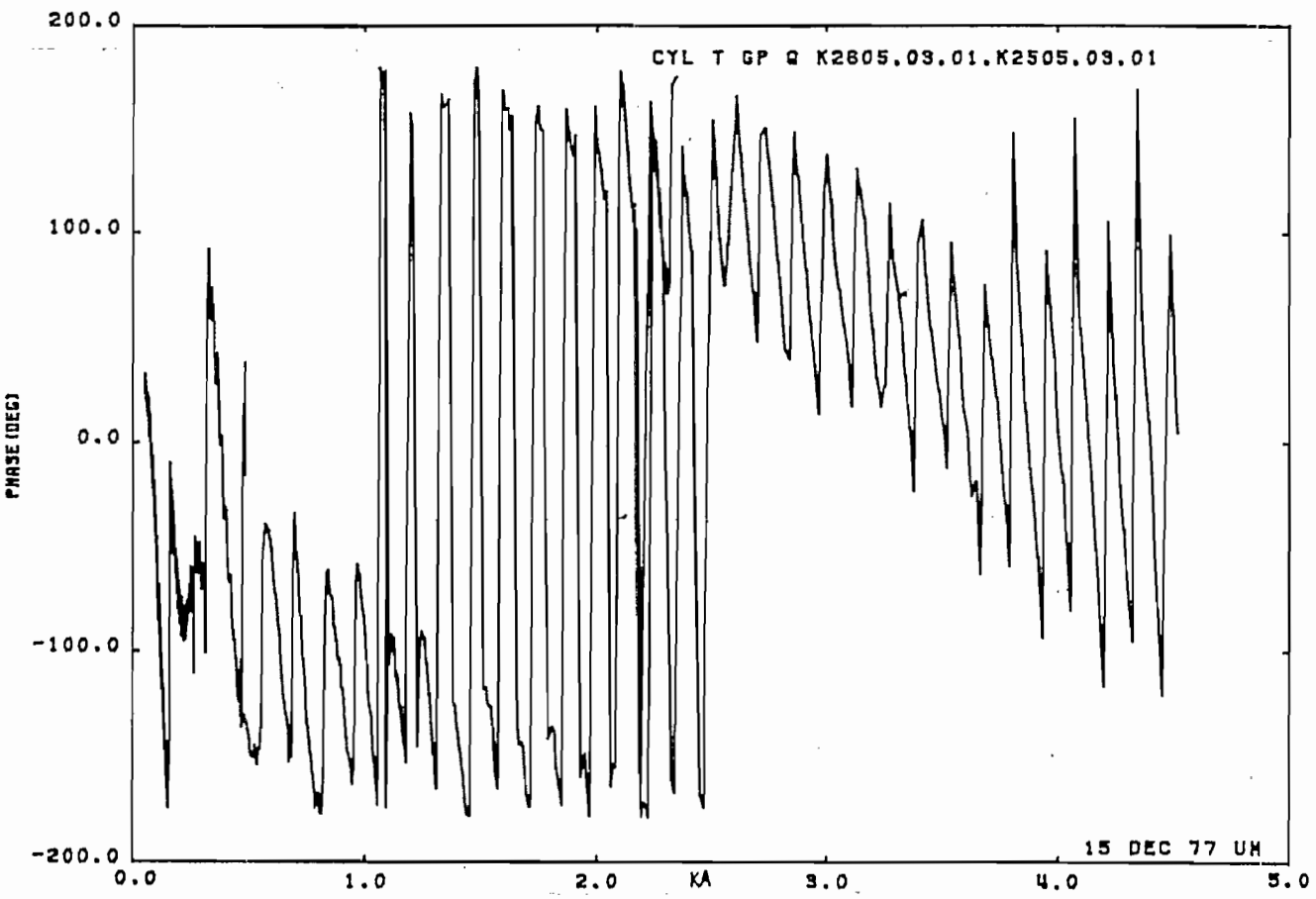

Figure 41a. Charge on cylinder at STA:T; h = 20a, near perfectly conducting ground plane.

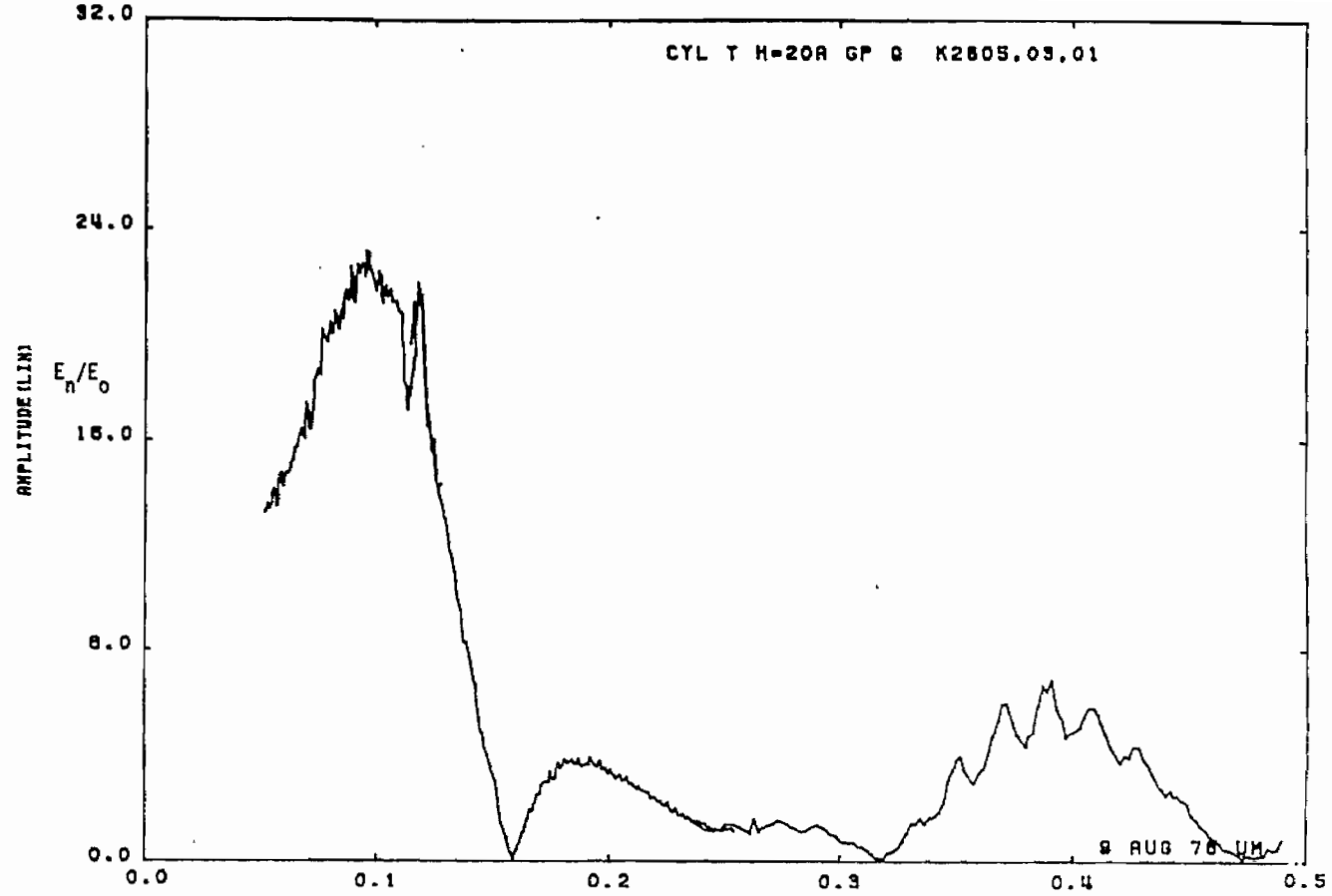

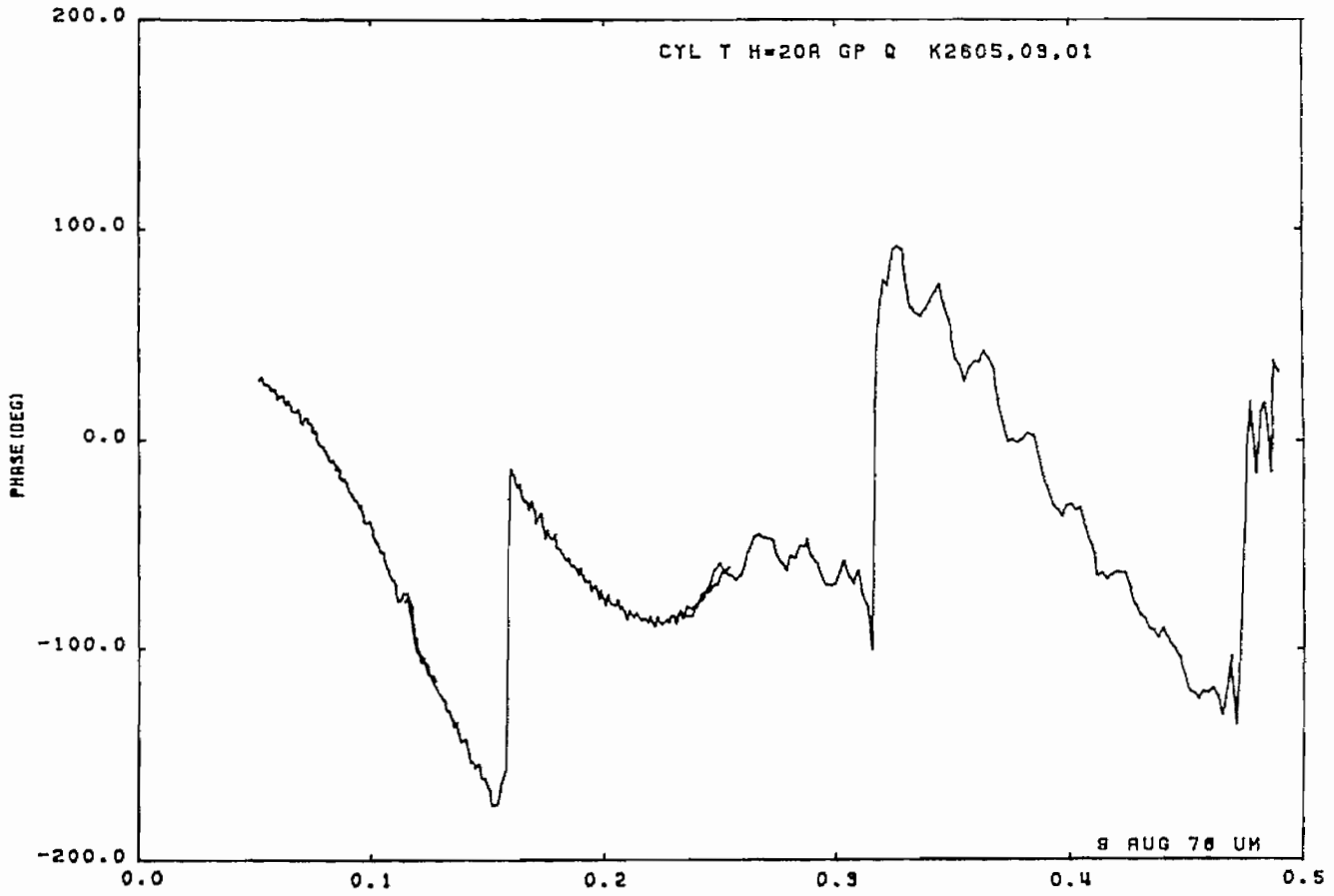

Figure 41b. Charge on cylinder at STA:T; h = 20a, near perfectly conducting ground plane (expanded scale).

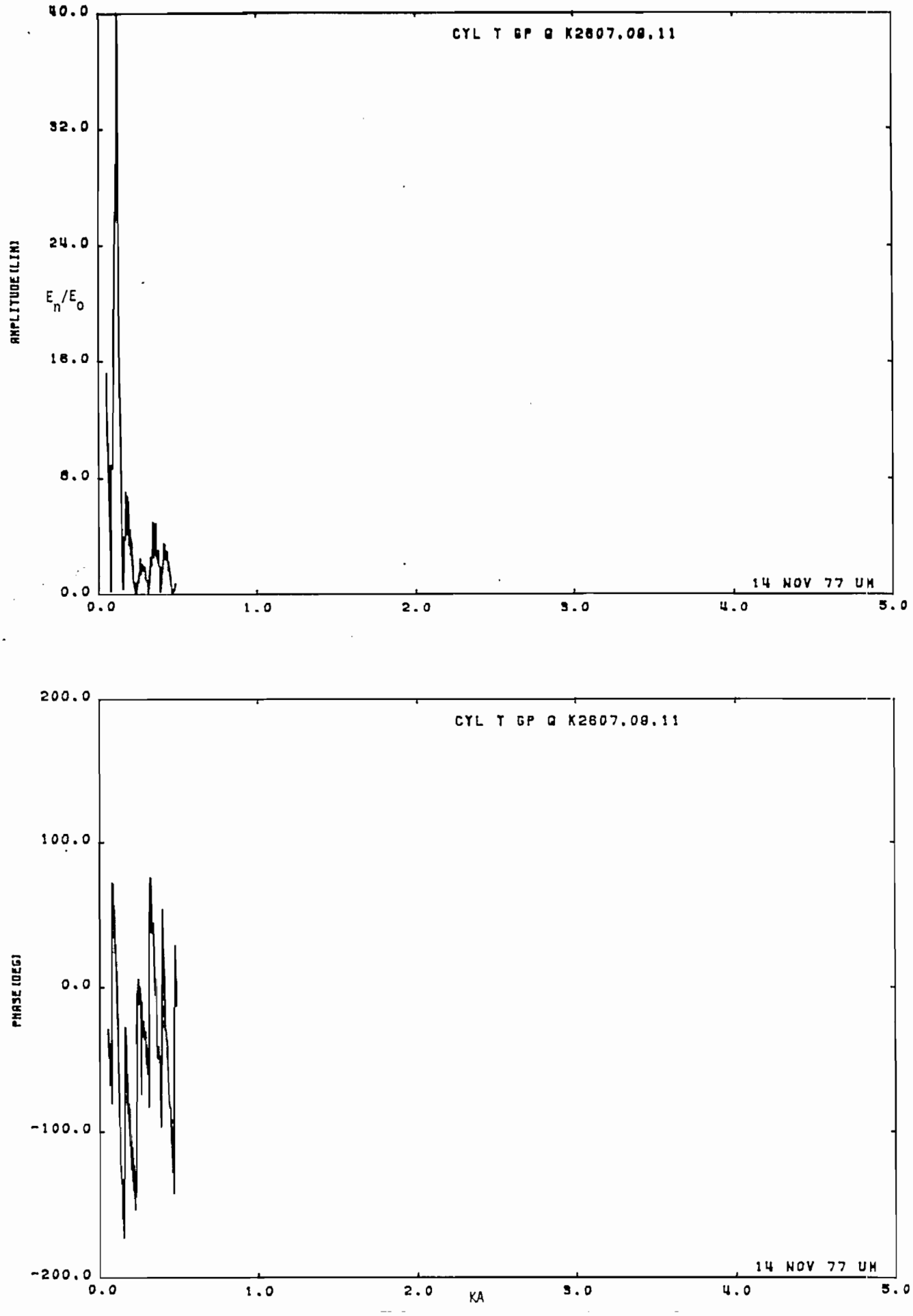

Figure 42a. Charge on cylinder at STA:T; h = 40a, near perfectly conducting ground plane.

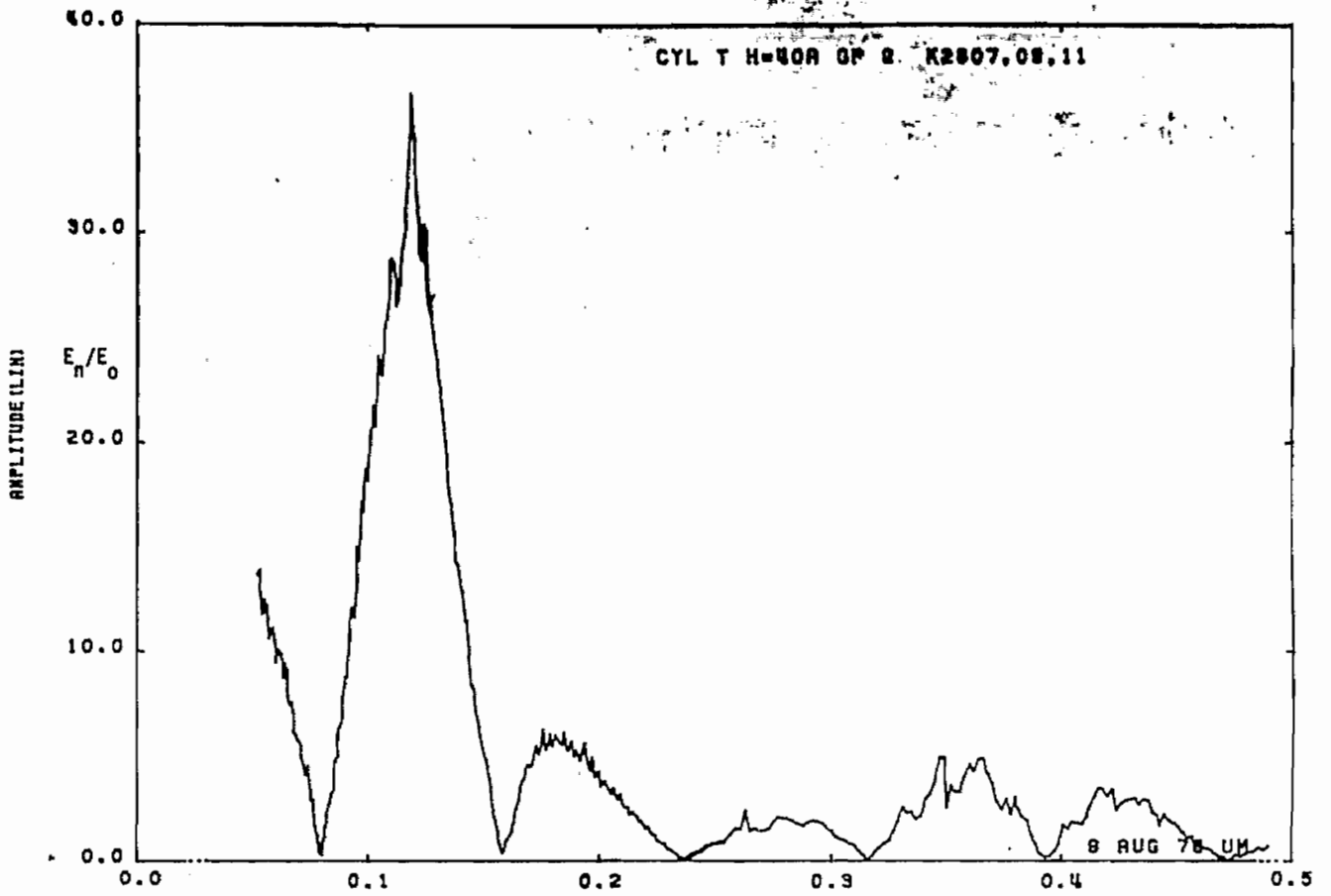

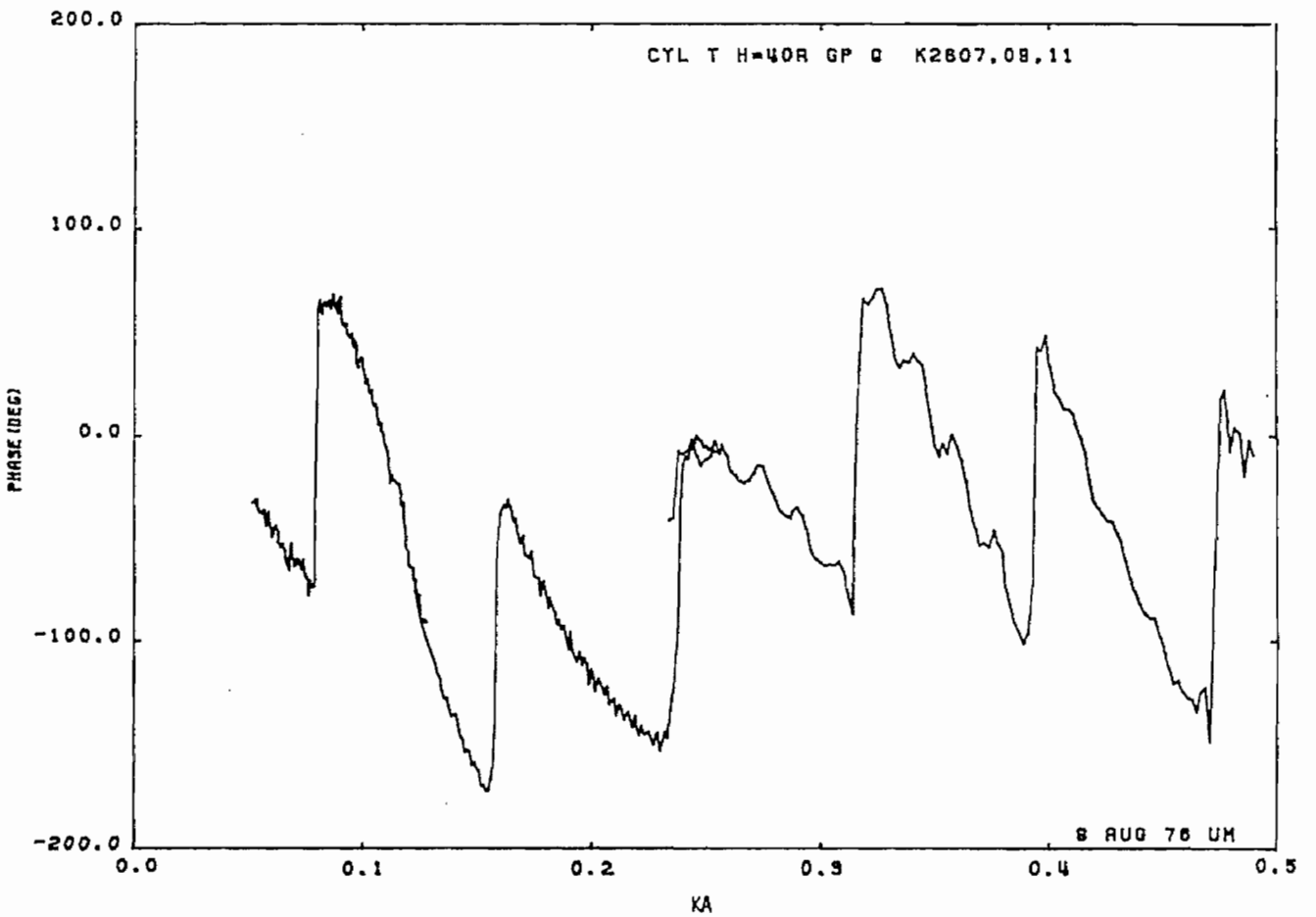

Figure 42b. Charge on cylinder at STA:T; h = 40a, near perfectly conducting ground plane (expanded scale).

3.1.3 Cylinder Near Lossy Ground Plane

The current was measured at the back ($\phi = 180°$) of the cylinder near the base (STA: +5D) and the charge at the top (STA: T) for various cylinder to ground plane spacings. The spacing h is measured from the center of the cylinder to the ground plane and is expressed in terms of the radius a. To be consistent with the data for the cylinder in the free space case, and near the perfectly conducting ground plane, the data presented here are also plotted as a function of ka. However, due to the frequency dependant complex permitivity of the lossy ground plane material, the measurements made on the small and the large cylinders at different frequencies but corresponding to the same ka values are not expected to match. The data definitely indicate this at ka = 0.5. For $0 < ka < 0.5$ data were obtained on the small cylinder while for $ka > 0.5$, they were measured on the large cylinder. Table 5 summarizes the data presented.

TABLE 5: CYLINDER NEAR LOSSY GROUND PLANE

h	J, STA: +5D	Q, STA: T
1.5a	Figure 43	Figure 49
2a	44	50
5a	45	51
10a	46	52
20a	47	53
40a	48	54

Each figure has two parts:

a) amplitude and phase, full plot

b) amplitude and phase, expanded plot

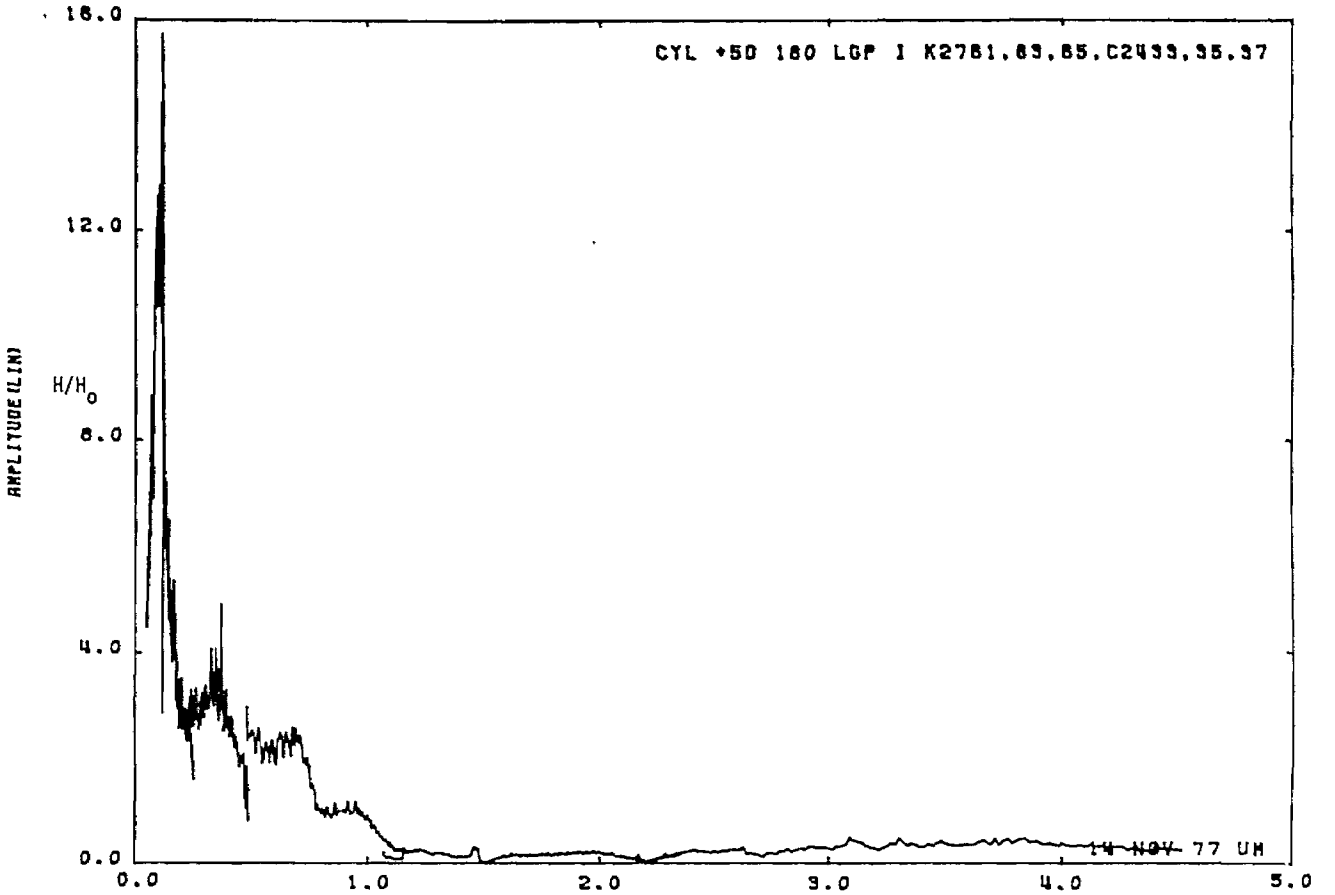

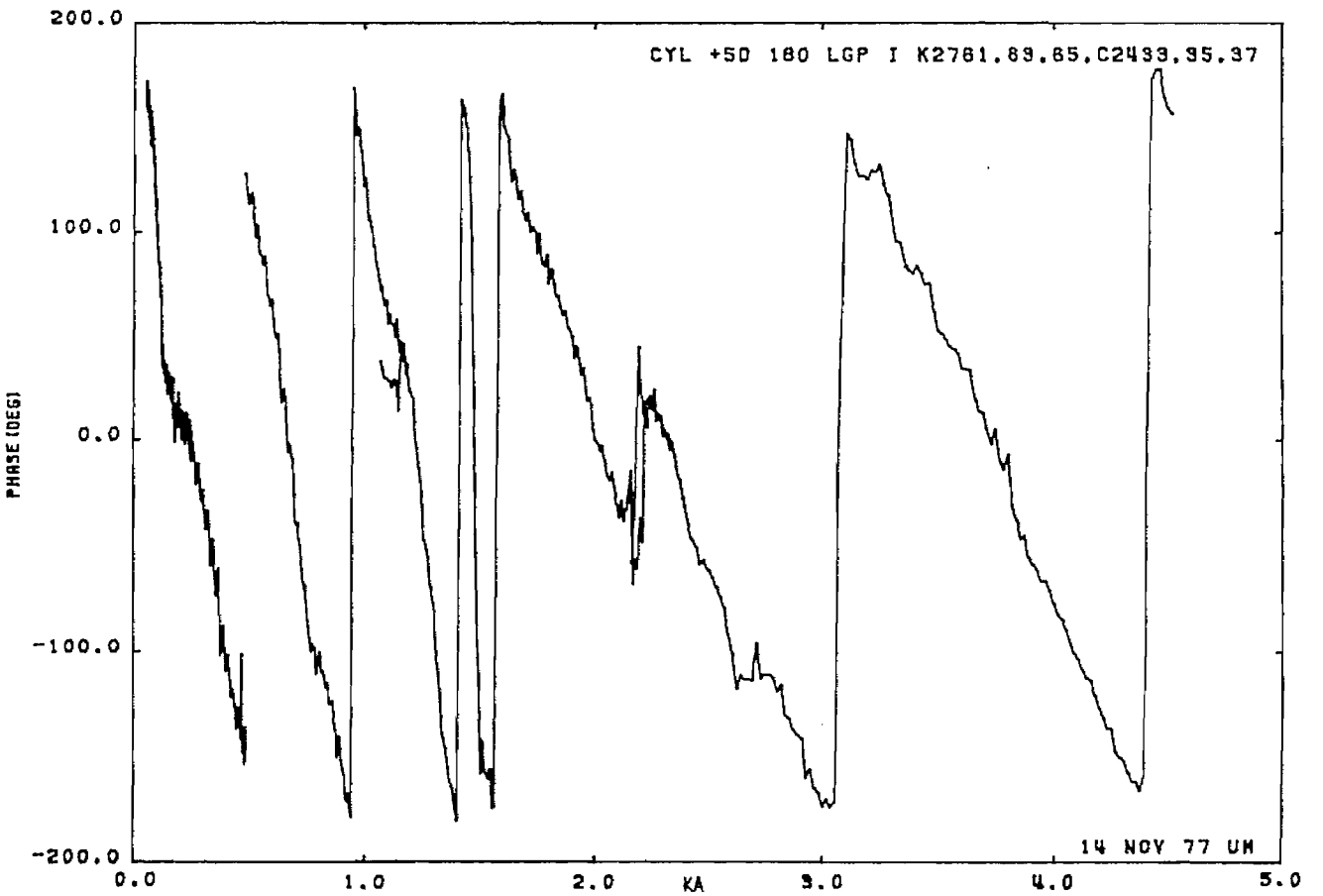

Figure 43a. Current on cylinder at STA:+5D; ϕ = 180°, h = 1.5a, near lossy ground plane.

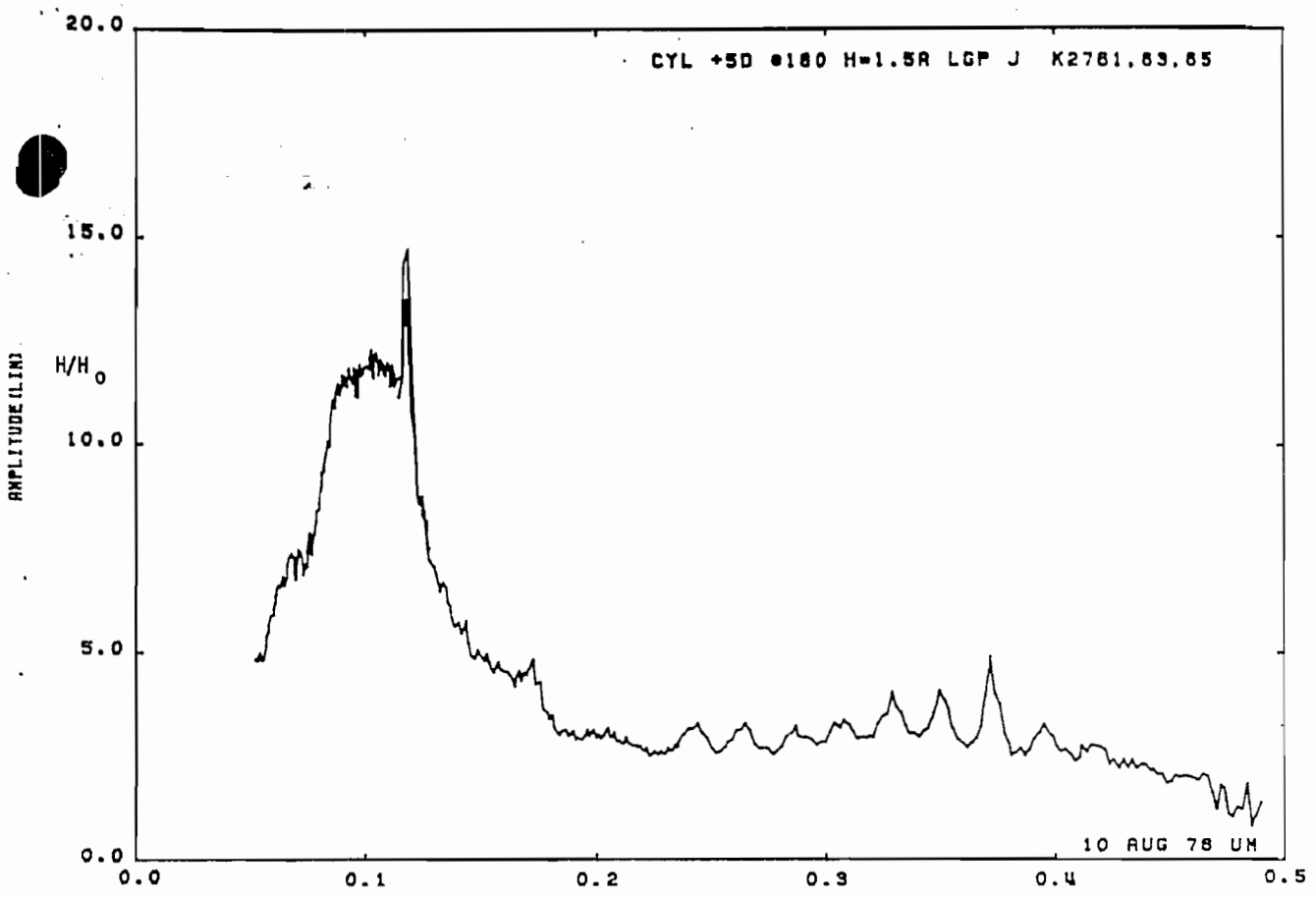

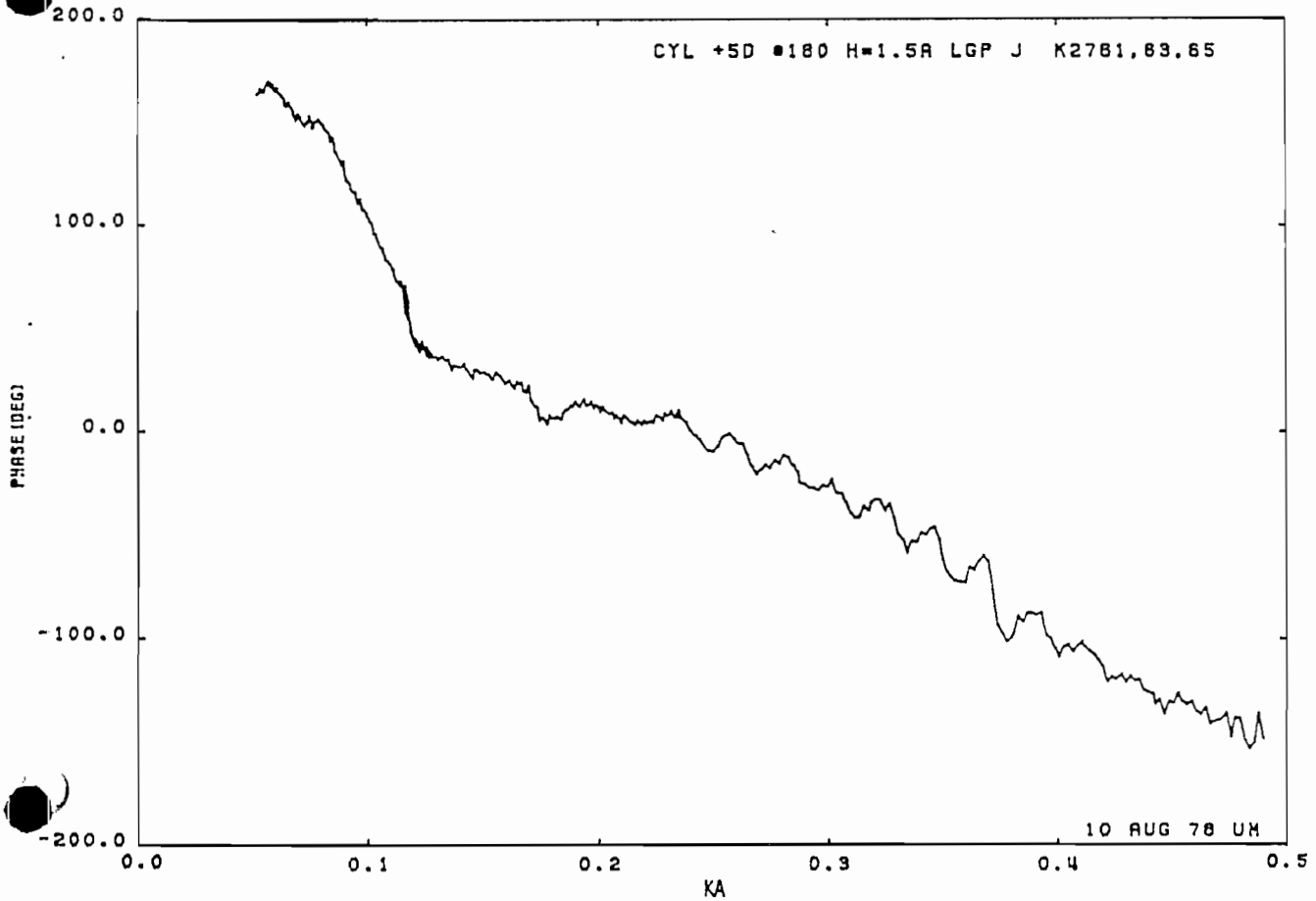

Figure 43b. Current on cylinder at STA:+5B; 180°, h = 1.5a, near lossy ground plane (expanded scale).

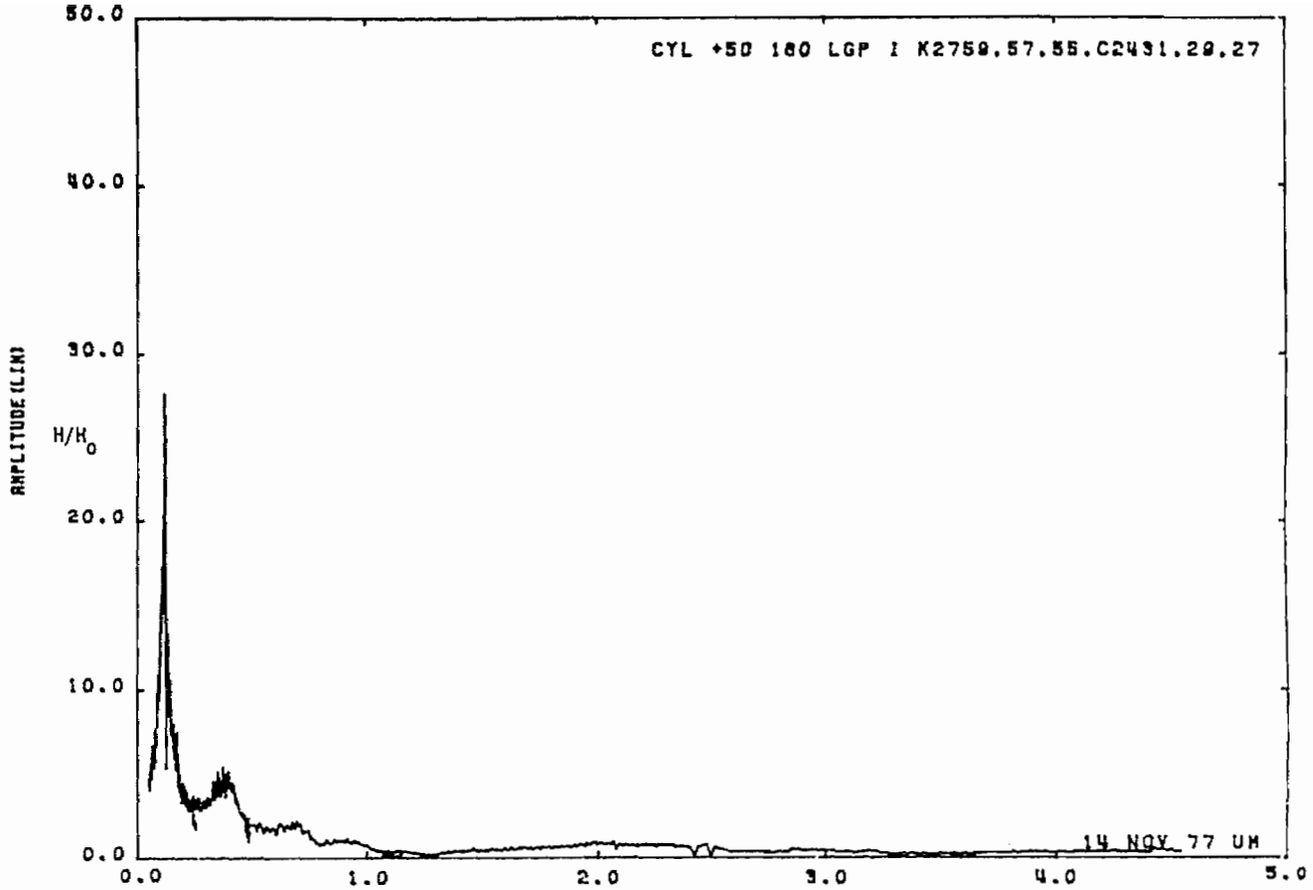

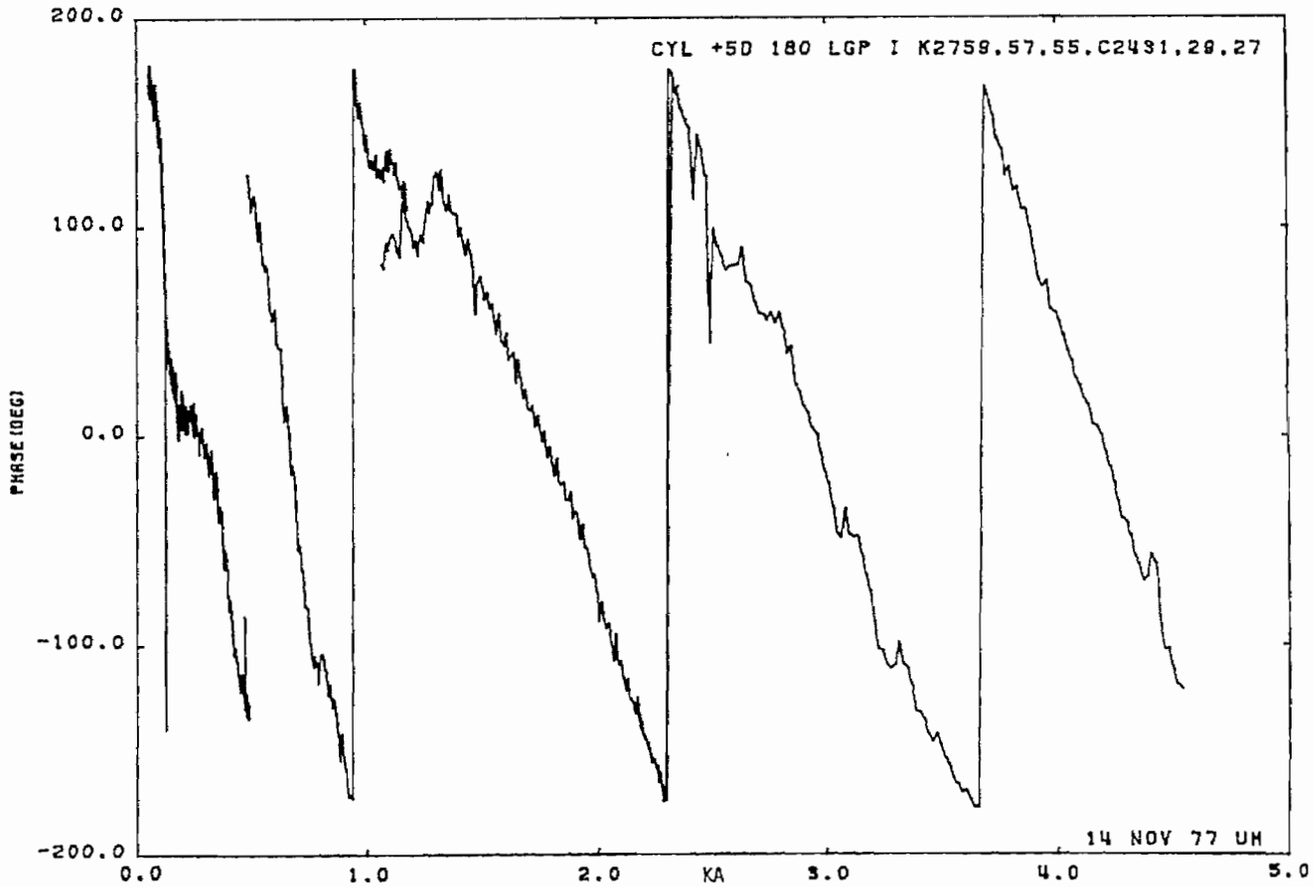

Figure 44a. Current on cylinder at STA:+5D; $\emptyset$ = 180°, h = 2a, near lossy ground plane.

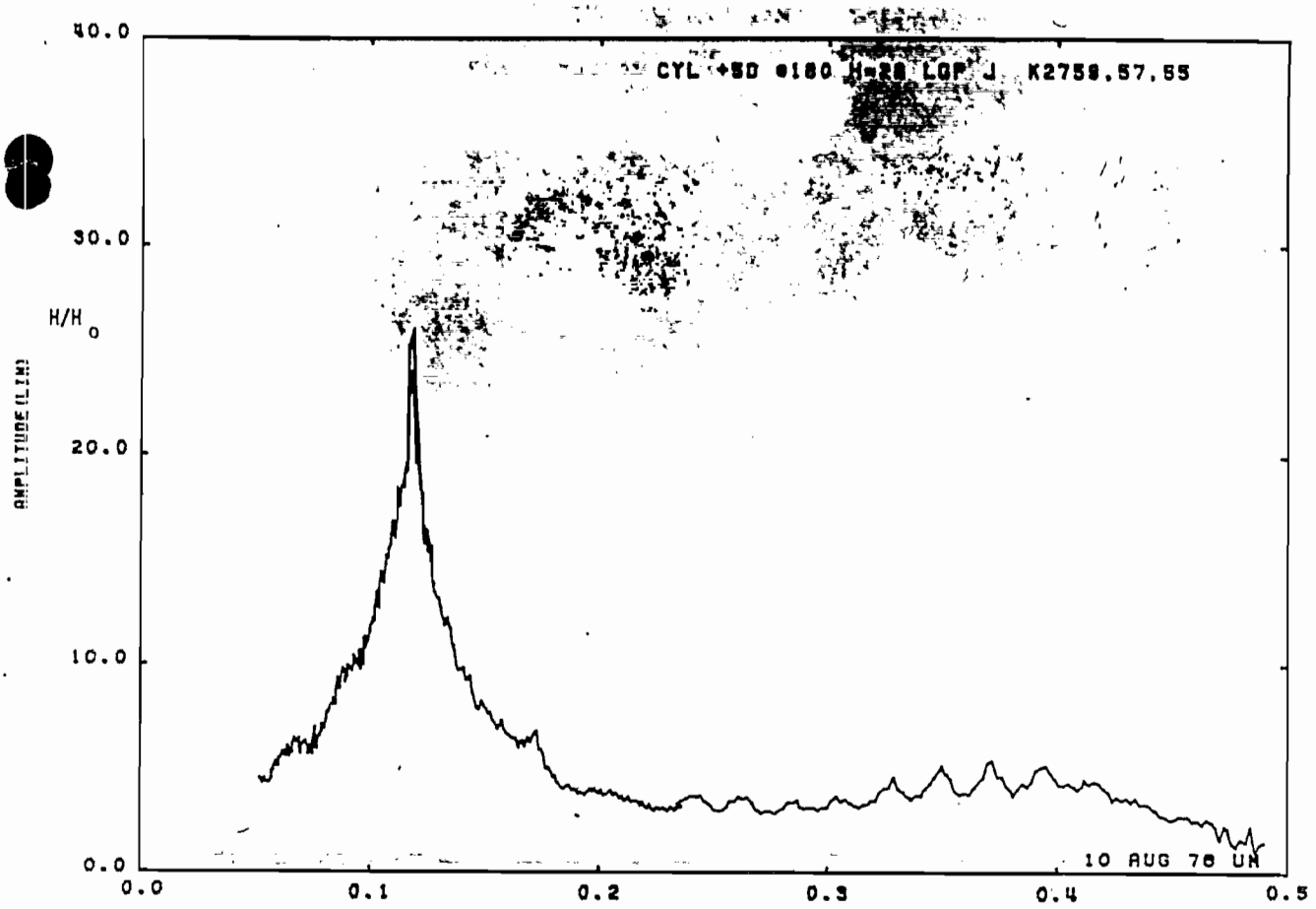

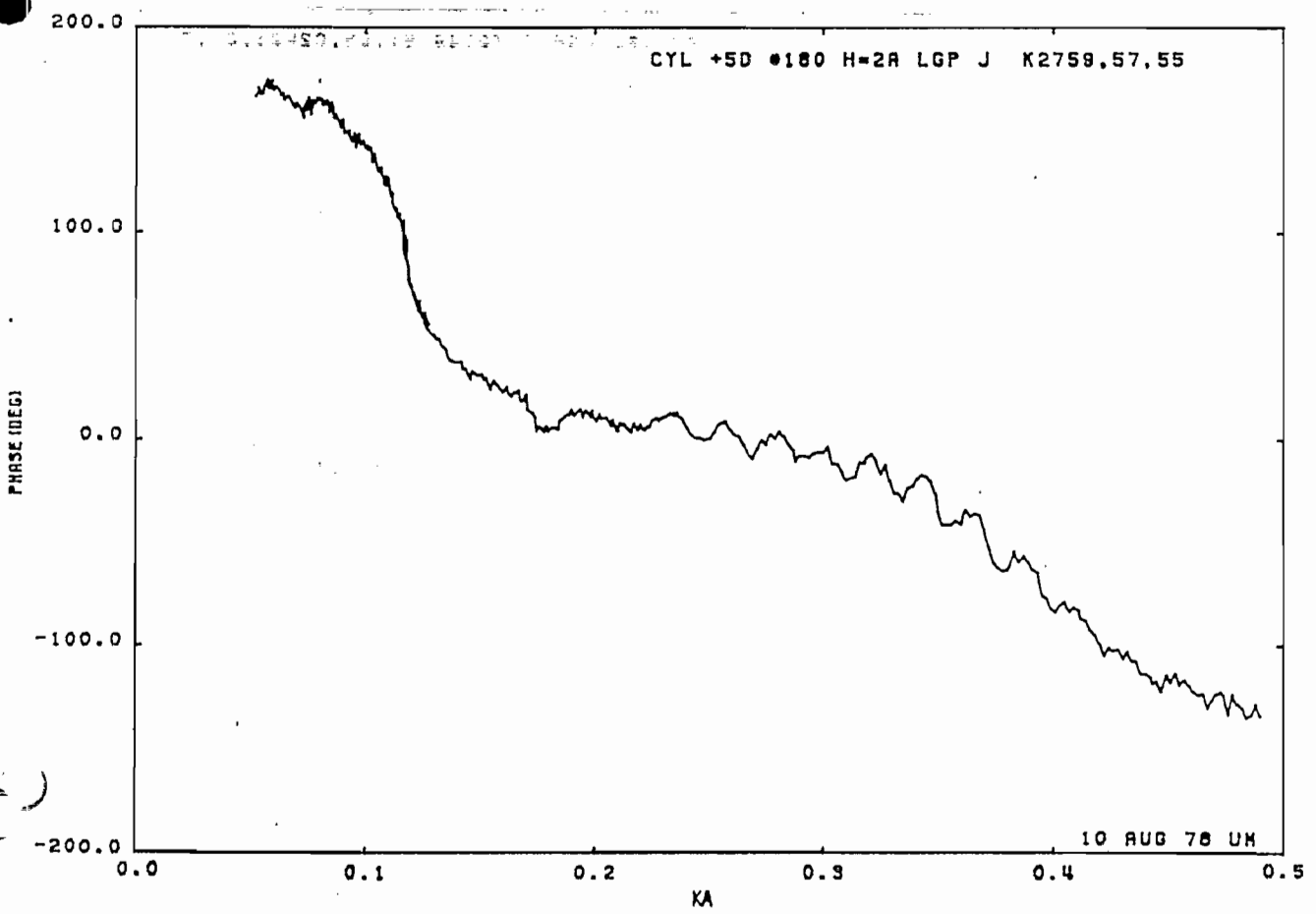

Figure 44b. Current on cylinder at STA:+5D; β = 180°, h = 2a, near lossy ground plane (expanded scale).

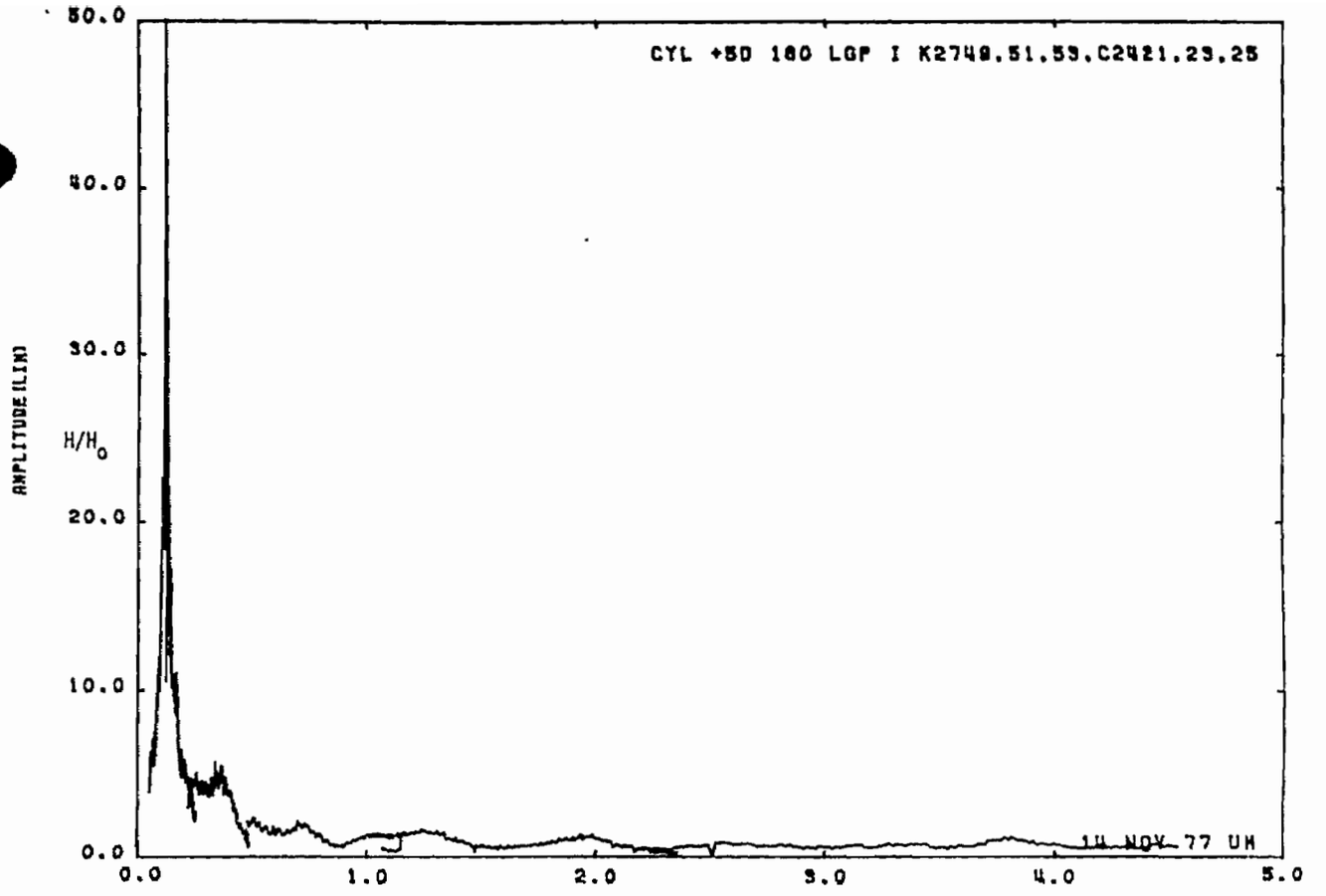

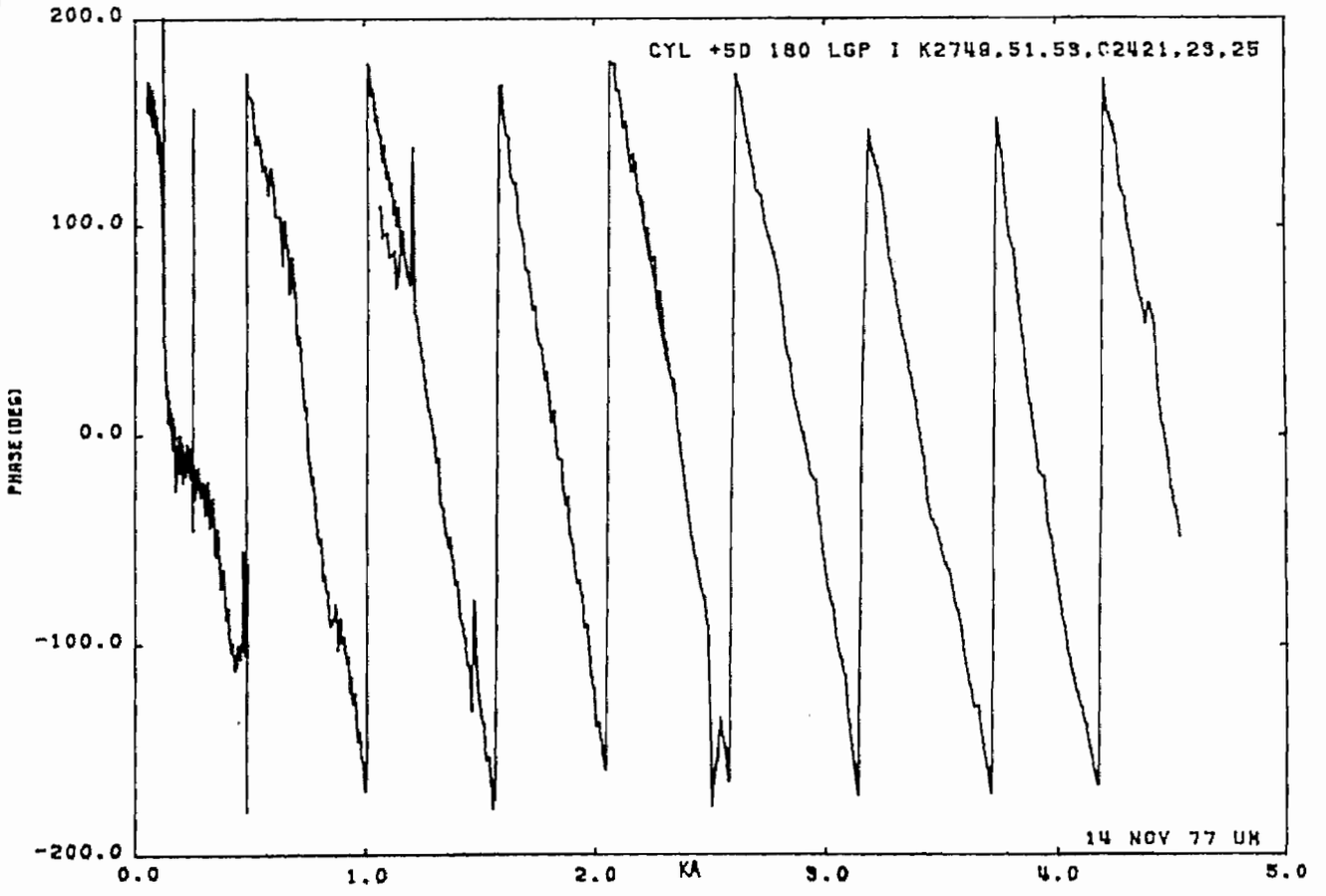

Figure 45a. Current on cylinder at STA:+5D; ϕ = 180°, h = 5a, near lossy ground plane.

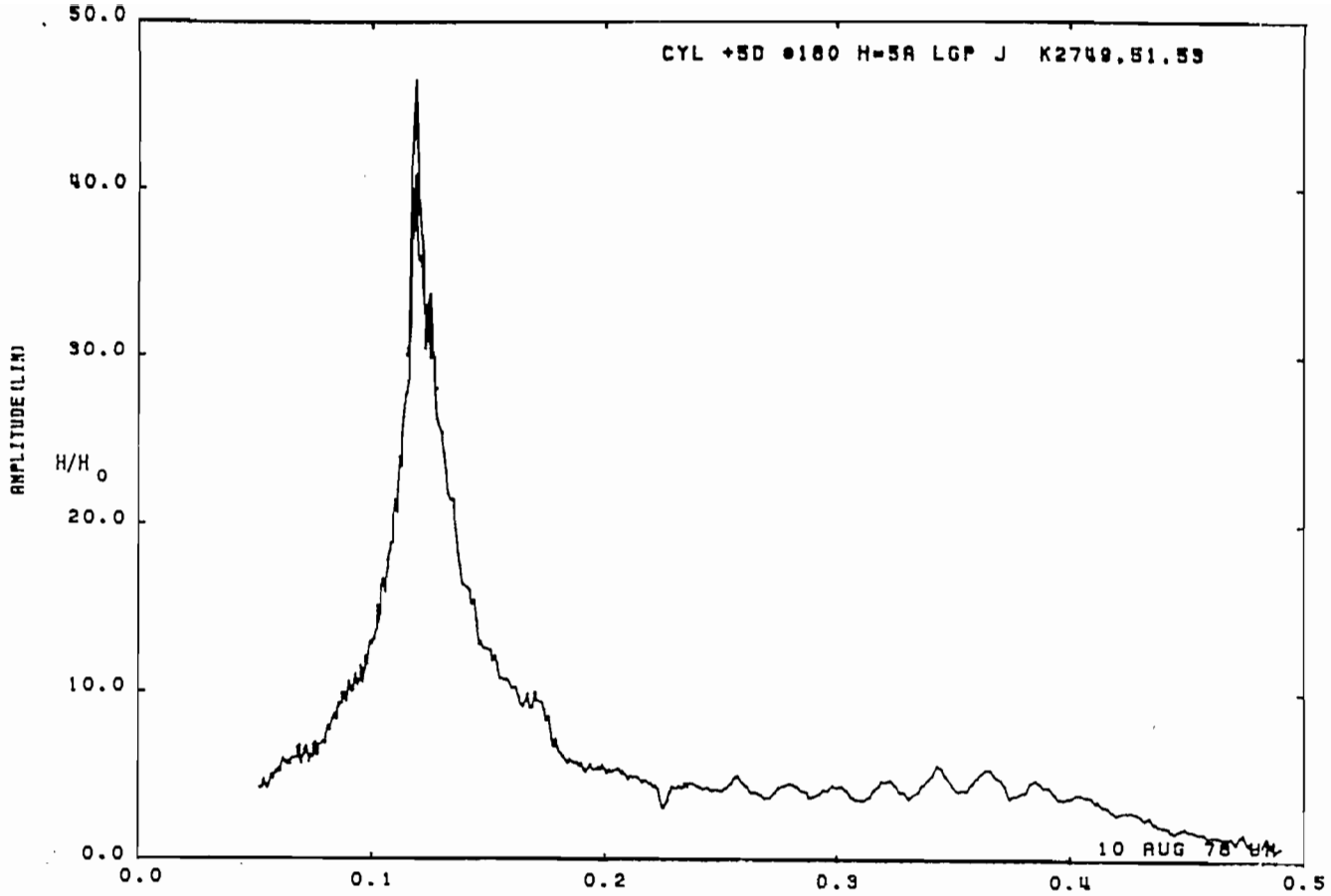

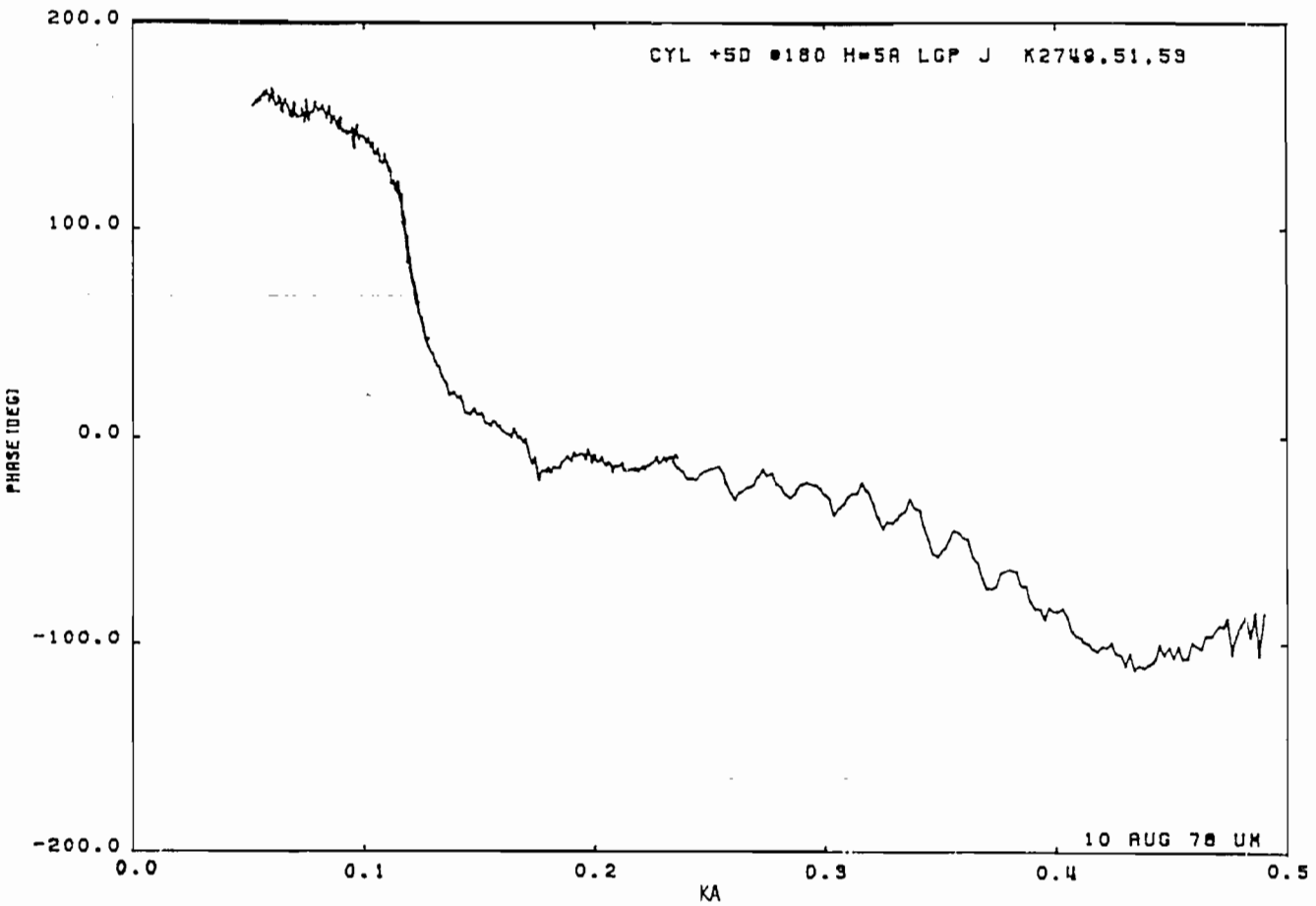

Figure 45b. Current on cylinder at STA:+5D; β = 180°, h = 5a, near lossy ground plane (expanded scale).

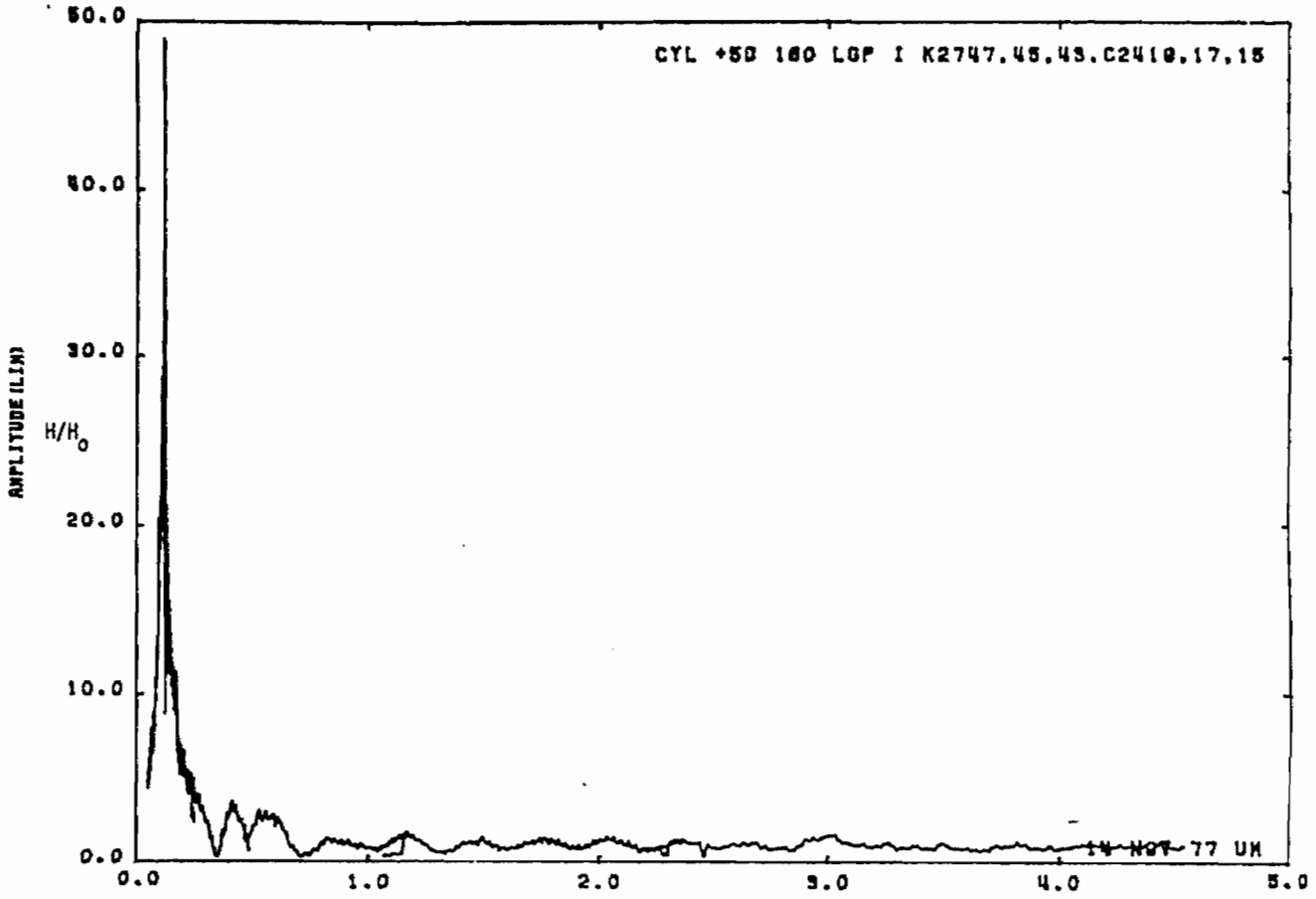

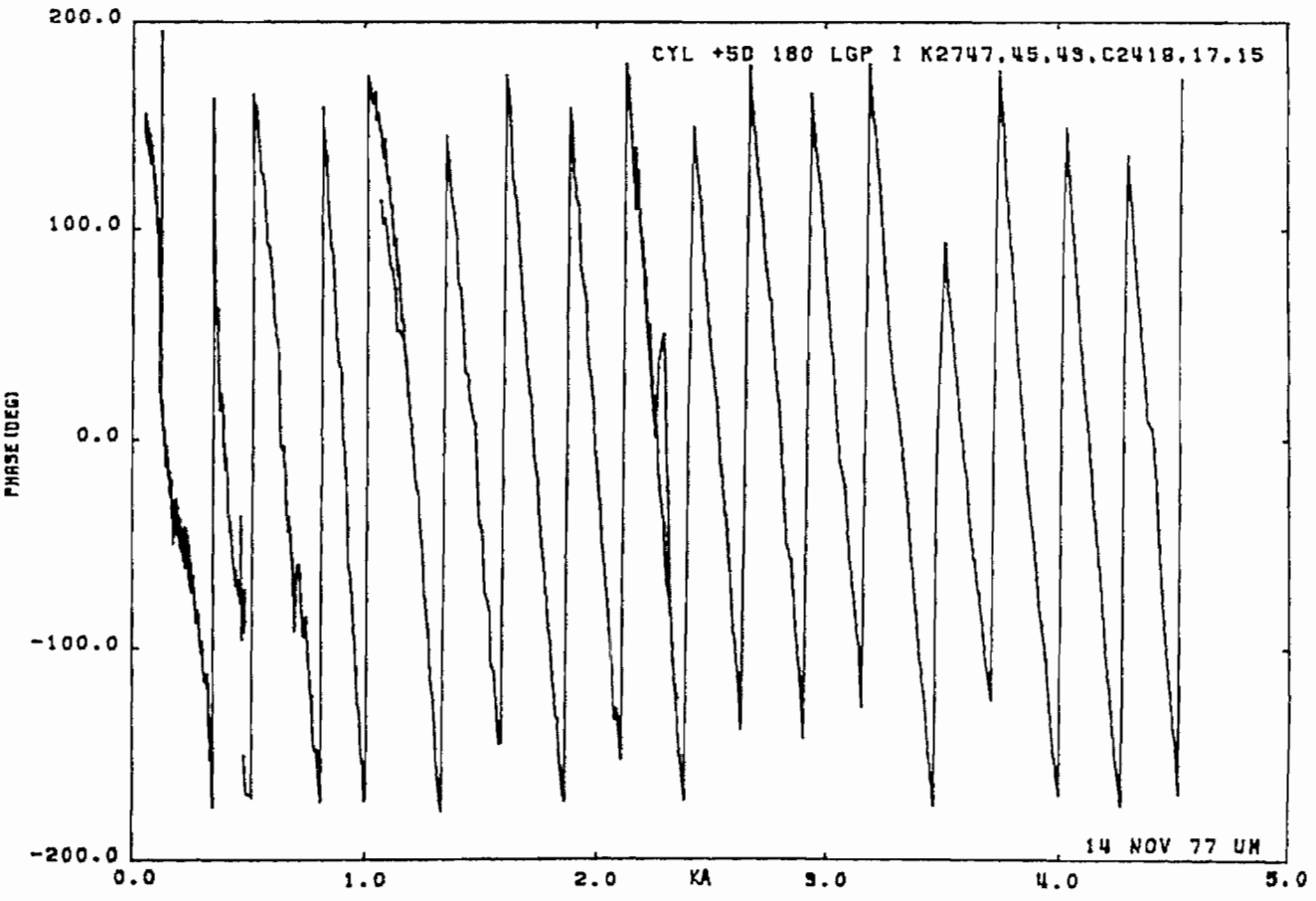

Figure 46a. Current on cylinder at STA:+5D; ϕ = 180°, h = 10a, near lossy ground plane.

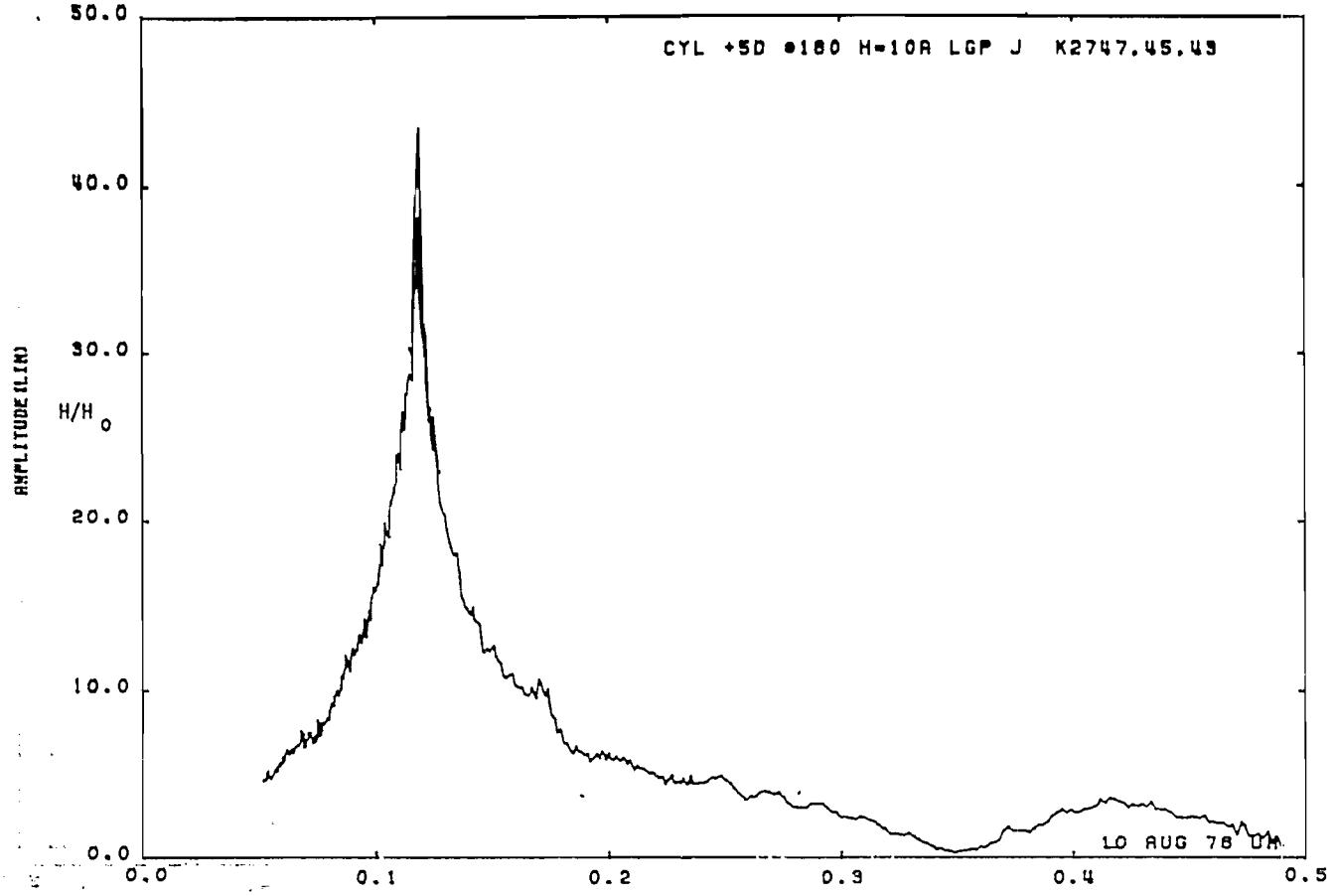

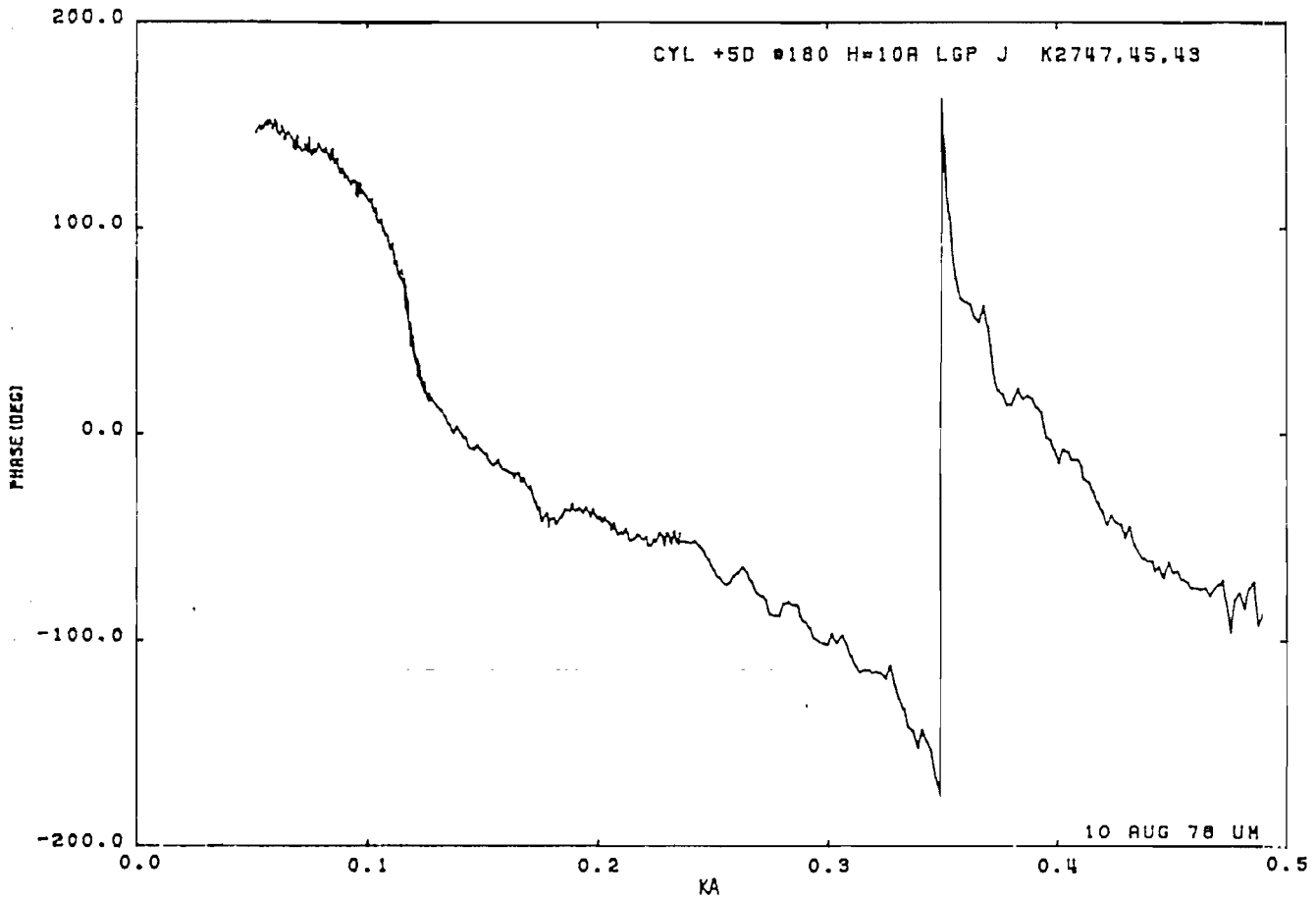

Figure 46b. Current on cylinder at STA:+5D; ϕ = 180°, h = 10a, near lossy ground plane (expanded scale).

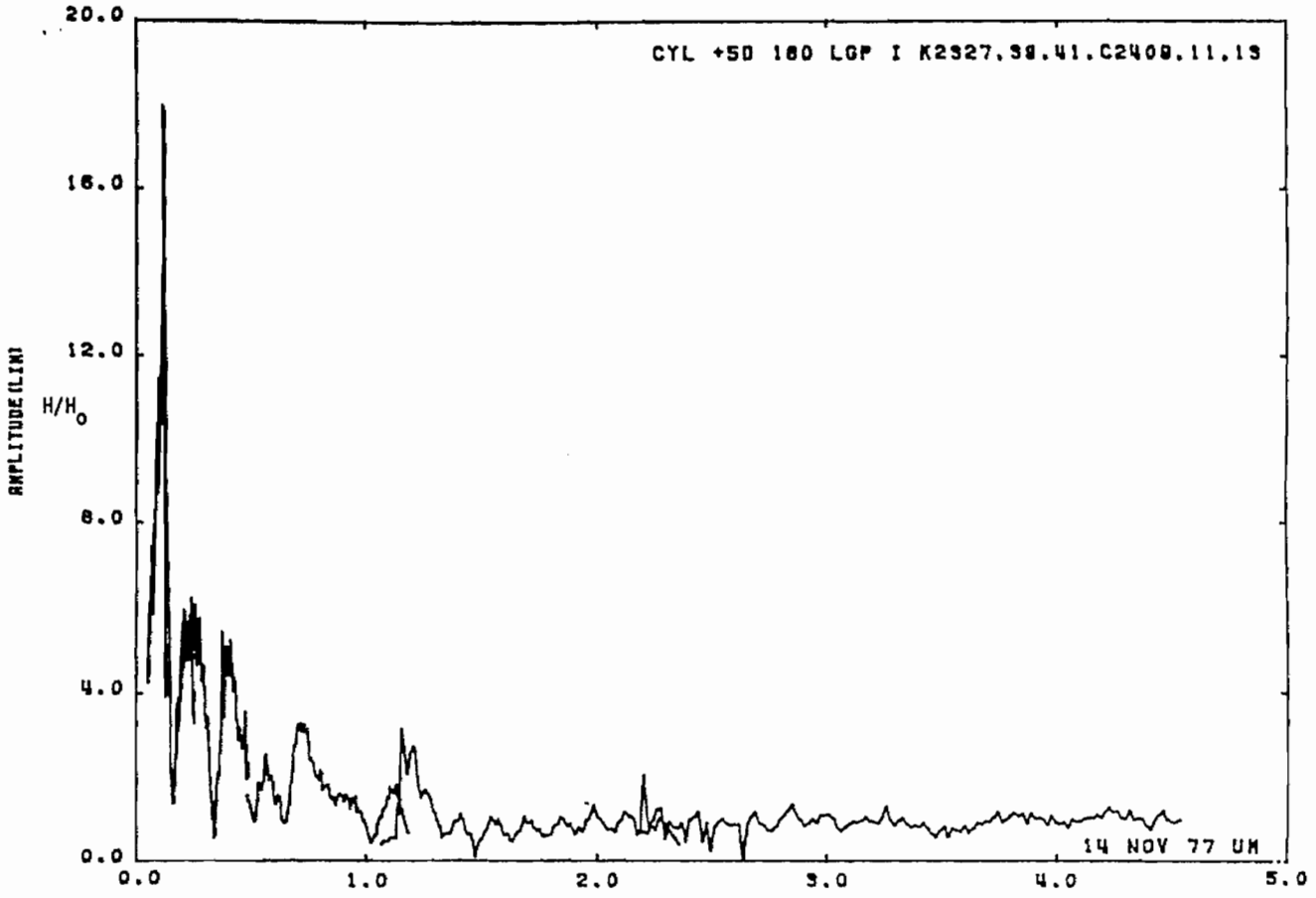

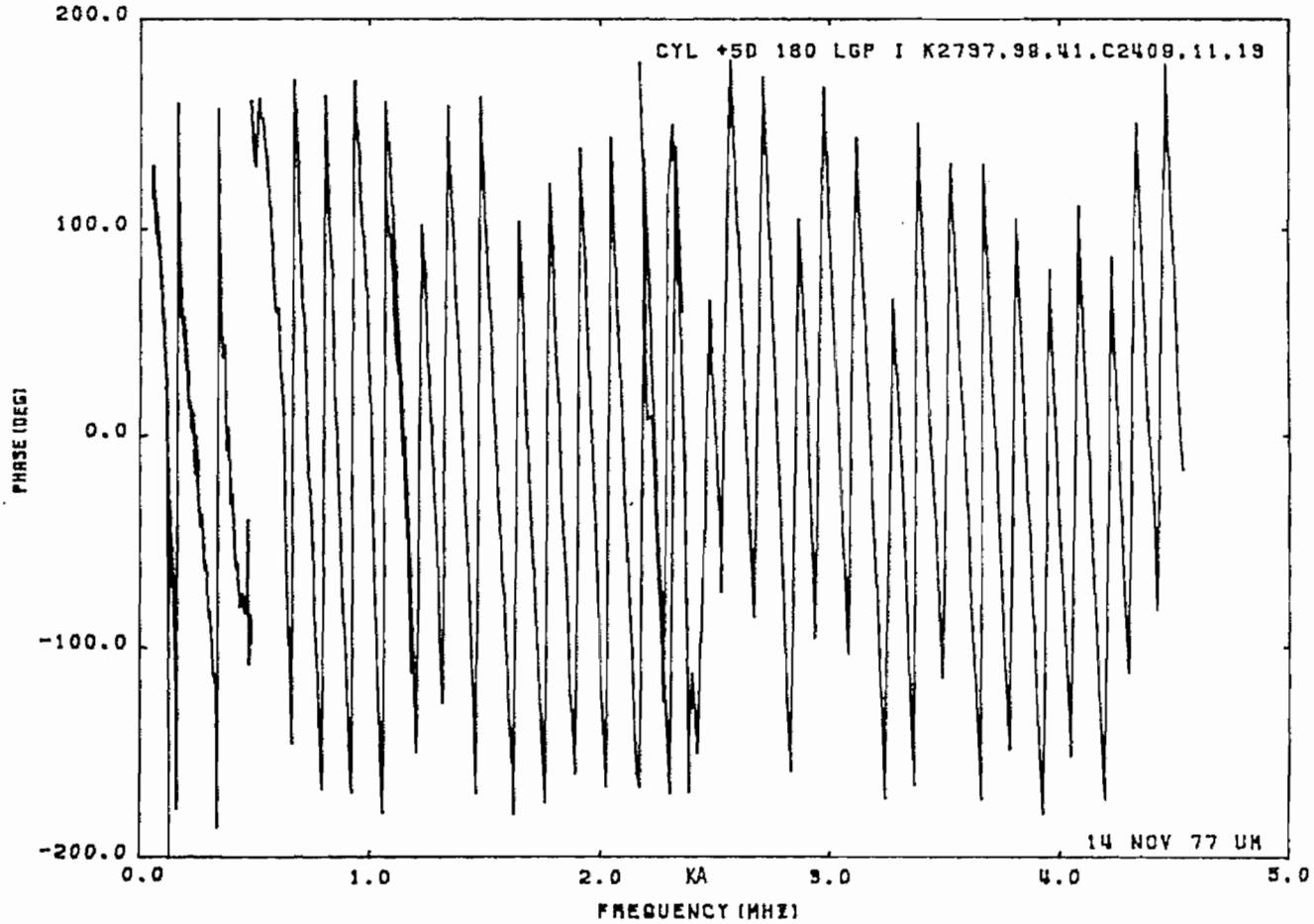

Figure 47a. Current on cylinder at STA:+5D; ϕ = 180°, h = 20a, near lossy ground plane.

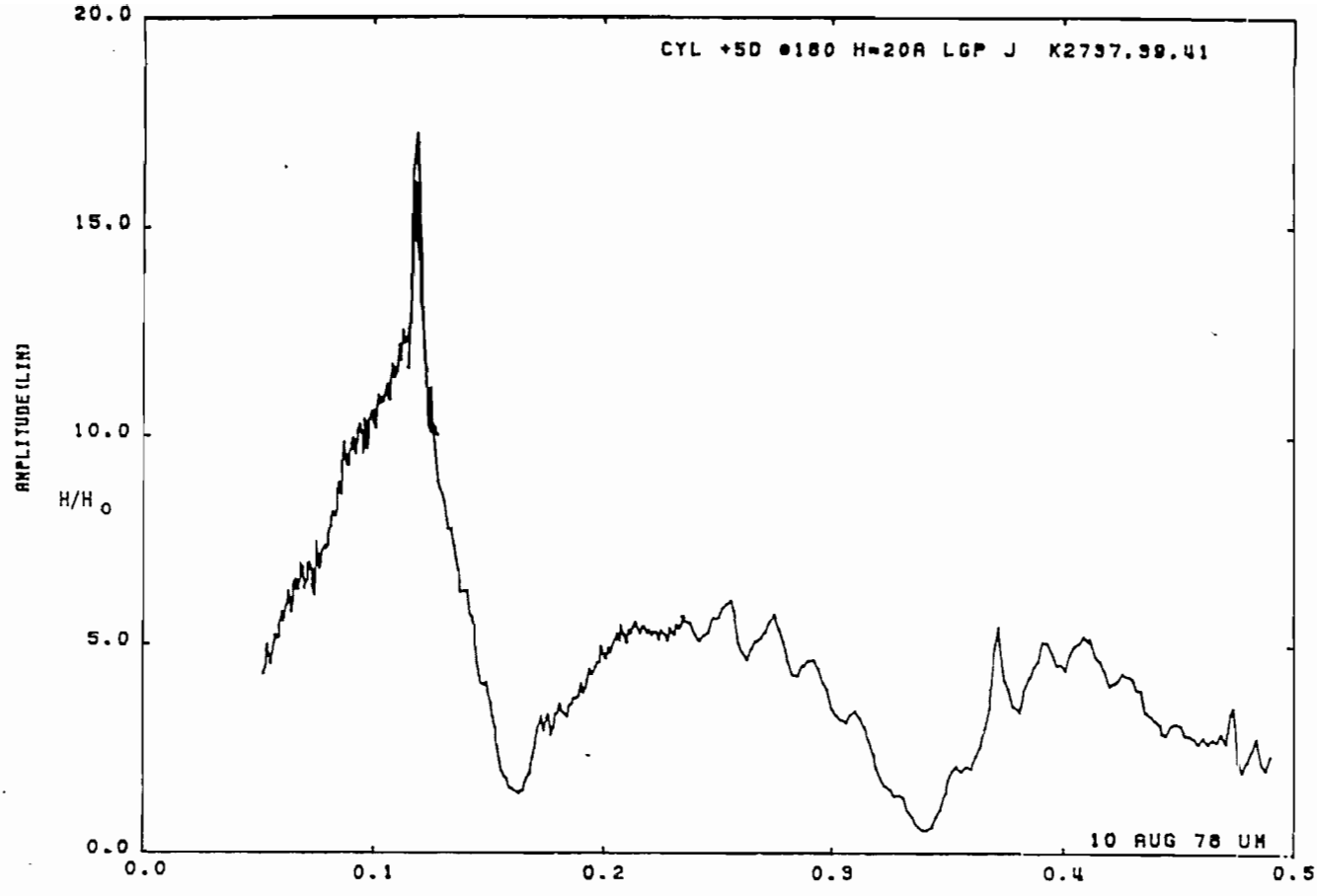

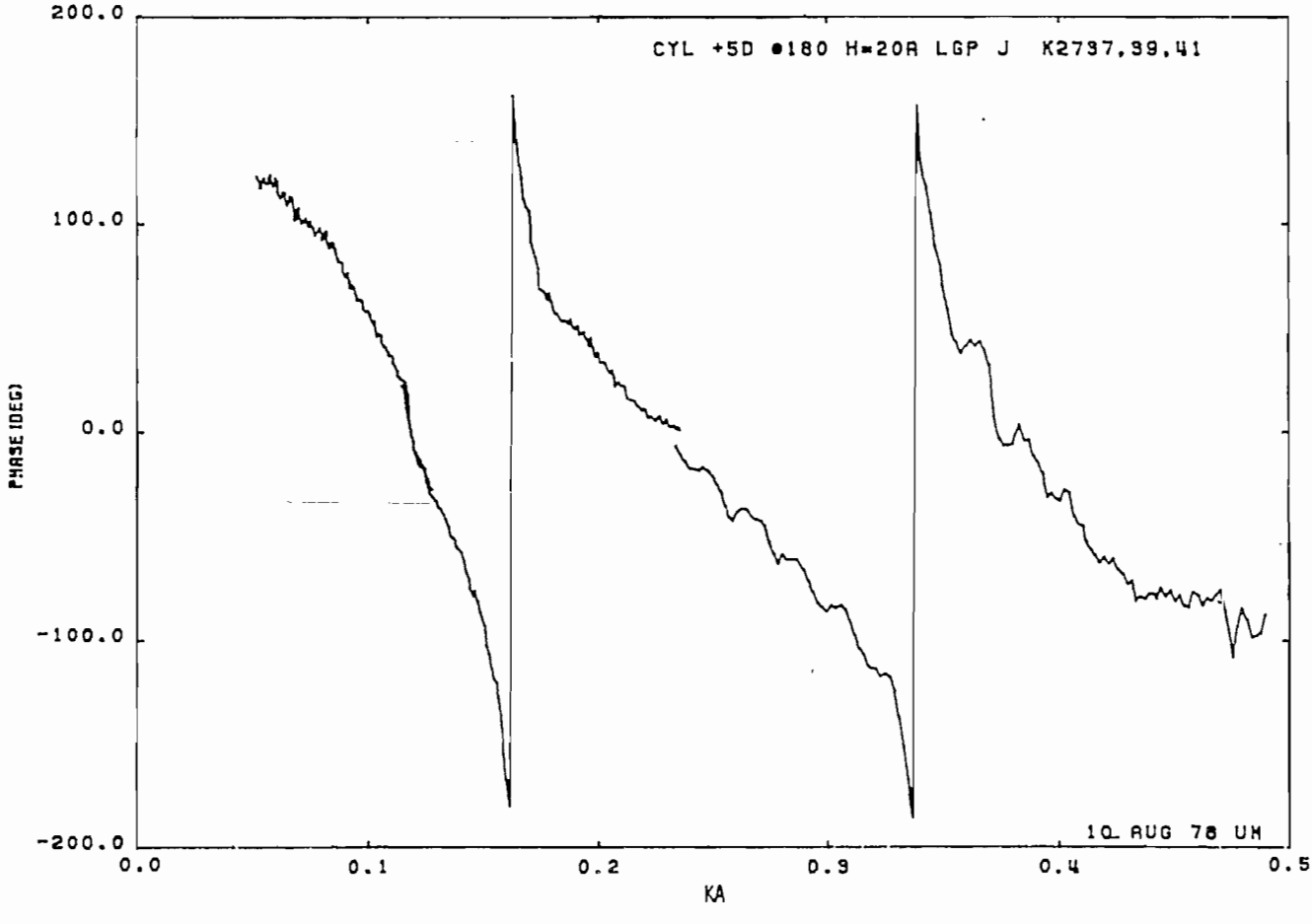

Figure 47b. Current on cylinder at STA:+5D; ø = 180°, h = 20a, near lossy ground plane (expanded scale).

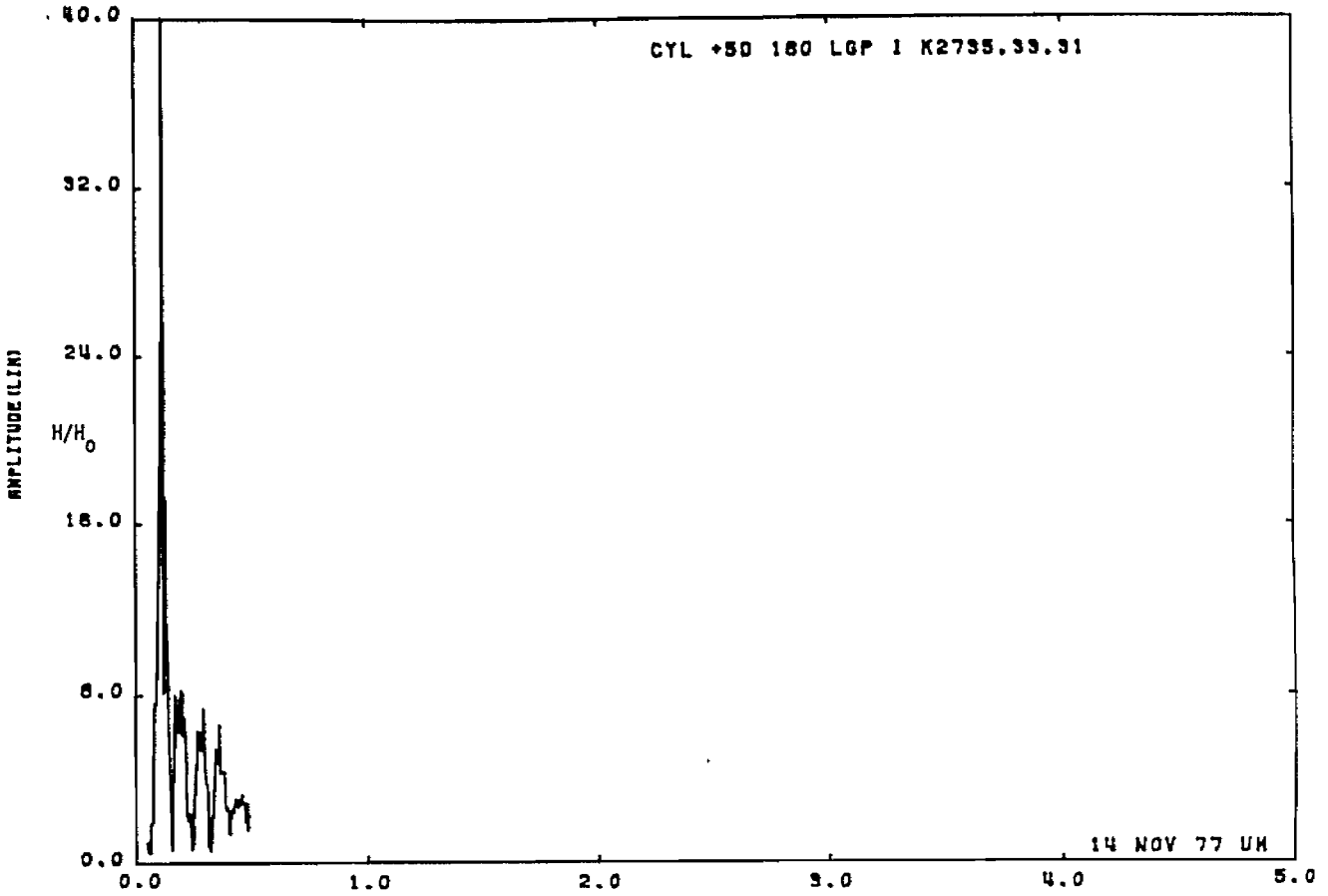

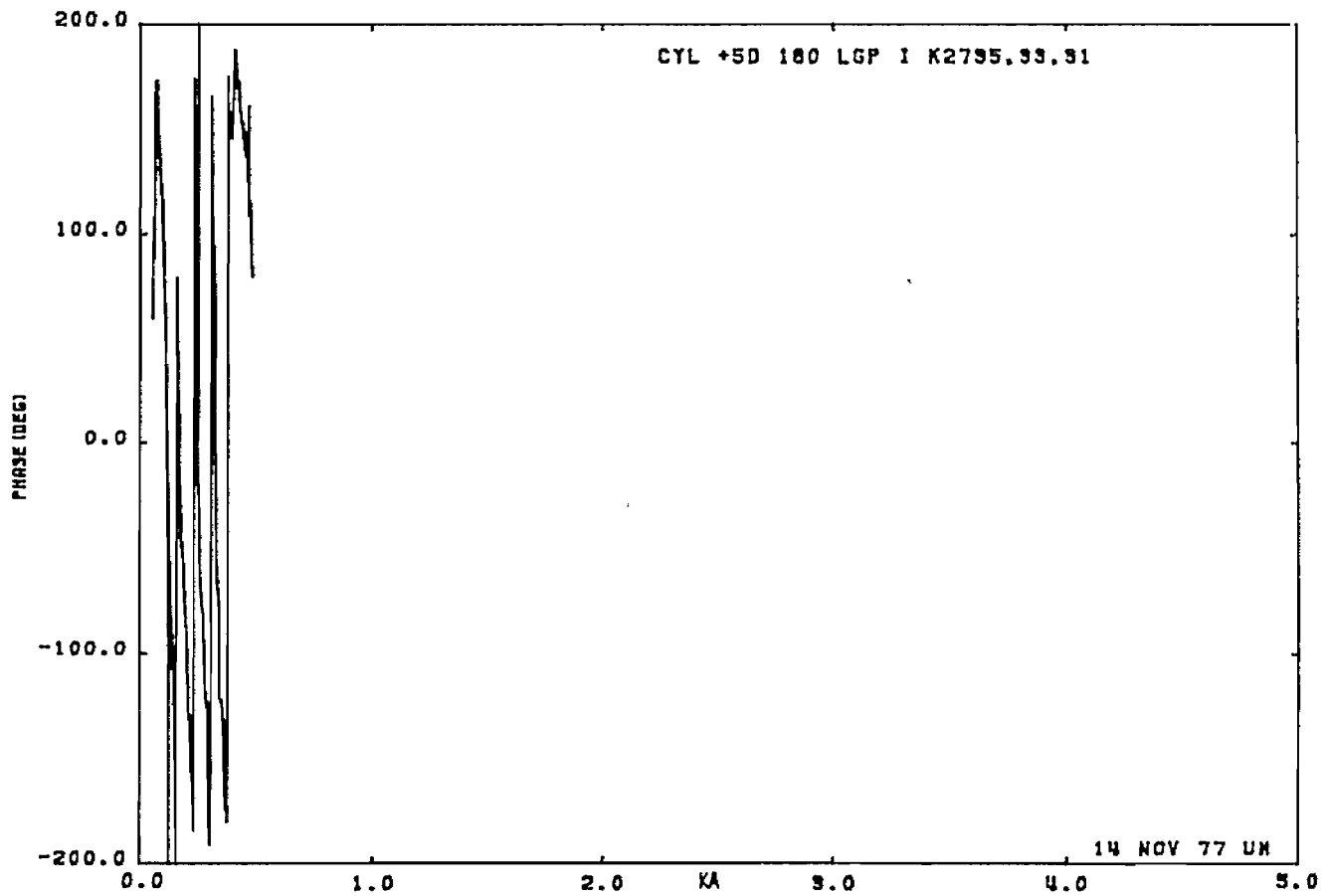

Figure 48a. Current on clyinder at STA:+50; β = 180°, h = 40a, near lossy ground plane.

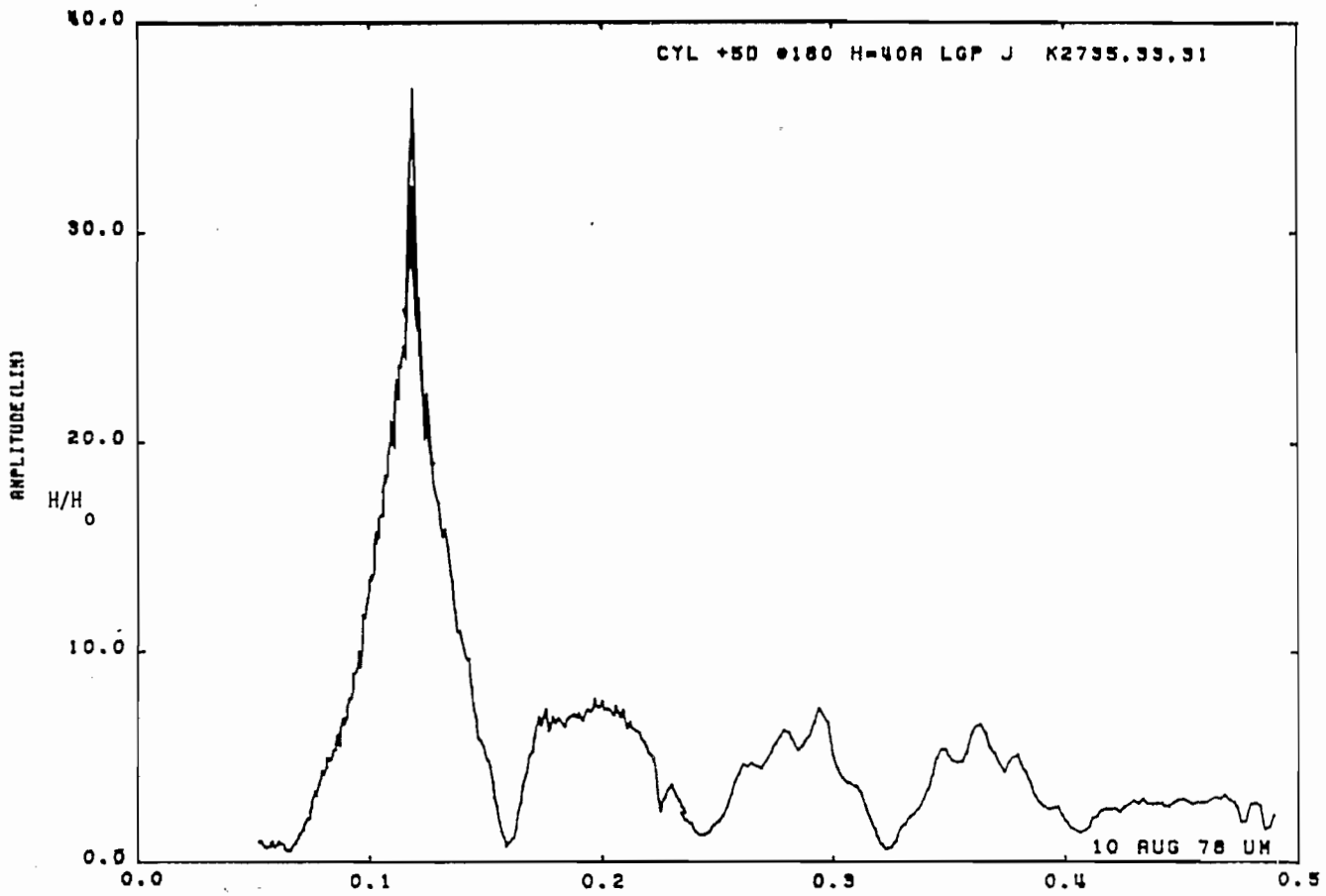

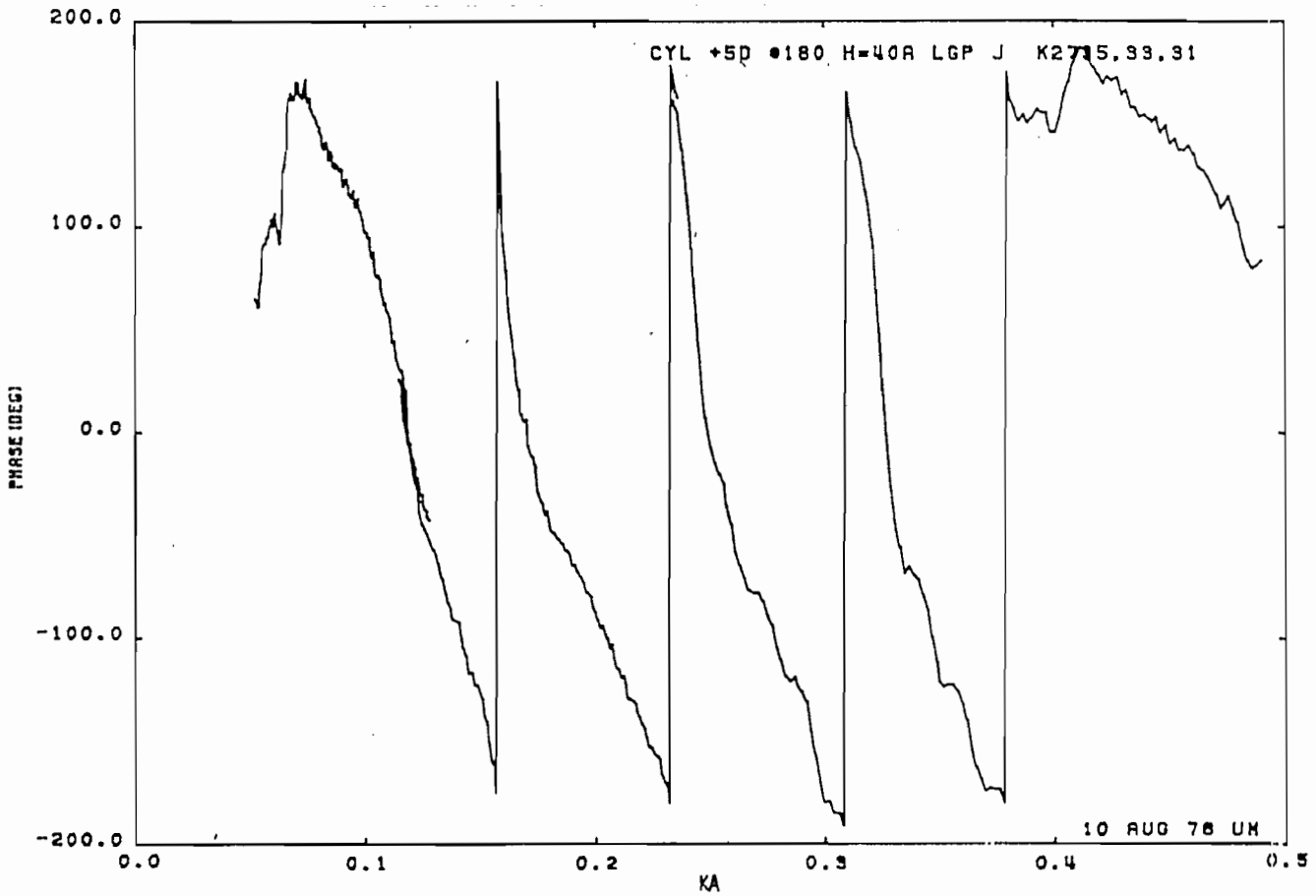

Figure 48b. Current on cylinder at STA:+5D; β = 180°, h = 40a, near lossy ground plane (expanded scale).

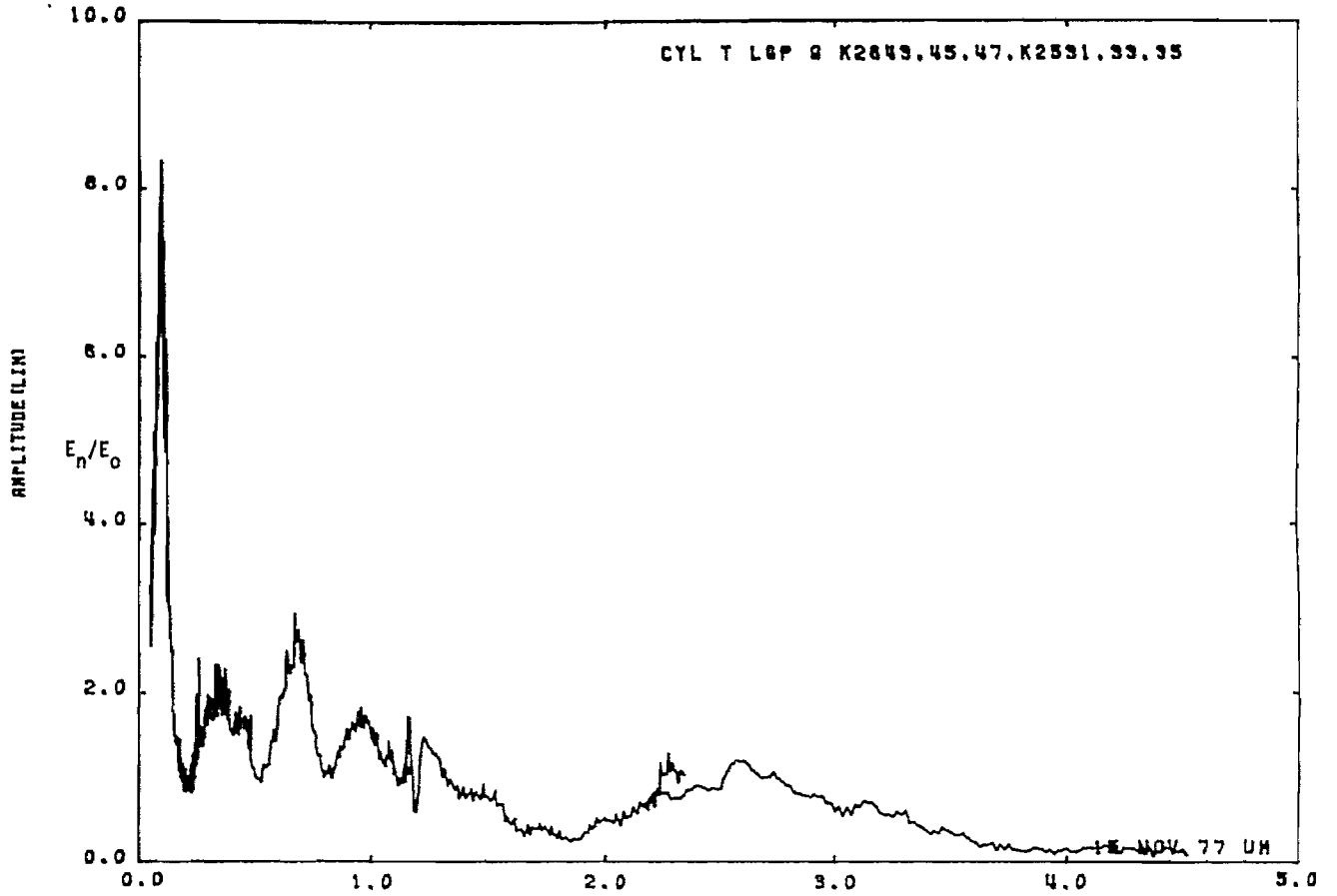

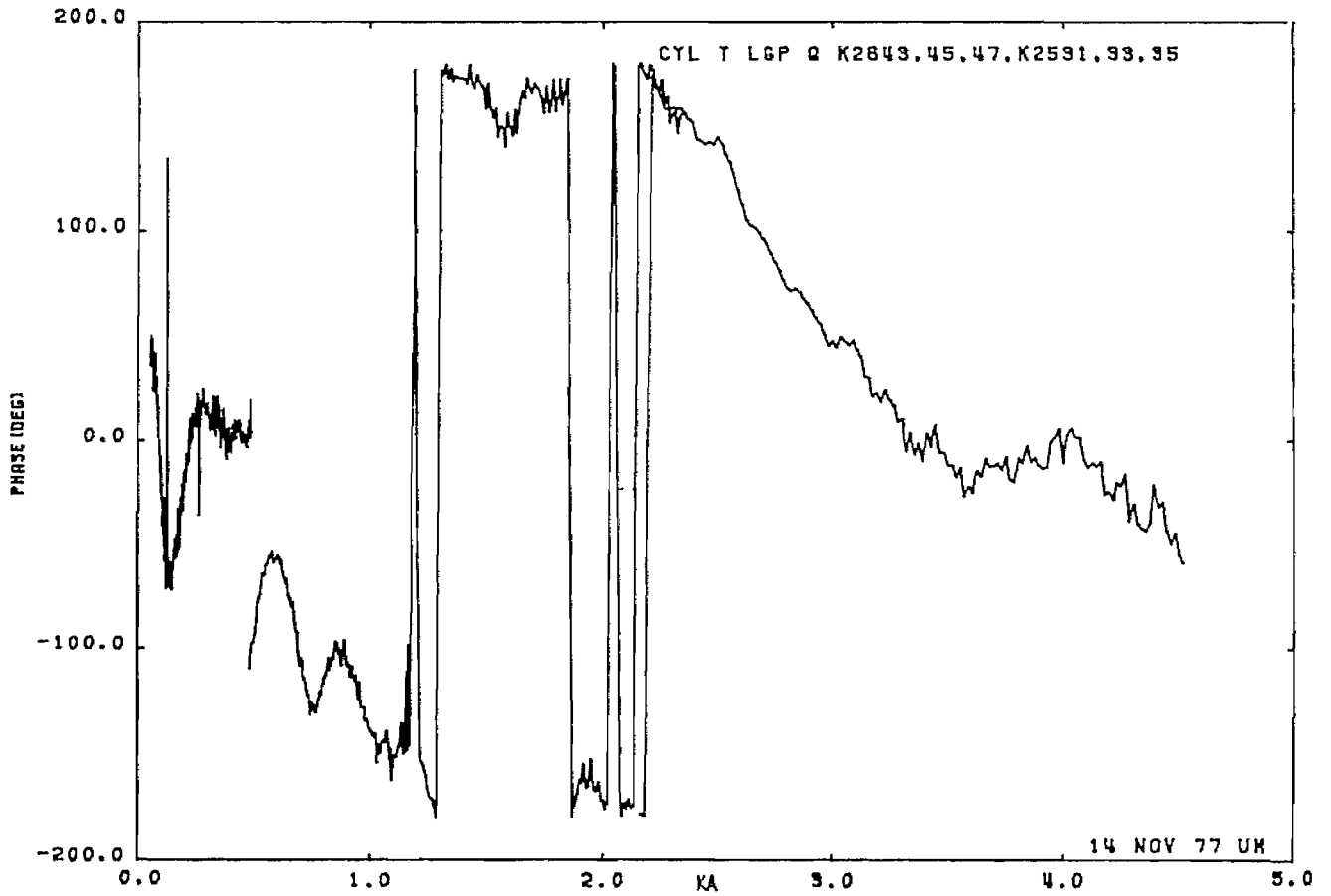

Figure 49a. Charge on cylinder at STA:T; h = 1.5a, near lossy ground plane.

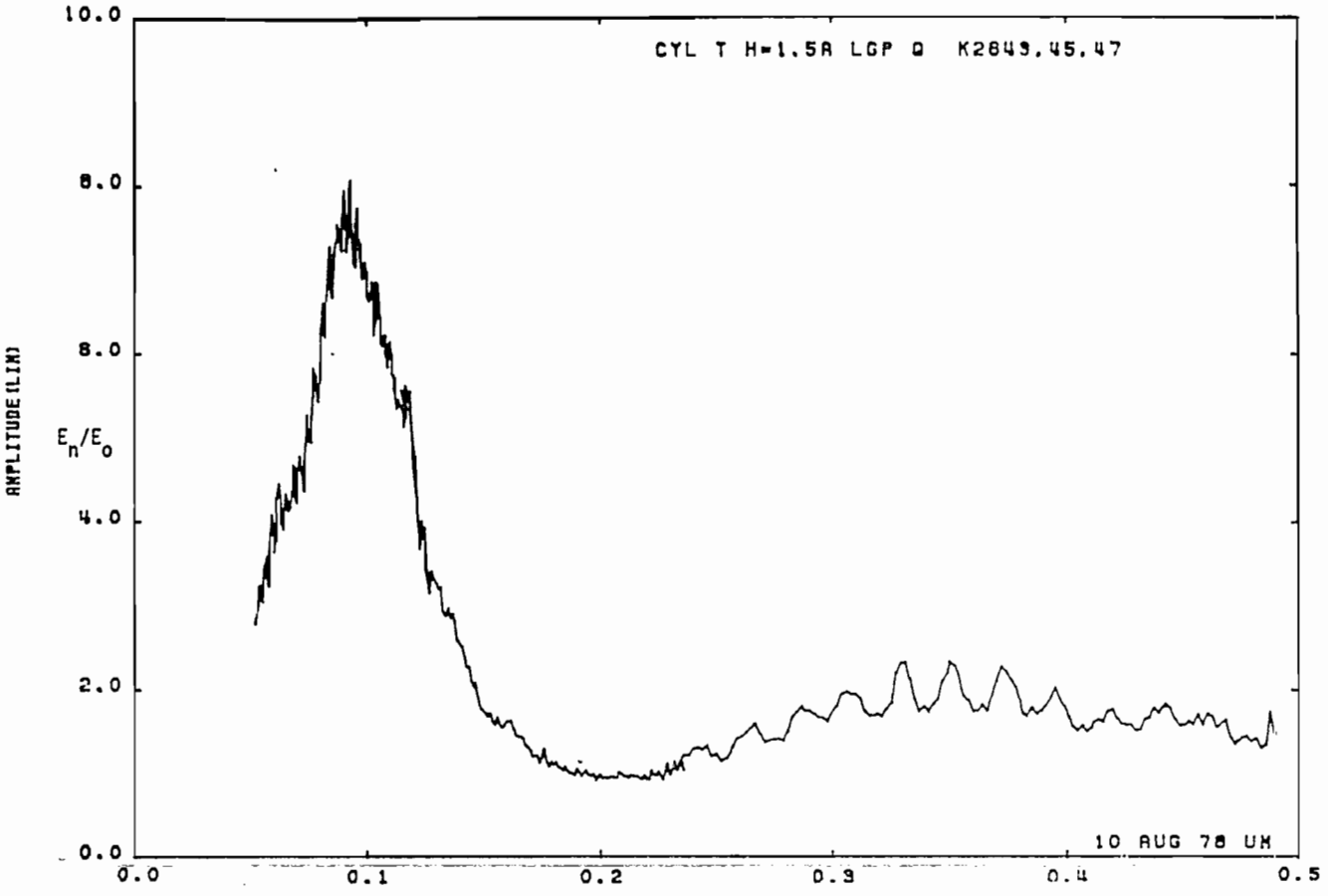

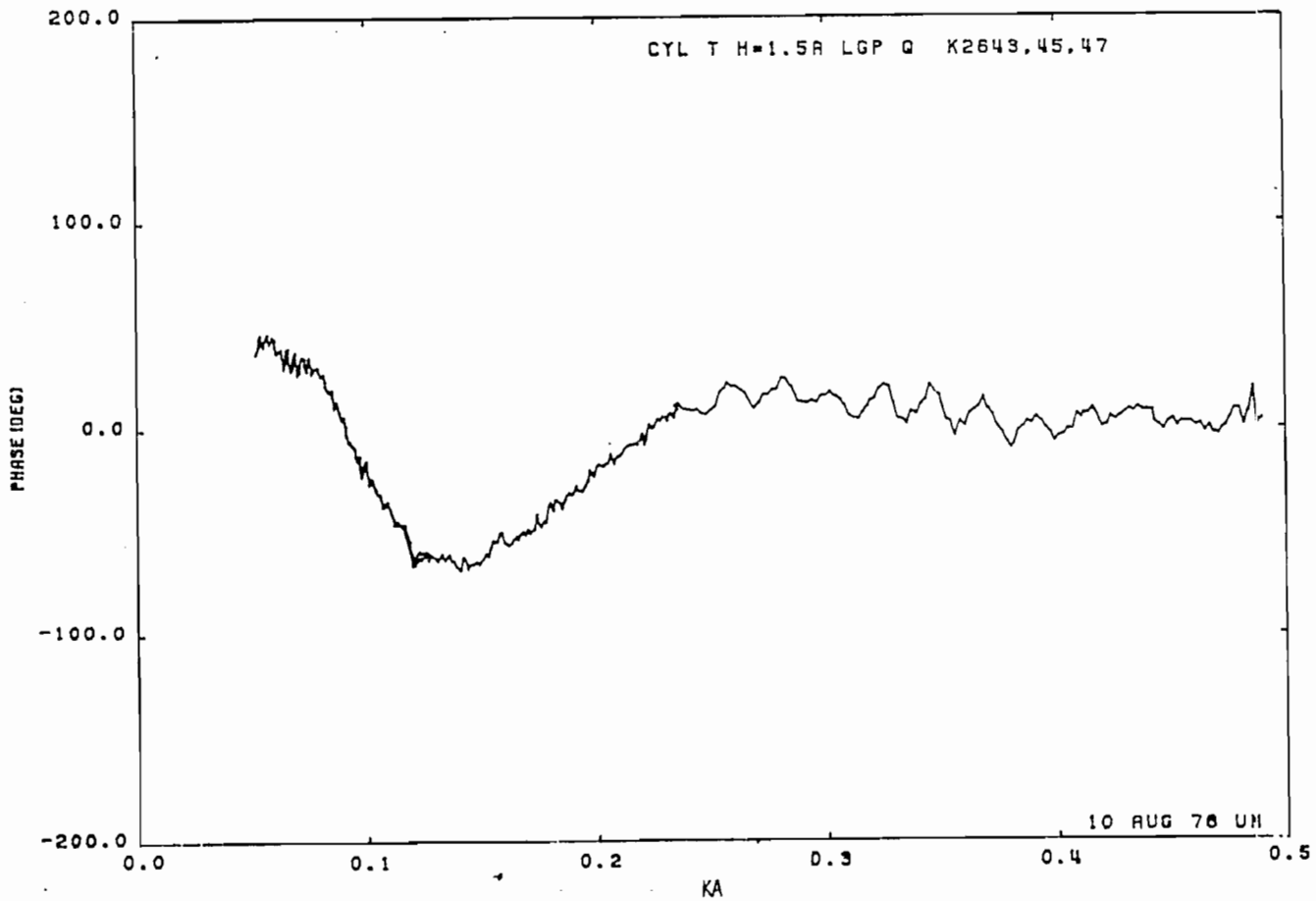

Figure 49b. Charge on cylinder at STA:T; h = 1.5a, near lossy ground plane (expanding scale).

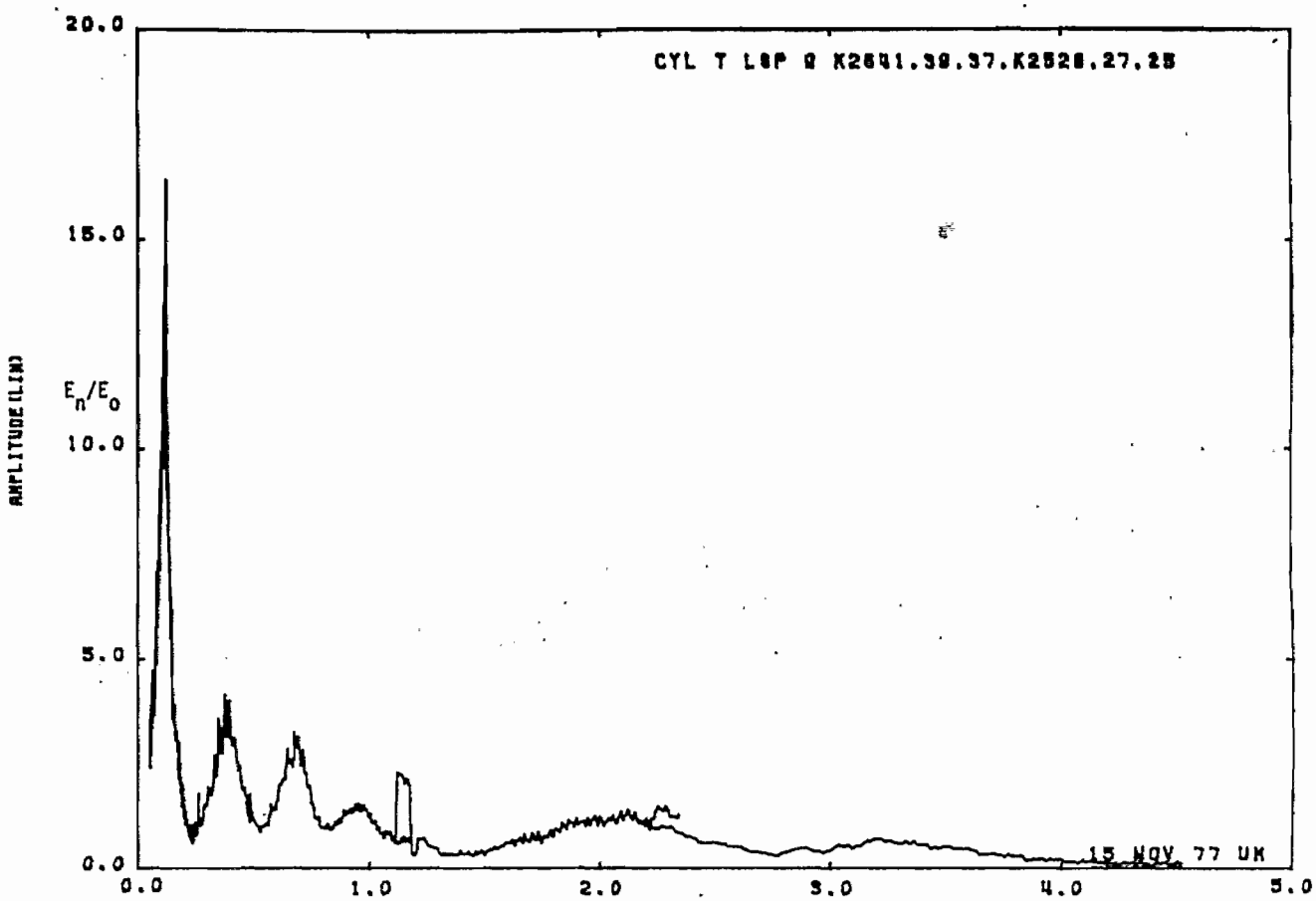

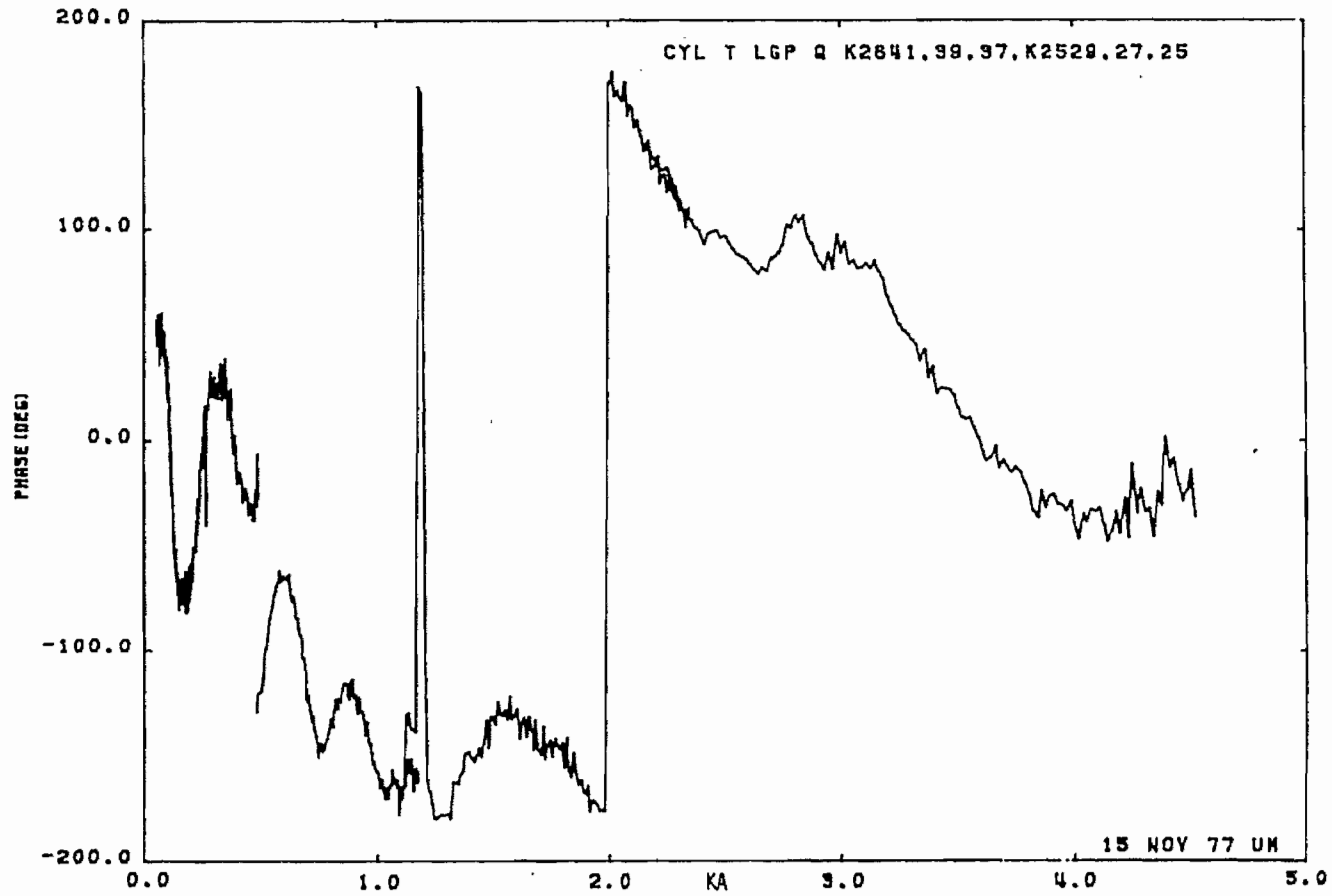

Figure 50a. Charge on cylinder STA:T; h = 2a, near lossy ground plane.

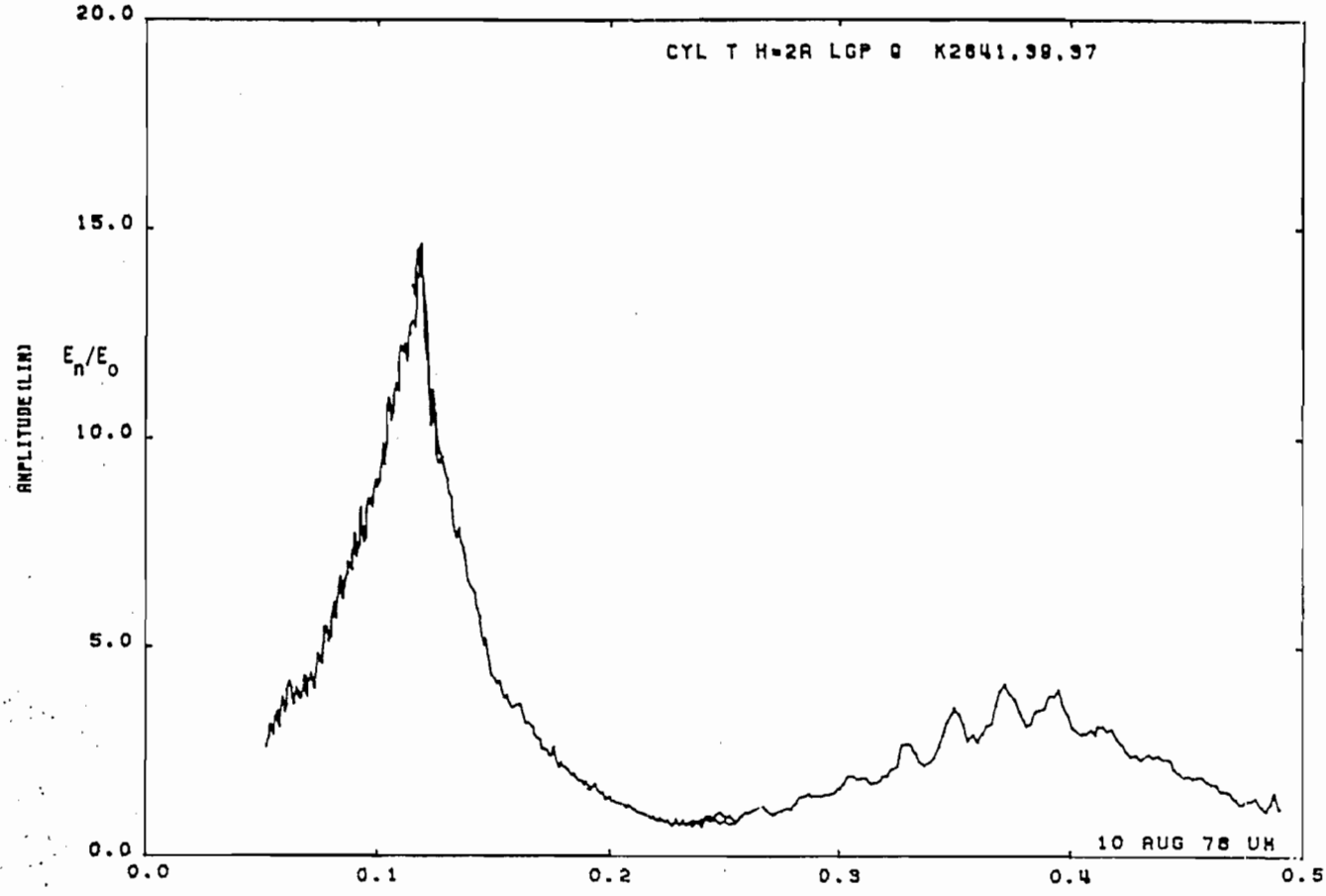

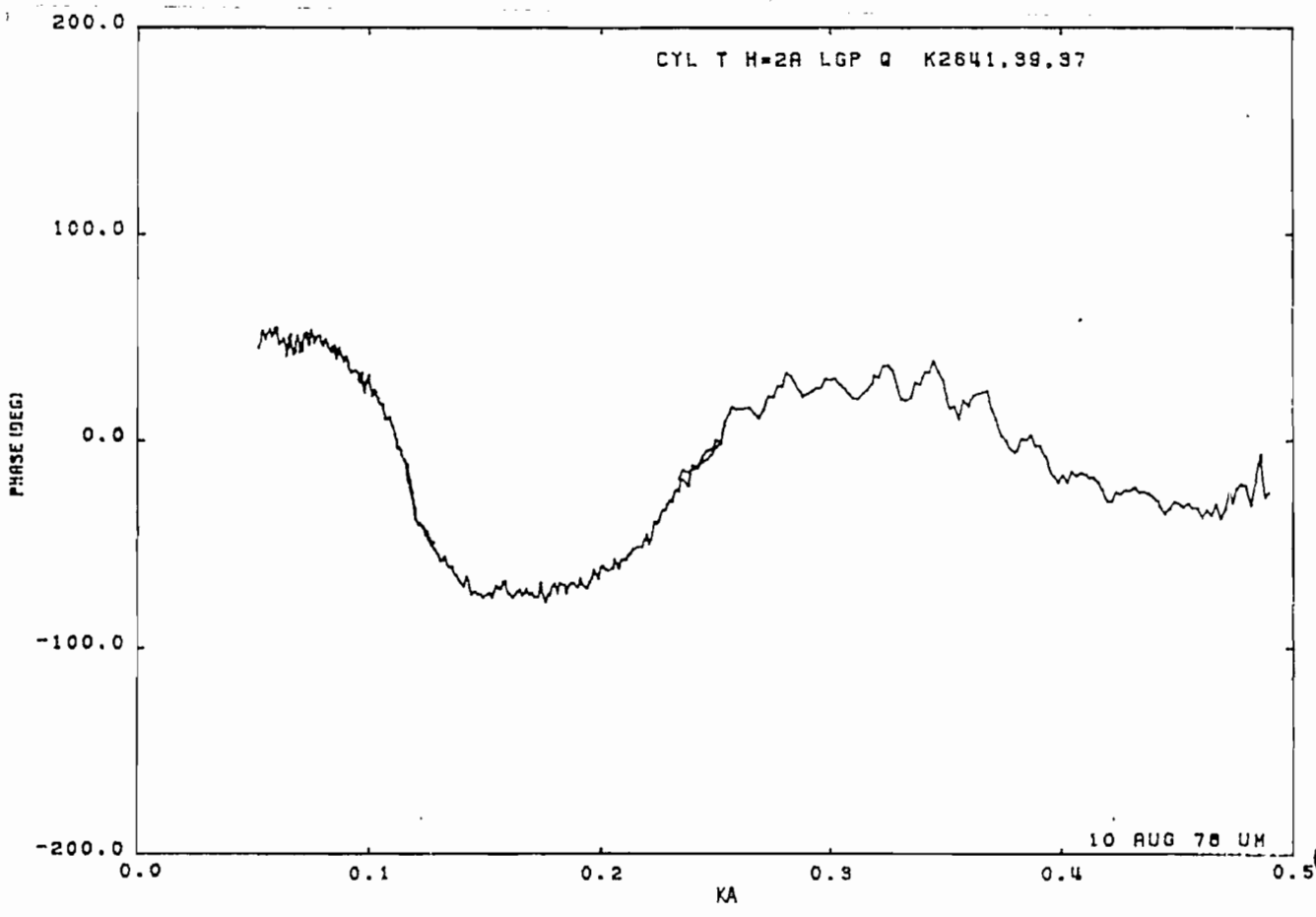

Figure 50b. Charge on cylinder at STA:T; h = 2a, near lossy ground plane (expanded scale).

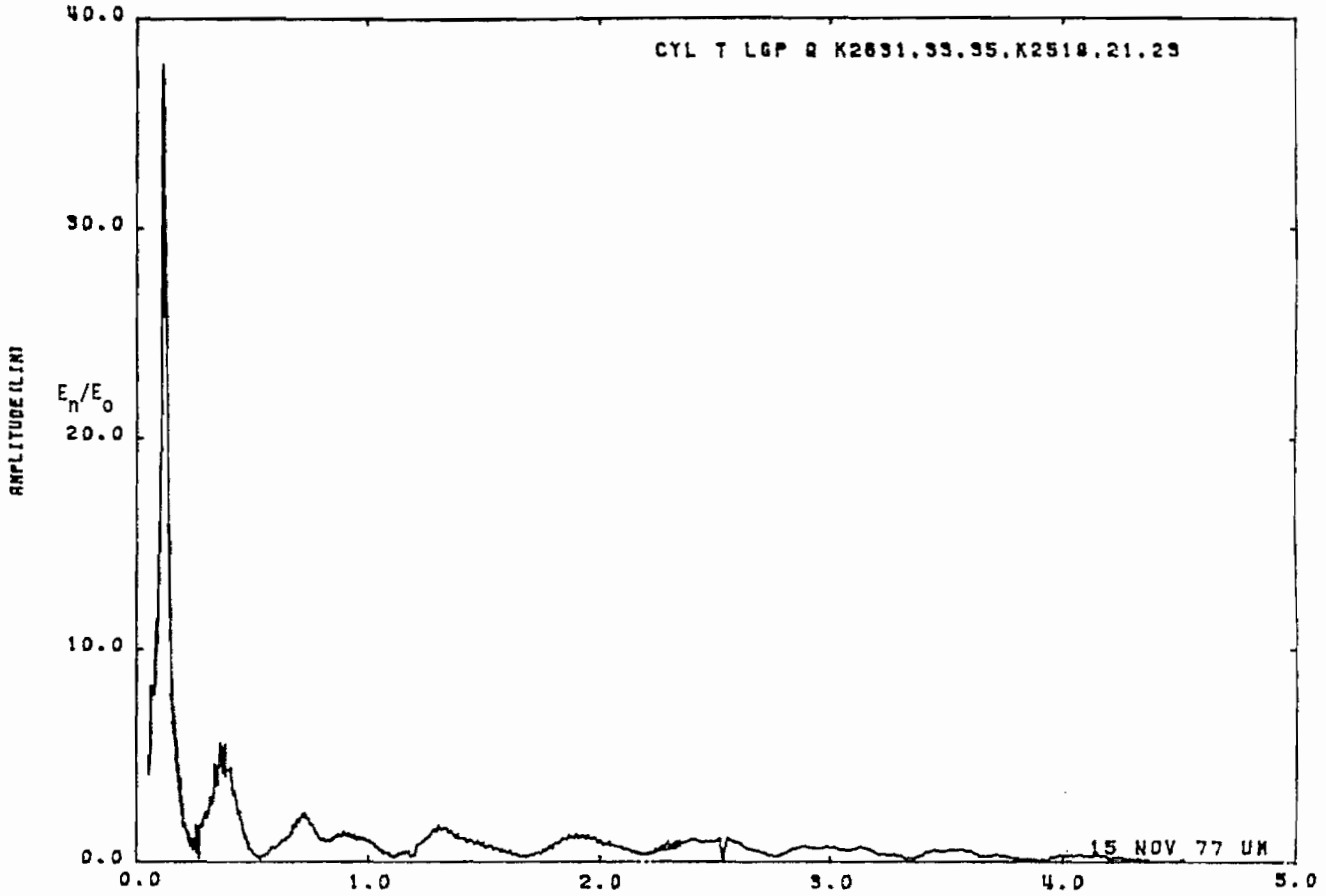

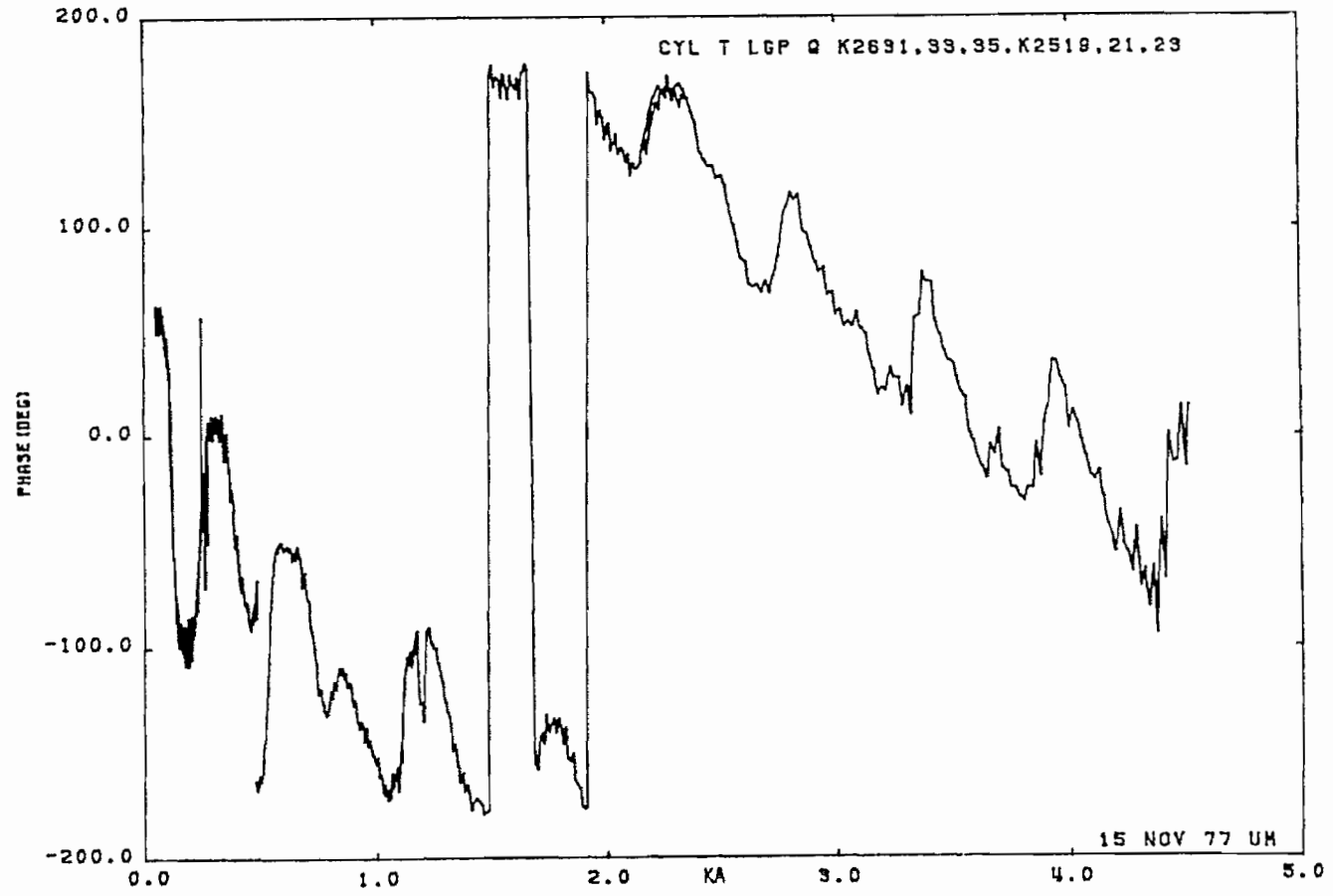

Figure 51a. Charge on cylinder at STA:T; h = 5a, near lossy ground plane.

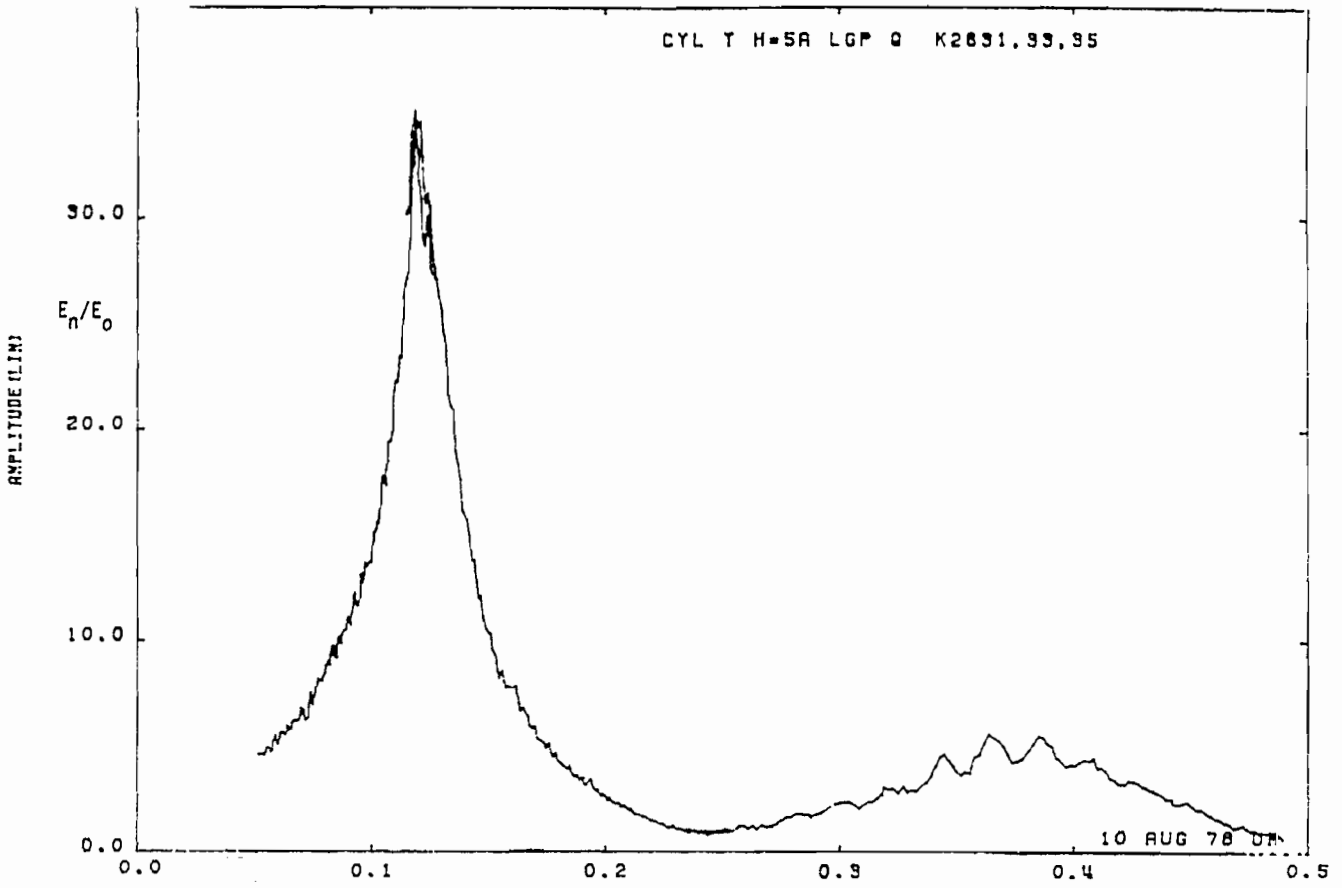

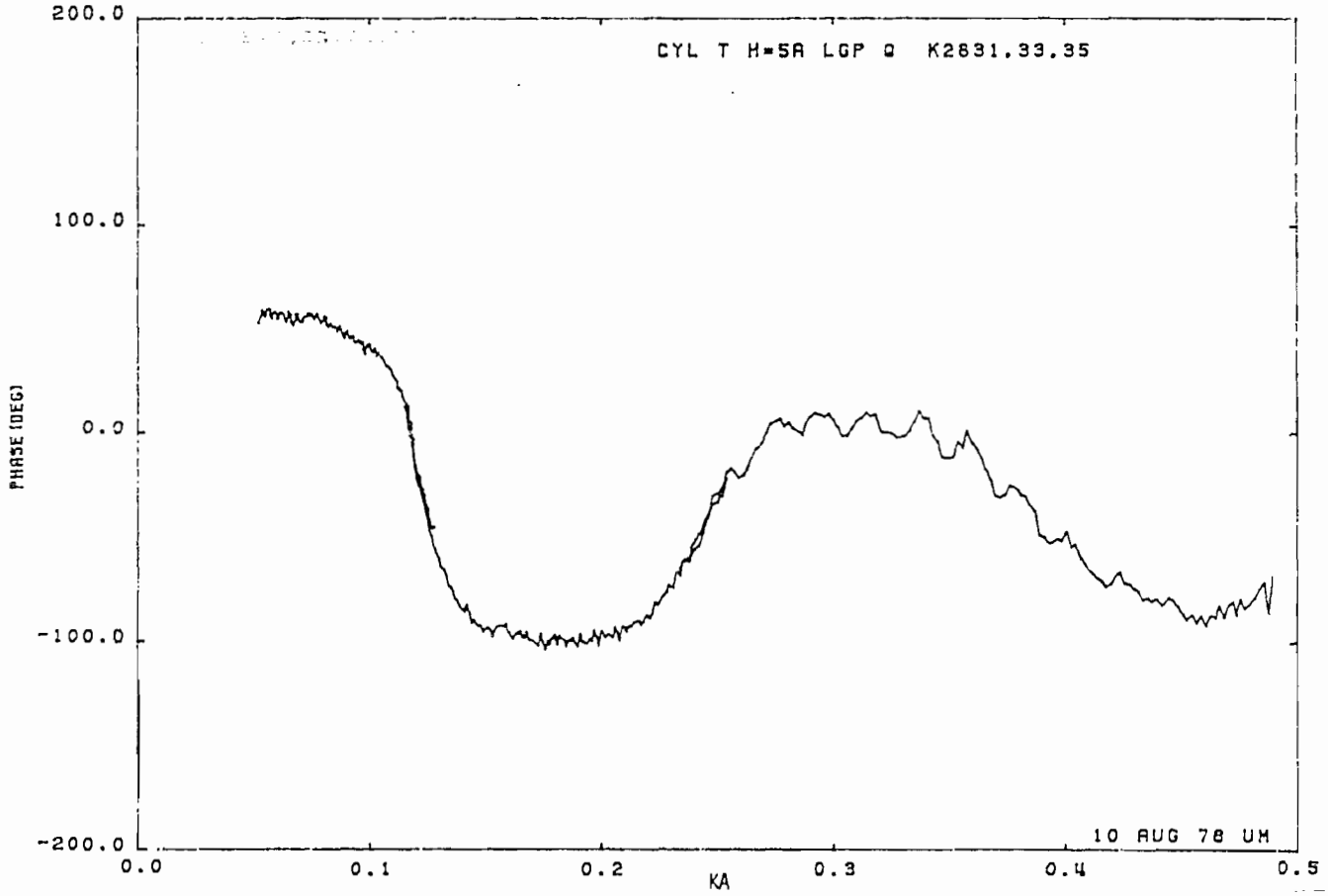

Figure 51b. Charge on cylinder at STA:T; h = 5a, near lossy ground plane (expanded scale).

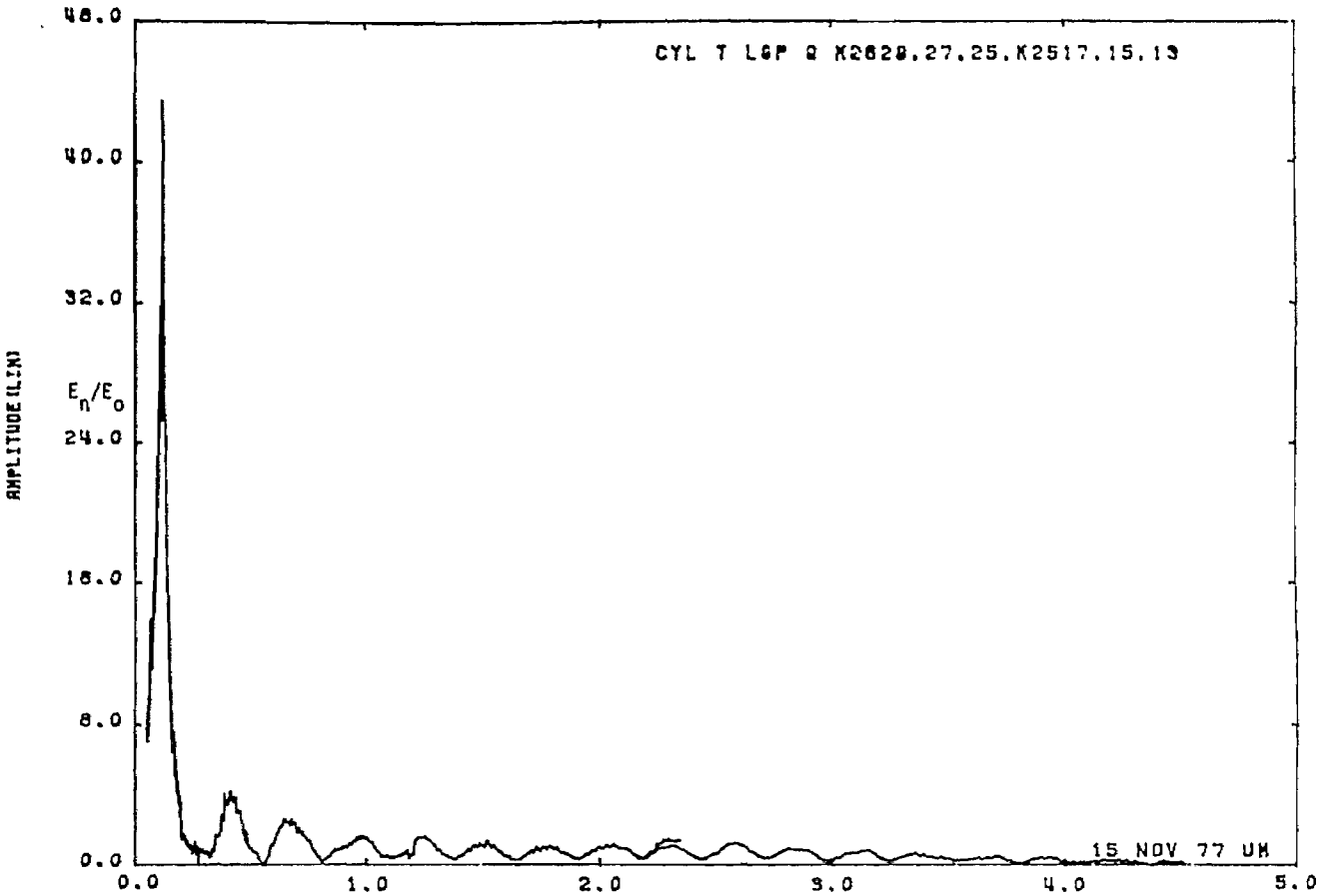

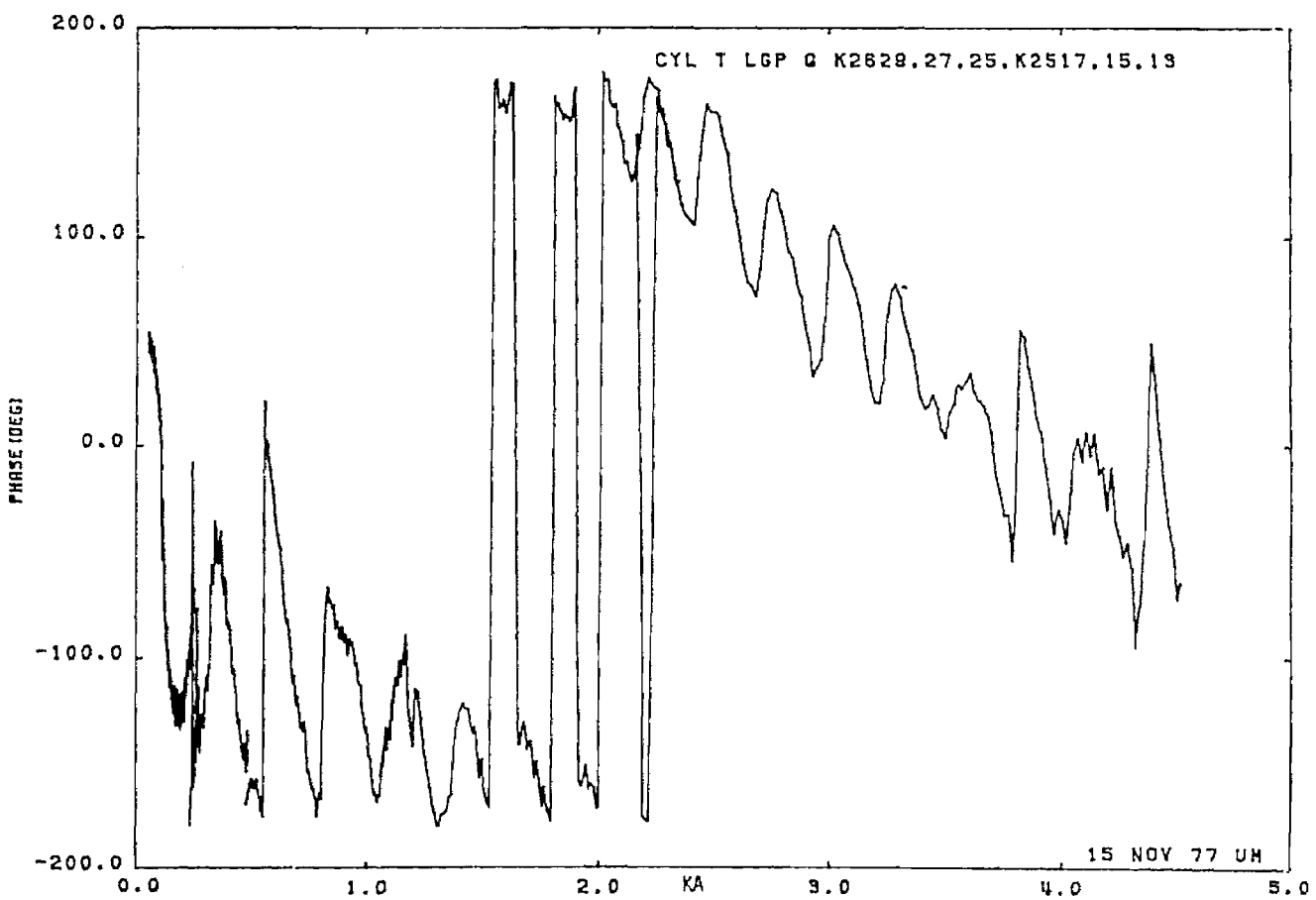

Figure 52a. Charge on cylinder at STA:T; h = 10a, near lossy ground plane.

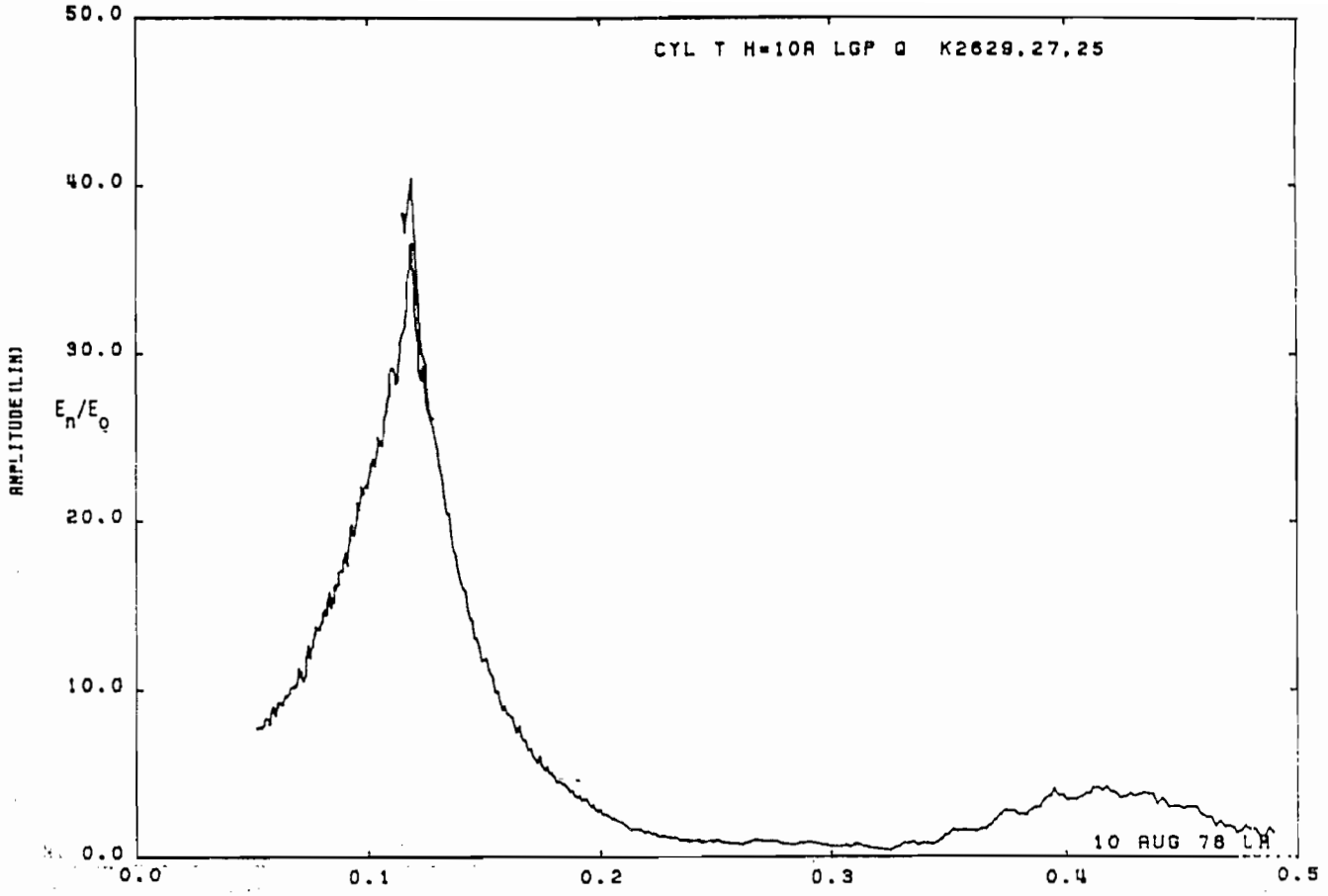

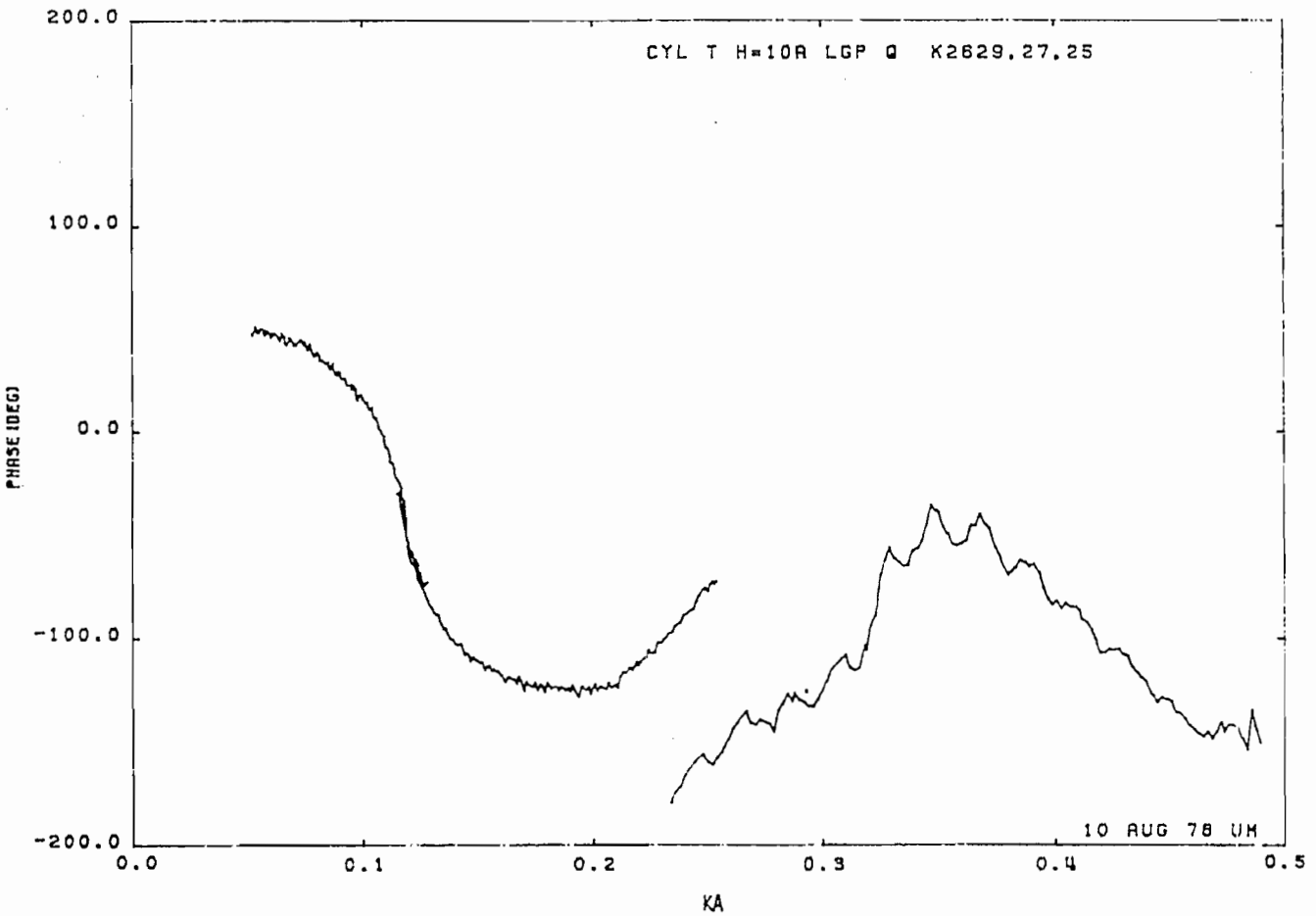

Figure 52b. Charge on cylinder at STA:T; h = 10a, near lossy ground plane (expanded scale).

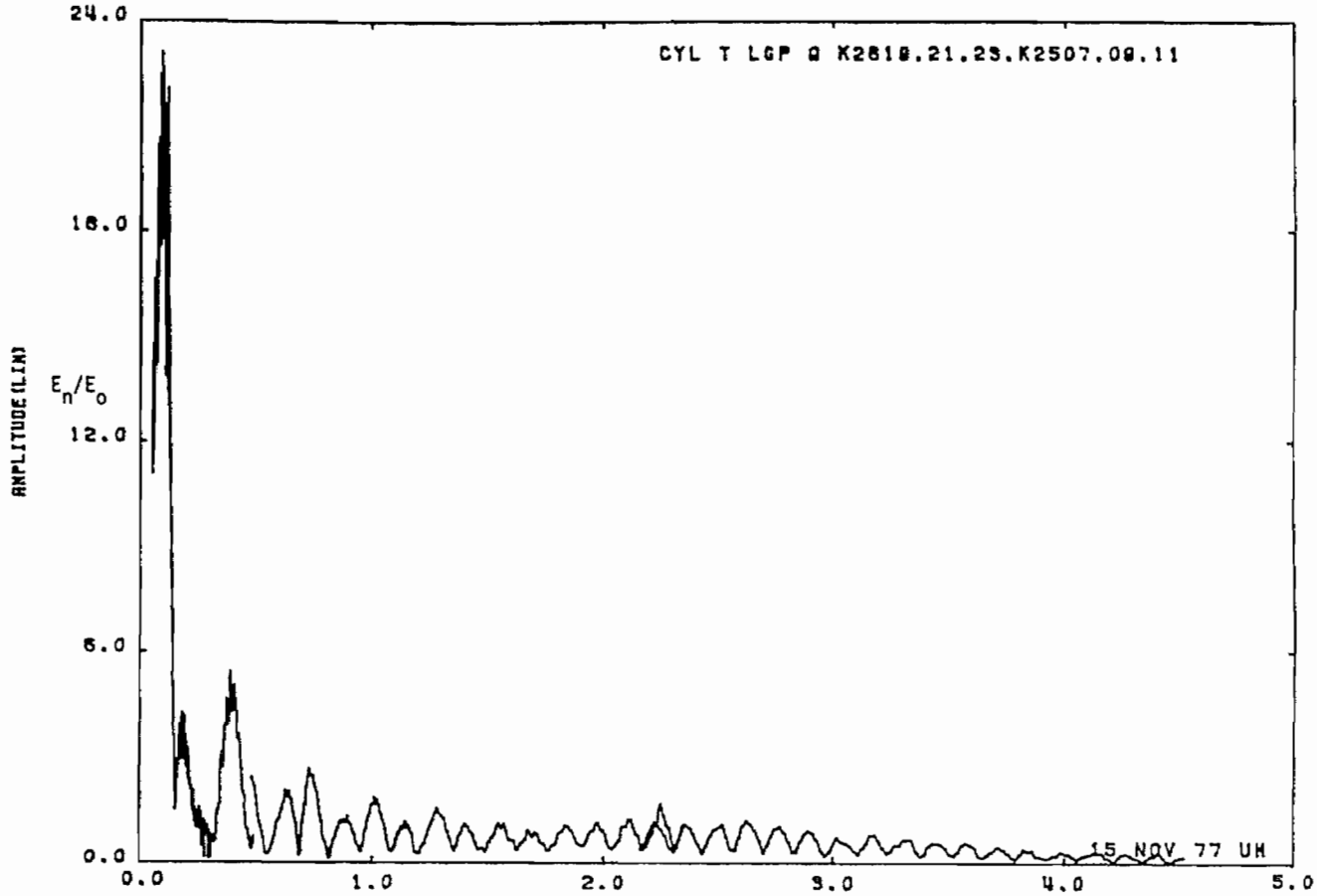

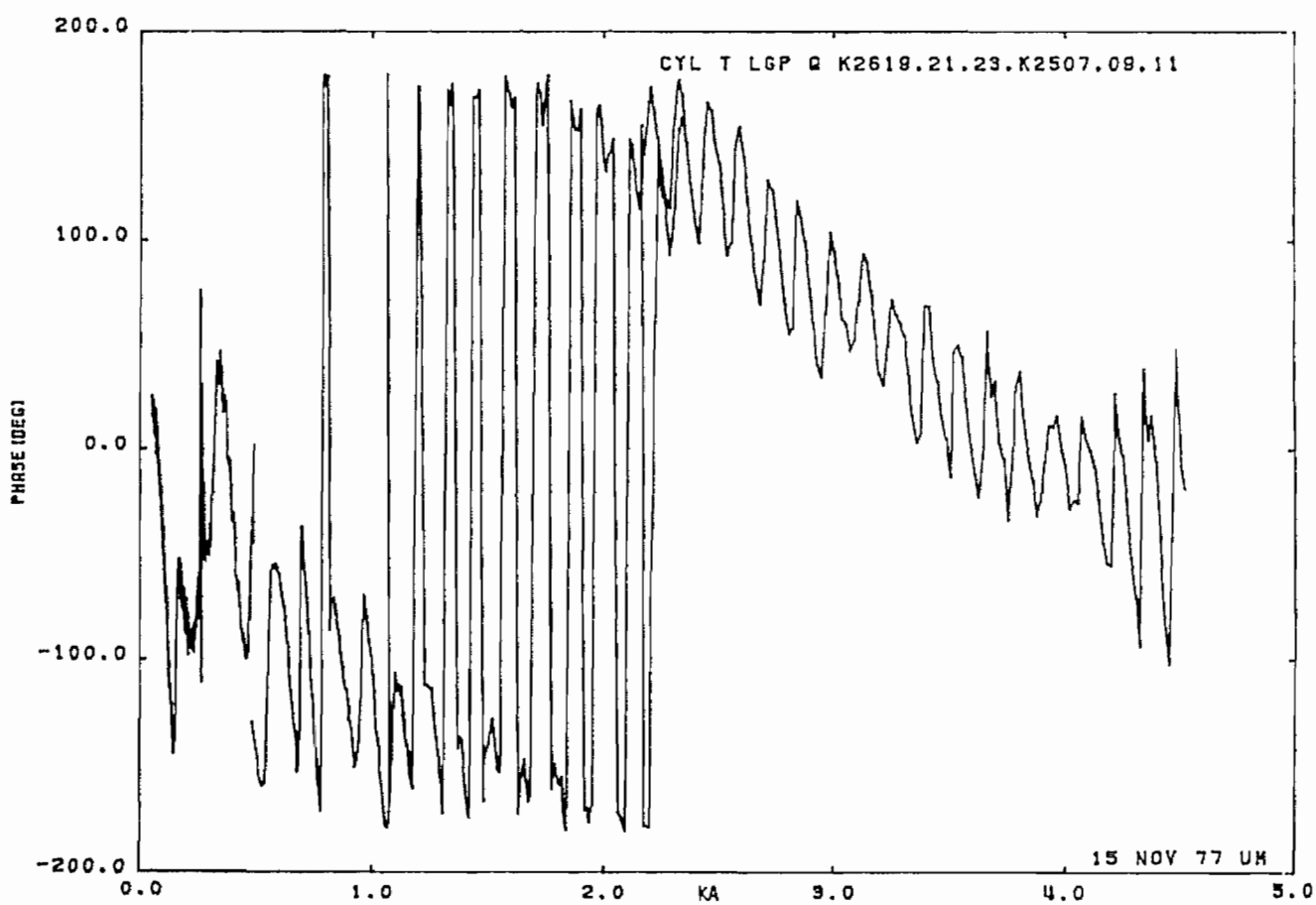

Figure 53a. Charge on cylinder at STA:T; h = 20a, near lossy ground plane.

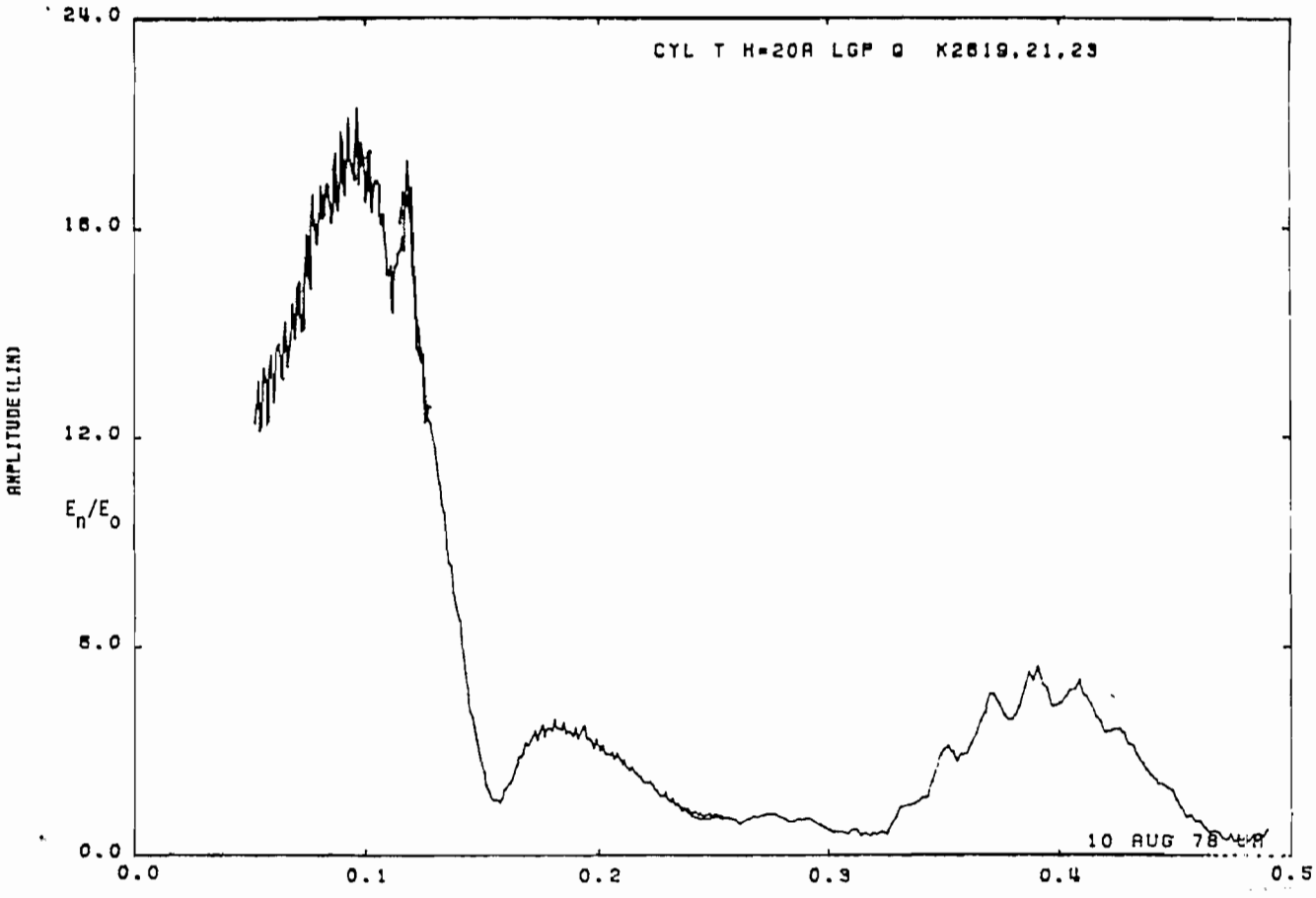

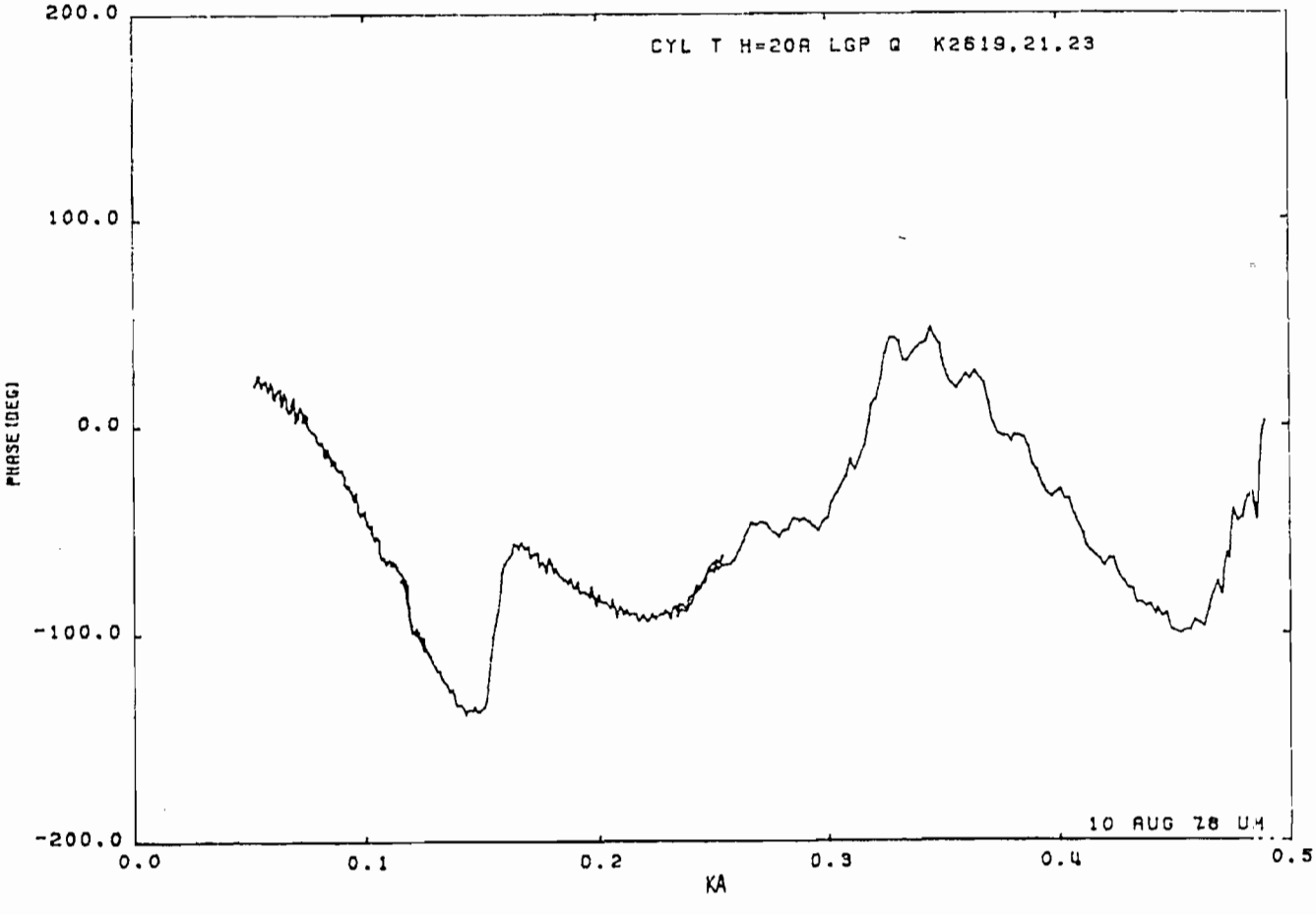

Figure 53b. Charge on cylinder at STA:T; h = 20a, near lossy ground plane (expanded scale).

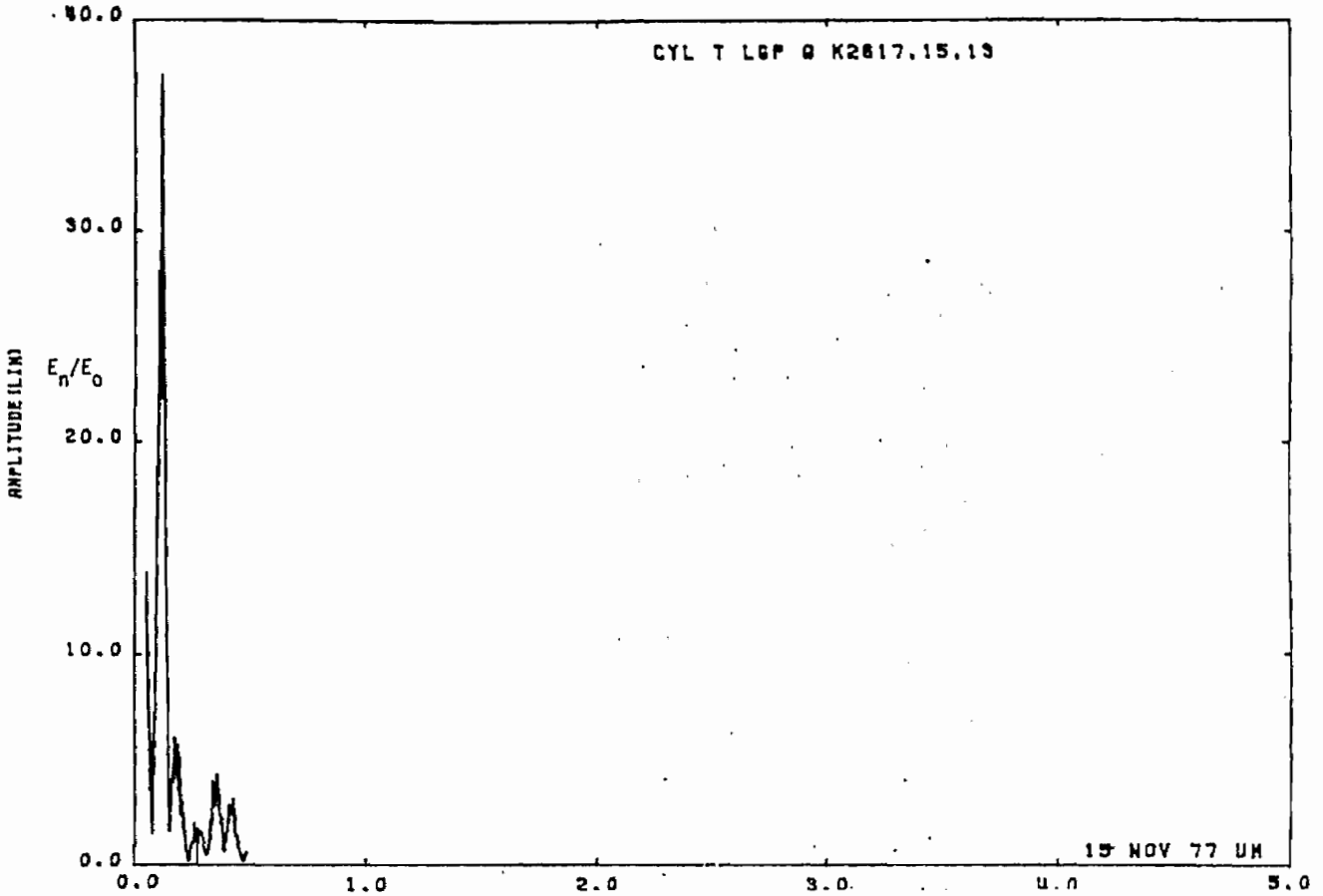

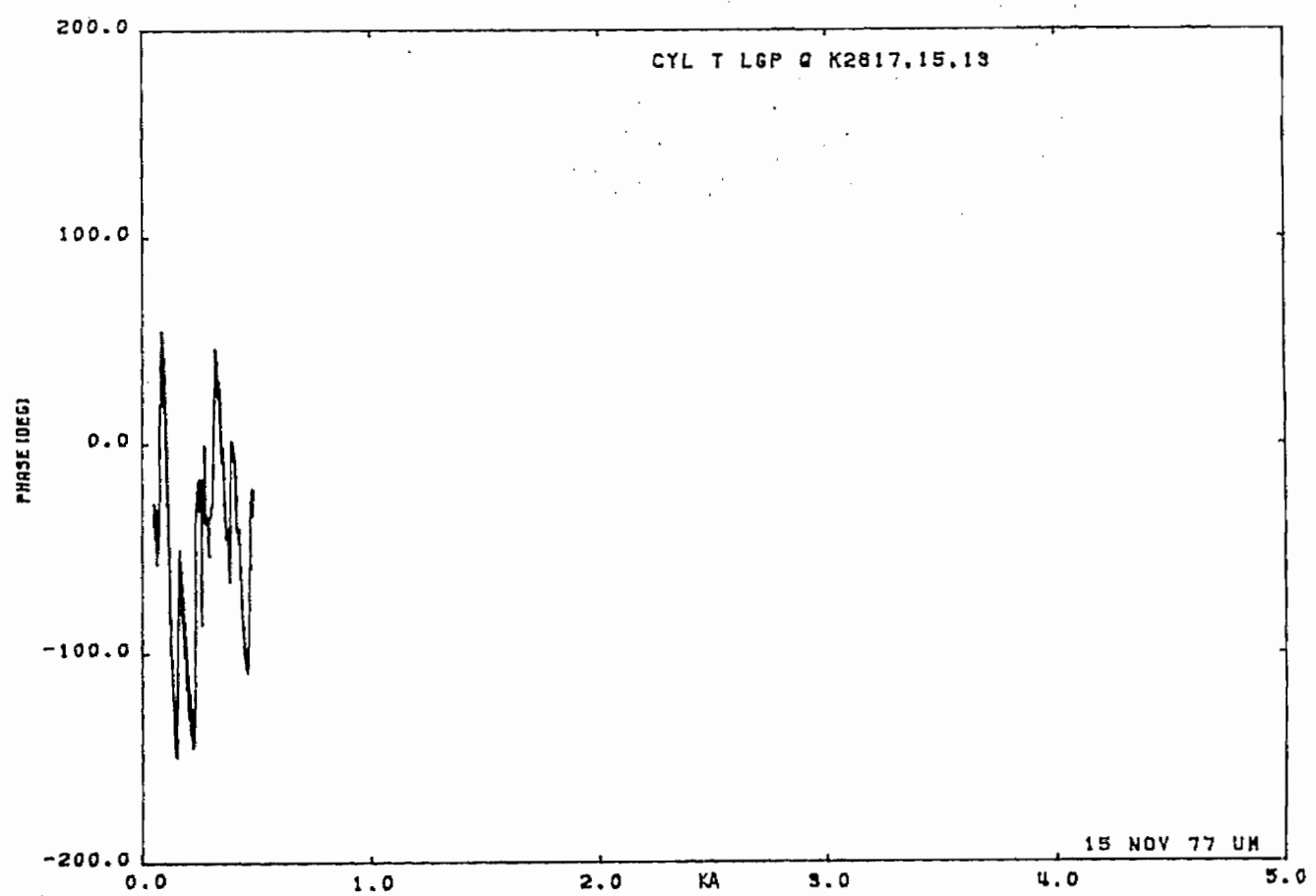

Figure 54a. Charge on cylinder at STA:T; h = 40a, near lossy ground plane.

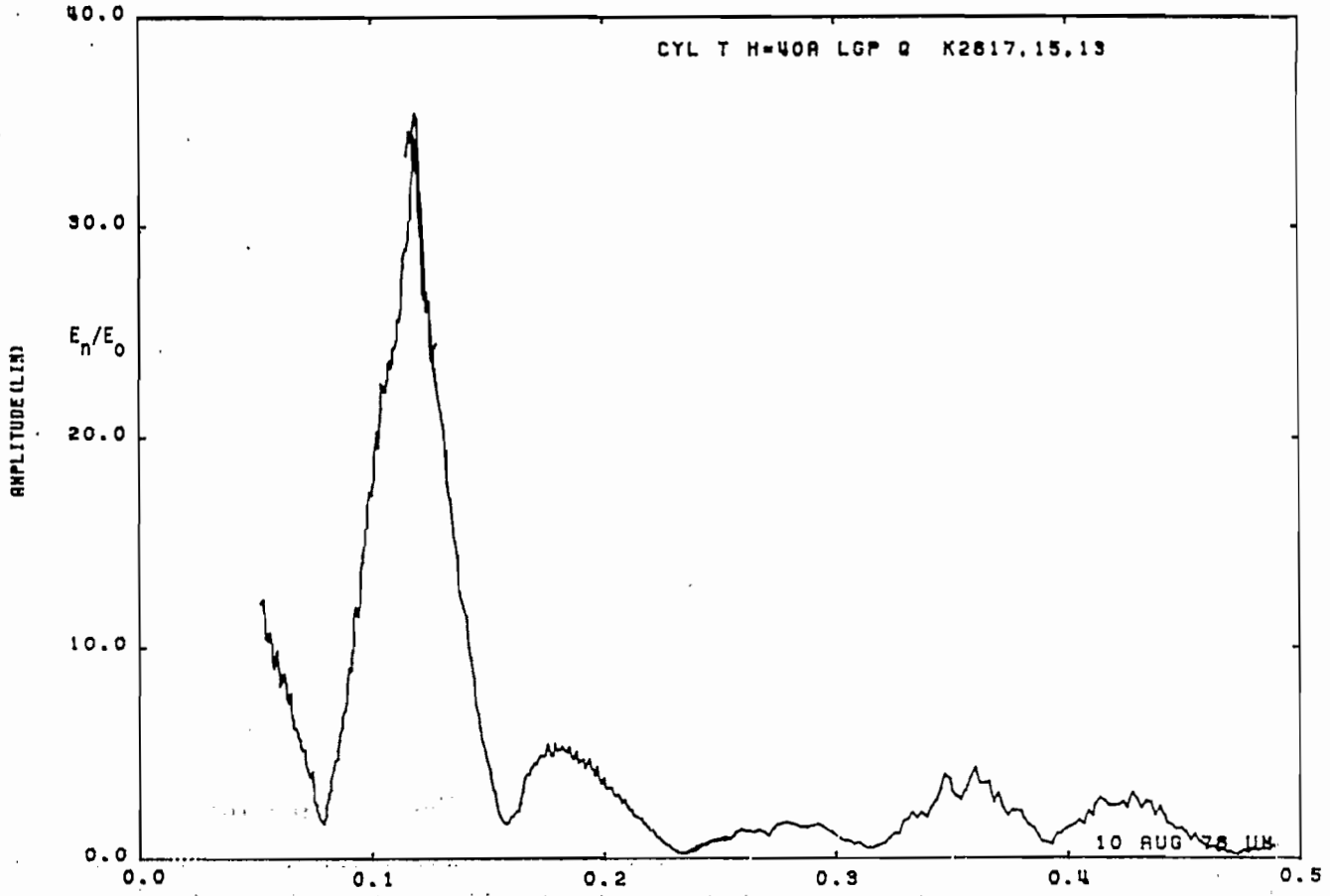

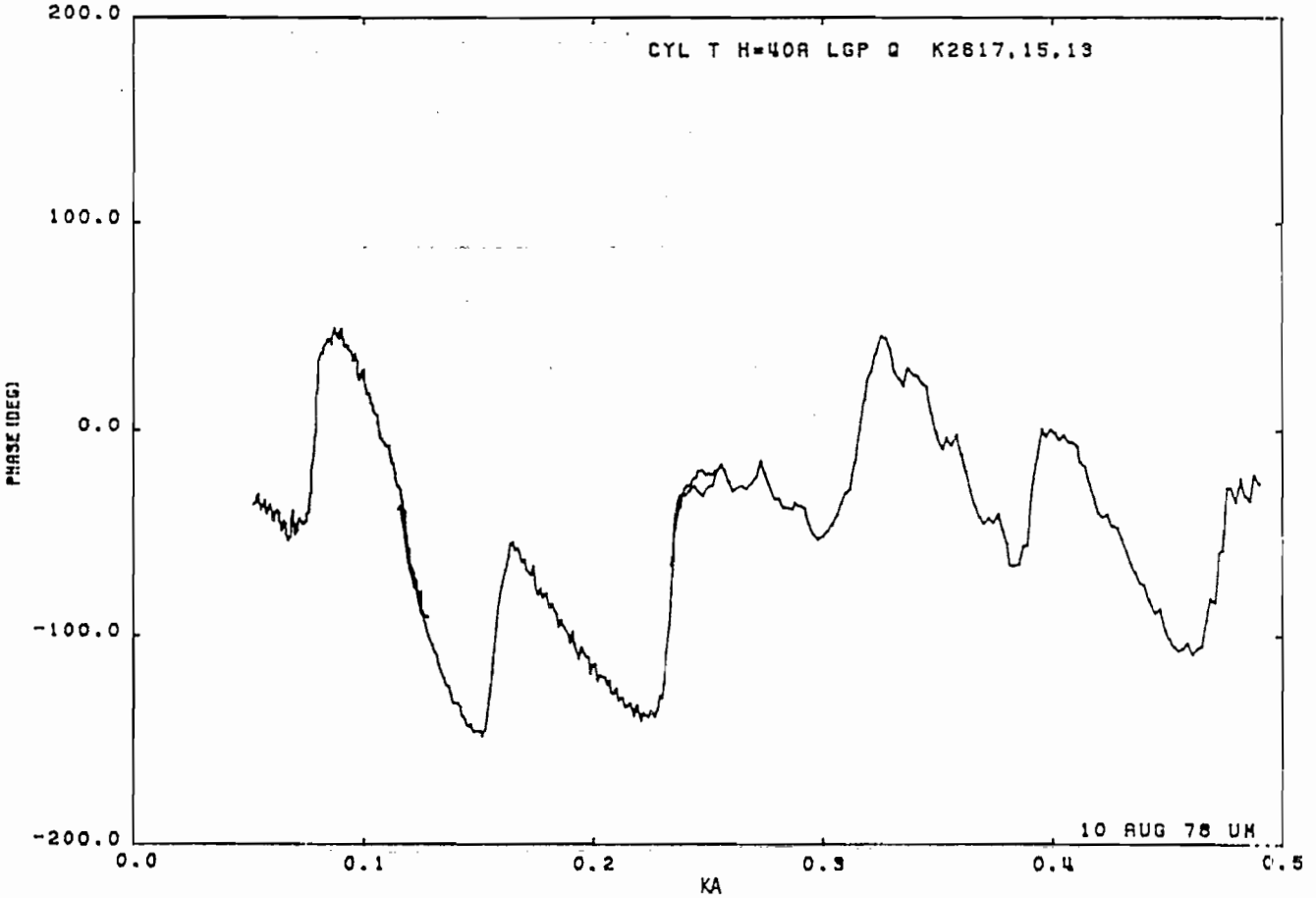

Figure 54b. Charge on cylinder at STA:T; h = 40a, near lossy ground plane (expanded scale).

3.2 Body of Revolution

The data are presented as functions of the full scale frequency using the full scale dimensions shown in Figure 8. This same figure also shows the location of measurement stations, as follows:

F/S - Fuselage, Side

WR/T - Wing Root, Top

WC/T - Wing Center, Top

WT/T - Wing Tip, Top

The current component measured was the axial one. The data are for simulated free space, and near to perfectly conducting and lossy ground planes. In the latter cases, the spacing between the model and the ground plane is a/2 where a is the (maximum) radius of the fuselage. The phase reference is at the top of the fuselage, midway along its length. The electrical properties of the lossy ground plane are given in Section 2.2.

The data presented are summarized in Table 6.

TABLE 6: BODY OF REVOLUTION DATA

STA	J/Q	F/S	GP	LGP *
F/S	J	Figure 55	Figure 59	Figure 61
WR/T	J	56		
WC/T	J	57	59	62
WT/T	Q	58		

*See section 3.1.3 on problems when scaling lossy ground plane measurements.

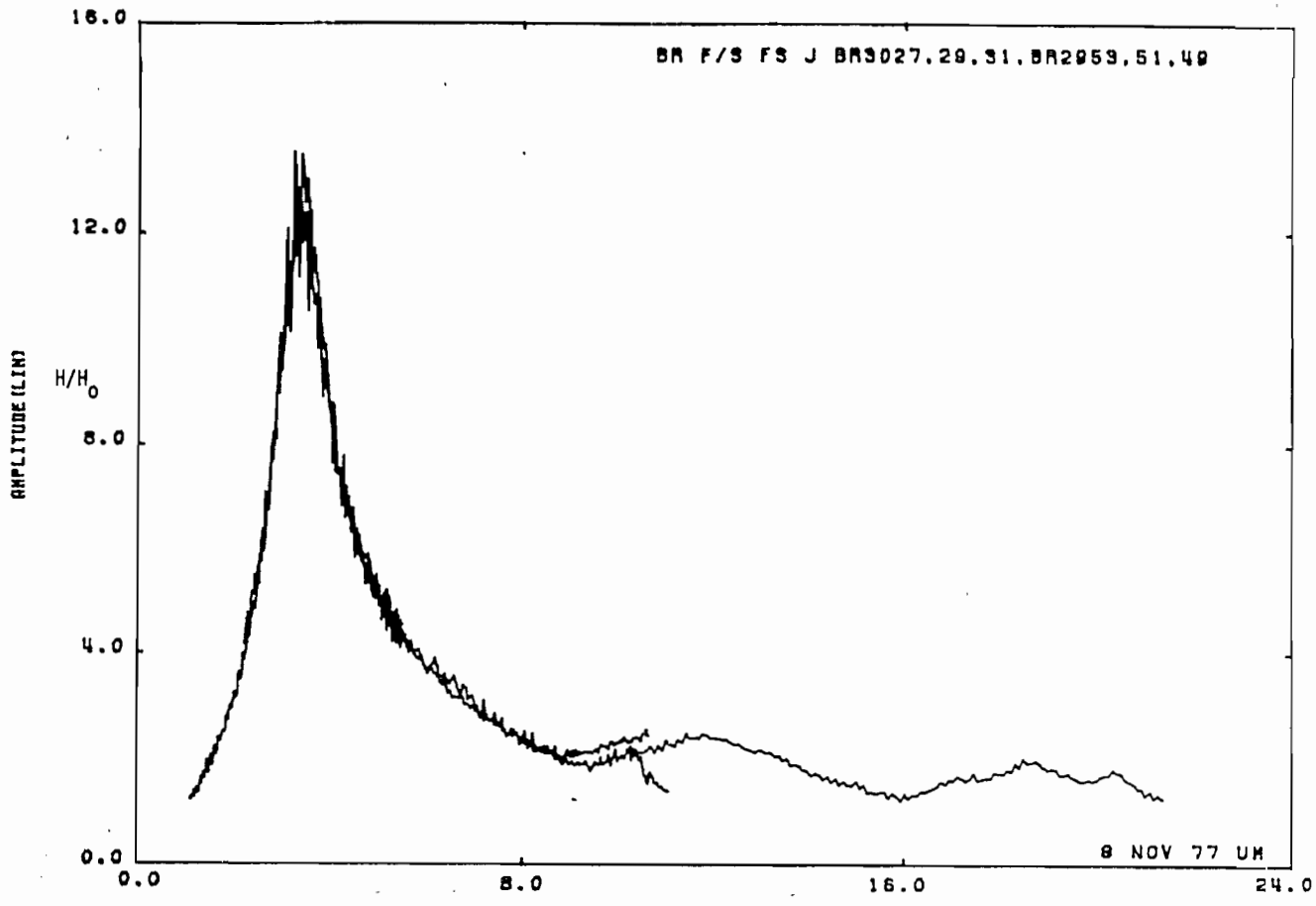

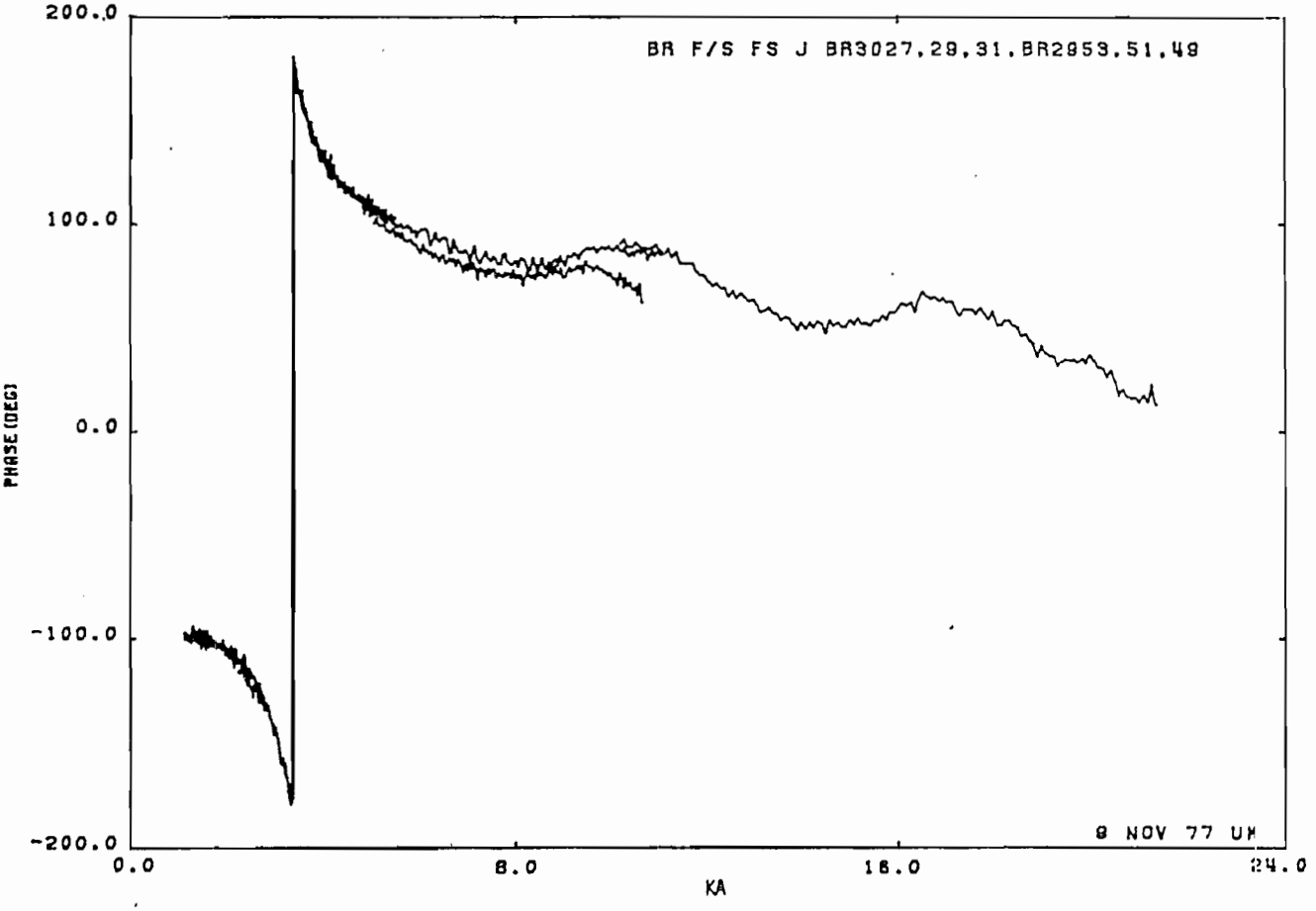

Figure 55. Current on body of revolution at STA:F/S; free space.

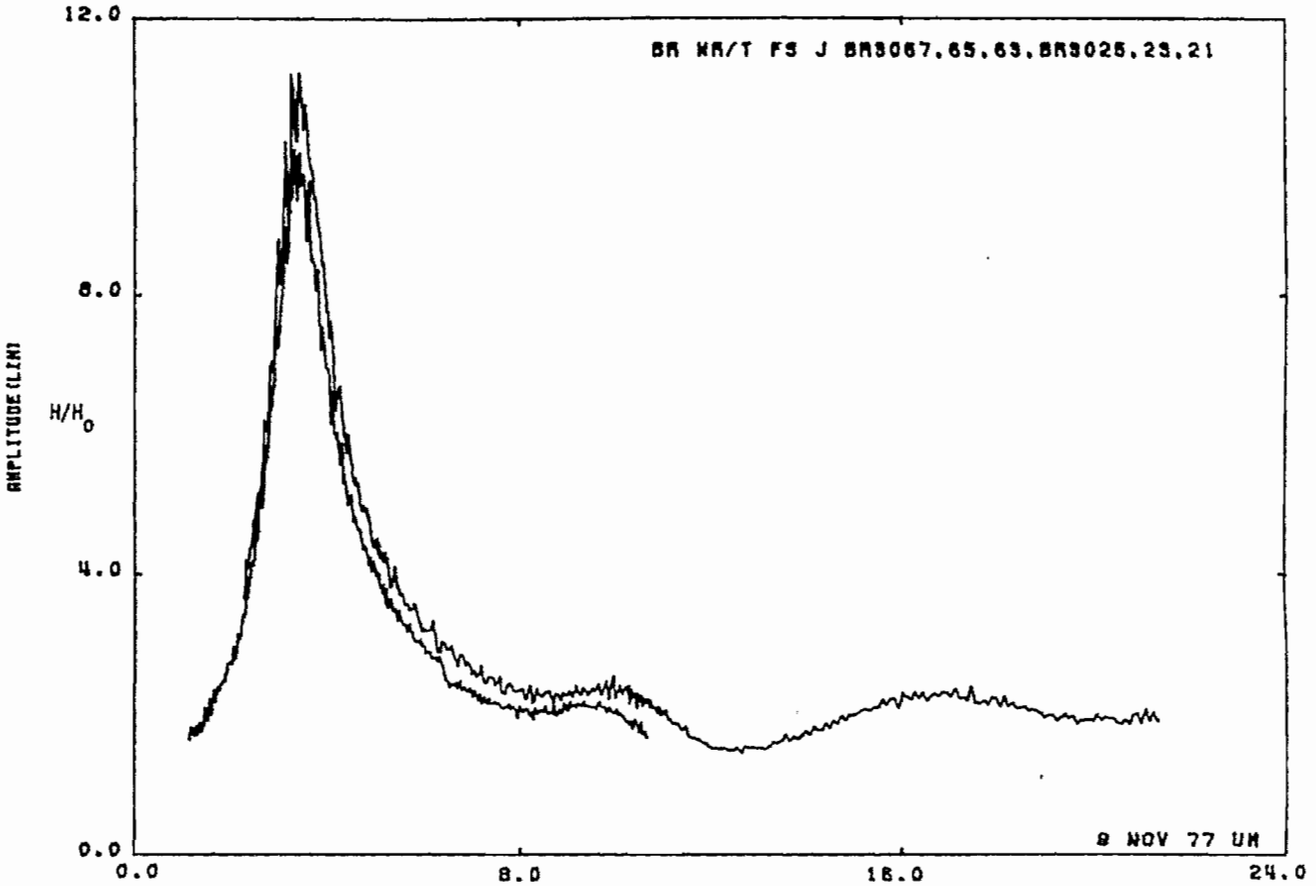

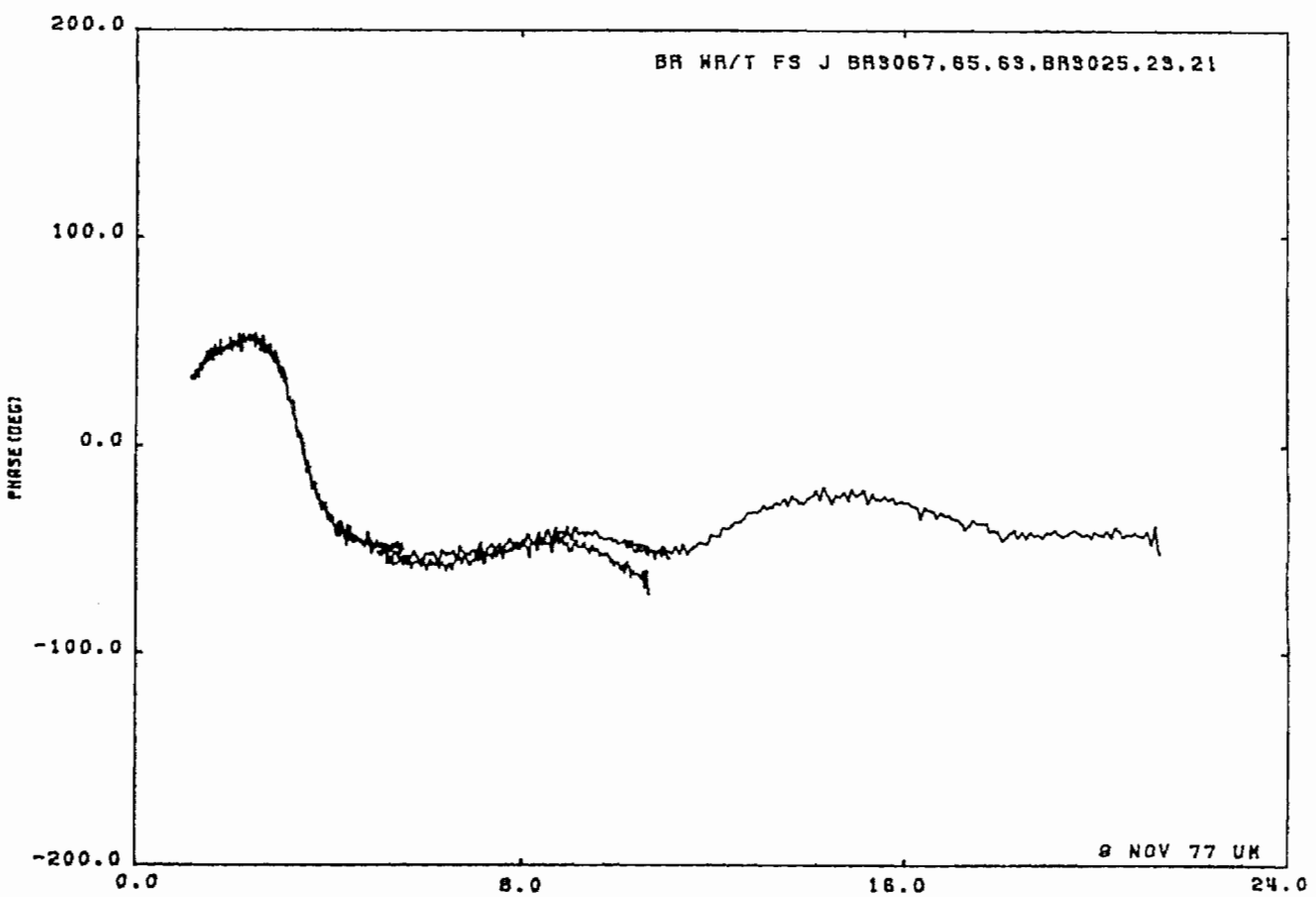

Figure 56. Current on body of revolution at STA:WR/T; free space.

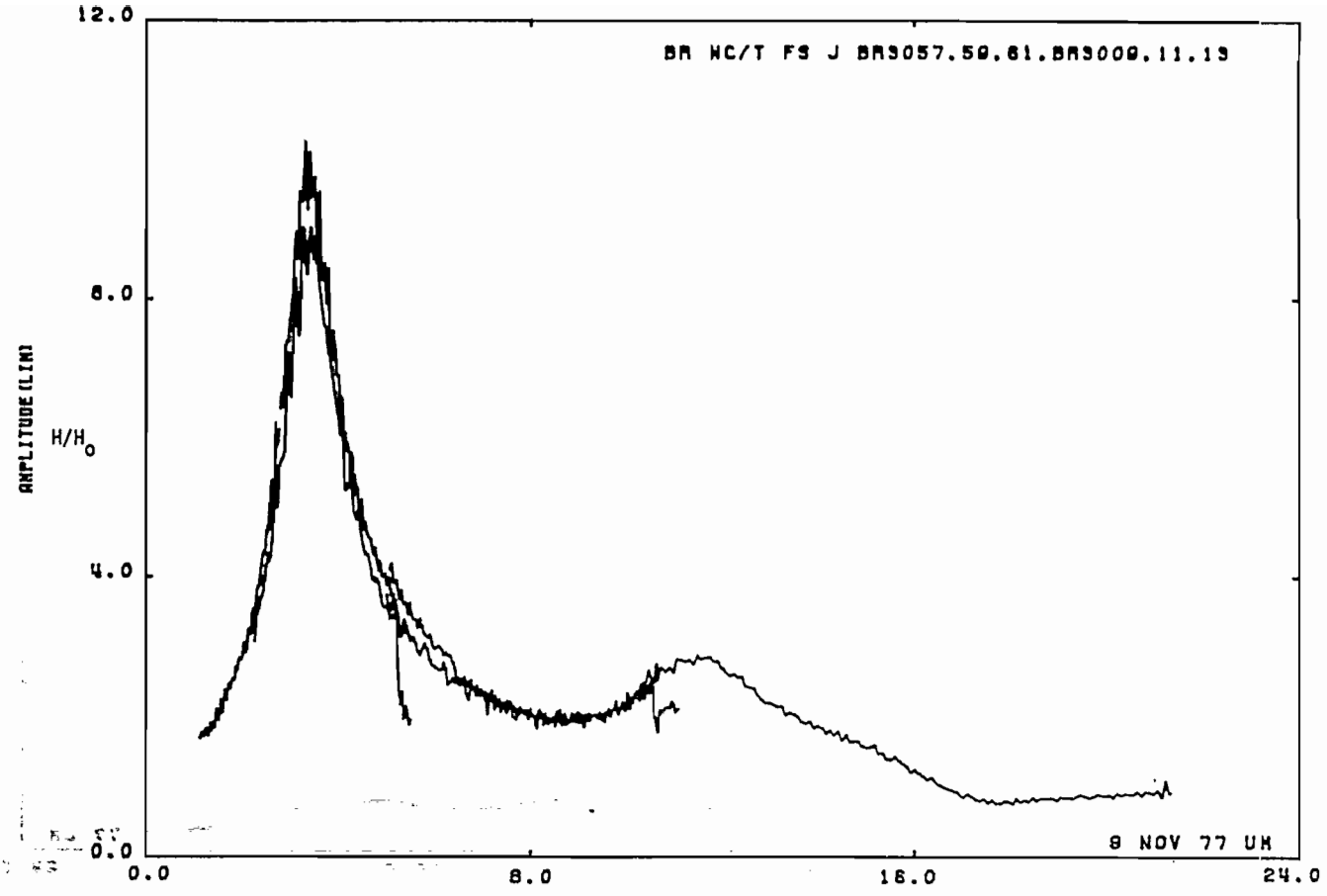

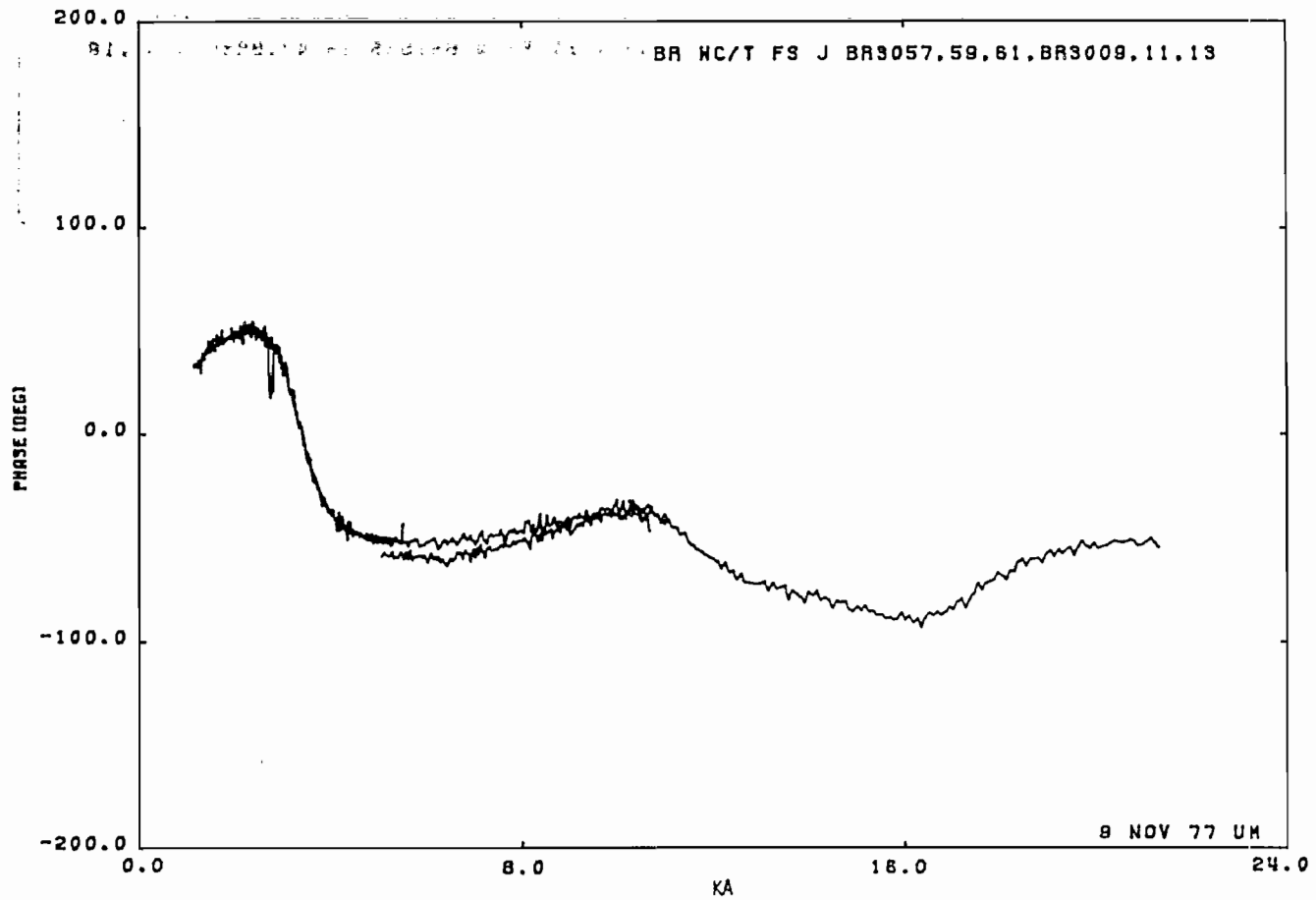

Figure 57. Current on body of revolution at STA:WC/T; free space.

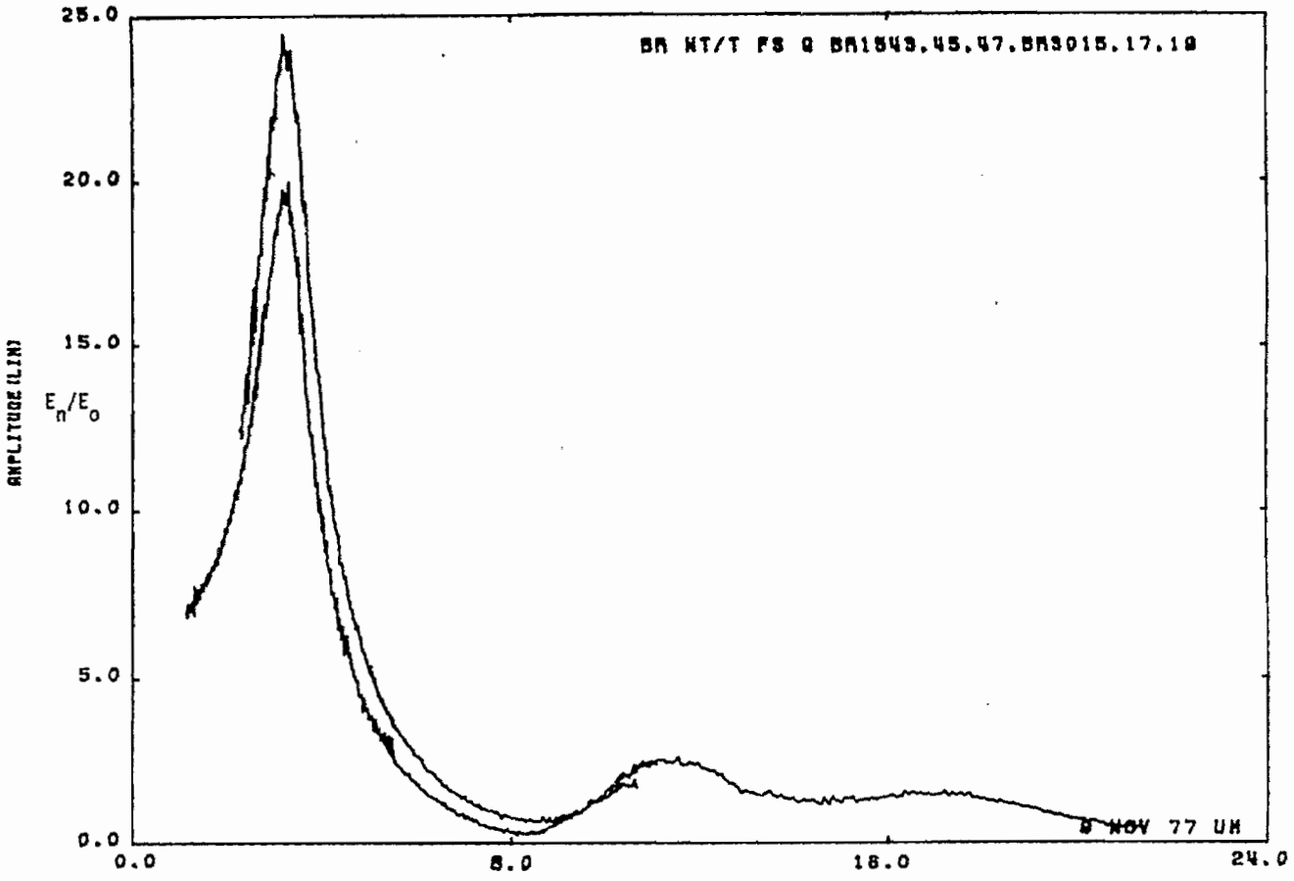

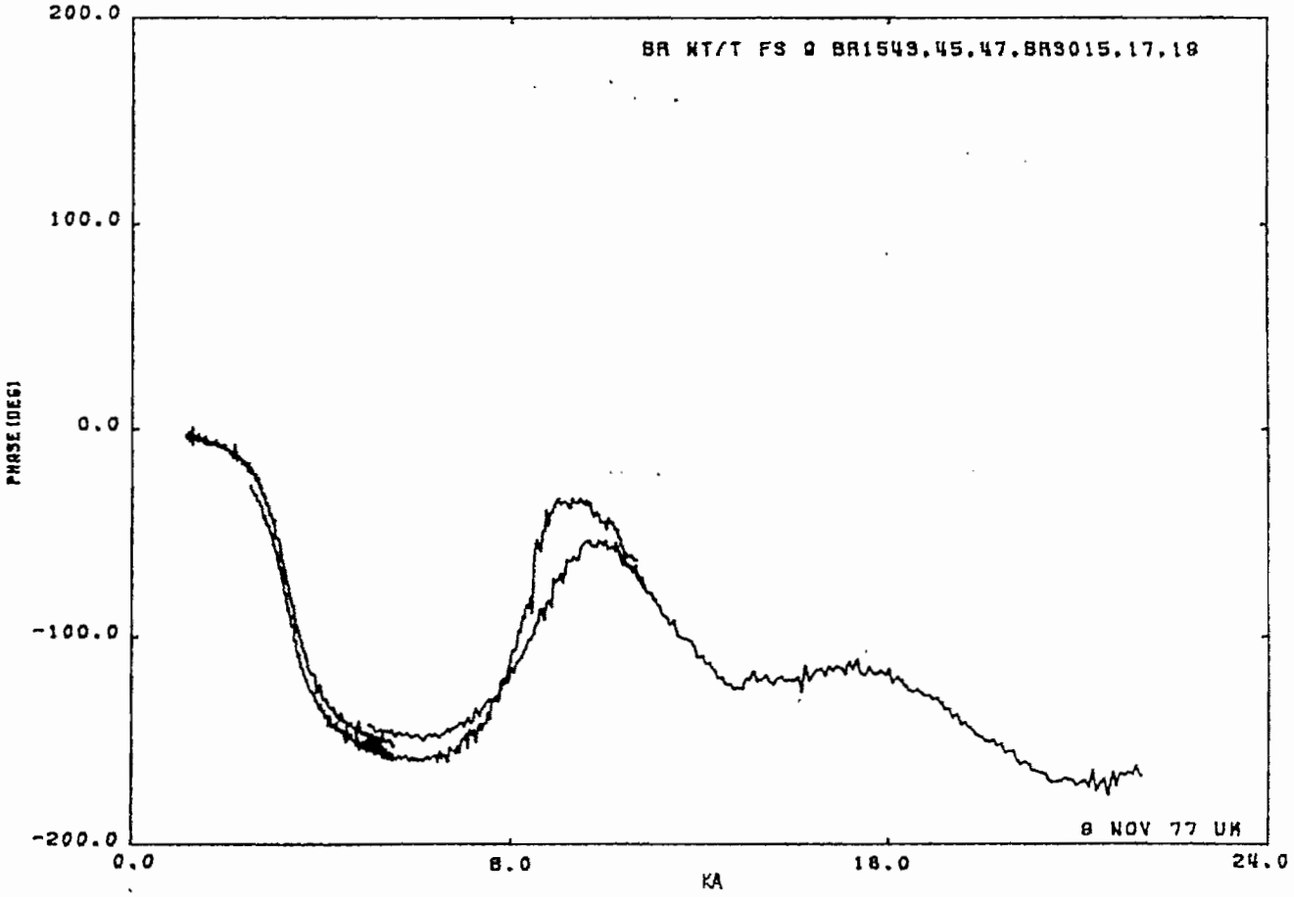

Figure 58. Charge on body of revolution at STA:WT/T; free space.

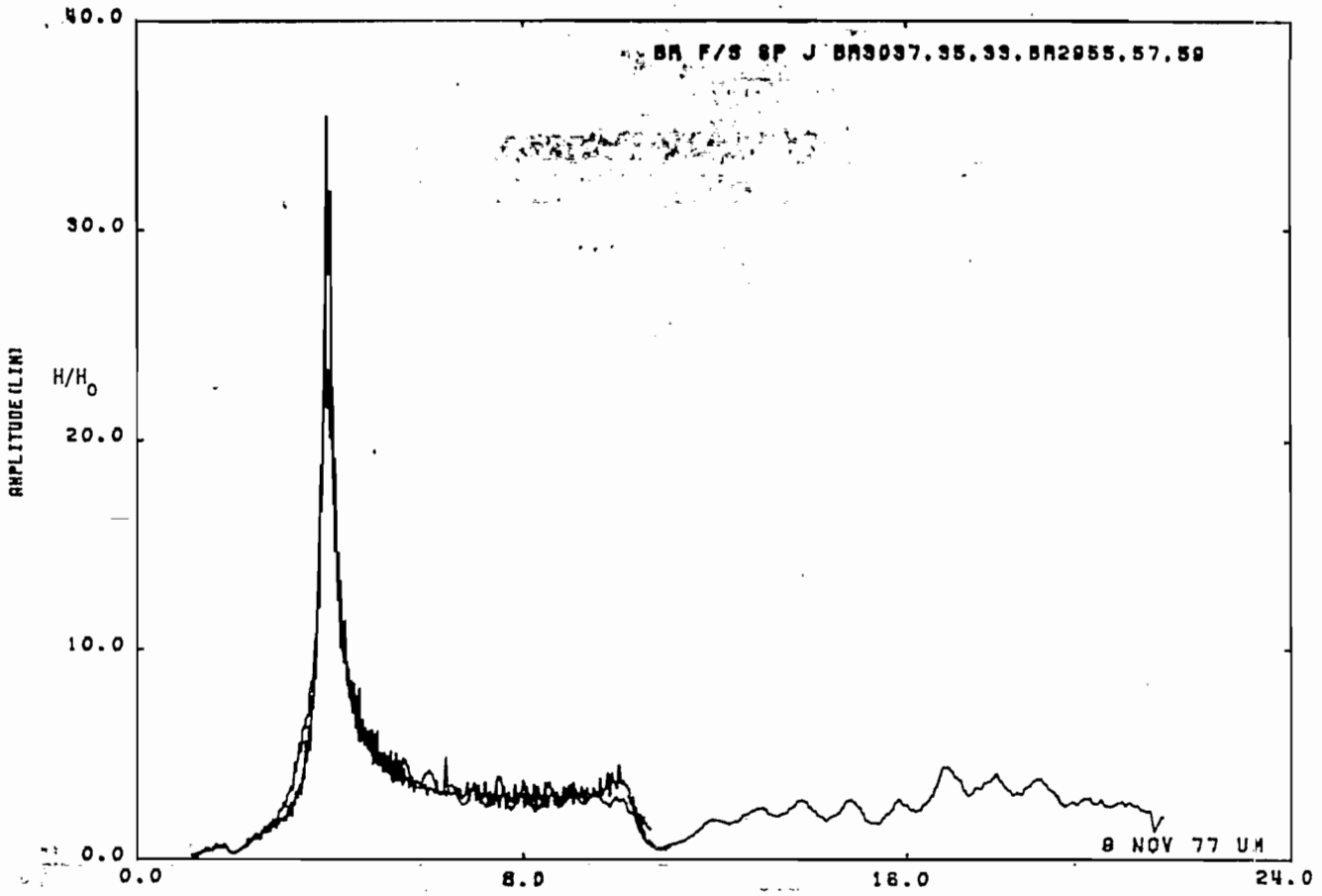

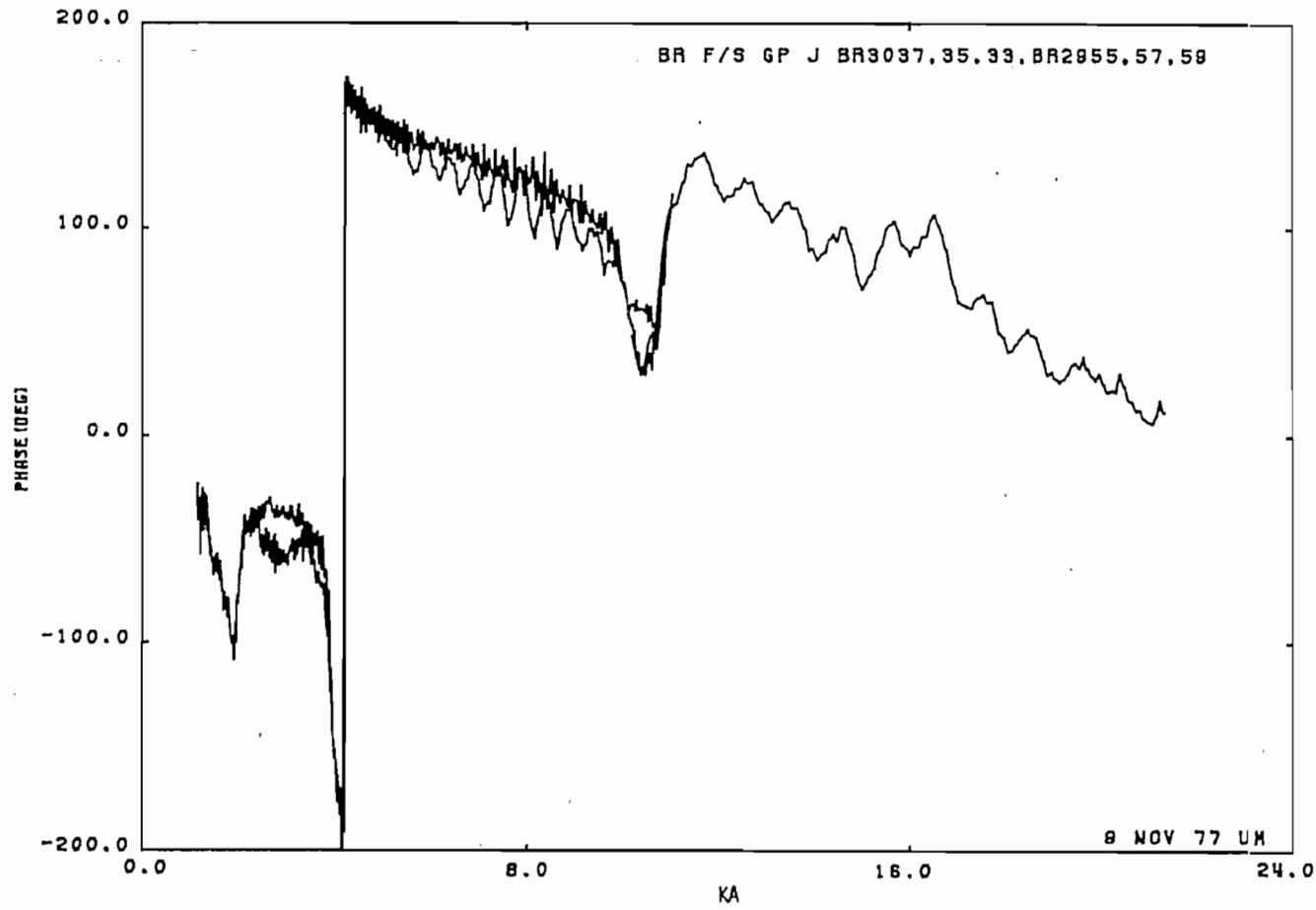

Figure 59. Current on body of revolution at STA:F/S; near perfectly conducting ground plane.

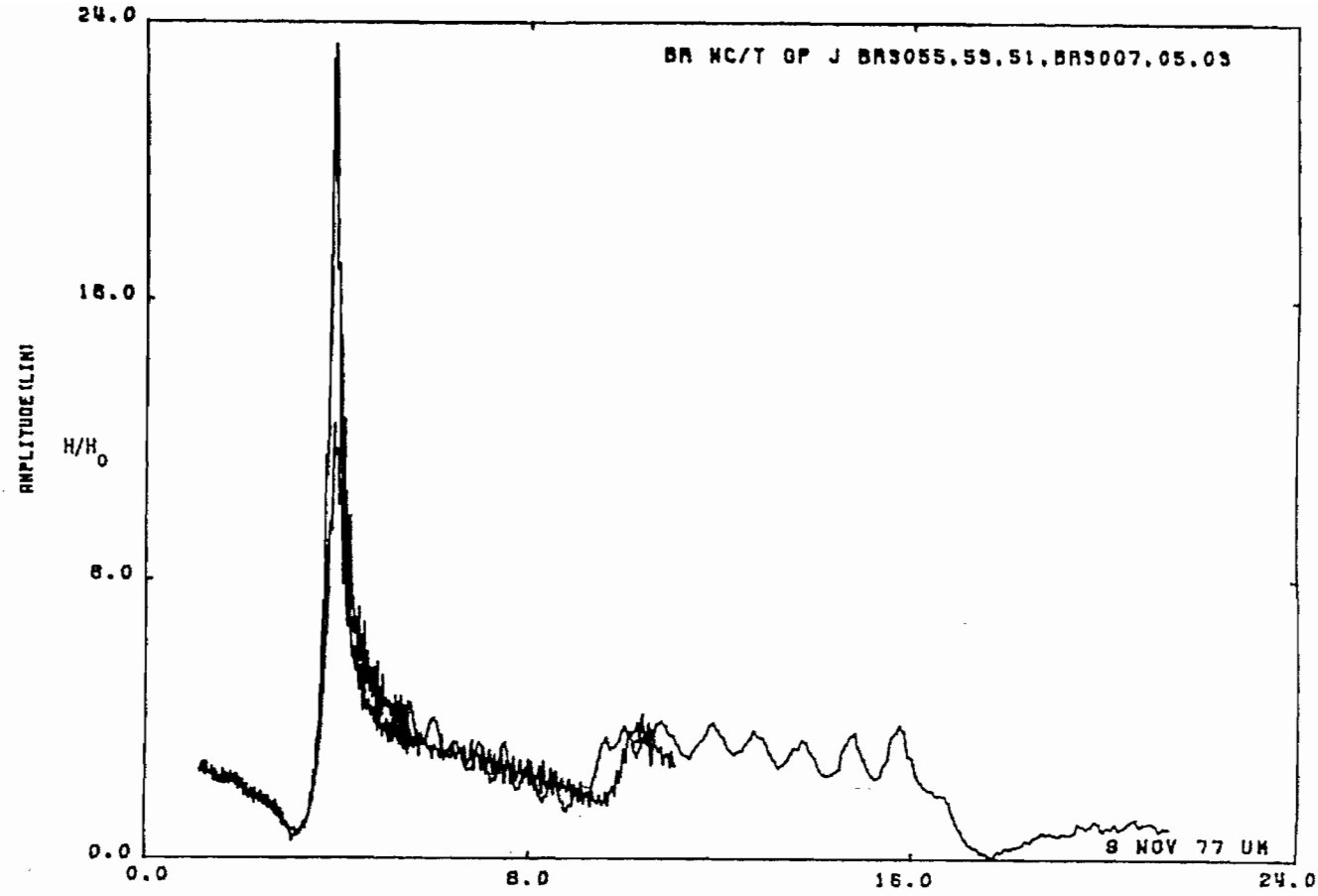

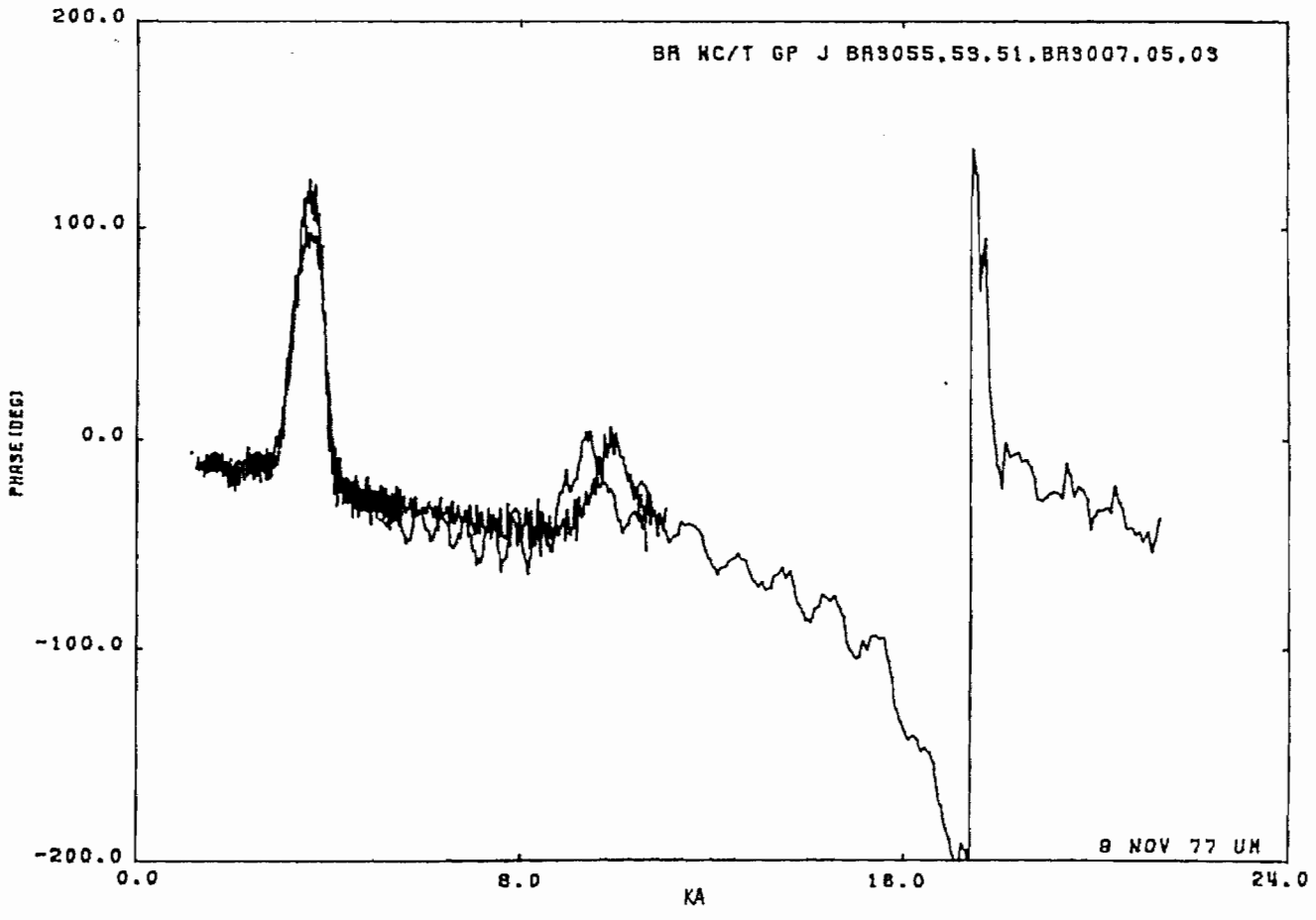

Figure 60. Current on body of revolution at STA:WC/T; near perfectly conducting ground plane.

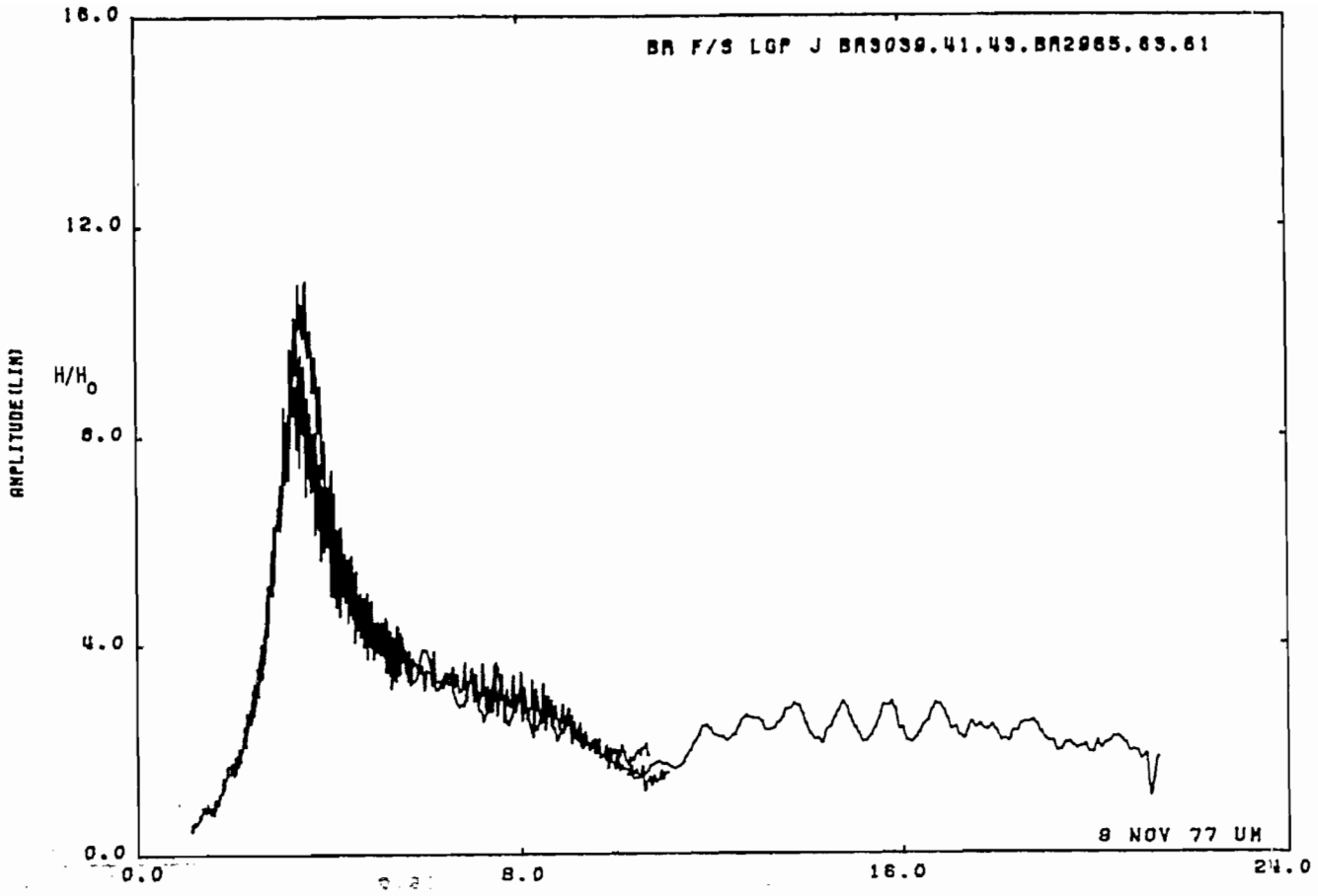

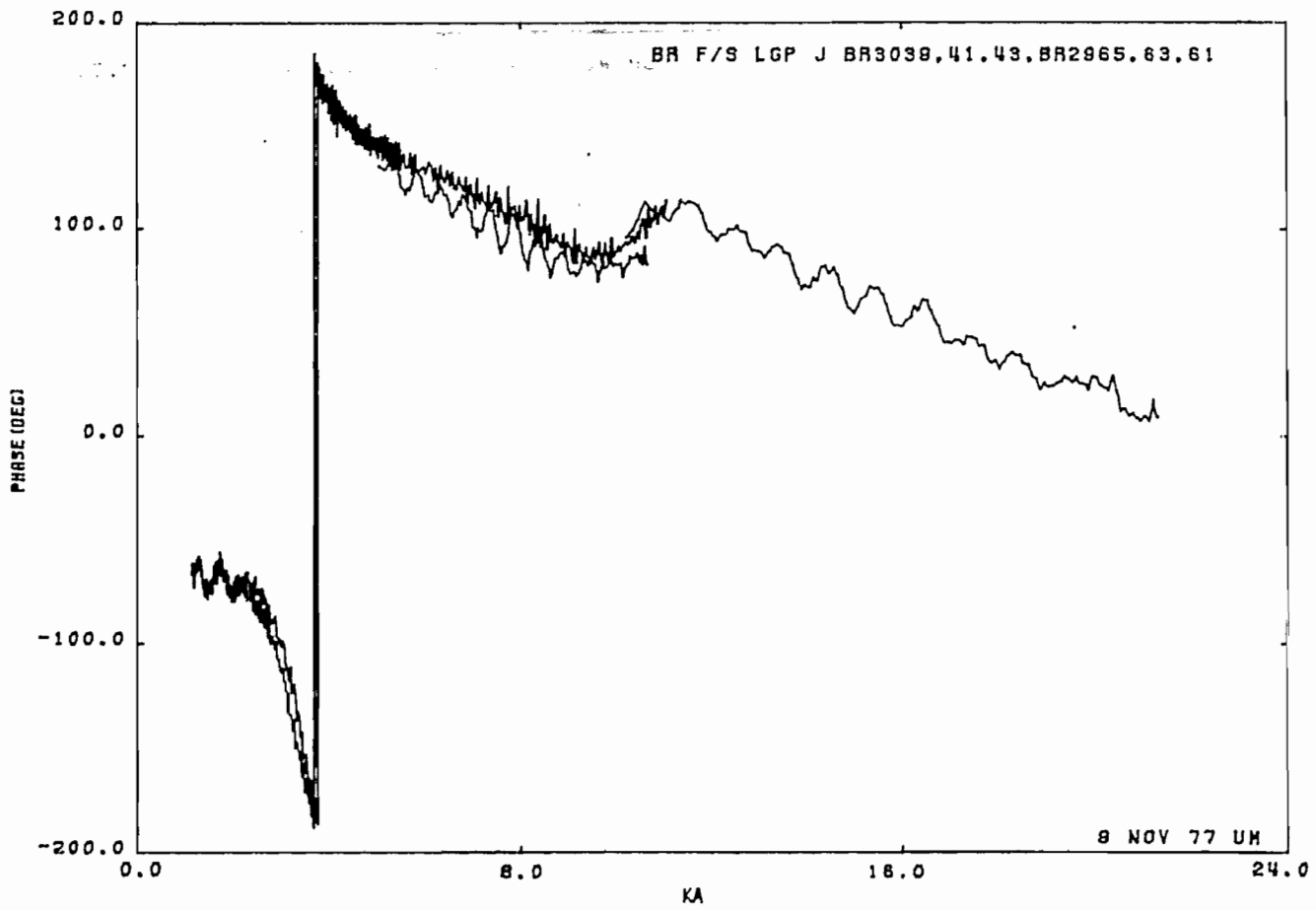

Figure 61. Current on body of revolution at STA:F/S; near lossy ground plane.

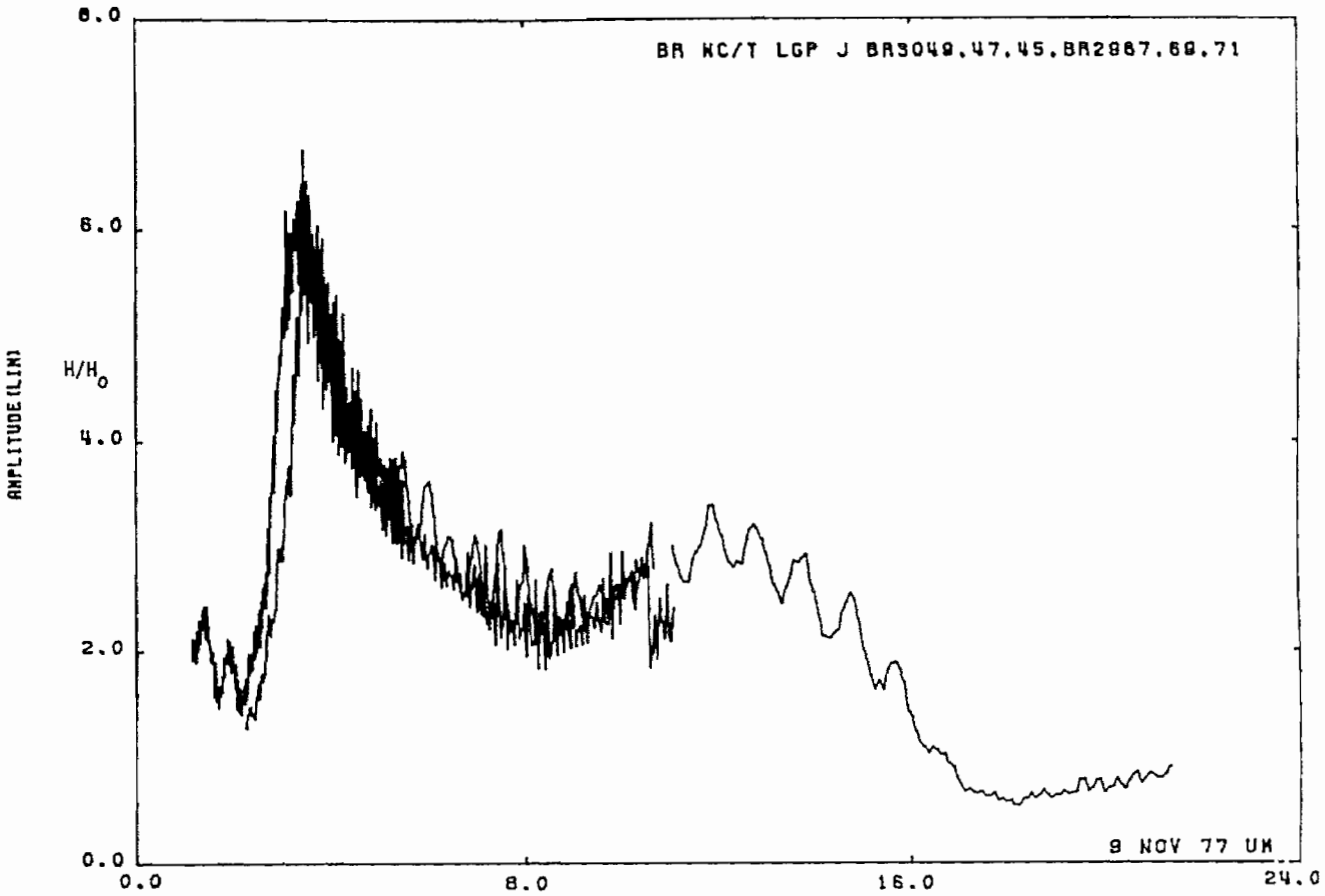

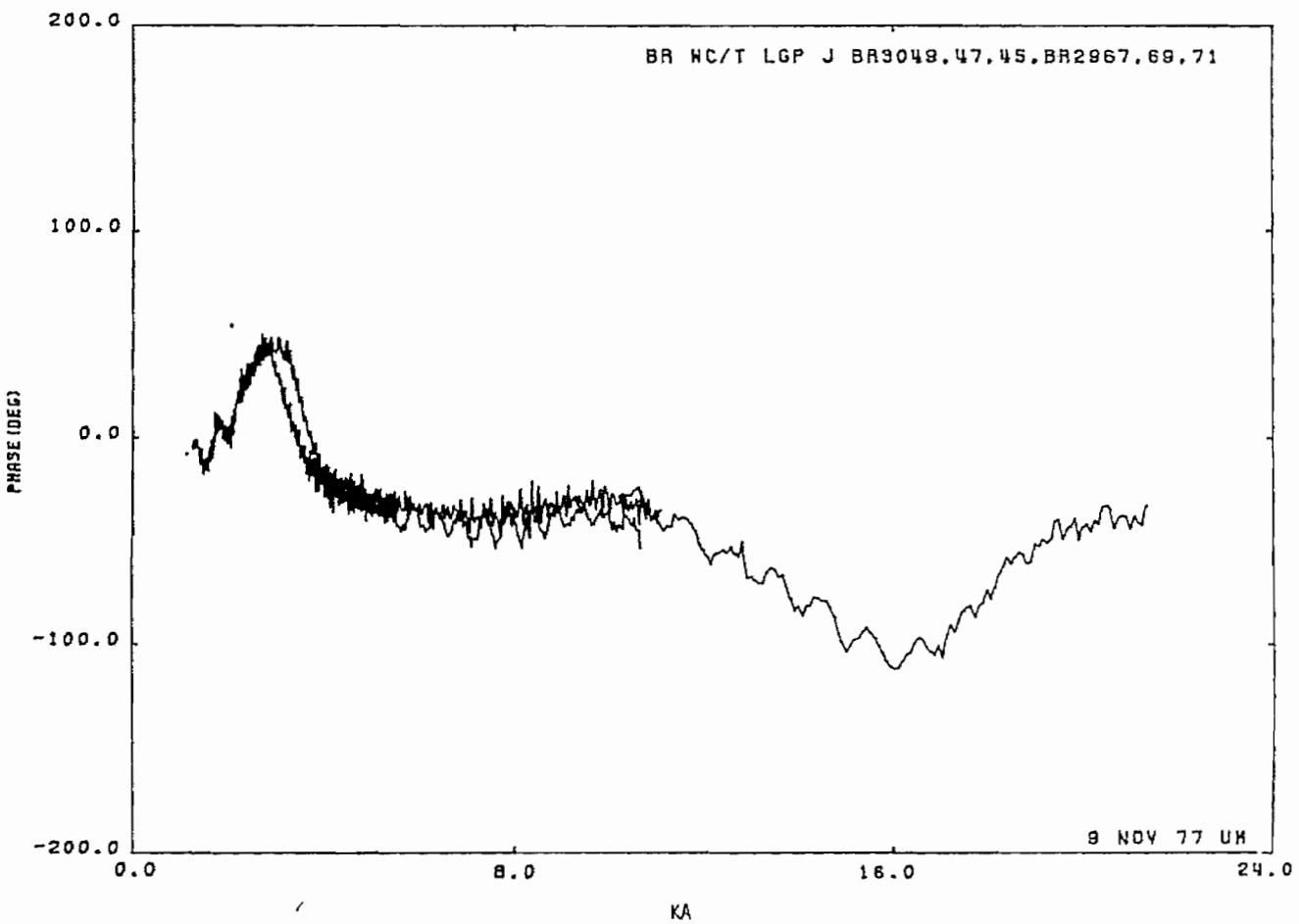

Figure 62. Current on body of revolution at STA:WC/T; near lossy ground plane.

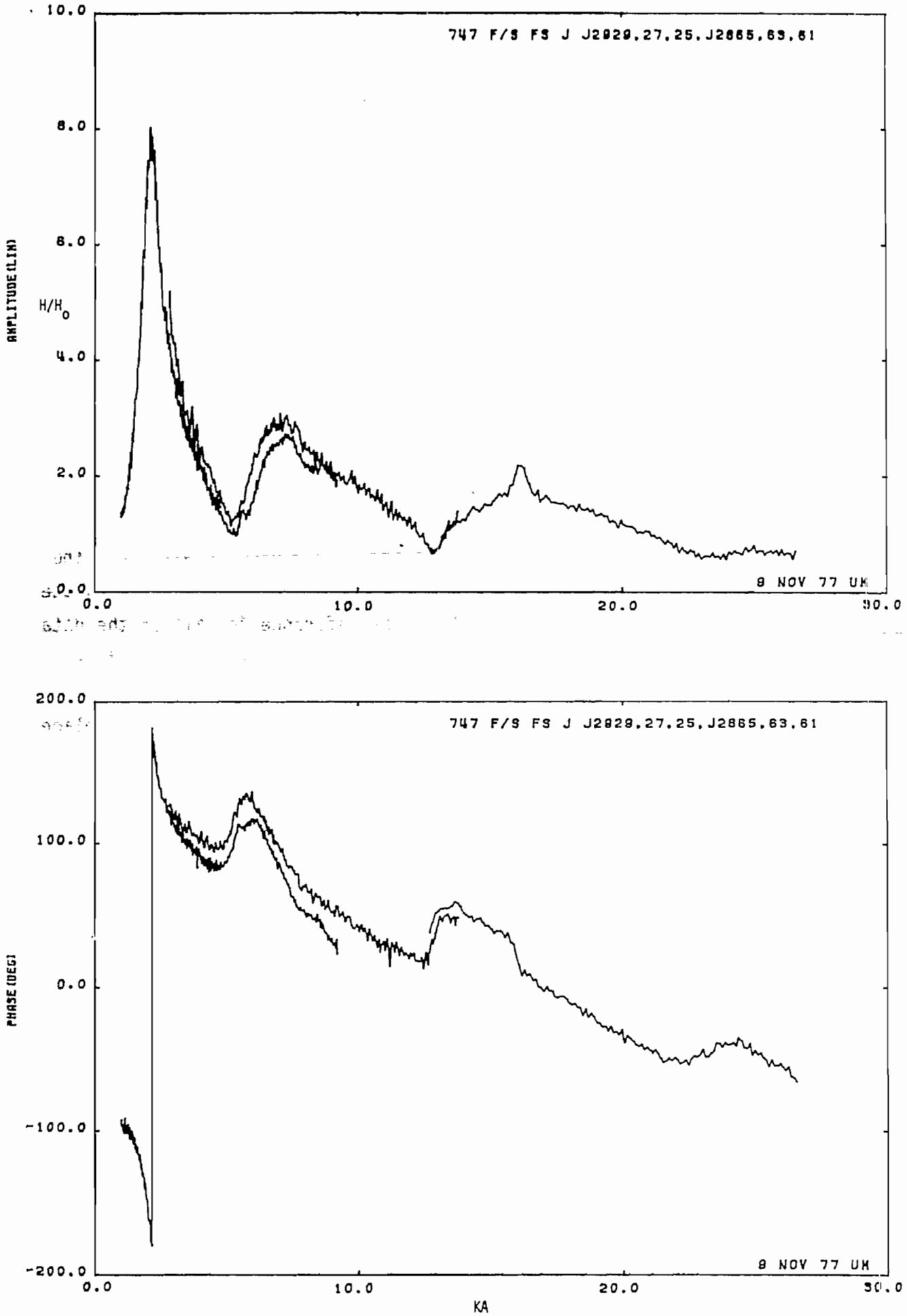

Figure 63. Current on 747 at STA:F/S; free space.

3.3 747 Aircraft

These data are also presented as functions of the full scale frequency, using the dimensions shown in Figure 10. The measurement locations were

F/S - Fuselage, Side

WR/T - Wing Root, Top

WC/T - Wing Center, Top

WT/T - Wing Tip, Top

and are indicated in Figure 10. The current component measured was again the axial one, but it should be noted that on the wing this component is along the bisector of the wing (see Figure 10). The phase reference for all of the data is the top of the fuselage midway along its length. The data are for simulated free space, and near perfectly conducting and lossy ground planes. The spacing between the model and the ground plane is a/2, where a is the fuselage radius at its midpoint.

Table 7 summarizes the data provided.

TABLE 7: 747 DATA.

STA	J/Q	FS	GP	LGP *
F/S	J	Figure 63	Figure 67	Figure 69
WR/T	J	64		
WC/T	J	65	68	70
WT/T	Q	66		

*See section 3.1.3 on problem when scaling lossy ground plane measurements

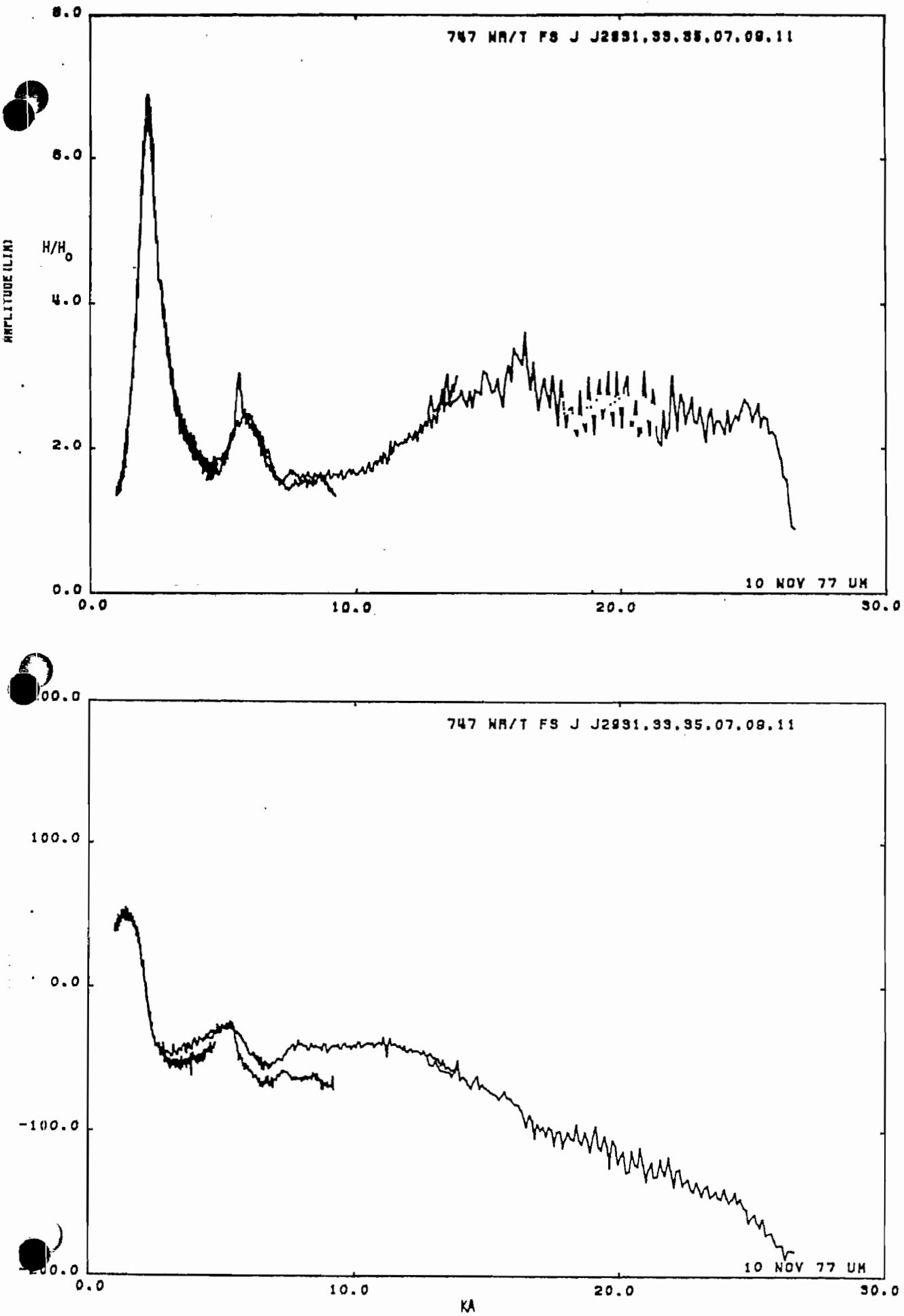

Figure 64. Current on 747 at STA:WR/T; free space.

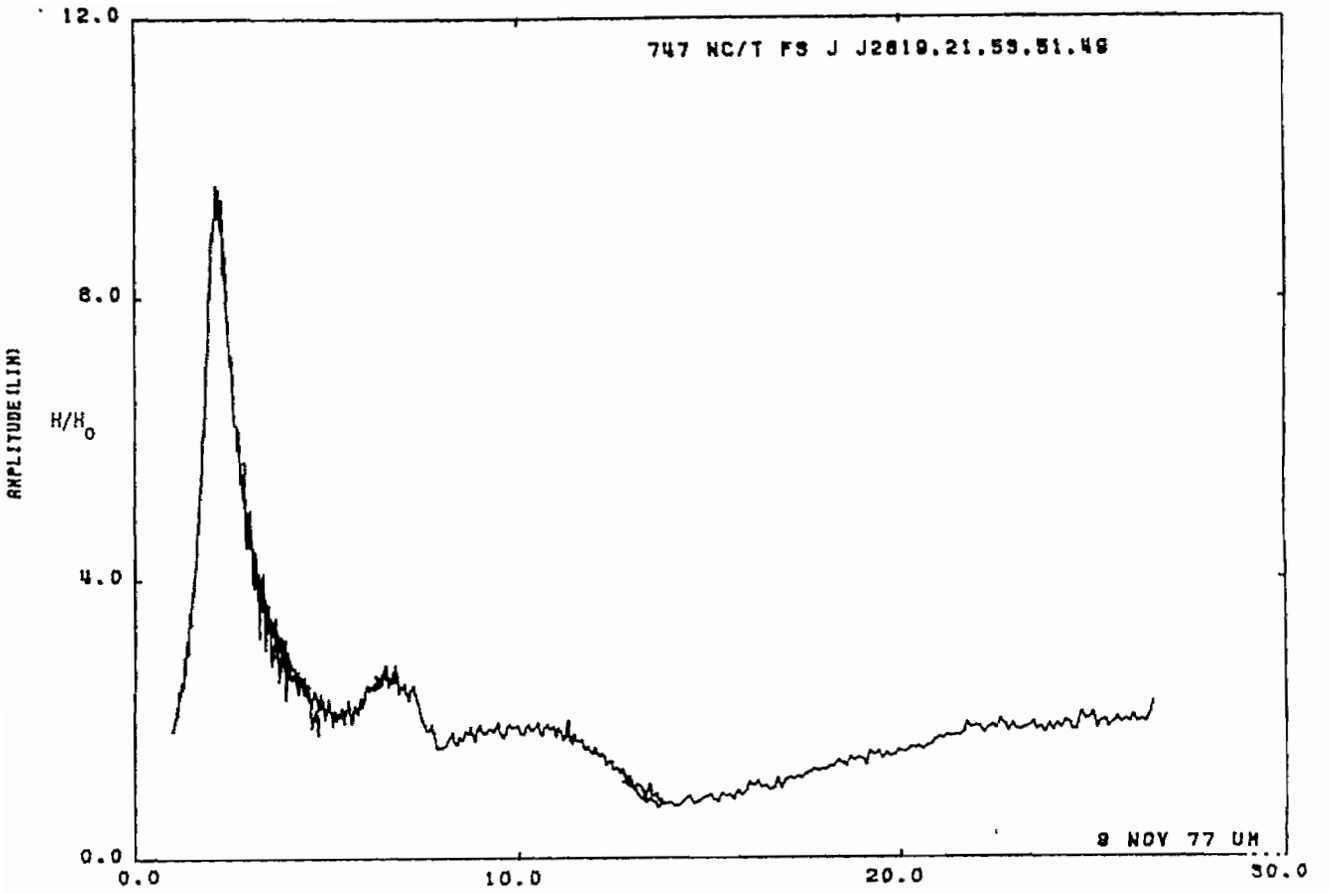

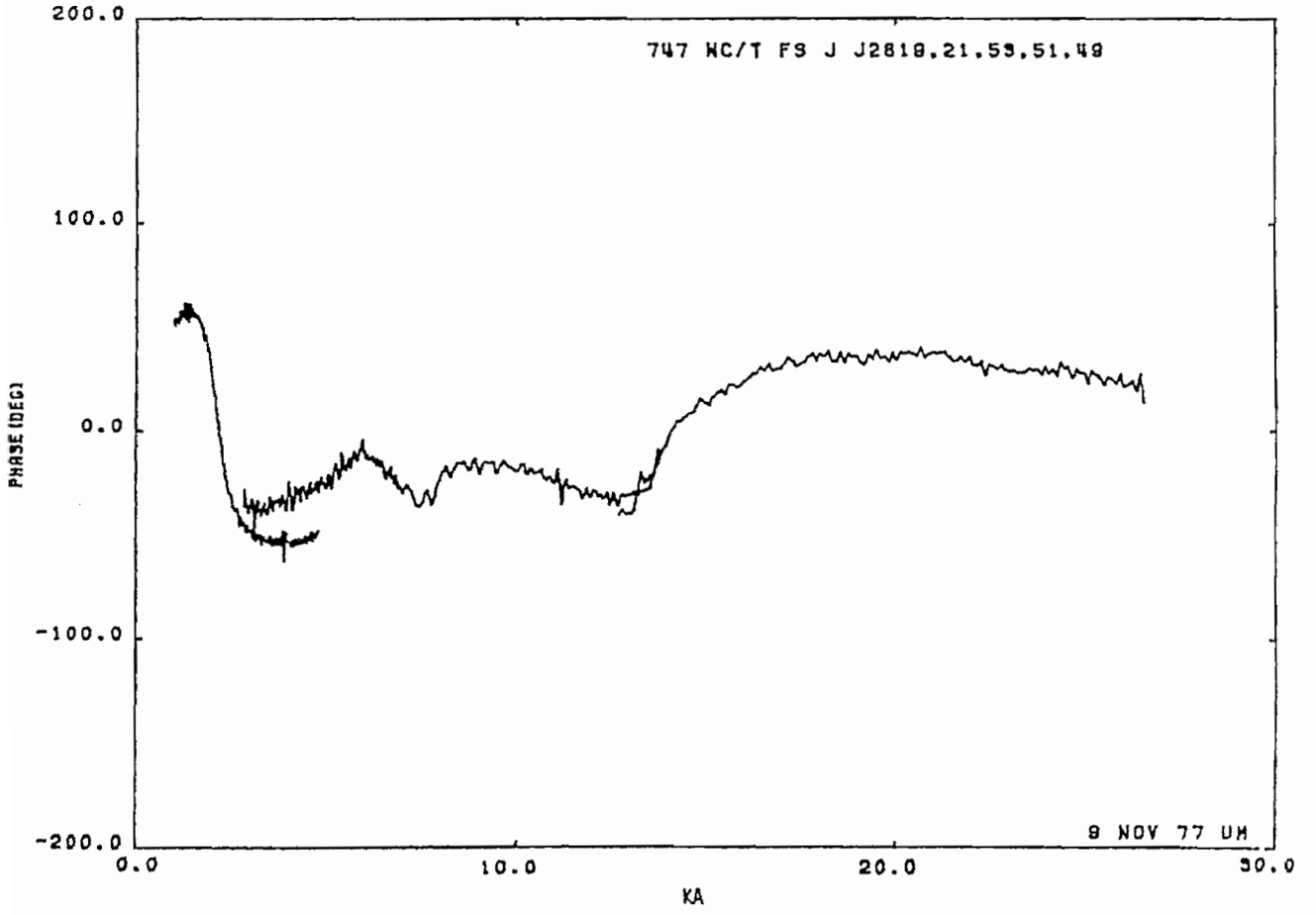

Figure 65. Current on 747 at STA:NC/T; free space.

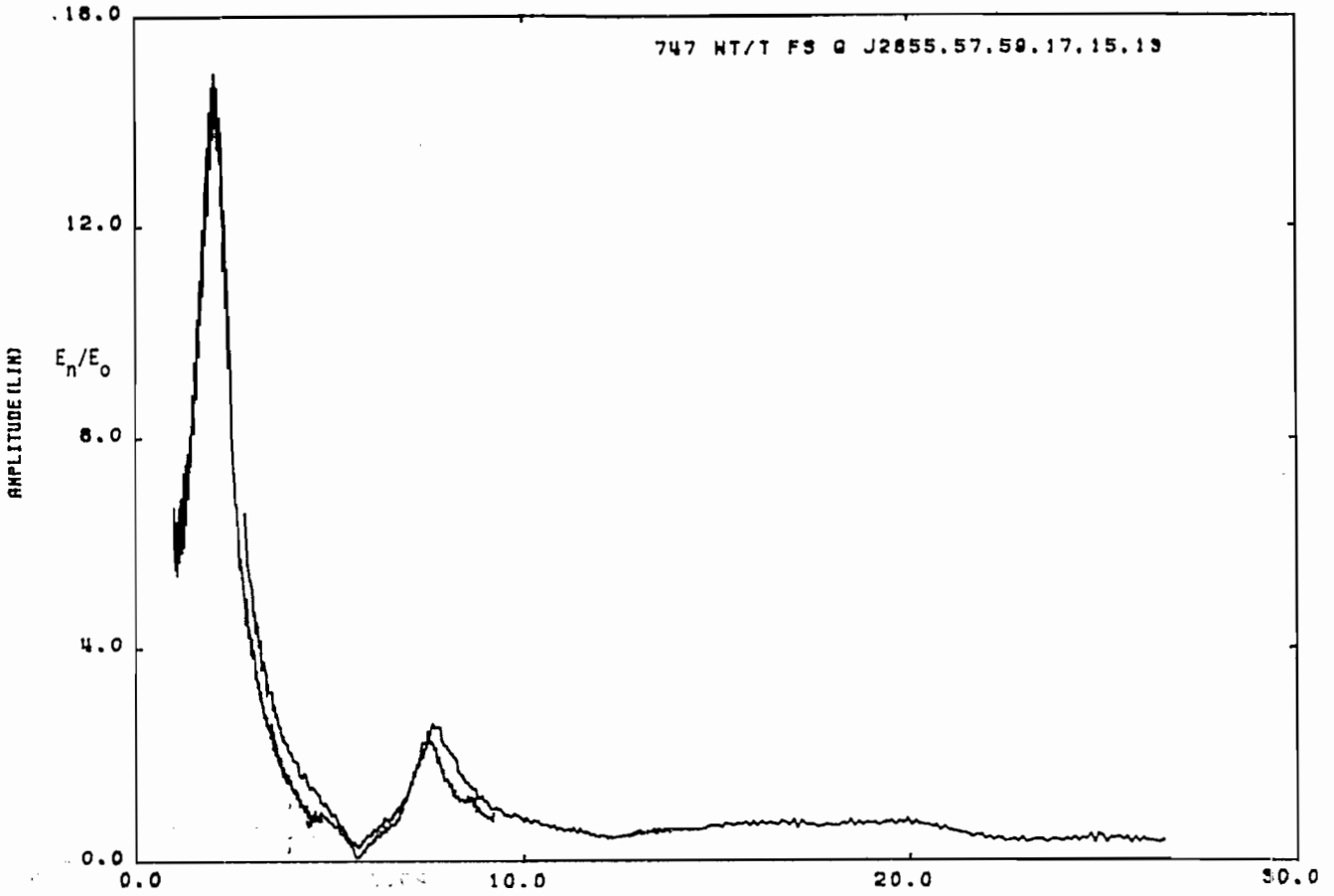

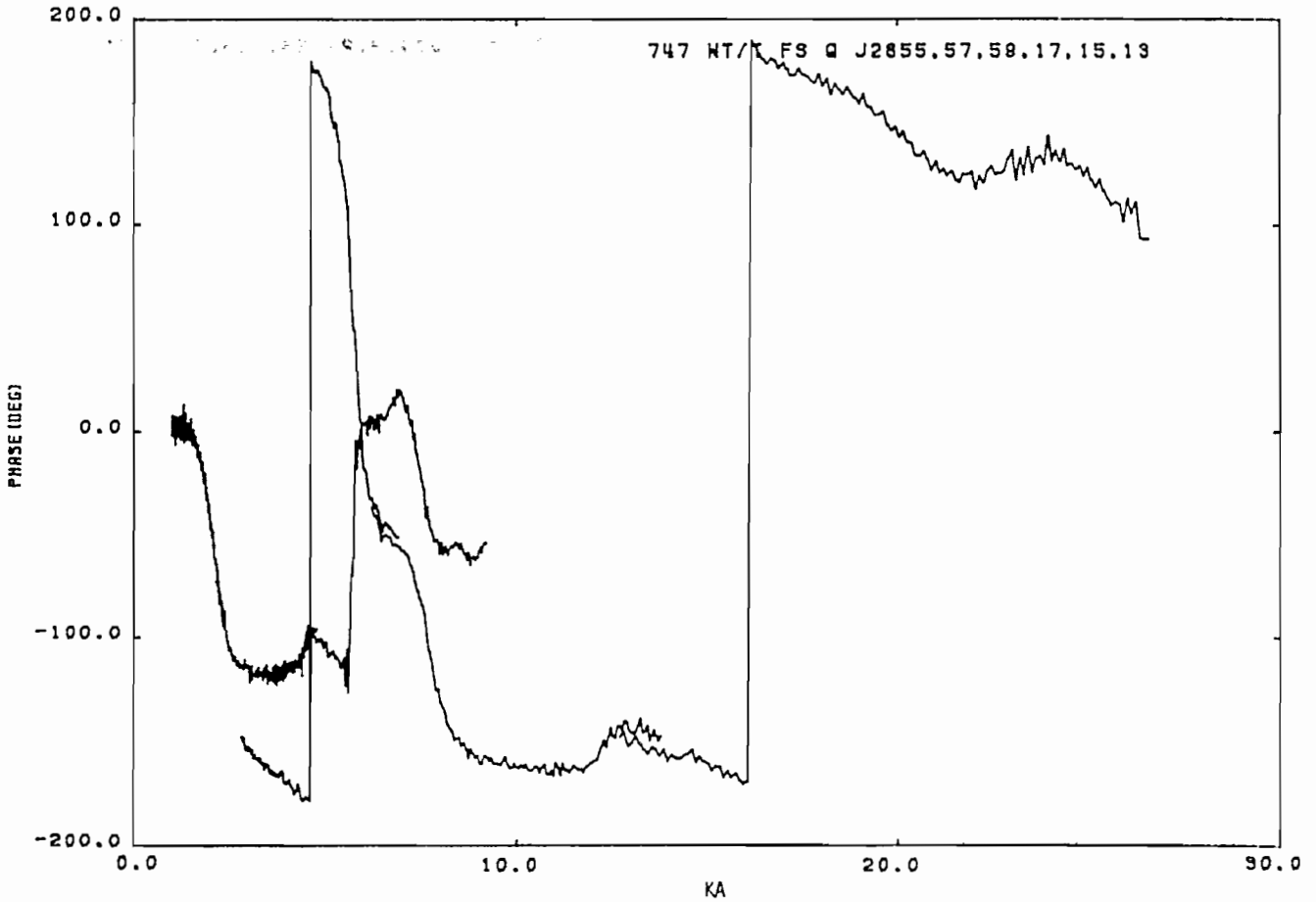

Figure 66. Current on 747 at STA:WT/T; free space.

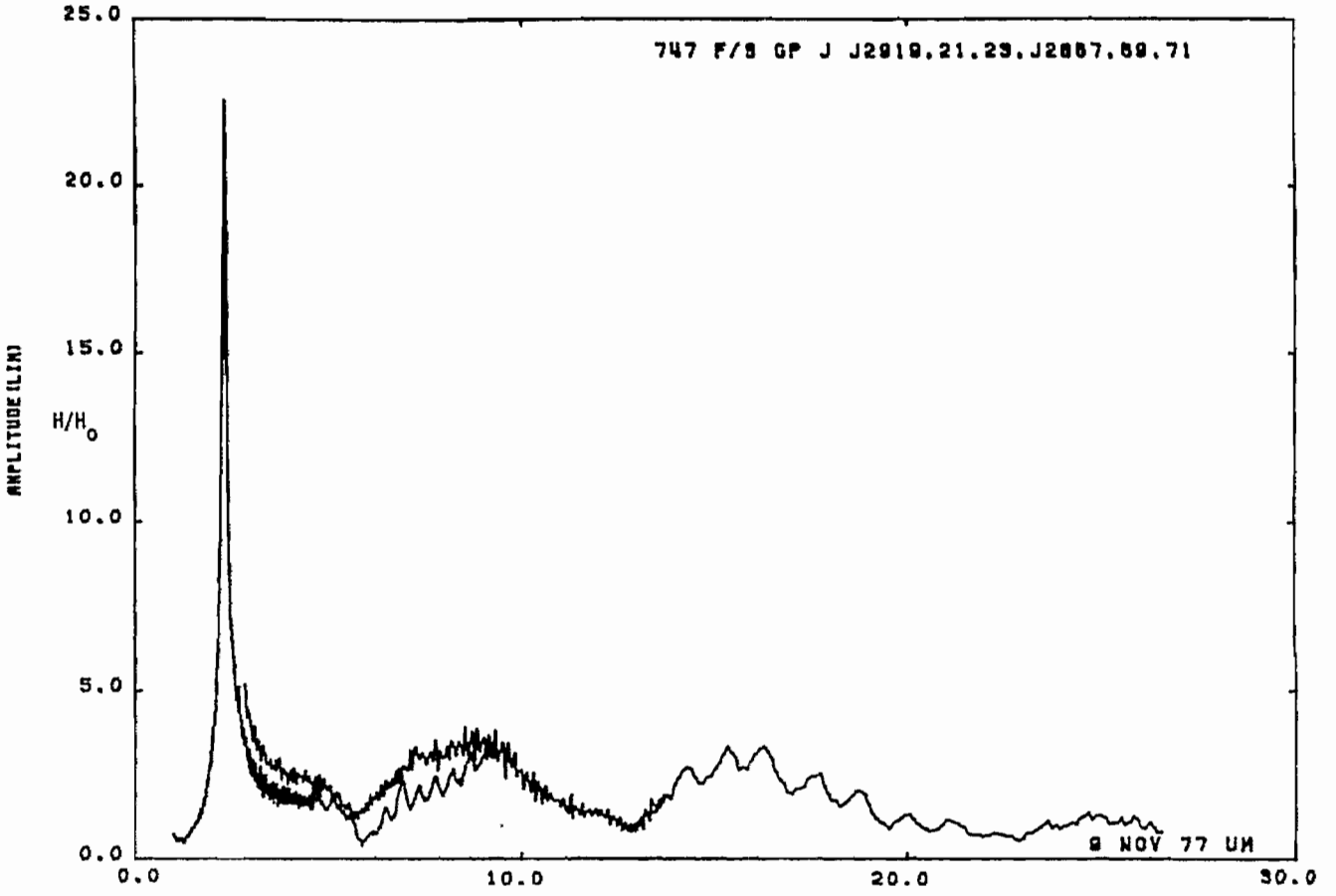

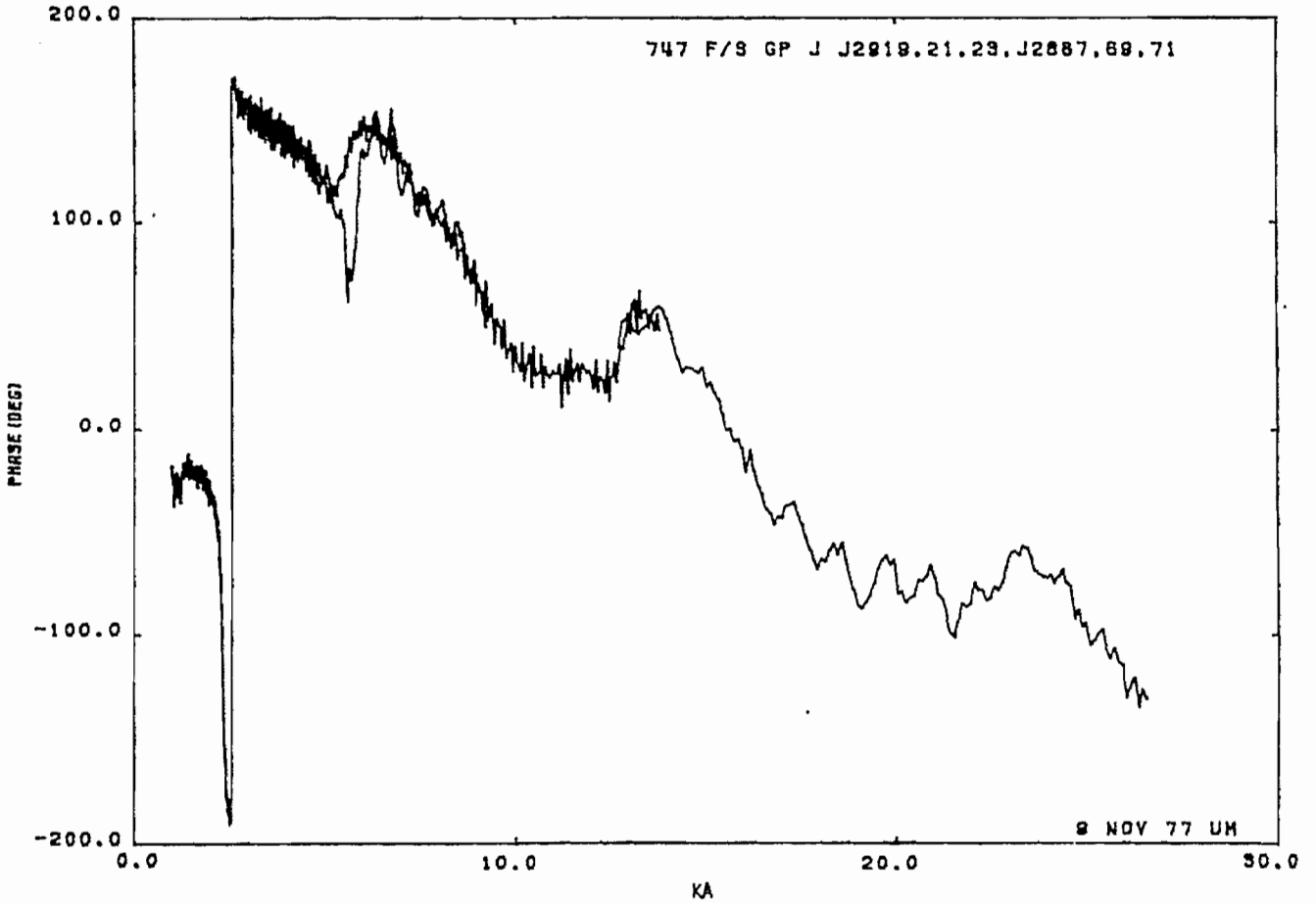

Figure 67. Current on 747 at STA:F/S; near perfectly conducting ground plane.

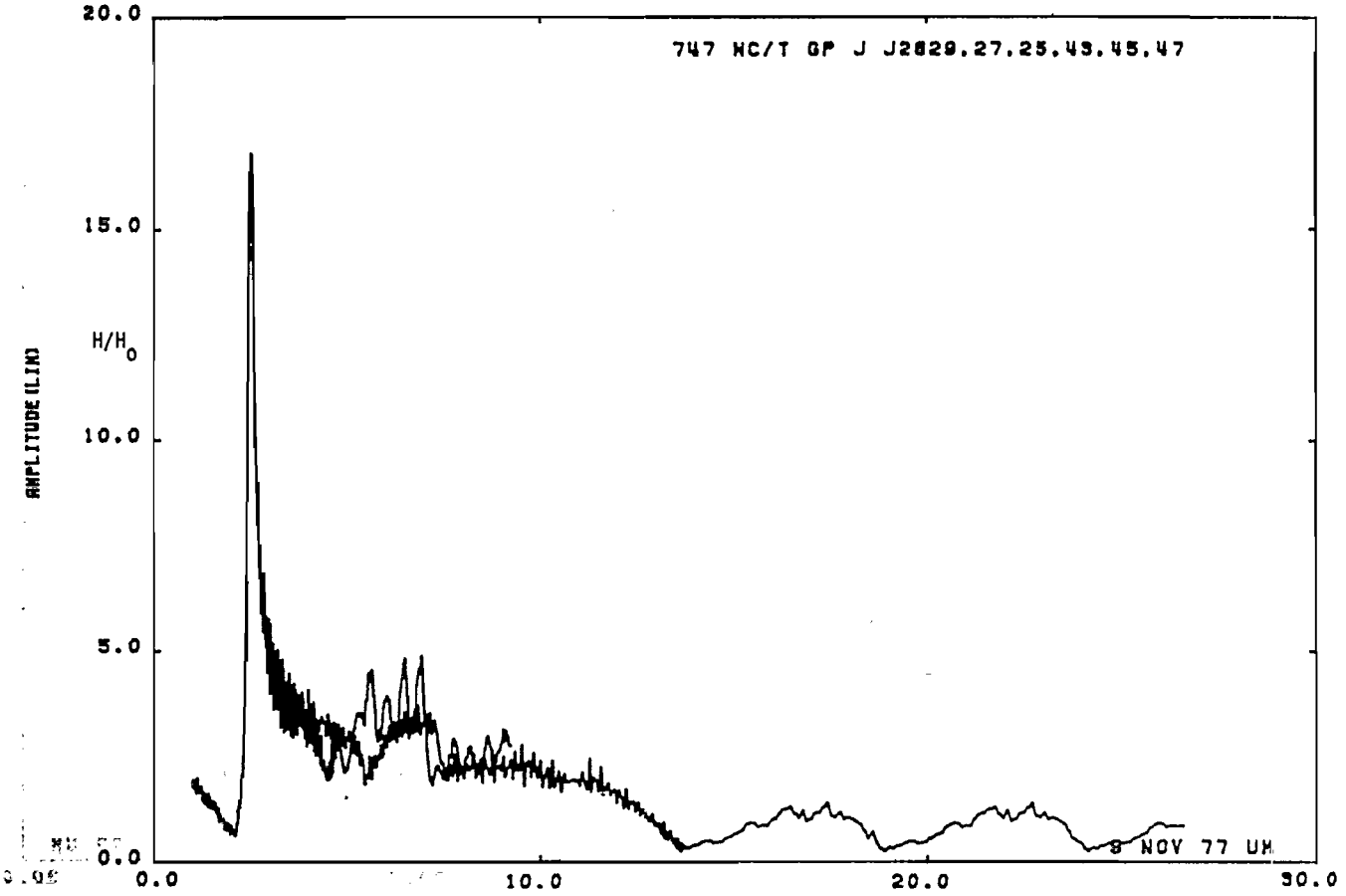

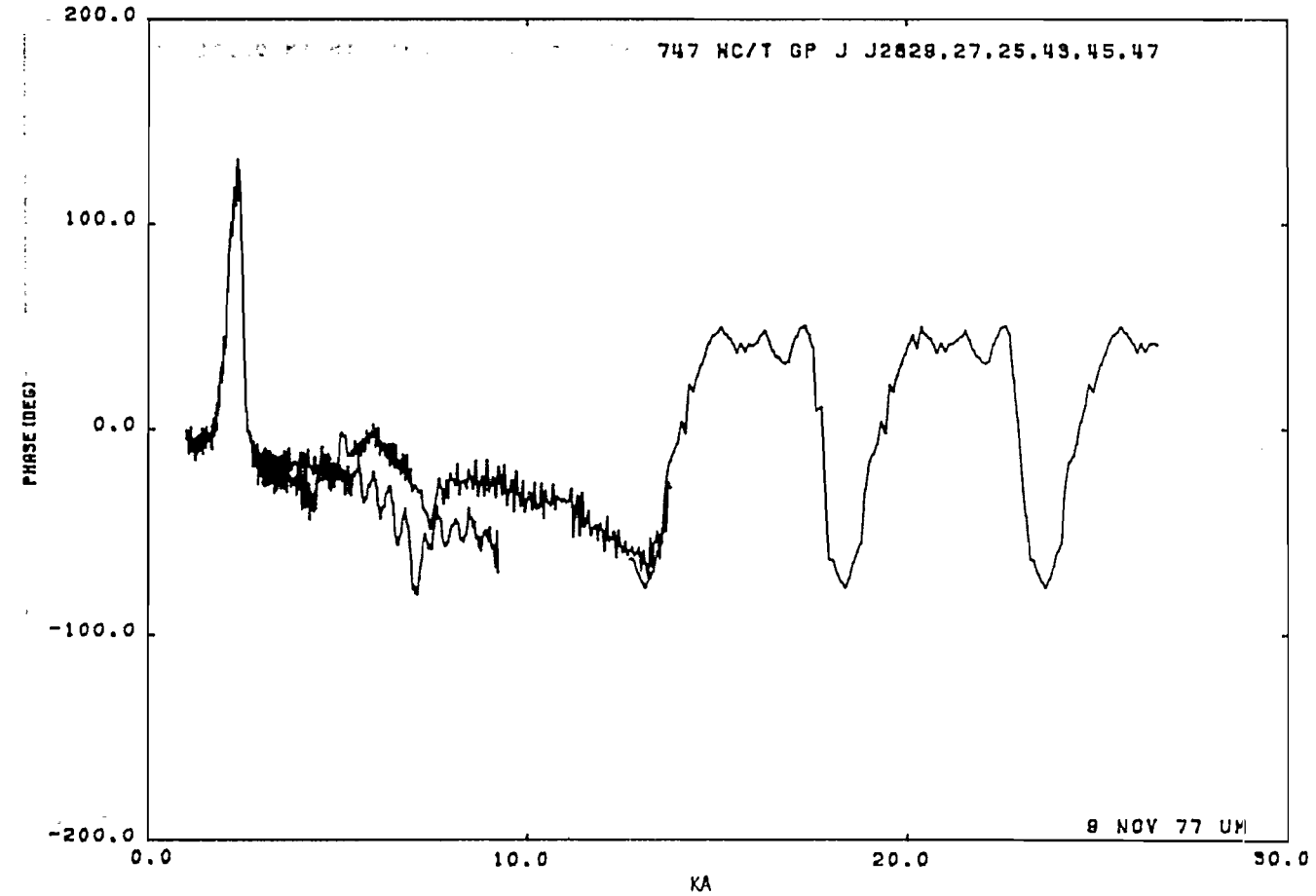

Figure 68. Current on 747 at STA:WC/T; near perfectly conducting ground plane.

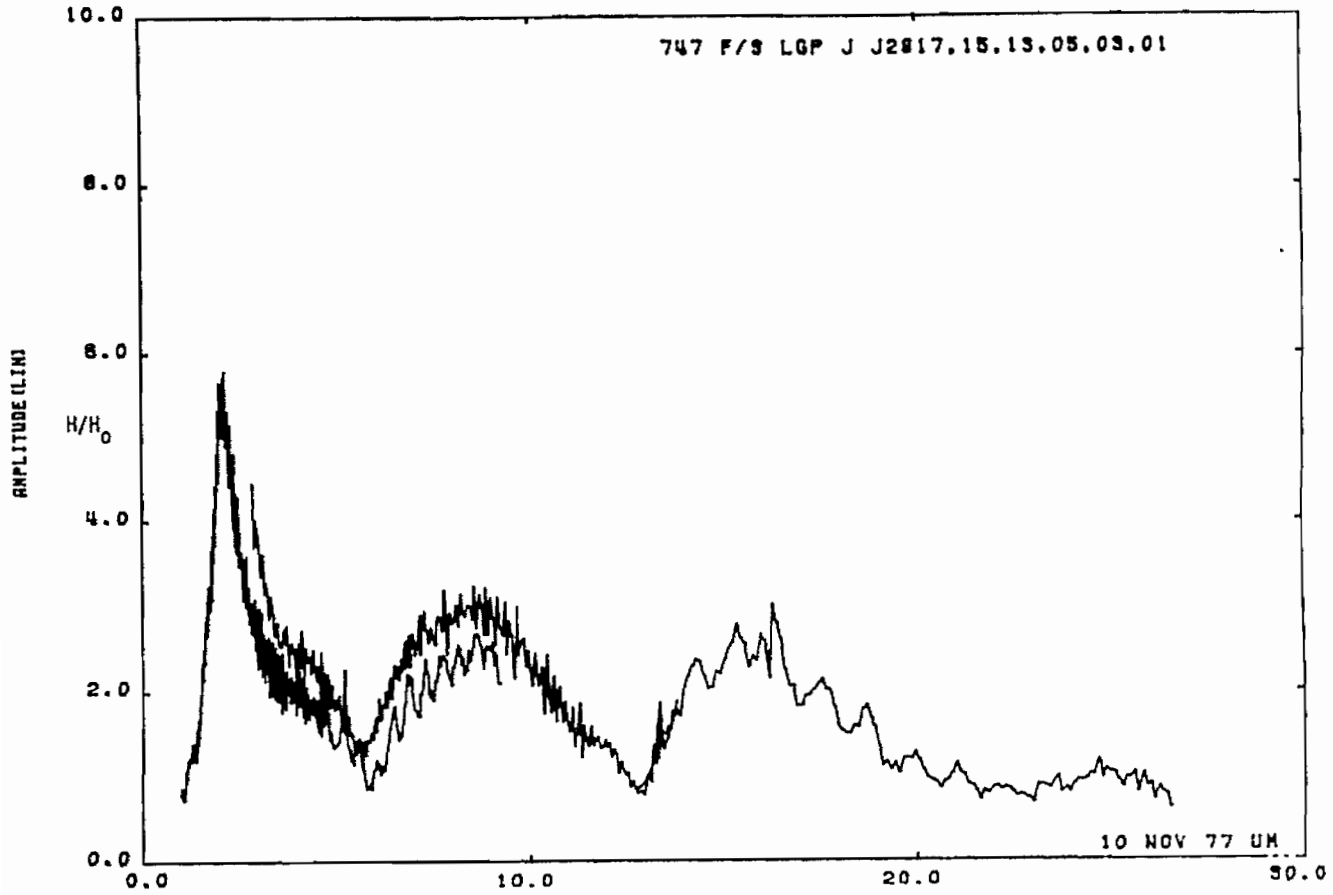

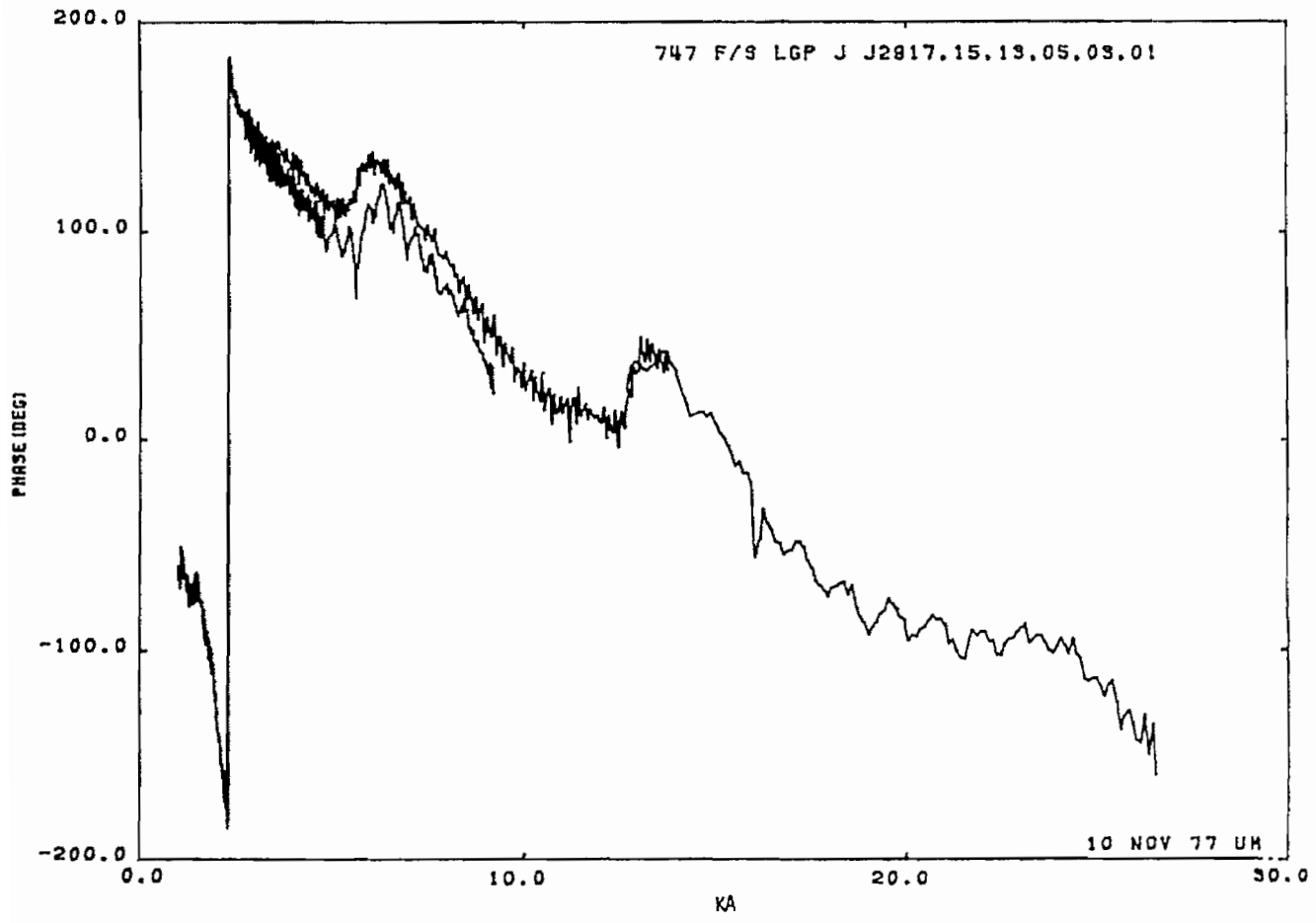

Figure 69. Current on 747 at STA:F/S; near lossy ground plane.

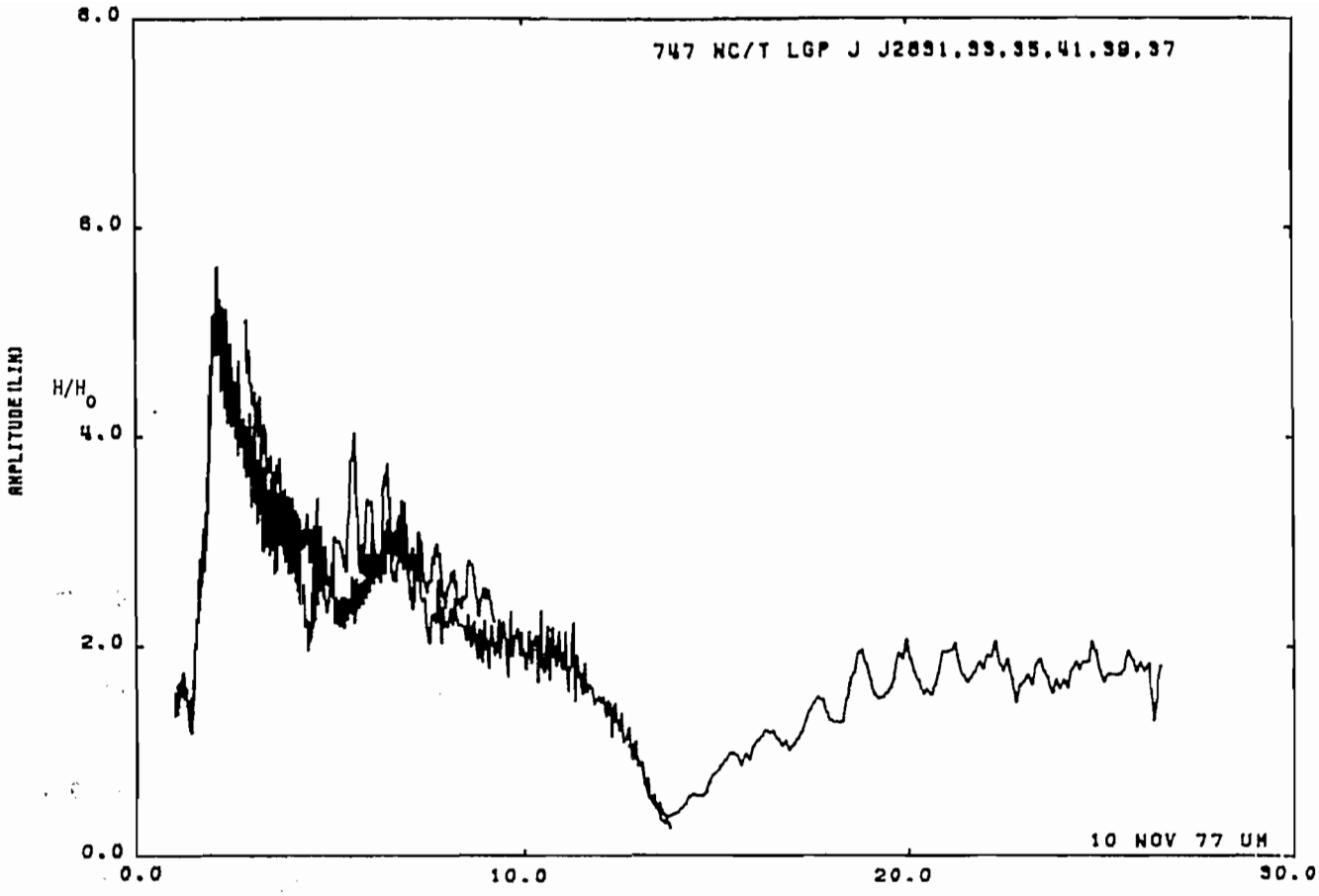

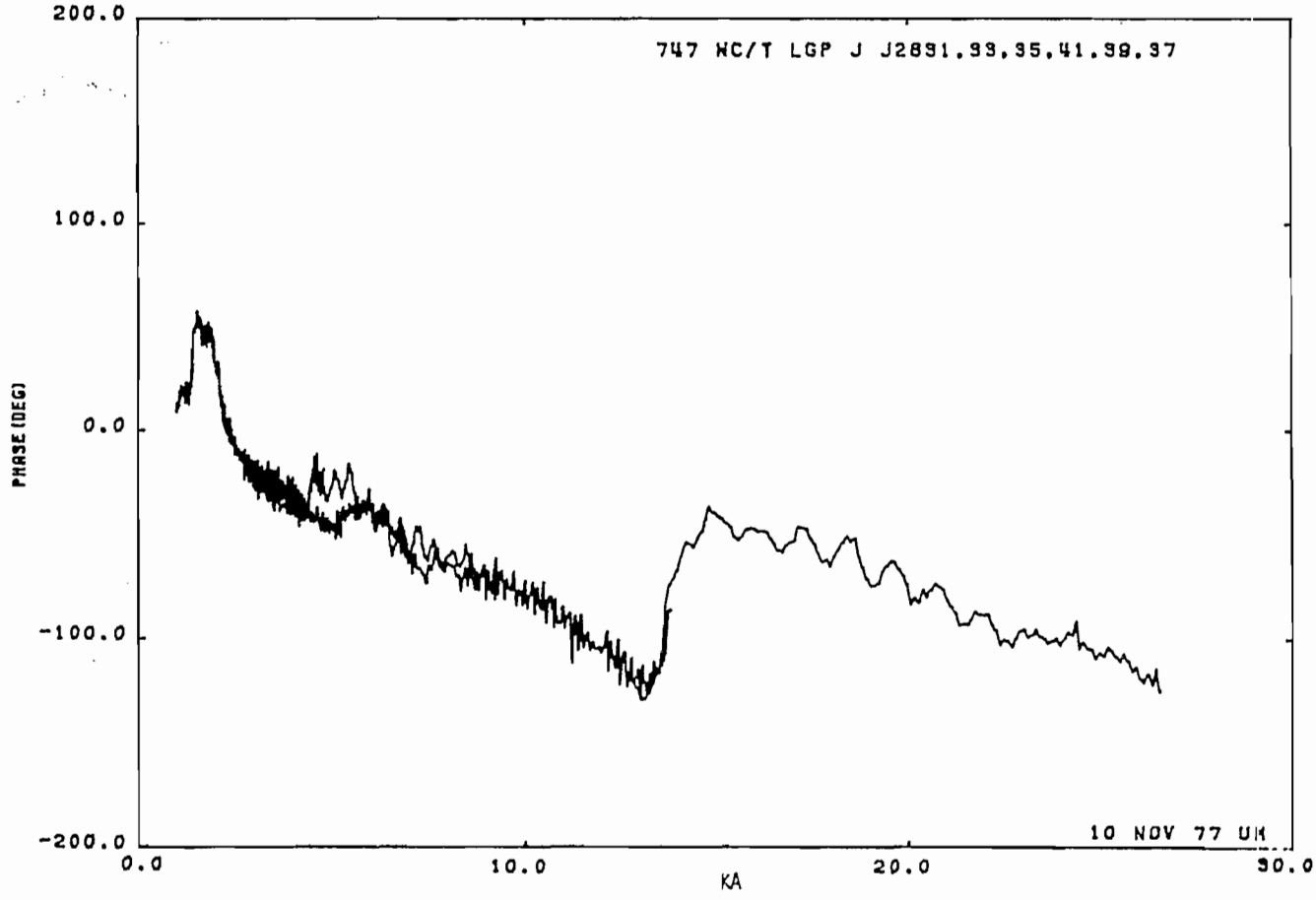

Figure 70. Current on 747 at STA:WC/T; near lossy ground plane.

4. CONCLUSIONS

A total of 57 transfer functions have been presented. A glance at these indicates that the data points are too crowded near the resonance regions and do not show explicitly the details of the resonance characteristics. This is due to the linear scale used to show the results over the wide band of frequencies required. Plotting the frequency on a log scale would have increased the resolution at the lower frequency end but at the expense of that at the higher.

Some of the curves have blank areas where data points are missing. In most cases these were caused by an inability to retrieve the recorded data from the cassette tapes, and the situation is made worse if calibration data required to reduce a set of test data are lost. There is also the problem of noise. As discussed in Section 2.7, the noise-like appearance of the raw data is due to the nonuniform frequency response of the system. The calibration procedure removes most of this noise. Some of the more important conditions that a facility must satisfy in order to successfully calibrate it are:

The physical layout must be fixed apart from the models;

The sampling frequencies must be the same for the test and calibration data;

The receiver or network analyzer must have a linear response.

The fact that not all of these requirements were met has some effect on the data.

The large physical layout required long lengths of cable in the crawl space under the chamber, and their electrical lengths can change due to variations in humidity and temperature. Temperature changes can also affect the frequency stability of the generator; and as a result of such instabilities, the frequencies at which the calibration data are taken may differ from those of the test data taken at a later time.

Problems were experienced with the network analyzer, and we did not become aware of these until the cylinder measurements were completed. The slow but progressive failure of the harmonic converter (HP 8411A) made its response nonlinear, and also reduced its ability to track the signals properly. Much of the noise in the cylinder data is attributable to this. The equipment was repaired prior to measuring the body of revolution and 747 aircraft, and resulted in much improved data for these models.

With the cylinder models, the data for ka $\gtrsim$ 3 may be questionable due to the nonuniform nature of the illumination associated with the image plane, and the variation is most pronounced in the data taken on the top of the cylinder. It should also be recognized that the test models were scaled but the sensors were not, and the effects of this are clearly evident in the measured data for the body of revolution models (for example, Figures 58 and 60). In addition, the distance of a cylinder from the perfectly conducting or lossy ground plane was difficult to control exactly. The jumps in the data for some cylinder models are attributable to some slight variations in the distances (for example, Figures 47 and 53).

Our final remarks concern the large noise-like spikes present in some of the data. Most of these are due to experimental and/or equipment shortcomings and, being spurous, should be ignored in any comparisons of the data with the results of other experimental or numerical investigations.

APPENDIX A. THEORETICAL ANALYSIS OF REFLECTIONS FROM A FINITELY CONDUCTING GROUND PLANE

We here examine the reflection of plane electromagnetic wave at normal incidence on a ground plane consisting of a slab of finitely conducting material. It is required that over the model frequency range 0.4 to 4.0 GHz the ground plane simulate the electrical properties of the earth immediately beneath the Air Force Weapons Center Dipole Facility at Kirtland Air Force Base. The full scale frequency range being 1.5 to 15 MHz, the required scale factor for simulation is about 267.

A.1 Earth Constants at Full Scale Frequencies

The results of the experimental investigation at 1 to 100 MHz described in [5] indicate that the earth immediately beneath the Dipole Facility contains three layers of contrasting electrical properties within 3 m of the surface. Subsurface resistivities at the site range from 2 to 82 ohm-m depending on the layer and the frequency of interest and average dielectric constants range from 6 to 6×10^6. The permeability of the earth may be assumed equal to that of free space.

The electrical characteristics of the top two layers of the earth beneath the Dipole Facility are shown in Table A-1. The relative permittivity (or the dielectric constant) and the resistivity shown in Table A-1 are the measured values obtained from [5], and the other quantities represent the corresponding calculated values. The relative complex permittivity of the medium is

$$\varepsilon = \varepsilon' - i\varepsilon'' \tag{A.1}$$

where

ε' is the dielectric constant

$$\varepsilon'' = \frac{\sigma}{\omega \varepsilon_0} \tag{A.2}$$

σ is the conductivity in mhos/m

TABLE A-1. ELECTRICAL CHARACTERISTICS OF THE EARTH BENEATH THE DIPOLE FACILITY [5]

Depth of Layer (m)	Thickness of Layer (m)	Frequency (MHz)	ρ (Ω-m)	σ (℧/m)	ε'	ε''	δ (m)
0.0 - 0.15	0.15	1.5	48	2.083×10^{-2}	19	250	2.87
		15	44	2.273×10^{-2}	13	27	0.87
0.15 - 0.18	0.73	1.5	73	1.370×10^{-2}	16	164	3.54
		15	65	1.538×10^{-2}	11	18	1.07

ω is the radian frequency

$\varepsilon_o = \frac{1}{36\pi} \times 10^{-9}$ Farad/m is the permittivity of free space

and $\rho = \frac{1}{\sigma}$ is the resistivity in ohm-m.

With this notation the skindepth δ is given by

$$\delta \simeq \frac{68}{f_{MHz}} \frac{1}{\sqrt{\varepsilon''}} \text{ m} \qquad \text{(A.3)}$$

where f_{MHz} is the frequency in MHz.

We shall assume that the earth constants to be simulated are the averages of the values for the top two layers, and these are shown in Table A.2.

TABLE A-2. AVERAGE VALUES OF THE EARTH CONSTANTS AT THE FULL SCALE FREQUENCIES

Frequency (GHz)	ρ (Ω-m)	σ (℧/m)	ε'	ε''	δ (m)
1.5	61	1.639×10^{-2}	18	197	3.23
15	55	1.818×10^{-2}	12	22	0.97

A.2 Simulated Ground Plane

For a scale factor of 267, the required values for the electrical constants of the simulated ground plane at the model frequencies are shown in Table A.3.

TABLE A-3. REQUIRED VALUES OF THE ELECTRICAL CONSTANTS FOR THE SIMULATED GROUND AT THE MODEL FREQUENCIES

Frequency (GHz)	ρ (Ω-m)	σ (℧-m)	ε'	ε''	δ (m)
0.4	0.23	4.4	18	197	$1.2\text{h} \times 10^{-2}$
4.0	0.21	4.9	12	22	3.62×10^{-2}

Emerson and Cuming, Inc. makes a material under the trade name Eccosorb LS-26 which has $\varepsilon' = 10$ and $\sigma = 0.6$ ℧/m at 1.0 GHz. The material is available in 2 by 2 ft. panels 3/4 inch in thickness. The conductivity of this material is about 1/8th of the desired values shown in Table A-3, and the measured values of the electrical constants of Eccosorb LS-26 at 0.5 and 5 GHz are shown in Table A-4.

TABLE A-4. MEASURED VALUES OF VARIOUS ELECTRICAL CONSTANTS FOR ECCOSORB LS-26

Frequency (GHz)	ρ (Ω-m)	σ (℧/m)	ε'	ε''	δ (m)
0.5	1.67	0.6	20	20	3.04×10^{-2}
5.0	0.71	1.4	5	5	0.6×10^{-2}

In the light of the above results and for lack of a more appropriate material, the decision was made to construct our simulated ground plane from a 2-1/4 inch ($\simeq$ 5.7 cm) thick layer of Eccosorb LS-26. The thickness corresponds to 9.52δ and 1.88δ respectively at the high and low ends of the frequency range.

A.3 Reflections From The Simulated Ground Plane

In the present section we discuss theoretically the reflection of a plane electromagnetic wave incident normally on an infinite slab of Eccosorb LS-26. Three arbitrary media are considered as shown in Figure A-1, where the various fields are displayed. Medium 2 is an infinite slab of thickness d in the z-direction. With assumed time dependence $e^{i\omega t}$, the field quantities in the three media can be written as follows.

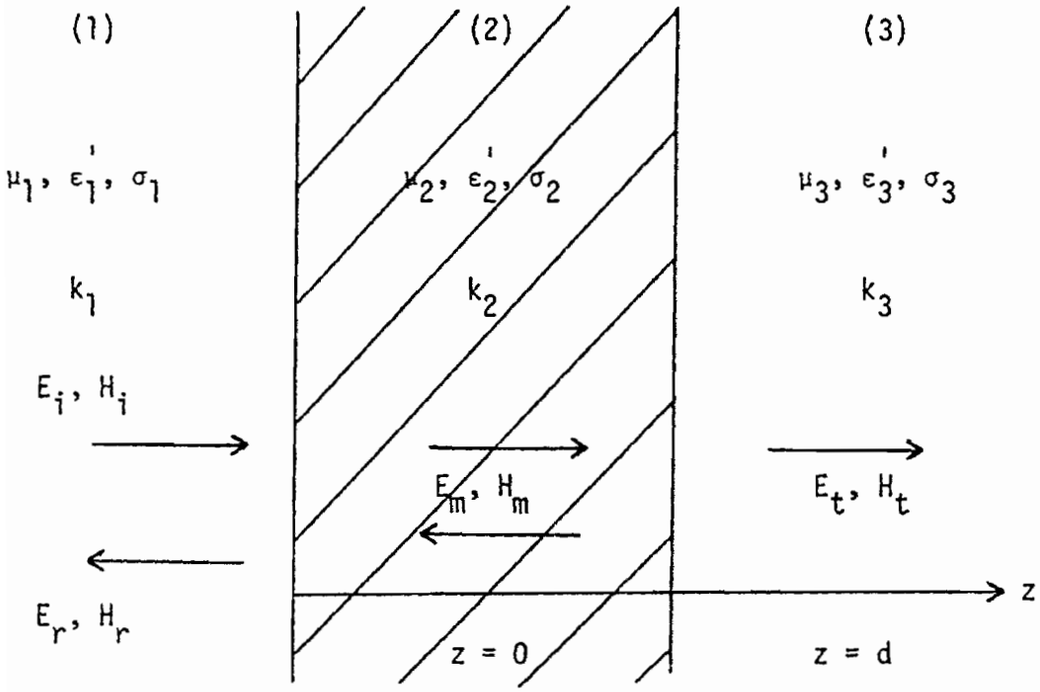

Figure A-1. Reflection and transmission of plane waves by an infinite slab at normal incidence.

$$E_i = E_o e^{-ik_1 z}, \quad H_i = \frac{k_1}{\omega\mu_1} E_i \tag{A.4}$$

$$E_r = E_1 e^{+ik_1 z}, \quad H_r = \frac{k_1}{\omega\mu_1} E_r \tag{A.5}$$

$$E_m = E_2^+ e^{-ik_1 z} \pm E_2^- e^{ik_2 z} \tag{A.6}$$

$$H_m = \frac{k_2}{\omega\mu_2} E_2^+ e^{-ik_2 z} - E_2^- e^{ik_2 z}$$

$$E_t = E_3 e^{ik_3 z}, \quad H_t = \frac{k_3}{\omega\mu_3} e^{ik_3 z} \tag{A.7}$$

where the propagation constants k_1, k_2, k_3 in the three media are defined by

$$k_j = \alpha_j - i\beta_j , \qquad j = 1, 2, 3 \tag{A.8}$$

with

$$\alpha_j = \omega \left[\frac{\mu_j \varepsilon_o \varepsilon_j}{2} \left(\sqrt{1 + \frac{\sigma_j^2}{\omega^2 \varepsilon_o^2 \varepsilon_j^2}} + 1 \right) \right]^{1/2} \tag{A.9}$$

$$\beta_j = \omega \left[\frac{\mu_j \varepsilon_o \varepsilon_j}{2} \left(\sqrt{1 + \frac{\sigma_j^2}{\omega^2 \varepsilon_o^2 \varepsilon_j^2}} - 1 \right) \right]^{1/2} \tag{A.10}$$

Assuming $\mu_j = \mu_o$ and using Eq. (A.2) we can rewrite Eqs. (A.8) and (A.9) as

$$\alpha_j = k_o \left[\frac{\varepsilon_j'}{2} \left(\sqrt{1 + \left(\frac{\varepsilon_j''}{\varepsilon_j'} \right)^2} + 1 \right) \right]^{1/2} \tag{A.11}$$

$$\beta_j = k_o \left[\frac{\varepsilon_j'}{2} \left(\sqrt{1 + \left(\frac{\varepsilon_j''}{\varepsilon_j'} \right)^2} - 1 \right) \right]^{1/2} \tag{A.12}$$

where $k_o = \frac{2\pi}{\lambda}$ is the propagation constant in free space.

Application of the boundary conditions at z = 0 and d to the field quantities in Eqs. (A.4) to(A.7) leads to the following

$$E_o + E_1 = E_2^+ + E_2^-$$

$$E_o - E_1 = Z_{12}(E_2^+ - E_2^-)$$

$$E_2^+ e^{-ik_2 d} + E_2^- e^{ik_2 d} = E_3 e^{-ik_3 d}$$

$$E_2^+ e^{-ik_2 d} - E_2^- e^{ik_2 d} = Z_{23} E_3 e^{-ik_3 d} \tag{A.13}$$

from which the reflection and transmission coefficients of the infinite slab can be determined as

$$\Gamma = \frac{E_1}{E_o} = \frac{(1 - Z_{23})(1 + Z_{12}) + (1 + Z_{23})(1 - Z_{12})e^{i2k_2 d}}{(1 - Z_{23})(1 - Z_{12}) + (1 + Z_{23})(1 + Z_{12})e^{i2k_2 d}} \tag{A.14}$$

$$T = \frac{E_3}{E_o} = \frac{4e^{ik_3 d}}{(1 + Z_{12})(1 + Z_{23})e^{ik_2 d} + (1 - Z_{12})(1 - Z_{23})e^{-ik_2 d}} \tag{A.15}$$

where

$$Z_j = \frac{\omega \mu_j}{k_j} \quad , \quad Z_{jk} = \frac{Z_j}{Z_k} \quad , \quad j, k = 1, 2, 3, . \tag{A.16}$$

Note that

$$\left.\begin{aligned} Z_{jk} &= Z_{kj} = 1 \\ Z_{ij}\, Z_{jk} &= Z_{ij} \end{aligned}\right\} \tag{A.17}$$

For computational purposes it is convenient to define,

$$r_{jk} = \frac{1 - Z_{jk}}{1 + Z_{jk}} = \frac{Z_k - Z_j}{Z_k + Z_j} = -r_{kj} \tag{A.18}$$

Using Eqs. (A.8), (A.16) and (A.18) it can be shown that

$$r_{jk} = \frac{(\mu_k \alpha_j - \mu_j \alpha_k) - i(\mu_k \alpha_j - \mu_j \alpha_k)}{(\mu_k \alpha_j + \mu_j \alpha_k) - i(\mu_k \alpha_j + \mu_j \alpha_k)} \tag{A.19}$$

Thus, the reflection coefficient Γ can be written in the following form

$$\Gamma = \frac{r_{12} + r_{23}\, e^{-2\beta_2 d}\, e^{-i2\alpha_2 d}}{1 + r_{12} r_{23} e^{-2\beta_2 d}\, e^{-i2\alpha_2 d}} \tag{A.20}$$

where r_{jk} is given by Eq. (A.19). Observe that if $d = \infty$ (i.e., medium 3 is missing) Eq. (A.20) implies

$$\Gamma_\infty = r_{12} \tag{A.21}$$

A computer program has been written to determine $|\Gamma|$ and arg Γ as functions of d under various conditions, and the program is listed in Section A.5.

A.4 Numerical Results and Discussion

Figure A-2 shows $|\Gamma|$ vs. d for normal incidence on an infinite slab of Eccosorb LS-26 at two selected frequencies. The curves marked F in Figure A-2 are for a slab in free space, i.e., when media 1 and 3 are free space, and the dotted curves are for a slab of infinite thickness. Observe that at both frequencies $|\Gamma|$ initially fluctuates around $|\Gamma_\infty|$ before asymptotically approaching $|\Gamma_\infty|$. The curves labelled "with absorber backing" refer to the cases when medium 1 is free space and medium 3 is filled with an absorbing material having $\varepsilon_3' = 5$, $\varepsilon_3'' = 1$ at both frequencies. With absorber backing the slab behaves as though it were infinitely thick at smaller values of d. Figure A-3 shows the corresponding values of arg Γ vs. d at the two frequencies. The results shown in Figures A-2 and A-3 indicate that as far as the reflection of a normally incident plane electromagnetic wave is concerned, a thickness d of Eccosorb LS-26 material behaves like infinitely thick slab at 5 GHz and 0.5 GHz for $d \gtrsim 2$ cm and $d \gtrsim 8$ cm, respectively.

As seen from Table A-4 the skin depths of Eccosorb LS-26 at these two frequencies are 0.6 cm and 3.04 cm, respectively, suggesting that a slab of thickness $d \gtrsim 3\delta$ will behave as if it were infinitely thick.

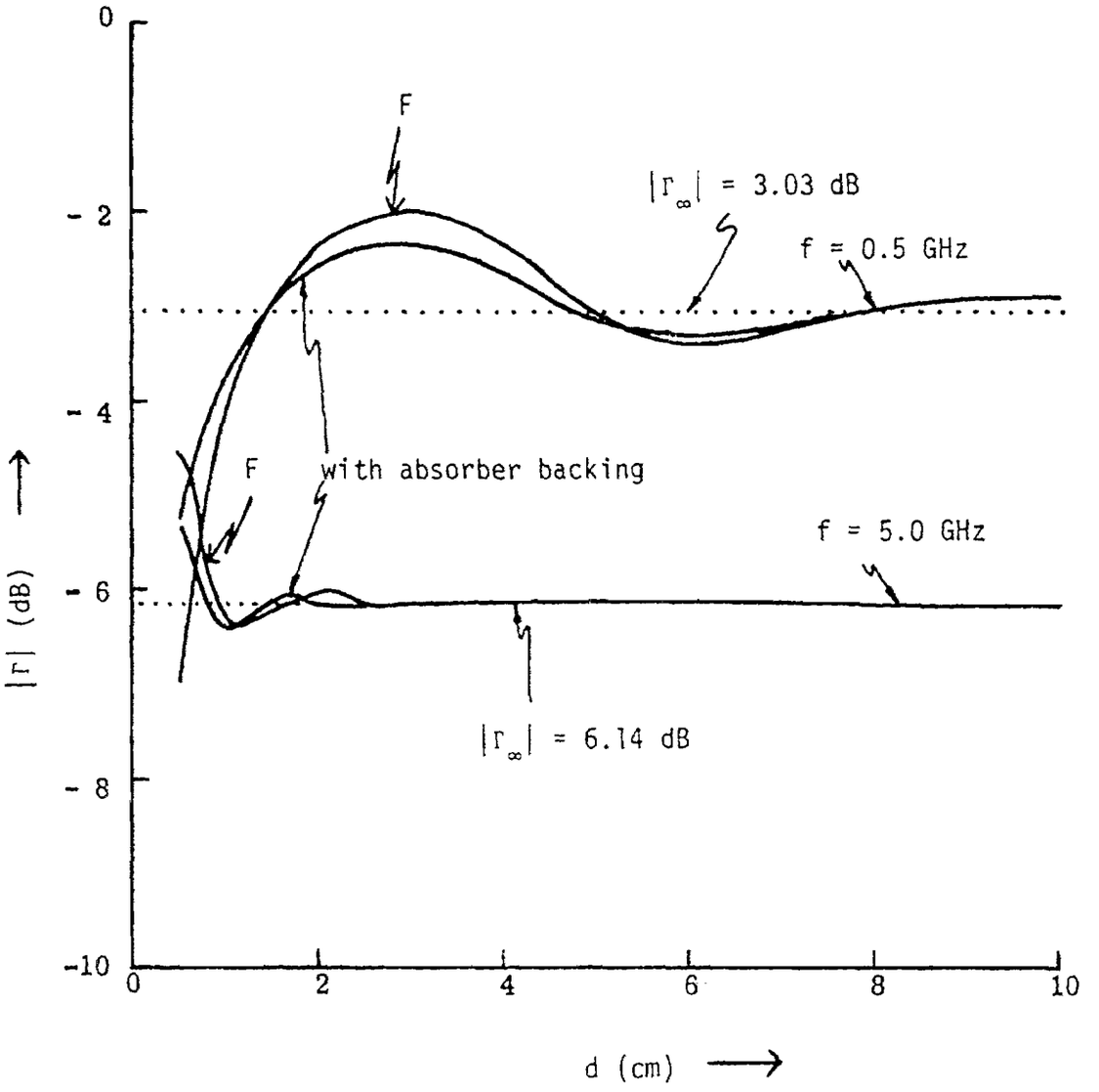

Figure A-2. $|\Gamma|$ vs. d for an infinite slab of Eccosorb LS-26.

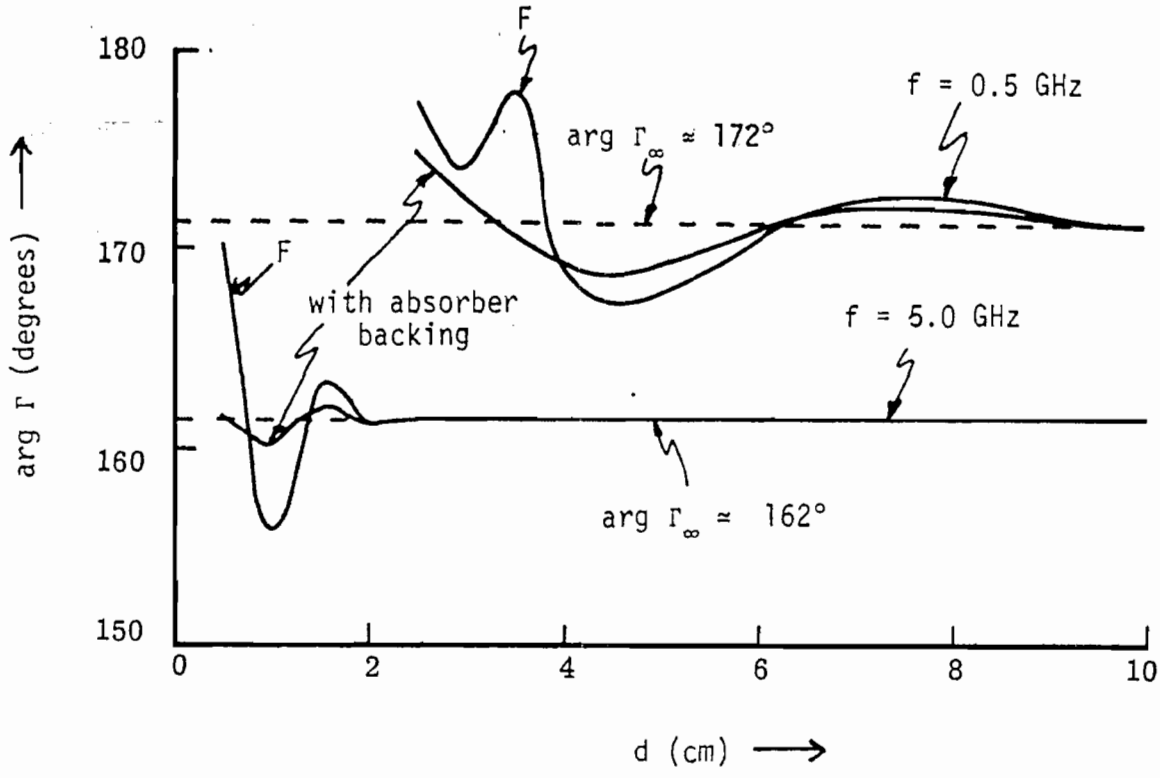

Figure A-3. Arg Γ vs. d for an infinite slab of Eccosorb LS-26.

As discussed in Section 2b we have fabricated ground plane out of a 5.7 cm-thick slab of Eccosorb LS-26. From the results shown in Figures A-2 and A-3, it can be seen that even with d = 4 cm the simulated ground plane may be considered to be infinitely thick at the upper region of the model frequency range. At the lower end of the model frequency range $|\Gamma|$ differs from $|\Gamma_\infty|$ by about 0.5 dB which is well within the experimental accuracy. Thus the 5.7 cm-thick ground plane should provide an adequate simulation of an infinitely thick ground of the same material.

A.5 Computer Program Listing

See next page.

SGFE:GAMMA

03-18-77 10:13:41 GAMMA

```
      COMPLEX GAMMA,R12,R23,EXPO,ECE
      REAL K0
      DATA PI/3.1415927/,DEG/57.2957795/
100   READ(5,500) DI,DINC,DF,FREQ,EP1,EPP1,EP2,EPP2,EP3,EPP3
500   FORMAT(4F10.4,6F5.1)
      K0=(PI*FREQ)/150.
      WRITE (6,510) FREQ,EP1,EP2,EP3,EPP1,EPP2,EPP3
510   FORMAT(1H1,4X,'FREQ =',F7.1,' MHZ'/
     &5X,'EPR1  =',F5.1,3X,'EPR2  =',F5.1,3X,'EPR3  =',F5.1/
     &5X,'EPPR1 =',F5.1,3X,'EPPR2 =',F5.1,3X,'EPPR3 =',F5.1)
      ROOT=SQRT(1.+(EPP1/EP1)**2)
      A1=K0*SQRT(EP1*(ROOT+1.)/2.)
      B1=K0*SQRT(EP1*(ROOT-1.)/2.)
      ROOT=SQRT(1.+(EPP2/EP2)**2)
      A2=K0*SQRT(EP2*(ROOT+1.)/2.)
      B2=K0*SQRT(EP2*(ROOT-1.)/2.)
      ROOT=SQRT(1.+(EPP3/EP3)**2)
      A3=K0*SQRT(EP3*(ROOT+1.)/2.)
      B3=K0*SQRT(EP3*(ROOT-1.)/2.)
      R12=CMPLX((A1-A2),-(B1-B2))/CMPLX((A1+A2),-(B1+B2))
      AMPR=CABS(R12)
      PHAR=DEG*ATAN2(AIMAG(R12),REAL(R12))
      DBR=20.*ALOG10(AMPR)
      WRITE(6,530) AMPR,PHAR,DBR
530   FORMAT(1H ,4X,'MOD(R12) =',F7.2,3X,'PHASE =',F7.2,3X,
     &'DB =',F7.2/)
      R23=CMPLX((A2-A3),-(B2-B3))/CMPLX((A2+A3),-(B2+B3))
      D=DI
      WRITE(6,520)
520   FORMAT(1H ,5X,'D (CM)',5X,'MOD(GAMMA)',5X,'PHASE',7X,'DB'/)
200   EXPO=CMPLX(0.,-2.*A2*D)
      ECE=EXP(-2.*B2*D)*CEXP(EXPO)
      ECE=R23*ECE
      GAMMA=(R12+ECE)/((1.0,0.)+R12*ECE)
      AMP=CABS(GAMMA)
      PHASE=DEG*ATAN2(AIMAG(GAMMA),REAL(GAMMA))
      DB=20.*ALOG10(AMP)
      DCM=100.*D
      WRITE(6,550) DCM,AMP,PHASE,DB
550   FORMAT(1H ,2X,F6.2,4X,F7.2,7X,F7.2,5X,F7.2)
      D=D+DINC
      IF(D.LE. DF) GO TO 200
      GO TO 100
      END
```


☆ U.S. GOVERNMENT PRINTING OFFICE: 1979-678-432-286